Distribution Agreement

In presenting this thesis or dissertation as a partial fulfillment of the requirements for an advanced degree from Emory University, I hereby grant to Emory University and its agents the non-exclusive license to archive, make accessible, and display my thesis or dissertation in whole or in part in all forms of media, now or hereafter known, including display on the world wide web. I understand that I may select some access restrictions as part of the online submission of this thesis or dissertation. I retain all ownership rights to the copyright of the thesis or dissertation. I also retain the right to use in future works (such as articles or books) all or part of this thesis or dissertation.

Signature:

_____ _____

Alexander Shih-Juin Chen Date

Understanding the Mechanism of Protein Kinases Drak/STK17A and RIOK2 function in Glioblastoma

By

Alexander Shih-Juin Chen
Doctor of Philosophy

Graduate Division of Biological and Biomedical Sciences
Cancer Biology

_____
Renee D. Read, Ph.D.
Advisor

_____
Brian G. Petrich, Ph.D.
Committee Member

_____
Anita Corbett, Ph.D.
Committee Member

_____
Anna Kenney, Ph.D.
Committee Member

_____
Kenneth H. Moberg, Ph.D.
Committee Member

_____
Dolores Hambardzumyan, Ph.D.
Committee Member

Accepted:

_____
Lisa A. Tedesco, Ph.D.
Dean of the James T. Laney School of Graduate Studies

_____
Date

Understanding the Mechanism of Protein Kinases Drak/STK17A and RIOK2 function in Glioblastoma

By:

Alexander Shih-Juin Chen
B.A., Lehigh University, 2012

Advisor: Renee D. Read, Ph.D.

An abstract of
A dissertation submitted to the Faculty of the
James T. Laney School of Graduate Studies of Emory University
in partial fulfillment of the requirements for the degree of
Doctor of Philosophy
in Graduate Division of Biological and Biomedical Sciences
Cancer Biology
2020

Abstract

Understanding the Mechanism of Protein Kinases Drak/STK17A and RIOK2 function in Glioblastoma

By: Alexander Shih-Juin Chen

Glioblastoma (GBM) is the most common adult primary malignant brain tumors and is resistant to current therapies. Genomic analyses reveal that signature genetic lesions in GBM include copy gain and amplification of chromosome 7, amplification, mutation, and/or overexpression of receptor tyrosine kinases (RTKs), such as EGFR, and activating mutations in components of the PI-3 kinase (PI3K) pathway. In *Drosophila melanogaster*, constitutive co-activation of RTK and PI3K signaling in glial progenitor cells recapitulate key features of human gliomas. Using our *Drosophila* glioma model to elucidate new downstream effectors of EGFR and PI3K signaling pathways, we discovered two novel protein kinases involved in GBM tumorigenesis through two disparate mechanisms: Death-associated protein kinase (Drak), a cytoplasmic serine/threonine kinase orthologous to the human kinase STK17A, and right open reading frame kinase 2 (RIOK2), an atypical serine/threonine kinase.

We discovered that Drak is necessary for glial neoplasia, but not for normal glial proliferation and development and cooperates with EGFR to promote glial cell transformation. Furthermore, our results indicate that Drak phosphorylates Sqh, the *Drosophila* ortholog of MRLC (non-muscle myosin regulatory light chain), and recruits Anillin, a binding partner of phosphorylated Sqh, to drive glial cell transformation. The Drak-Sqh-Anillin complex co-localizes in neoplastic cells undergoing mitosis and cytokinesis. These functional relationships were conserved in human GBM. Our results indicate that Drak/STK17A, the substrate Sqh/MRLC, and the effector Anillin/ANLN regulate mitosis and cytokinesis in gliomas.

We also discovered that dRIOK2 forms a complex with RNA-binding protein, Imp, the *Drosophila* ortholog of IGF2BP3 (IMP3), and that both dRIOK2 and Imp are necessary for glial neoplasia, but not for normal glial proliferation and development. Furthermore, our results indicate that RIOK2 catalytic activity is important for glial neoplasia and recruits TORC2 to phosphorylate IMP3, and in turn, regulate levels of MYC protein, a known target mRNA of IMP3. These functional relationships were conserved in human GBM. Collectively, our data indicates that RIOK2 autophosphorylation recruits TORC2 and IMP3, which in turn, modulates MYC protein expression to promote GBM tumorigenesis. The novel Drak/STK17A-Sqh/MRLC-Anillin/ANLN and RIOK-IMP3-TORC2 complexes may provide new therapeutic targets for gliomas.

Understanding the Mechanism of Protein Kinases Drak/STK17A and RIOK2 function in Glioblastoma

By:

Alexander Shih-Juin Chen
B.A., Lehigh University, 2012

Advisor: Renee D. Read, Ph.D.

A dissertation submitted to the Faculty of the
James T. Laney School of Graduate Studies of Emory University
in partial fulfillment of the requirements for the degree of
Doctor of Philosophy
in Graduate Division of Biological and Biomedical Sciences
Cancer Biology
2020

Acknowledgements

I would like to thank my advisor Dr. Renee D. Read for all of her assistance over the 6 years I was a graduate student in her lab. Her passion and love for science is contagious and instilled on me the very same drive and curiosity about whatever scientific idea I am pursuing. She was always there when I needed her assistance may it be preparing manuscripts, talking about data, or even just ruminating about the many podcasts I listen to on a regular basis. Her guidance and mentorship were what made me the scientist I am today, and for that, I am eternally grateful.

I would like the thank the members of my committee, Dr. Anita Corbett, Dr. Dolores Hambardzumyan, Dr. Anna Kenney, Dr. Ken Moberg, and Dr. Brian Petrich for all their assistance over the years. Their support and guidance were a tremendous help during my research endeavors and helped me through the frustrating times when experiments did not work as intended.

I would like to thank my family who were always there for me when I needed them most. They were considerate and patient with me during the time I was in graduate school and was always there to lend an ear during the long walks home from lab to talk about my day. Their love was a constant anchor and their kind words were a source of comfort. I would like to thank my brother who always there for me and knew that it was best not to ask me when I would be done with graduate school. His love, his humor, and his friendship always brought a smile to my face, may it be a random postcard or just a call now and then to check up on me. I would like to thank my family that are no longer with me. I would like to thank my grandmother and grandfather for always believing in me no matter what, and teaching me that when in doubt, always pursue your passion.

I would like to thank my friends at Emory for game nights, wing nights, and outings. Through the fun times, you made my time at Emory feel just a bit shorter, and for my Lehigh friends who were always supportive during my time as a graduate student. Through visits, videogame sessions, and phone conversations, you were always there to listen to me and were genuinely interested in what I was doing during graduate school.

Finally, I would like to thank my lab family both past and present. I am eternally grateful for your assistance in experiments or just talking shop. I greatly appreciate you making my time in lab as memorable as it was.

Table of Contents

List of Figures and Tables:

Figure 3.5. The RIOK2-IMP3 complex recruits TORC2 to phosphorylate IMP3.

Figure 3.6. dRIOK2/RIOK2 and Imp/IMP3 modulate dMyc/MYC expression in a conserved pathway.

Figure 3.7. A model for the role of the RIOK2-IMP3-TORC2 complex in regulating MYC expression to promote GBM tumorigenesis.

Supplementary Figure S3.1. RIOK2 RNAi induces minor defects in ribosome biogenesis and disrupts TORC2 activation.

Supplementary Figure S3.2. Overexpressed catalytically inactive RIOK2 does not induce defects in ribosome biogenesis.

Supplementary Figure S3.3. *Drosophila* orthologs of RIOK2 associated RNA-binding proteins are required for EGFR-PI3K glial neoplasia.

Supplementary Figure S3.4. Imp and dRIOK2 knockdown in wild-type background produced no gross morphological defects in *Drosophila* glia.

Supplementary Figure S3.5. dRIOK2 or kinase-dead dRIOK2 overexpression induced no gross development or morphological defects in *Drosophila* glia.

Supplementary Figure S3.6. RIOK2 autophosphorylates itself but does not directly phosphorylate IMP3.

Supplementary Figure S3.7: RIOK2 and IMP3 modulate MYC expression in GBM cells in a conserved pathway.

Supplementary Figure S3.8: RIOK2-IMP3 complexes include other RNA-binding proteins and rely on the presence of RNA.

Supplementary Table S3.1: Proteomic approach to identify endogenous RIOK2 binding proteins.

Supplementary Table S3.2: RNAi screen of *Drosophila* orthologs for RIOK2 binding proteins.

Supplementary Table S3.3: IMP3 does not strongly co-immunoprecipitate with catalytically inactive RIOK2.

List of Abbreviations:

ANLN: Anillin
BBB: Blood Brain Barrier
Brat: Brain Tumor
CNS: Central Nervous System
DAPK: Death-Associated Protein Kinase
DAPK1: Death-Associated Protein Kinase 1
DAPK2: Death-Associated Protein Kinase 2
DAPK3: Death-Associated Protein Kinase 3
Drak: Death-Associated Protein Kinase
DRAK1: DAPk-related Apoptosis-Inducing Protein Kinase-1
DRAK2: DAPk-related Apoptosis-Inducing Protein Kinase-2
DRP-1: DAPk-Related Protein 1
ECM: Extracellular Matrix
EGFR: Epidermal Growth Factor Receptor
$EGFR^{vIII}$: EGFR Mutant Variant III
FGFR: Fibroblast Growth Factor Receptor
GBM: Glioblastoma multiforme
GSC: Glioma Stem Cells
HNPC: Normal Human Neural Progenitor Cells
HNSCC: Head and Neck Squamous Cell Carcinoma
IDH1: Isocitrate Dehydrogenase 1
IMP: Insulin Growth Factor 2 mRNA Binding Protein
IMP1: Insulin Growth Factor 2 mRNA Binding Protein 1
IMP2: Insulin Growth Factor 2 mRNA Binding Protein 2
IMP3: Insulin Growth Factor 2 mRNA Binding Protein 3
IP: Immunoprecipitation
KD: Kinase Dead
KH: hnRNP KH domains
LGG: Low Grade Gliomas
Lox: Lysyl oxidase
MLCK: Myosin Light Chain Kinase
MRLC: Myosin Regulatory Light Chain
mRNA: Messenger RNA
mTORC1: Mammalian Target of Rapamycin Complex 1
mTORC2: Mammalian Target of Rapamycin Complex 2
NMII: Nonmuscle Myosin Type II
NSC: Neural Stem Cells
PAR-CLIP: Photoactivatable Ribonucleoside-Enhanced UV Crosslinking and Immunoprecipitation
PDGFRA: Platelet-Derived Growth Factor Receptor Alpha
PI3K: Phosphatidyl-Inositol-3-Kinase
PIP3: *PTEN* Phosphatidyl-Inositol-3-Phosphate Lipid Phosphatase
PKC: Protein Kinase C
RBP: RNA-Binding Proteins

RIP: RNA-binding protein Immunoprecipitation
RIOK2: Right Open Reading Frame Kinase 2
RNAi: RNA Interference
ROCK: RhoA Kinase
ROS: Reactive Oxygen Species
RRMs: RNA Recognition Motifs
RTK: Receptor Tyrosine Kinase
Sqh: Spaghetti Squash
STK17A: Serine Threonine Kinase 17A
TCGA: The Cancer Genome Atlas
TMA: Tissue Microarrays
TSC1/2: Tuberous Sclerosis Protein 1/2
UTR: Untranslated Region
wHTH: N-Terminal Winged Helix
WHO: World Health Organization
WT: Wild-Type

Chapter 1. Introduction

1.1 Glioblastoma

Glioblastoma multiforme (GBM) is the most common primary malignant adult brain tumor. GBM originates primarily in the cerebral hemispheres, though tumors may also arise in the brain stem, cerebellum, and spinal cord (1). Standard of care for GBM involves surgical resection followed by concomitant radiotherapy with adjuvant chemotherapy with the DNA alkylating agent, temozolomide. Despite this treatment, median survival for GBM remains poor at 14-15 months after initial diagnosis (1). The World Health Organization (WHO) has classified GBM based on the histopathological and clinical presentation as grade IV glioma due to its highly aggressive, malignant, invasive, and undifferentiated nature (2, 3). GBMs can be further subclassified as either primary or secondary GBMs. Primary GBMs are far more common in patients aged 65 and older, are *de novo* tumors, and do not arise from lower grade gliomas. Conversely, secondary GBMs are much rarer and occur in patients below the age of 40. Secondary GBMs arise from the progression of lower grade gliomas, with approximately 70% of grade II gliomas transforming into either grade III or grade IV gliomas in a timespan of approximately 5-10 years after diagnosis (3). While both primary and secondary GBMs present similarly in the clinic, recent genomic characterizations reveal that in terms of transcriptional patterns and recurrent DNA copy number aberrations, these two subclasses are quite distinct from one another (4, 5). Further contributing to the difficulty of treatment, GBMs have considerable intratumoral heterogeneity and arise from glial cells and glial cell progenitors, though the precise cell-of-origin for gliomas remains controversial, with data supporting neural stem cells, astrocytes, or oligodendrocyte precursor cells as possible cells-of-origin (6). As such,

it is imperative to better understand the biology of GBM in order to develop more effective treatments.

To discover genetic mutations essential to gliomagenesis, large-scale genomic projects such as The Cancer Genome Atlas (TCGA) analyzed hundreds of GBM tumor tissue specimens (7, 8). Common alterations in GBMs include genomic amplification, activating mutations, and overexpression of receptor tyrosine kinases (RTKs), such as *epidermal growth factor receptor* (*EGFR), platelet-derived growth receptor alpha (PDGFRA),* and *fibroblast growth factor receptor* (*FGFR),* and genes in core RTK signal transduction pathways, such as the *phosphatidyl-inositol-3-kinase (PI3K)* pathway, and inactivation of the *TP53/RB* pathway (7, 8). Genetic alterations in RTKs occur in over 80% of GBMs, and one of the most frequent alterations is amplification and mutation of *EGFR* (7, 8). The most common EGFR mutation is variant III ($EGFR^{vIII}$), a constitutively active version of EGFR created by an internal deletion of the ligand-binding domain (exons 2-7) that results in overactivation of downstream cell growth pathways (9, 10). Constitutive activation of RTKs through amplification and/or mutation contributes to GBM pathogenesis by promoting proliferation, migration, and resistance to apoptosis (11-14).

Common genetic alterations in GBM occur in the PI3K pathway, including activating missense mutations in *PIK3CA*, which encodes the p110α catalytically active subunit of PI3K (15, 16), and *PIK3R1*, which encodes the p85α regulatory subunit of PI3K (7, 17). Loss of the *PTEN* phosphatidyl-inositol-3-phosphate (PIP3) lipid phosphatase, which is inactivated through point mutations, deletions, and epigenetic silencing, results in constitutive activation of PI3K signaling as a consequence of elevated PIP3 levels (18-20). As a response to PI3K activation, AKT kinases are upregulated in approximately 70% of GBMs (16, 18). Other common mutations

inactivate the TP53/RB pathways, including homozygous *CDKN2A/CDKN2B* or *RB1* loss, *TP53* mutations, *MDM4* and *MDM2* amplification, and *CDK4* amplification (7, 8). Another common genetic alteration in GBM are activating mutations in the promoter of telomerase reverse transcriptase (*TERT*), which occurs in 70% of GBM patients (8, 21). These mutations inactivate cell cycle checkpoints, immortalize glial cells, and, together with RTK alterations, promote GBM tumor initiation and progression (reviewed in (3)). Studies in mice indicate that co-mutation of these pathways cooperate to promote GBM tumorigenesis (22-26). However, due to limited drug absorption into tumors, cellular and genetic heterogeneity in tumors, and emergence of drug resistance over time, efforts to therapeutically target these genetic alterations have shown limited efficacy in the clinic (27-30). To improve outcomes for GBM patients, there must be a concerted effort to translate these data to develop new therapies that target underlying biological mechanisms that drive GBM.

1.2 *Drosophila melanogaster*: an effective tool to model GBM

One of the most effective models for advancing our understanding of cancer is *Drosophila melanogaster* (reviewed in (31)). As a cancer model, *Drosophila* has numerous advantages over traditional animal models, including a relatively short lifespan, a large number of progeny, a fully sequenced and annotated genome, and powerful modalities to analyze complex tissues. Furthermore, there are tools available for targeted or insertional mutagenesis and RNA interference (RNAi) for almost all genes in the genome. The binary UAS/GAL4 system allows for Gal4-driven cell-type specific gene manipulation in fly tissues, including the central nervous system (CNS), and expression of multiple UAS-containing transgenes within the same cell type allows for complex genetic manipulation (32-36). Most importantly, 75% of

genes associated with human diseases have functional fly orthologs, and 30% of them have enough similarity such that human and fly proteins have identical functions (37).

Drosophila is also an excellent model organism for neurological diseases due to extensive cellular homologies between *Drosophila* and humans. The *Drosophila* CNS consists of two bilaterally symmetrical brain hemispheres and a central nerve cord that, like humans, is comprised of glia and neurons. *Drosophila* glia share similar developmental origins, cellular properties, and physiological functions of human glia, such as astrocytes, oligodendrocytes, and Schwann cells (38). In *Drosophila*, there are several types of CNS glia that are derived from neural stem cells, known as neuroblasts, and that are defined by their morphology and associations with neurons, including astrocytes, cortex glia, and peripheral glia (reviewed in (38)). Astrocytes, which restructure neuronal circuits and regulate synapses, similar to mammalian astrocytes, primarily localize in the cortex and extend processes into the neuropil, a histologically distinct region of the *Drosophila* CNS where dendrites and axons project and connect (38). Cortex glia, which have similarities to mammalian astrocytes, localize in the cortex, where neuronal cell bodies are localized, and support development and maturation of neuroblasts, neurons, and other glial cell types in response to local and systemic signals (39-41). Perineural glia along with the subperineural glia act as a chemical and physical barrier for the CNS and make up the blood-brain barrier (BBB) (38). Perpherial glia, similar to Schwann cells, ensheath the peripheral sensory and motor nerves (42, 43).

In support of their relevance as a cancer model, *Drosophila* do in fact develop neoplastic tumors that share key features of vertebrate neoplasms: rapid autonomous growth, invasion into adjacent healthy tissue, metastasis into distant organs, lethality to host, loss of tissue structure, lethal autonomous growth after transplantation, and lack of contact inhibition (31). Studies show

that subjecting wild-type *Drosophila* to genetic manipulation, carcinogens, and X-ray irradiation can result in heritable tumor-causing mutations, producing malignant cells that are a source of uncontrolled cell growth (44-46). Furthermore, *Drosophila* models demonstrate a crucial characteristic of malignant tumors, unlimited growth after transplantation. In a seminal study, Gateff et al. demonstrated that pieces of larval wild-type brains transplanted into the abdominal cavity of female adult flies neither grew nor killed their hosts, whereas pieces from tumor suppressor mutant brains grew rapidly up to 300 times the size of the original transplant and prematurely killed their hosts (44).

Several genetic pathways involved in gliomagenesis are conserved between *Drosophila* and humans, and single orthologs exist for many genes involved in gliomagenesis, simplifying complex genetic analysis. For example, there are single functional orthologs for genes such as *EGFR (dEGFR), PIK3CA (dp110), PTEN (dPTEN), RAS (dRas)*, *RAF (dRaf)*, and *AKT (dAkt)*. Moreover, many essential genes involved in human gliomagenesis were first discovered in flies: for example, the gene *Notch* is named for *Drosophila* mutant phenotypes (47), and human orthologs of Notch are involved in GBM tumorigenesis (48).

1.3 *Drosophila* models for RTK-driven GBM

Given the homologies between *Drosophila* and mammals, Read *et al*. developed a *Drosophila* GBM model to investigate how signaling pathways cooperate during neural tumorigenesis (49). Similar to published mouse models, in *Drosophila*, co-activation of EGFR and PI3K signaling in a glial-specific manner resulted in glial neoplasia (Figure 1.1) (49). This was achieved using glial-specific *repo-Gal4* to co-overexpress constitutively active versions of dEGFR and dp110, the catalytic subunit of PI3K, or downstream effectors, such as dRas or dRaf

combined with *dPTEN* RNAi. In contrast, glial-specific activation of EGFR-Ras or PI3K signaling alone did not induce neoplasia, indicating that EGFR and PI3K work together synergistically to drive glial tumorigenesis (49). Mutant variants of EGFR found in GBM, such as $EGFR^{vIII}$, also produced neoplastic phenotypes in *Drosophila* (50). Moreover, co-activation of either dEGFR or dRas with PI3K did not induce neoplasia in neuroblasts or neurons, indicating that neural tumorigenesis in response to these pathways is glial-specific (49).

Read *et al.* used transplant assays and FLP-FRT clonal analysis to investigate developmental origins, malignant properties, and invasive potential of neoplastic glia. EGFR-PI3K mutant glia transplanted into the abdomen of adult host flies yielded large lethal tumors in which neoplastic glia invaded adjacent tissues (49). These tumors were associated with excess trachea, which are oxygen delivery tubules, suggesting that they stimulated tracheal growth in a process similar to angiogenesis (49). FLP recombinase was used to induce clones of mutant glia in otherwise normal tissue in late development or young adult flies. While single $dPTEN^{null}$ mutant clones or clones overexpressing dEGFR showed a slight increase in glial cells compared to wild-type control clones, *dEGFR* or *dRas*; $dPTEN^{null}$ double mutant clones created highly proliferative and invasive tumor-like neoplastic growths (49).

This *Drosophila* GBM model recapitulates a key aspect of human GBM in that tumor formation relies on activation of multiple pathways that work synergistically to promote uncontrolled proliferation and migration (49). At least four pathways downstream of EGFR and PI3K co-activation promote glial neoplasia, all of which have orthologous gliomagenic human genes (49): dMyc (MYC) promoted cell cycle entry, Pnt (ETS-family transcription factor) promoted cell cycle progression, and the Tor-S6K pathway promoted protein translation and

cellular growth (49). Thus, *Drosophila* GBM models show evolutionary conservation of oncogene cooperativity.

Read *et al.* established that, in *Drosophila*, glial progenitor cells are prone to malignant transformation in response to oncogenes that drive human gliomagenesis, and that *Drosophila* models of RTK-driven glial neoplasia are effective tools to characterize gliomagenic pathways. These models have now been used by several groups to evaluate the capacity of other RTK and Ras pathway components to promote glial neoplasia, to identify novel genes and pathways that contribute to neuro-glial tumorigenesis, and to identify subtypes of glia prone to transformation (40, 50-59). GBM is by nature a highly invasive tumor, and RTK and PI3K signaling pathways promote invasive behavior of tumor cells; *Drosophila* can be used to investigate this aspect of tumor biology (3). To better understand how these signaling pathways govern migration and invasion in GBM, Witte *et al*. used imaging to track changes in proliferation and migration of EGFR-PI3K transformed glia in the visual system (52). During larval development, repo-positive glia originate in the optic stalk and migrate into the retina but not the Bolwig's organ, at predictable times during development (60, 61). Neoplastic transformation by EGFR and PI3K signaling dramatically increased the number of migratory glia in the optic stalk, with some glia invading along the Bolwig's organ nerves, and importantly, this increase was rescued using pharmacological inhibitors of EGFR and PI3K, consistent with the conclusion that, in *Drosophila* glia, these pathways are sufficient to drive neoplastic invasion and migration (52). Moreover, Witte *et al*. observed that overexpressing other RTKs such as *Pvr* (PDGFR/VEGFR), *htl* (FGFR1), and *Inr* (Insulin receptor), also increased the proportion of migratory and invasive neoplastic glia (52). This study indicates that *Drosophila* can be effectively used to model GBM migration and invasion in response to constitutive activation of RTKs and PI3K signaling.

However, pharmacological agents that target a single RTK show limited efficacy in GBM patients (62). Therefore, RTK effector pathways in glial tumorigenesis, which could be identified in *Drosophila*, may be more relevant to therapeutic development.

Due to the ease of cell-type specific genetic manipulation, *Drosophila* are also effective tools to identify glial cells-of-origin in GBM tumorigenesis and investigating their propensity to be transformed in relation to their developmental roles. Mouse models have identified glial progenitors as cells-of-origin in gliomas, including astrocytic and oligodendrocyte progenitor cells (OPCs), because driver mutations associated with human GBM can transform these cells (6). As discussed previously, *Drosophila* possess glia and glial progenitor cells that share many features with their mammalian counterparts. In a study of neuroblast development, Pvr ligands produced by neuroblasts were found to stimulate Pvr signaling in cortex glia, supporting their survival and morphogenesis, which, in turn, is required for their ability to support neuroblast and neuron development (40). Importantly, constitutively active Pvr or EGFR-PI3K induced neoplastic transformation of cortex glia, and, as they grew during early stage tumorigenesis, neoplastic cortex glia colonized the developing brain at the expense of neuroblasts and neurons (40). Like cortex glia, OPCs similarly depend on PDGFR signaling for their normal development, become transformed by constitutive PDGFR or RTK-Ras signaling, and outcompete neural stem cells in the mouse brain (6, 63). However, the pathways that mediate cell-cell interactions to allow tumor cells to colonize the brain during early-stage tumorigenesis and effectively killing neuronal cells are not clear. In the future, *Drosophila* GBM models may help elucidate the mechanisms involved in competition between normal and RTK-driven tumor cell populations.

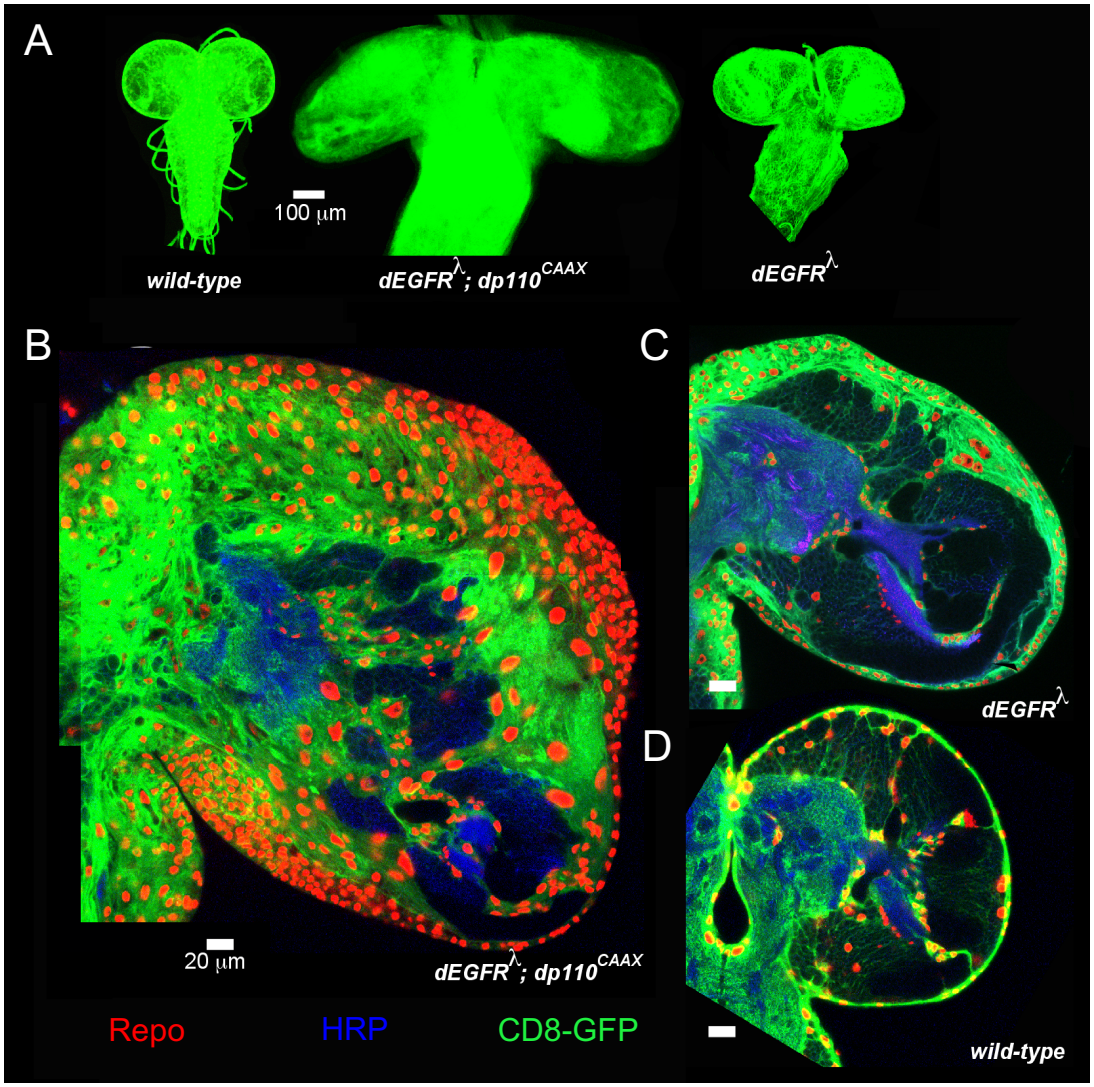
A
100 μm
wild-type
dEGFRλ; dp110CAAX
dEGFRλ
B
20 μm
dEGFRλ; dp110CAAX
C
dEGFRλ
D
wild-type
Repo
HRP
CD8-GFP

Figure 1.1. Co-activation of EGFR and PI3K in Drosophila glia causes neoplasia.

(A) Optical projections of whole brain-nerve cord complexes from late 3rd instar larvae, displayed at the same scale. Glia are labeled with CD8-GFP (green) and constitutively activated EGFR (dEGFR$^{\lambda}$) and PI3K(dp110^{CAAX}) driven by repo-Gal4. Each brain is composed of 2 symmetrical hemispheres attached to the ventral nerve cord. In *repo>dEGFR$^{\lambda}$;dp110^{CAAX}* larvae, both brain hemispheres are enlarged and elongated relative to other genotypes. (B–D) 2 μm optical sections of larval brain hemispheres from late 3rd instar larvae approximately, displayed at the same scale. Glial cell nuclei labeled with Repo (red); anti-HRP for neuropil (blue). In *repo>dEGFR$^{\lambda}$;dp110^{CAAX}* brains (B) there is a dramatic increase in glia relative to *repo>dEGFR$^{\lambda}$* (C) or wild-type animals (D). Figure adapted from [35].

1.4 *Drosophila* models identify mechanosensory mechanisms in GBM

As genomic analyses of GBMs continues, new RTK mutations are being uncovered. For example, a subset of adult GBMs carry gene fusion mutations in which the C-terminal tyrosine kinase domains from FGFR RTKs are fused in frame to the N-terminal regions of the TACC family proteins, which drive oligomerization and kinase activation (64, 65). Recent studies show that FGFR-TACC fusion proteins drive glioma cell proliferation and invasion, and that tumor cells positive for FGFR-TACC fusion proteins can be sensitive to FGFR kinase inhibitors *in vitro* and *in vivo* (64, 65). FGFR-TACC proteins drive tumorigenesis in mammalian astrocytes, although they localize to the nucleus and fail to activate canonical FGFR signaling pathways, indicating that they have aberrant activity distinct from full-length FGFR proteins (64, 65). Thus, there is great enthusiasm for understanding how these lesions contribute to tumorigenesis and for using such knowledge to therapeutically target FGFR-TACC mutant tumors.

To understand how FGFR-TACC proteins promote glial transformation, the human FGFR3-TACC3 fusion was overexpressed specifically in *Drosophila* glia (54). Like co-activation of EGFR and PI3K, FGFR3-TACC3 induced neoplastic transformation of larval glia, and tumorous glia showed increased deposition of extracellular matrix (ECM) proteins and increased ECM stiffness (54). Glial tumor tissues have altered ECM stiffness that contributes to altered mechanosignaling within tumor and stromal tissues (66). These ECM changes actively promote tumor progression by increasing cellular proliferation, survival, migration, drug resistance, and angiogenesis (67-69). However, the molecular mechanisms involved in this process are not well understood.

In *Drosophila* models of EGFR-PI3K and FGFR-TACC driven GBM, function of the dPiezo ion channel was required for GBM tumorigenesis, and required for increased ECM

deposition and tissue stiffness in neoplastic glial tissues but not in normal glia (54). Research studies have shown that ion channels play a critical role in regulating ECM stiffness and cellular rigidity (70). The evolutionarily conserved PIEZO transmembrane ion channels, which normally function in sensory neurons, are mechanosensitive and open in response to membrane tension to allow for permeation of potassium, calcium, and sodium ions (71-74). Loss of dPiezo function was rescued by increased integrin signaling or overexpression of ECM proteins, indicating that these pathways act downstream of dPiezo function genetically in glial neoplasia (54). The human ortholog of dPiezo, PIEZO1, is overexpressed in human GBM cells and tissues, and its overexpression is inversely correlated with patient survival (54). In cell-culture and xenograft models of human GBM, PIEZO1 is required for tumor cell growth and sustained integrin signaling through pathways that regulate tissue and ECM stiffness, such as the FAK kinase pathway, in a manner dependent on channel activity (54). Thus, key aspects of dPiezo function in *Drosophila* GBM models are recapitulated in human GBM tumor models. Given that ion channels are well-established pharmacologic drug targets (75), these results open a way forward to the possible development of new therapeutics for GBM.

In a related imaging-based study, Kim *et al*. identified Lysyl oxidase (Lox), which mediates ECM stiffness and regulates cell migration, as a potential mediator of Pvr-dependent neoplastic glial migration (56). They found that Lox operates through integrin signaling in a positive feedback loop promotes cell migration in local extracellular microenvironment (56). Similar results were observed in mammalian GBM model systems (56). Mechanisms that influence ECM stiffness are of particular interest, because increased ECM rigidity favors migration of glioma cells (76, 77). Moreover, integrins mediate ECM stiffness by providing mechanical coupling to the matrix, adhesion to surrounding cells, and signal transduction to the

cytoskeleton and nucleus (78, 79). Collectively, these studies show that *Drosophila* models and modifier screens are invaluable tools for uncovering novel biological pathways involved in GBM.

1.5 *Drosophila* models identify metabolic mechanisms in GBM tumorigenesis

In his seminal work on cancer metabolism, Otto Warburg discovered that tumor cells generate the majority of their ATP through aerobic glycolysis regardless of extracellular signals, and that tumor cells use this altered metabolism to generate biosynthetic precursors, which in turn allow for production of nucleotides, fatty acids, membrane lipids, and proteins to increase tumor cell proliferation and survival (80-82). This shift in metabolic processes is particularly important in adult GBM tumors (81). GBM is a late onset disease with a median age of 62 years (1), as such, an adult *Drosophila* GBM model may better reflect adult human GBM biology. Dr. Hueng's group has expanded on the aforementioned *Drosophila* GBM model developed by Read *et al*., and designed a *Drosophila* model that uses a temperature sensitive $GAL80^{ts}$ temporal expression system to allow for the induction of glioma formation in adult flies (57). In adult flies, EGFR-PI3K neoplastic glia induced grossly enlarged brains, a progressive decline in neurological function, and shorter lifespans (57). Using a bioinformatics approach to analyze the REMBRANDT tumor genomics database, Chi *et al.* identified four key metabolic genes that are correlated with poor prognosis in adult GBM patients, *ALDOA*, *ACAT1*, *ELOVL6*, and *LOX* (57). Of particular interest was ACAT1, a key metabolic enzyme involved in ER-cholesterol homeostasis and lipid metabolism and is highly expressed in many different types of cancers. Although the mechanisms by which ACAT1 promotes GBM tumorigenesis remain poorly understood, *ACAT1* knockdown in the adult GBM *Drosophila* model dramatically reduced

glioma brain enlargement and improved lifespan (57). These results were recapitulated in human models wherein *ACAT1* expression was upregulated in human GBM cell lines in a EGFR-PI3K-dependent manner, and *ACAT1* knockdown dramatically reduced GBM tumorigenesis (57). This study shows that *Drosophila* models are well suited to test the biological relevance of metabolic pathways and alterations identified from tumor genomic databases.

Drosophila GBM models are also effective at elucidating evolutionarily conserved roles for metabolic genes in glioma. Agnihotri *et al.* conducted a screen for gliomagenic mutations and found PINK1, a mitochondrially localized serine/threonine kinase that regulates mitophagy, reactive oxygen species (ROS) production, and OXPHOS (58). In primary murine and human astrocytes, PINK1 loss promotes aerobic glycolysis and an altered metabolic state that is conducive to GBM tumor progression (83, 84). Subsequent experiments indicate that PINK1 expression is downregulated in human GBM tumors, and that PINK1 restoration in human GBM cell lines reduced ROS and blocked tumor cell growth (58). In the *Drosophila* GBM model developed by Read *et al.,* dPink1 overexpression similarly reduced EGFR-PI3K dependent glial neoplasia (58), demonstrating an evolutionarily conserved metabolic function of PINK kinases in glioma. Thus, *Drosophila* GBM models can provide an efficient system to functionally characterize poorly understood metabolic enzymes that impact tumorigenesis.

1.6 *Drosophila* models and glioma stem cells

Despite treatment with surgery, radiation, and chemotherapy, GBM tumors invariably recur (1). These tumors display considerable cellular heterogeneity, and recent studies show that there exists a subset of cells within GBMs called glioma stem cells (GSCs) that have neural stem-cell like self-renewing properties (85-88). GSCs derived from human tumors express many

of the same transcription factors and receptors present in neural stem/progenitor cells, maintain capacity to generate tumors resembling human GBM in serial transplantation, and exhibit radiation and chemotherapy resistance (reviewed in (89)). RTK and PI3K signaling are required for normal development of neural stem/progenitor cells and for maintenance of stem cell-like properties of GSCs, and gliomagenic mutations in RTKs and PI3K pathway components confer GSC-like properties to neural stem/progenitor cells in mouse GBM models (89). Given that neoplastic *Drosophila* glia transformed by RTK-Ras and PI3K display many properties of GSCs, namely the ability to form malignant tumors upon transplantation and ectopic expression of factors that confer neural stem cell-like properties like dMyc, *Drosophila* GBM models are attractive systems for identifying and characterizing factors that govern the biological properties of GSCs (49). For example, the previously described RTK-PI3K pathway components RIOK1, RIOK2, and STK17A are all required for GSC proliferation, maintenance, and survival (50, 53).

In particular, RTK-Ras driven *Drosophila* GBM models have been used to evaluate functional requirements for transcription factors altered in GSCs. For example, Cheng *et al*. identified several transcription factors ectopically upregulated in patient-derived GSCs relative to human normal neural stem/progenitor cells (59). One of these transcription factors, FOXD1, which is a member of the Forkhead family of transcription factors, regulates organogenesis, mediates induced pluripotent stem cell dedifferentiation, and promotes tumor cell proliferation in various cancers (90-92). In GSCs, FOXD1 transcriptionally upregulates Aldehyde dehydrogenase 1A3 (ALDH13), which is involved in glycolytic pathways (93) and may provide a link between GSC identity and metabolic reprogramming. Using RNAi, Cheng *et al.* showed that fly orthologs of *FOXD1* (*fd59a)* or *ALDH1A3* (*dALDH)* were required for tumor cell proliferation in neoplastic *Drosophila* larval glia transformed by co-activation of the Ras and

PI3K pathways (59), thereby demonstrating that FOXD1 and ALDH1A3 form an evolutionary conserved gliomagenic pathway.

Drosophila models are also useful for testing the function of transcription factors that normally promote neural differentiation. For example, overexpression of Achaete-scute homolog 1 (ASCL1), which is orthologous to *Drosophila acheate*, is correlated with improved patient prognosis (51). ASCL1 promotes cell cycle exit and neuronal differentiation of human neural progenitors cells (94, 95). To understand how ASCL1 functions in GBM, Park *et al.* overexpressed either fly Acheate or human ASCL1 in EGFR-PI3K mutant *Drosophila* glia (51), which dramatically reduced neoplastic proliferation and induced a switch from glial-to-neuronal cell fate in neoplastic glia (51). Subsequent experiments revealed that ASCL1 reduces GBM tumorigenicity by transcriptionally suppressing glial cell and neuronal progenitor cell fate and promoting differentiation (51). Thus, *Drosophila* models can reveal how genes that regulate differentiation can limit gliomagenesis.

During development, stem cells undergo asymmetric cell division in which one daughter cell self-renews and retains the stem-cell fate and the other daughter generates a more specialized and differentiated cell. GSCs are thought to undergo both symmetric cell division, wherein both daughter cells generate GSCs, as well as asymmetric cell division, wherein one daughter cell maintains GSC fate and the other daughter cell of limited proliferative potential gives rise to tumor bulk (89, 96). While processes of symmetric and asymmetric cell division are not well understood in *Drosophila* glia, much of the pioneering work on mechanisms of asymmetrical cell division have been carried out in *Drosophila* neuroblasts (97, 98).

In *Drosophila* neuroblasts, asymmetric cell division requires setting up an axis of polarity and differential segregation of cell fate determinants between daughter cells (97, 98). Among

those determinants is Brat (encoded by the *brain tumor* gene), which normally asymmetrically segregates into the differentiating daughter cell during neuroblast division, where Brat inhibits self-renewal and promotes cell cycle exit and differentiation (98). *brat* loss-of-function clones or RNAi dysregulate differentiation of neuroblasts and their daughter cells, causing these cells to maintain self-renewal and to express neuroblast and glial markers, with *brat* mutant cells maintaining the ability to create malignant tumors in adult brains and in transplantation assays (99, 100). The human Brat ortholog TRIM3, which is only normally expressed in the brain, is genomically deleted in 25% of GBMs and is not detectably expressed in nearly all GBMs (101). In *Drosophila* and human GSCs, loss of Brat/TRIM3 function led to increased active cleaved Notch (NICD), and to NICD nuclear accumulation (102), whereas restored Brat/TRIM3 expression suppressed Notch signaling and attenuated NICD nuclear localization due to direct interactions between TRIM3 and nuclear import proteins (102). Furthermore, in a *Drosophila* modifier screen designed to identify downstream factors that mediate the tumorigenic effects of *brat* mutation, Mukherjee *et al.* discovered that the *brat* mutant phenotype is rescued by *Cdk5a* knockdown or pharmacological kinase inhibition, and that Cdk5a overexpression promoted the neuroblast-like fate stem-cell like (103). In human GBM, *CDK5A* is frequently genomically amplified and overexpressed, and in GSCs *CDK5A* RNAi or pharmacological kinase inhibition decreased tumorigenicity and reduced expression of stem cell markers, indicating that CDK5A regulates GSC self-renewal (103). These studies reveal a novel and evolutionarily conserved connection between Brat/TRIM3 and dCdk5a/CDK5A, and demonstrates that GSCs are particularly sensitive to targeting of this pathway, although the connections between CDK5 and Notch signaling remain to be determined. Collectively, these studies demonstrate that *Drosophila* is an effective model for studying how defects in asymmetrical cell division and

neural differentiation can contribute to tumorigenesis. Collectively, *Drosophila melanogaster* as a model organism has proven to be suited to experimentally investigate the signaling pathways and cellular mechanisms involved in gliomagenesis. As previously described, these models have also been used to address evolutionarily conserved hallmarks of cancer, including uncontrolled proliferation, invasion and metastasis, and altered cellular metabolism (Figure 1.2), and will be an effective tool to discover novel GBM pathways and mechanisms.

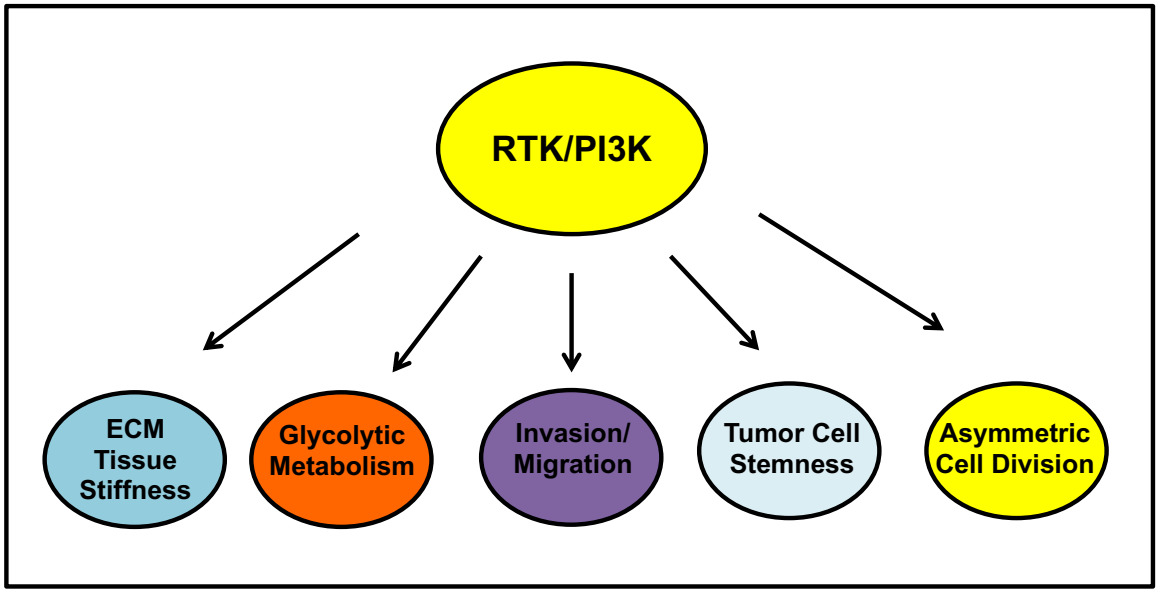

Figure 1.2. RTK and PI3K signaling regulate a wide range of gliomagenic pathways. Diagram depicting that ectopic constitutive RTK and PI3K signaling is responsible for a range of functions including but not limited to ECM-based regulation of tissue stiffness, glycolytic metabolism, invasion/migration, tumor stem cell self-renewal, and asymmetric cell division that drive GBM tumorigenesis.

1.7 Tumor stem cells: a model for investigating essential biological pathways of GBM

In additional to our *Drosophila* GBM model, another model system that we use in the lab is patient-derived GBM stem cells grown in serum-free neural basal media supplemented with EGF and FGF growth factors. Cancer cell lines have long been regarded as the standard model in investigating the basic biology of human tumors, as well as, a useful tool in the preclinical screening of potential therapeutic treatments for various cancers, including GBM (104). There are a number of advantages in using cell culture-based systems to the previously mentioned *Drosophila* GBM models and cancer mouse models. Most striking is the simplicity of the system in testing specific signaling transduction pathway components relevant in GBM tumorigenesis. However, the well-documented failure of GBM clinical trials based on preliminary experiments conducted in serum-based cancer cell culture models reveal that serum-based cancer cell models may not recapitulate key aspects of the primary tumor (105-108). Furthermore, extensive genetic differences between serum-cultured cancer cell lines and the human disease may lead to misidentification of tumor-driving pathways. Therefore, there is a pressing need to develop more biologically relevant models.

The development of GBM stem cell cultures, where single cell suspensions of freshly resected and dissociated from patient GBM tissues are grown in serum-free neural basal media supplemented with FGF and EGF, are a major improvement over serum-based cell culture models (88, 109). Studies performed by Lee *et al.* identifies the essential differences between GBM cell cultured in serum-free conditions (NBE) and GBM cells culture in serum-containing media (109). Lee *et al.* observed that cells cultured in NBE have drastically different proliferation profiles compared to cells cultured in serum (109). Cells cultured in NBE form nonadherent, multicellular spheres and proliferate at a constant rate regardless of passage

number, while cells cultured in serum grew as an adherent monolayer and proliferated at a much greater rate at higher passage numbers (109).

Furthermore, cells cultured in NBE conditions expressed neural stem cells (NSCs) markers Nestin, Sox2, and SSEA-1, and had consistent telomerase activity compared to cells culture in serum conditions, indicating that cells cultured in NBE conditions more closely resembled NSCs based on their self-renewal and differentiation characteristics (109). In terms of phenotypic and genotypic characteristics of cells cultured in NBE conditions, xenografts in SCID mice reveal that cells culture in NBE conditions have similar histopathology as human GBM in that they have extensive infiltration into the surrounding cerebral cortex and tend to migrate along white matter tracts and migrate toward the olfactory bulb (109). Importantly, gene expression profiles of cells cultured in NBE conditions more closely resemble the human disease and tend to maintain their expression profiles even in higher passage cells (109). Other studies conducted by Yuan *et al*. reached similar conclusions in that when a small subpopulation of GBM cells isolated from patients were grown in EGF and bFGF neural basal media, these cells grew as neurospheres and were able to self-renew and could differentiate into multi-lineage progenies (110). Furthermore, Yuan *et al.* found that only cells that formed neurospheres developed into tumors when transplanted into athymic nude mice (110). Larger studies performed by Gunther *et al.* and Laks *et al*. reached similar conclusions that cells isolated from GBM patient tumor tissue only formed tumors in immunosuppressed mice if they grew as spheroids (88, 111). Laks *et al*. found that the tumorigenic capacity of the tumors that formed in the immunosuppressed mice strongly correlated with patient outcome, and that neurosphere formation was a strong, independent indicator of glioma disease progression (88). Collectively, these studies indicate that patient-derived GBM stem cells grown under NBE conditions

recapitulate key genotypic and phenotypic characteristics of adult GBM tumors and may provide more useful insights into the functionally relevant drivers of GBM tumorigenesis, potentially translating into more effective therapeutic treatments.

1.8 STK17A: a novel protein kinase

Serine/Threonine Kinase 17A (STK17A), also known as DAPk-related apoptosis-inducing protein kinase-1 (DRAK1), was identified in a kinome-wide screen using the *Drosophila* GBM model (50), and may prove to be a promising candidate for targeted therapy based on its tumor-specific effect on glial cell proliferation in initial screens. As such, elucidating the mechanism by which STK17A/Drak drives GBM tumorigenesis is one of my research topics in my dissertation.

STK17A belongs to the death-associated kinase (DAPK) family, whose members share sequence and functional homology (112-115). The DAPK family consists of five members: DAPK1, DAPK2 (aka DAPK-related kinase 1 (DRP1)), DAPK3 (aka Zipper-interacting protein kinase, DAP-like kinase, Dlk), and DRAK1 and DRAK2 (DAPK-related apoptosis-inducing protein kinase 1 and 2, aka STK17A and STK17B, respectively) (116). DRAK1 and DRAK2 belong to the superfamily of calcium/calmodulin (Ca^{2+}/CaM) regulated STKs (116). While all five members belong to the same family of protein kinases, there exists considerable differences between the DAPKs and DRAKs in terms of sequence homology. While the kinase domain of DAPK2 and DAPK3 share 80% and 83% sequence homology with that of DAPK1 (113-115), respectively, the kinase domain of DRAKs share only about 50% sequence homology with DAPK1 and exhibit homology to both calcium/calmodulin-dependent kinase 2 (CaMK2) and myosin light chain kinase (MLCK) (117). Interestingly, even within DRAK proteins, there exists

considerable differences in sequence homology. While the kinase domain of DRAK1 and DRAK2 share 67.1% sequence homology, the extra-catalytic C-terminal domain only share 24.2% sequence homology (118). The extra-catalytic domain of both DRAK1 and DRAK2 contain a nuclear localization signal, and thus, DRAKs are primarily localized in the nucleus (116). DRAK2 translocates to the cytoplasm upon activation with protein kinase C (PKC) (116).

Though the DAPK family of protein kinases were initially discovered to have roles in promoting apoptosis (116, 119, 120), recent studies suggest that DAPK family members are involved in a wide variety of biological functions that depends largely on cellular setting (116). In the context of cell death, DAPK1 interacts with other proteins to regulate apoptosis, autophagy, and membrane blebbing, often through myosin regulatory light chain (MRLC) as an intermediary (116). For example, DAPK1 can bind ERK, which results in DAPK1 phosphorylation at Ser735, increasing DAPK1's ability to phosphorylate MRLC (121, 122). DAPK1 binding to ERK stimulates ERK-cytoplasmic retention, thus inhibiting ERK signaling in the nucleus and in turn, initiates apoptosis (116). Furthermore, under amino acid starvation conditions, the DAPK1 kinase domain binds to microtubule-associated protein 1B (MAP1B) and forms a stable immune complex to induce autophagy and membrane blebbing (123).

In the context of cancer, DAPK1, interestingly, has a dual function in that DAPK1 can both suppress and enhance tumor growth, depending on cellular context. Studies show that DAPK1 can activate $p19^{ARF}$/p53-mediated apoptotic checkpoint and in turn suppress transformation of normal cells to cancer cells (124). In pancreatic cancer cells, upregulation of DAPK1 significantly reduced cellular proliferation and invasion, suggesting that DAPK1 may behave as tumor suppressor in this context (124). Interestingly, studies have also shown that DAPK1 can also promote tumor growth. In P^{53} mutant triple negative breast cancer and prostate

cancer, studies show that DAPK1 disrupted the tuberous sclerosis protein 1 and 2 (TSC1/2) complex which in turn activated the mTOR/S6K pathway and increased cell growth (125, 126).

Studies also show that DRAKs are implicated in promoting cancer tumorigenicity. In head and neck squamous cell carcinomas (HNSCC), cytoplasmic DRAK1 binds to Smad3, interfering with Smad3/4 complex formation, and in turn, prevents the induction of the tumor suppressor $p21^{War1/Cip1}$ (127). Furthermore, knockdown of DRAK1 in a variety of GBM cell lines drastically reduced cell proliferation, motility, and invasion (128). DAPK family can also regulate cytokinesis. In fact, studies in *Drosophila* show that Drak, the *Drosophila* ortholog of DRAK1/2, acts downstream of Rho-GTPase to phosphorylate spaghetti squash (Sqh) and regulates actin cytoskeleton and promotes epithelial morphogenesis (129, 130). In humans, myosin regulatory light chain (MRLC), the human ortholog of Sqh, is a regulator of nonmuscle myosin type II (NMII) motor proteins, and upon phosphorylation, MRLC binds to NMII and stimulates NMII-dependent contractile activity to promote cytoskeletal re-organization, morphogenesis, and cytokinesis (131, 132). Importantly, studies show that DRAK1/STK17A is overexpressed in GBM and can directly phosphorylate MRLC *in vitro* (118, 129). However, the mechanism in which STK17A promotes GBM tumorigenesis remains to be elucidated.

1.9 RIOK2: a novel protein kinase

As previously mentioned, RIOK2 was identified in a kinome-wide screen using the *Drosophila* GBM model (50). Based on previous published studies, RIOK2 has a role in driving GBM tumorigenesis (50); however, the mechanism in which RIOK2 drives GBM tumorigenesis remains unknown and was one of my research topics in my dissertation.

RIOK2 belongs to the RIO family of protein, which consists of at least four members RIOK1, RIOK2, RIOK3, and RIOKB (133, 134). RIOK1 and RIOK2 are an evolutionarily ancient group of proteins and are found in both archaea and eukaryotes, RIOK3 is found exclusively in eukaryotes, and RIOKB is found in some archaea and eubacteria (133, 134). The defining characteristic of RIO family members is the presence of a RIO kinase domain (133, 134). While the RIO kinase domain shares some similarities to eukaryotic protein kinases, the RIO kinase domain lacks key regions including the activation loop and helices H and I (135), regions important in eukaryotic protein kinases for interacting with its substrates and converting the enzyme from an inactive to an active state (135), and as such, RIO kinases are typically referred to as atypical protein kinases. However, the RIO kinase domain still retains the N-terminal and C-terminal lobes, which is connected by a hinge region where ATP and magnesium can still bind (136-139). Furthermore, RIO kinase domains still retain in the C-terminal, the catalytic loop and the metal-binding loop and thus, can catalyze phosphoryl transfer; however, to date, a bona fide substrate of RIOK2 has yet to be identified (134).

In yeast, both Rio1 and Rio2 have been shown to autophosphorylate, and researchers have identified the autophosphorylation site in Rio1 to be Ser-108 and the autophosphorylation site in Rio2 to be Ser-128 (139-141). Structurally, one of the primary differences between Rio1 and Rio2 is that Rio2 has an N-terminal winged helix (wHTH) (133), which consists of four α-helices followed by two β-strands and a fifth α-helix (133). It is reported that the most common function of the wHTH structure is DNA-binding (142, 143).

In terms of function, studies in yeast show that Rio1 is required for proper cell cycle progression and chromosome maintenance, and lacking Rio1, cell cycle arrest occurs at G_1 phase or mitosis (140). Moreover, in yeast, Rio1 and Rio2 have roles as non-integral ribosomal

assembly factors necessary for late 18S rRNA processing (141, 144). Interestingly, loss of either Rio1 and Rio2 in yeast is lethal, indicating that they have distinct non-overlapping functional roles (144, 145). Studies show that the human Rio2 ortholog RIOK2 is important in the export of the pre-40S subunit from the nucleus to the cytoplasm (146). Also, Zemp *et al.* determined that the presence of human RIOK2, not its kinase activity, is important for the release of ENP1, a known component of pre-40S particles (146), and that RIOK2 catalytic activity is important in the second phase of cytoplasmic 40S maturation, where the 18S-E pre-rRNA is cleaved and ribosome assembly factors DIM2, LTV1, and NOB1 are released (146).

Furthermore, recent studies have shown that instead of directly phosphorylating substrates, RIOK2 may instead act as an ATPase, where the phosphoryl transfer of ATP to Asp257 in the RIOK2 active site and subsequent hydrolysis of aspartylphosphate induces a conformational change in RIOK2 that releases it from the pre-40S particle along with other *trans*-acting factors such DIM2, LTV1, and NOB1 from the pre-40S particle (146, 147). Interestingly, studies have shown that RIOK2 regulates the export of the pre-40S particle by binding to the nuclear export receptor, CRM1 (147).

Importantly, RIO kinase family members have been implicated in a number of different types of cancers including breast, lung, and gliomas (50, 148-150). In non-small cell lung cancer tumors, high expression of RIOK2, along with ribosome assembly factor NOB1, is correlated with poor patient prognosis (151). Importantly Read *et al.* identified that in GBM downstream of EGFR and PI3K signaling, RIOK2 is upregulated in response to AKT activation and forms a complex with TORC2, which in turn, forms a positive feedforward loop with AKT to drive GBM tumorigenesis (50). Read *et al.* demonstrated that RIOK2 promoted GBM tumorigenesis; however, the mechanism by which RIOK2 drives tumorigenesis is unclear.

1.10 IMP3: a potential downstream effector of RIOK2

In preliminary studies using both immunoprecipitations coupled with proteomics analysis along with screens using our *Drosophila* GBM model, we identified IMP3, an RNA-binding protein as a possible downstream effector of RIOK2. RNA-binding proteins (RBPs) are important regulators of gene expression and are involved in all facets of messenger RNA (mRNA) metabolism, including transcription, 5' end capping, precursor mRNA splicing, 3' end processing, nuclear export, transport, translation, and stability (152). Over 600 RBPs are annotated in the mammalian genome (153), and each RBP may have hundreds of mRNA targets (154). RBPs operate as structural components of messenger ribonucleoprotein particles (RNPs), and while many RBPs lack enzymatic activity, they exert their functions by recruiting other proteins into the complex (152, 155, 156). The composition of RBPs and associated proteins are what determines the fate of their target mRNAs (152). While there exist many RBPs, very few have been associated with cancer.

Among the RBPs associated with cancer, the oncofetal RBP family, IGF2BP (IMP) has been investigated by a number of different laboratories. The IMP family of RBPs consists of IMP1, IMP2, and IMP3 and are physiologically expressed in early development (157, 158). Structurally, the three family members are highly similar in terms of domain order and spacing (159), and have an overall amino acid sequence identity of 56% (160), with a 73% amino acid sequence identity between IMP1 and IMP3 (160). All three IMPs contain two RNA recognition motifs (RRMs) in the N-terminal region, and four hnRNP KH domains (KH) in the C-terminal region (161). However, in *Drosophila*, the lone form of IMP, Imp, lacks the RRM domain and contains only the four KH domains (160). *In vitro* data shows that KH domains are primarily

responsible for RNA binding, while RRMs contribute to the stabilization of the IMP-mRNA complex (162, 163). Interestingly, while analysis of the structure of the KH domains shows that KH domains can only recognize short sequences of RNA and only allow for weak binding affinity to their target mRNAs (164), structural analysis of IMP1 shows that the binding of multiple copies of the KH domains increases the binding affinity and specificity to allow IMPs to bind to specific target mRNAs (164). Recent studies utilizing photoactivatable ribonucleoside-enhanced UV crosslinking and immunoprecipitation (PAR-CLIP) in HEK293T cells have identified the putative IMP consensus recognition element as 5'-CAUH-3' (H=A, U, or C) (165). Furthermore, UV-CLIP studies in human pluripotent stem cells show that IMP1 and IMP2 primarily bind to the 3' UTR of target genes, while IMP3 primarily binds to the coding regions of target genes (166).

The physiological roles of IMPs have been identified through the use of loss-of-function and gain-of-function models. In *Drosophila*, Imp is required for axon guidance (167). IMP1 has roles in enhancing neurite outgrowth and axonal guidance (168, 169), regulating cell metabolism and/or stem cell maintenance (170), regulating the expansion of fetal NSCs (171), and regulating adhesion and survival (166). IMP2 has roles in cell metabolism and muscle cell motility (159). For IMP3, on the other hand, there has not been a concerted effort to characterize the phenotypic consequence of IMP3 in knockout models, as such, the physiological effects of IMP3 remain to be elucidated (159).

Recent studies reveal that IMP1, IMP2, and IMP3 are aberrantly expressed in a number of cancers (160, 172). Importantly, IMP3 has been shown to promote a number of tumorigenic functions including tumor cell proliferation, growth, drug-resistance, and invasiveness by modulating the activity of oncogenic target mRNAs (172). As its name implies, the most widely

studied mRNA target of IMP3 is IGF2. Studies have shown that IMP3 binds to the 5' UTR of the IGF transcript and promotes IGF2 synthesis through phosphorylation by mTOR at S183 (173). In GBM, studies show that IMP3 promotes tumor proliferation and invasion by promoting the translation of IGF2 mRNA and activating the downstream effectors of IGF2, PI3K and MAPK, and that high IMP3 is correlated with poor patient prognosis (174). Also, IMP3 regulates the expression of cyclins to promote tumor cell proliferation (175), stabilizes *ABCG2* mRNA to enhance chemo-resistance in breast cancer (176), and stabilizes CD44, CD164, MMP9, and PDPN encoding mRNA to enhance the invasive potential of tumor cells (172). Another important oncogenic target mRNA is *MYC* (172, 177). By better understanding how IMP3 interacts with its oncogenic target mRNAs, such as *MYC*, we may uncover the underlying mechanism in which IMP3 promotes GBM tumorigenesis.

1.11 MYC and mTOR in Cancer

As previously mentioned, *MYC* is an established target mRNA of IMP3, and establishing an interaction between MYC and the RIOK2-IMP3 complex is a critical research component of my dissertation. The MYC oncogene family consists of c-MYC, N-MYC, and L-MYC, and belongs to the so-called family of "super-transcription factors", in that they regulate at least 15% of the entire genome (178). MYC can act as either a transcription factor or a transcriptional signal amplifier (179). As a transcription factor, MYC-MAX dimer binds to the E-BOX sequence (CACGTG), which leads to the recruitment of chromatin-modifying complexes GCN5, TIP60, TIP48, and TRRAP, allowing for transcriptional activation (179). As a transcriptional signal amplifier, MYC does not bind to the E-BOX and instead accumulates in the promoter and enhancer region of active genes and causes transcriptional signal amplification (179). The

downstream target genes of MYC are implicated in a variety of pro-tumor functions including ribosome biogenesis, cell proliferation, differentiation, survival, and immune surveillance (178, 180). Upstream, the PI3K/AKT pathway regulates MYC protein levels in various MYC-dependent cancers, and the PI3K-AKT effector kinase mTOR plays a key role in regulating MYC levels (181-184).

mTOR exerts its effects as part of a larger protein complex known as either mammalian target of rapamycin complex 1 (mTORC1) or mammalian target of rapamycin complex 2 (mTORC2) (185), each with its unique set of complex members. mTORC1 consists of mTOR, raptor, and mLST8, and regulates growth through its downstream effectors, 4EBP1 and S6K1 (185). The mTORC2 complex, on the other hand, consists of RICTOR and SIN1, and is thought to be part of the PI3K/AKT pathway and directly phosphorylates AKT (185-187). Based on the well-established roles of MYC and mTOR in tumorigenesis, it is important to better understand the underlying mechanism in how these proteins influence or are influenced by the RNA-binding protein, IMP3.

1.12. Dissertation Goals

Given the prevalence of aberrant activation of the EGFR and PI3K pathways and the ineffectiveness of targeting these pathways in GBM, there must be a concerted effort to better understand the underlying biology downstream of these pathways in order to develop more effective targeted therapies. Contributions of Read *et al.* in developing a powerful *Drosophila* GBM model with glial-specific constitutive activation of EGFR and PI3K that recapitulates key aspects of human GBM, has led to the identification of two novel protein kinases, RIOK2 and STK17A, implicated in GBM tumorigenesis. My dissertation goals are to investigate the

mechanism by which RIOK2 and STK17A promote GBM tumorigenesis by utilizing a combination of *in vitro* and *in vivo* experimental approaches.

In the second chapter, using the *Drosophila* GBM model, I explore how Drak, the *Drosophila* ortholog of STK17A, promotes GBM tumorigenesis by activating essential pathway components of cytokinesis, Sqh and Anillin. Using a combination of patient-derived GBM stem cells, TCGA datasets, and human tissue microarrays, I investigate how essential findings regarding Drak function in *Drosophila* GBM models are recapitulated by STK17A in human GBM models.

In chapter 3, I investigate the mechanisms by which RIOK2 interacts with IMP3 to promote GBM tumorigenesis. Using a combination of *in vitro* and *in vivo* techniques, I explore how RIOK2 catalytic activity is involved in formation of the RIOK2-IMP3 complex and how IMP3 may promote GBM tumorigenesis by regulating MYC protein levels. In chapter 4, I will summarize my work on two novel protein kinases and how they function in two disparate pathways to drive gliomagenesis. Moreover, I discuss how RNA-seq and proteomic analyses can be used to identify how the RIOK2-IMP3 complex may regulate a novel set of target mRNAs, and how RIOK2 may interact with other RNA-binding proteins to promote GBM tumorigenesis. By elucidating novel pathways and mechanisms of GBM tumor biology, in the future we can apply that knowledge such that we can better design more effective target therapies to treat GBM patients and improve patient prognosis.

Chapter 2. Drak/STK17A drives neoplastic glial proliferation through modulation of MRLC signaling

Alexander Chen*, Joanna Wardwell-Ozgo*, Nilang Shah, Deidre Wright, Christina Appin, Krishanthan Vigneswaran, Daniel J. Brat, Harley I. Kornblum, and Renee D. Read (*Authors contributed equally)

2.1 Abstract

Glioblastoma (GBM) and lower grade gliomas (LGG) are the most common primary malignant brain tumors and are resistant to current therapies. Genomic analyses reveal that signature genetic lesions in GBM and LGG include copy gain and amplification of chromosome 7, amplification, mutation, and overexpression of receptor tyrosine kinases (RTK) such as EGFR, and activating mutations in components of the PI-3 kinase (PI3K) pathway. In *Drosophila melanogaster*, constitutive co-activation of RTK and PI3K signaling in glial progenitor cells recapitulates key features of human gliomas. Here we use this *Drosophila* glioma model to identify death-associated protein kinase (Drak), a cytoplasmic serine/threonine kinase orthologous to the human kinase STK17A, as a downstream effector of EGFR and PI3K signaling pathways. Drak was necessary for glial neoplasia, but not for normal glial proliferation and development, and Drak cooperated with EGFR to promote glial cell transformation. Drak phosphorylated Sqh, the *Drosophila* ortholog of MRLC (non-muscle myosin regulatory light chain), which was necessary for transformation. Moreover, Anillin, which is a binding partner of phosphorylated Sqh, was upregulated in a Drak-dependent manner in mitotic cells and co-localized with phosphorylated Sqh in neoplastic cells undergoing mitosis and cytokinesis, consistent with their known roles in non-muscle myosin-dependent cytokinesis. These functional relationships were conserved in

human GBM. Our results indicate that Drak/STK17A, its substrate Sqh/MRLC and the effector Anillin/ANLN regulate mitosis and cytokinesis in gliomas. This pathway may provide a new therapeutic target for gliomas.

2.2 Introduction

Glioblastomas (GBM), the most common primary malignant brain tumors, infiltrate the brain, grow rapidly, and are resistant to current therapies (188). Low grade gliomas (LGG), which are related infiltrative malignant neural neoplasms, have slower tumor growth rates, longer patient survival, and display more variable responses to therapeutics (189). To understand their genesis, these tumors have been subject to extensive genomic analyses, which show that signature genetic lesions in LGG and GBM include copy gain and amplification of chromosome 7, amplification, mutation, and/or overexpression of receptor tyrosine kinases (RTKs), such as EGFR, and activating mutations in components of the PI-3 kinase (PI3K) pathway (7, 188, 190). Nearly 60% of GBMs show focal EGFR copy gain or amplification, which are often accompanied by gain-of-function EGFR mutations (190). The most prevalent EGFR mutant variant in GBM is $EGFR^{VIII}$ (191), in which exon2-7 deletion confers constitutive kinase activity, which potently drives tumorigenesis (188, 192). The most frequent PI3K pathway mutation in gliomas is loss of PTEN lipid phosphatase (190), which results in unopposed PI3K signaling.

Recent mouse models demonstrate that co-activation of EGFR and PI3K pathways in glial cells or neuro-glial stems cells induces GBM-like tumors, although these tumors do not show the full range of GBM phenotypes (12, 26, 193). Furthermore, to date, pharmacologic inhibitors of EGFR and PI3K pathway components are ineffective in improving LGG and GBM outcomes (194). Genomic studies indicate that LGGs and GBMs have other genomic alterations (7, 190, 191); however, it is unknown how these changes contribute to gliomagenesis. Taken collectively, these data suggest that there are still undiscovered biological factors that drive tumorigenesis. Given the aggressive nature of these tumors, there is a pressing need to better understand their biology and to identify additional factors that could serve as new drug therapy targets.

To investigate the biology of malignant gliomas, we developed models in *Drosophila melanogaster* (49). *Drosophila* offers unique advantages for modeling gliomas: flies have orthologs for 70% of human genes, including most known gliomagenic genes (195); *Drosophila* neural and glial cell types are homologous to their human counterparts (196); and versatile genetic tools are available for *in vivo* cell-type specific gene manipulation including RNAi (31). Although *Drosophila* models cannot address all aspects of glioma biology, our model demonstrates that constitutive activation of EGFR and PI3K signaling in glial progenitor cells gives rise to malignant glial tumors that recapitulate key biological features of human gliomas (49).

To discover new pathways that contribute to EGFR-PI3K-mediated glioma, we performed a kinome-wide RNAi-based genetic screen in our EGFR-PI3K *Drosophila* GBM model (50). Kinases were screened because they are highly conserved in terms of protein function between *Drosophila* and mammalian systems. One of the top candidates from this screen was Drak (Death-associated protein kinase related) (50). Drak and its human ortholog, STK17A, are cytoplasmic serine/threonine kinases in the Drak subfamily of cytoplasmic death-associated protein (DAP) kinases, which regulate cytoskeletal dynamics, cytokinesis, and cell adhesion and mobility (129, 197, 198). In *Drosophila* development, Drak promotes epithelial morphogenesis, acting downstream of Rho-GTPase signaling to control the actin cytoskeleton through phosphorylation of Spaghetti Squash (Sqh) (129, 130). MRLC, the human Sqh ortholog, is a regulator of non-muscle myosin type II (NMII) motor proteins, and phosphorylated MRLC binds to NMII and stimulates NMII-dependent contractile activity to promote cytoskeletal re-organization, morphogenesis, and cytokinesis (131, 132). MRLC phosphorylation is dynamic and tightly regulated, which allows for precise temporal and spatial changes to the cytoskeleton (131). Like other Drak family kinases, STK17A, which is expressed in GBM (128), can directly phosphorylate

purified MRLC protein *in vitro* (118, 129). However, little is known about the mechanisms by which Drak/STK17A promotes tumorigenesis.

Here we characterize genetic and functional requirements for Drak in EGFR- and PI3K-driven neoplastic glia. We report that Drak operates downstream and in concert with EGFR signaling to phosphorylate and activate Sqh to drive proliferation of neoplastic glia. Moreover, our data show that, in mitotic neoplastic glial cells undergoing cytokinesis, phosphorylated Sqh co-localizes with Anillin, a cytoskeletal protein and known Sqh binding partner (199), and that Anillin is required for proliferation of neoplastic glia. We show that these interactions are conserved in human gliomas. STK17A is overexpressed in primary human GBM and LGG tumors and patient-derived GBM cell cultures, and elevated STK17A expression correlates with elevated EGFR, MRLC phosphorylation, and ANLN (human Anillin ortholog) levels. STK17A activity is required for tumor cell proliferation and for elevated levels of MRLC phosphorylation and ANLN. Moreover, we found that STK17A, phosphorylated MRLC, and ANLN are all co-localized to the cleavage furrow in tumor cells undergoing cytokinesis. Taken together, our data suggests that Drak/STK17A potentiates EGFR signaling to drive activation of Sqh/MRLC, which in turn regulates mitosis in gliomas through effects on Anillin/ANLN.

2.3 Materials and Methods

Drosophila Strains and culture conditions

Drosophila stocks were obtained from the Bloomington stock center and VDRC and the specific genotypes and stocks used are listed in the Supplemental Table 2.1 and Table 2.2. $Drak^{null}$($Drak^{del}$) was a gift of David Hipfner (129). *UAS-*sqh^{D20D21} was a gift of Guang-Chao Chen (200). *UAS- dEGFR*$^{\lambda}$ was a gift of Trudi Schupbach. All stocks were cultured on standard corn meal molasses food at 25°C. Prior to publication, the *UAS-*$Drak^{dsRNA}$ stocks were validated by PCR amplification of the dsRNA element followed by sequence validation against the published sequence available at the VDRC. To create *UAS-Drak* and *UAS-*$Drak^{KD}$ (kinase dead) constructs, the RE12147 *Drak* cDNA was cloned into pUAS-T, site directed mutagenesis was used to convert Lys-66 to Ala, and the resulting DNA was injected into embryos and stocks for each construct were established and sequence verified. All genotypes were established by standard genetic crossing.

Immunohistochemistry

Larval brains were dissected with forceps, fixed in 4% paraformaldehyde, processed, stained, and imaged as previously described (49). The following antibodies were used: 8D12 mouse anti-Repo (1:10, Developmental Studies Hybridoma Bank), anti-phospho-S21-Sqh (1:500, gift of Robert Ward) (201), anti-Anillin (1:500, gift of Maria Giansanti) (202). Secondary antibodies were conjugated to Cy3 (1:150), Alexa-488, or Alexa-647 (1:100) (Jackson Laboratories). Brains were mounted on glass slides ventral side down in vectashield and whole mount imaged on a Zeiss LSM 700 confocal system. For experiments where protein levels were compared between genotypes, all samples were prepared, subjected to immunohistochemistry,

imaged, and image processed in a parallel manner side by side. 6 or more brains were stained with each Ab combination, and representative images are shown for each result. All brain phenotypes shown were highly penetrant, with approximately 75-100% of animals showing the growth phenotypes described. Images were analyzed in Zeiss Zen Software and processed in Photoshop. Larval *Drosophila* brain hemisphere volumes were analyzed using Imaris software. Larval glial cells were counted manually in representative optical sections of age-matched brain hemispheres, matched for section plane. Statistical analyses were done using Prism.

Mammalian tissue culture

GBM39, shared by C. David James, was created from human GBMs serially xenografted. GBM157, GBM281, GBM301, and GBM309 gliomasphere cultures were derived at UCLA and maintained in culture as described (88). HNPCs were obtained from Lonza. U87 and U87-EGFR^{vIII} cells were gifts of Frank Furnari. Cell culture was performed as previously described (50). Lentiviral shRNAs were prepared and used as previously described on serum cultured cells and adherent serum-free cultured gliomasphere lines (50). WST-1 assays on shRNA-treated cells were performed as previously described (50). For immunofluorescence, U87-EGFR^{vIII} cells were plated on glass coverslips, fixed with 4% paraformaldehyde, and stained on the coverslips with anti-beta-tubulin (1:25, Developmental Studies Hybridoma Bank, AA4.3), anti-STK17A (1:1000, Sigma HPA037979), anti-ANLN (1:100, Sigma, HPA005680), anti-phospho-S19-MRLC (1:200, Abcam, ab2480; note this antibody detects S19 according to our sequence alignment and not S20), and/or DRAQ7 (Cell Signaling Technology, 1:200) to stain nuclear DNA and chromosomes.

Immunoblot Analysis

Cultured cells were collected and washed with 1xPBS and lysed in RIPA buffer containing protease and phosphatase inhibitors. Whole third instar larval brains were dissected were washed with 1xPBS and lysed in RIPA buffer containing protease and phosphatase inhibitors. The following antibodies were used for immunoblotting following the manufacturer's recommendations: anti-STK17A (1:1000, Sigma, HPA037979), anti-phospho-S19-MRLC (1:500, Cell Signaling 3671), anti-phospho-S19-MRLC (1:200, Abcam, ab2480), anti-MRLC (1:500, Cell Signaling, 3672), anti-EGFR (1:5000, BD), anti-ANLN (1:500, Sigma, HPA005680) and anti-actin (1:200, Developmental Studies Hybridoma Bank, JLA20). Bands were quantified using ImageJ.

***in silico* Analysis**

STK17A mRNA expression data was obtained from cBioportal (www.cbioportal.org) and exacted and analyzed using RStudio. All graphs and statistics were generated from this data using Prism (203, 204). The *in silico* analysis results shown here are based solely upon data generated by the TCGA Research Network (http://cancergenome.nih.gov) (7, 189, 190).

TMA processing

All human tumor specimens were collected from surgical specimens donated for research with written informed consent of patients and were collected and used according to recognized ethical guidelines (Declaration of Helsinki, CIOMS, Belmont Report, GCP, Nuremberg Code) in a protocol (IRB00045732) approved by the Institutional Review Board at Emory University. Paraffin embedded human brain tumor specimens and tumor tissue microarrays with matched control tissue were prepared and sectioned using the Winship Core Pathology Laboratory. Antigen

retrieval and immunohistochemical staining was performed as specified by manufacturer's guidelines for each specific antibody (50). The following antibodies were used: anti-STK17A (1:1000, Sigma HPA037979), anti-ANLN (1:50, Sigma, HPA005680), anti-phospho-S19-MRLC (1:200, Abcam, ab2480), anti-EGFR (1:50, Cell Signaling Technology, 4267). Results were scored by neuropathologists according to standard clinical criteria on a scale of 1 and 2 (low staining), 3 or 4 (high staining, with 4 being more uniform), and images of immunoreactivity were taken on an Olympus DP72 CCD camera.

Statistical analyses

Comparisons between two groups were performed by Mann-Whitney U Test (nonparametric) for TCGA RNA-seq data analyses. Comparisons between of three or more groups, were performed by one-way ANOVA with multiple comparisons to experimental controls. Comparisons between two groups were done using either paired or unpaired parametric T-Tests. Fisher's exact test was used to analyze correlations in IHC data.

2.4 Results

Drak is required for glial neoplasia in *Drosophila*

To understand GBM pathology, we developed a *Drosophila* GBM model. The model uses the glial-specific *repo-Gal4* transcriptional driver to co-overexpress constitutively active versions of dEGFR (dEGFR$^{\lambda}$) and dp110 (dp110^{CAAX}), the catalytic subunit of PI3K, that together drive malignant transformation of post-embryonic larval glia (49). The resulting glial tumors exhibit phenotypic and molecular characteristics similar to human GBM (49). To identify novel modifiers of EGFR-PI3K driven glial neoplasia, we used our *Drosophila* GBM model in a genetic screen, and identified Drak, which encodes the sole *Drosophila* ortholog of STK17A and STK17B serine/threonine kinases (50).

Glial-specific *Drak* RNAi reduced neoplastic glial proliferation and altered glial morphogenesis, with *Drak*$^{dsRNA\#1}$ yielding significantly reduced brain sizes and glial cell numbers compared to dEGFR$^{\lambda}$-dp110^{CAAX} (Figure 2.1A-C, 1D-I). The transforming effects of EGFR-PI3K signaling were also reduced in *Drak* null mutants (*Drak*^{null}) (129) or by co-overexpression of kinase-dead Drak (Drak^{KD}): such mutants showed near wild-type brain sizes and reduced glial cell numbers compared to dEGFR$^{\lambda}$-dp110^{CAAX} controls (Figure 2.1A-C, 1D-I), indicating that Drak catalytic activity is essential for proliferation of dEGFR$^{\lambda}$-dp110^{CAAX}-mutant glia.

Growth inhibition of neoplastic glia induced by *Drak* knockdown or loss-of-function was not due to nonspecific glial lethality: *Drak* is a nonessential gene and homozygous null mutants are viable and show normal brain morphology and glial development, and *Drak* RNAi in wild-type larval glia caused no obvious defects (50, 129) (Supplemental Figure S2.1A-B). Thus, while Drak is not required for normal glial proliferation and development, Drak kinase activity is essential for neoplastic glial proliferation.

Because reduced Drak function had a dramatic effect on dEGFR$^{\lambda}$-dp110^{CAAX} mutant neoplastic glia, and because Drak functions downstream of EGFR in epithelia (130), we predicted that Drak may function downstream of EGFR in neoplastic glia. Overexpression of constitutively active dEGFR$^{\lambda}$ alone elicits hyperplasia in glia (49), which we found was suppressed by loss of *Drak* function (Supplemental Figure S2.1C-D), consistent with our prediction.

Previous studies show that, in developing epithelia, Drak acts downstream of EGFR and RhoGTPase (RhoA) signaling in parallel with Rho kinase (Rok) (129, 130). To investigate whether RhoGTPases are also required in neoplastic glia, we tested *RhoA* RNAi and dominant negative constructs in our GBM *Drosophila* model. We found that *RhoA* loss-of-function caused a significant reduction in dEGFR$^{\lambda}$-dp110^{CAAX} mutant glial proliferation, but did not obviously affect wild-type glia proliferation (Figure 2.1A-C, 2.1D-I, Supplemental Table 2.1). Glial-specific inhibition of Rho family GTPases Cdc42 and RhoL and glial-specific *Rok* RNAi did not as strongly suppress neoplastic glial proliferation (50) (Supplemental Table 2.1). Thus, Drak may phosphorylate substrates to drive neoplastic glial proliferation downstream of RhoA GTPase signaling, independent of Rok. Together, our data demonstrate that Drak pathways are necessary for EGFR-PI3K-dependent glial neoplasia.

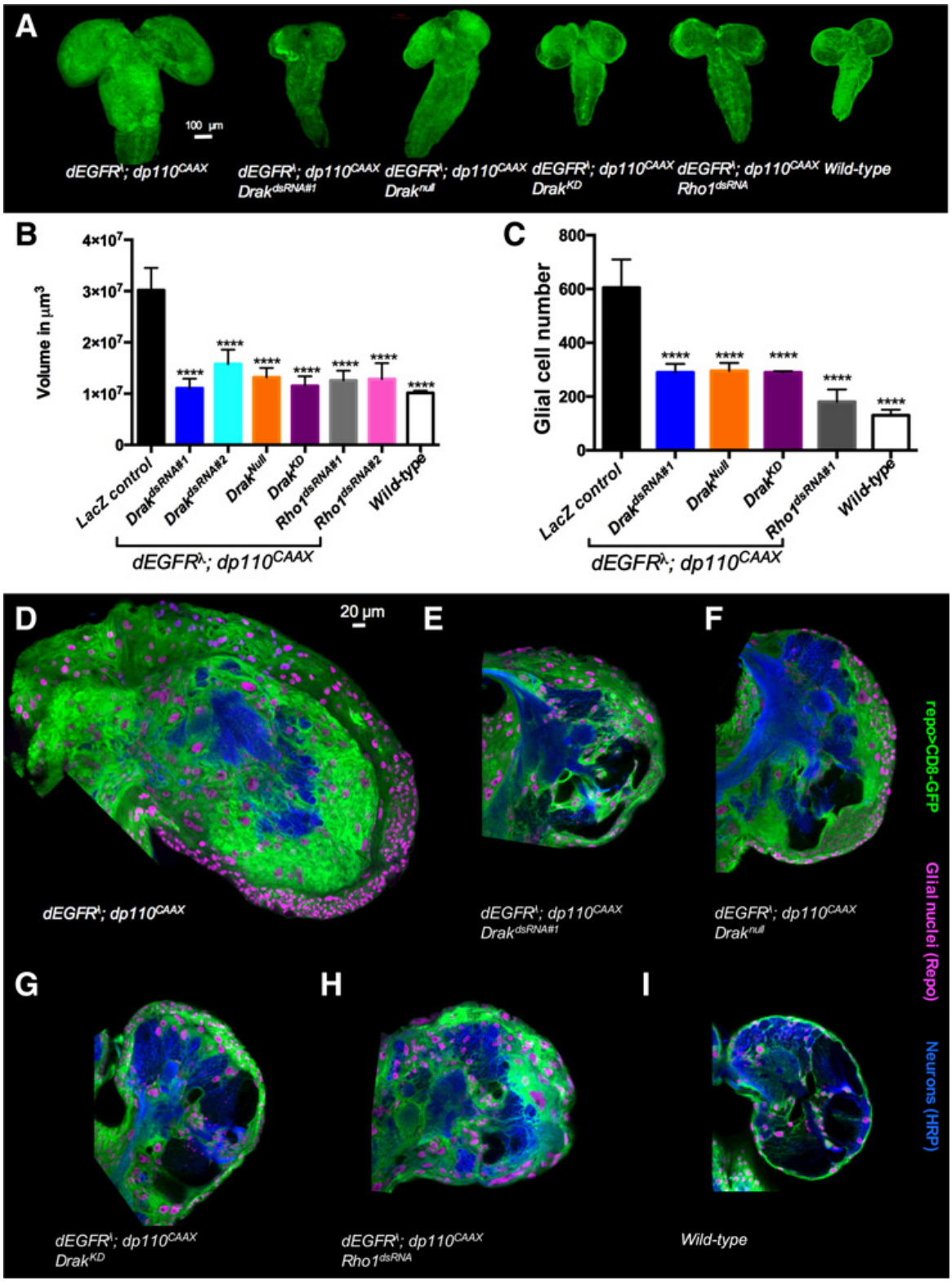
A
100 µm
dEGFRλ; dp110CAAX
dEGFRλ; dp110CAAX DrakdsRNA#1
dEGFRλ; dp110CAAX Draknull
dEGFRλ; dp110CAAX DrakKD
dEGFRλ; dp110CAAX Rho1dsRNA
Wild-type
B
Volume in µm3
4×10^7
3×10^7
2×10^7
1×10^7
0
****
LacZ control
DrakdsRNA#1
DrakdsRNA#2
DrakNull
DrakKD
Rho1dsRNA#1
Rho1dsRNA#2
Wild-type
dEGFRλ; dp110CAAX
C
Glial cell number
800
600
400
200
0
****
LacZ control
DrakdsRNA#1
DrakNull
DrakKD
Rho1dsRNA#1
Wild-type
dEGFRλ; dp110CAAX
D
20 µm
dEGFRλ; dp110CAAX
E
dEGFRλ; dp110CAAX DrakdsRNA#1
F
dEGFRλ; dp110CAAX Draknull
G
dEGFRλ; dp110CAAX DrakKD
H
dEGFRλ; dp110CAAX Rho1dsRNA
I
Wild-type
repo>CD8-GFP
Glial nuclei (Repo)
Neurons (HRP)

Figure 2.1. Drak is required for glial neoplasia in *Drosophila.*

(A) Optical projections of whole brain-nerve cord complexes from 3rd instar larvae approximately 130 hrs old. Dorsal view; anterior up. CD8-GFP (green) labels glial cell bodies. Knockdown of Drak (*repo>dEGFR$^{\lambda}$;dp110^{CAAX};Drak^{dsRNA}*) and Rho1 (*repo>dEGFR$^{\lambda}$;dp110^{CAAX};Rho1^{dsRNA}*), the Drak null genetic background (*Drak^{null}*; *repo>dEGFR$^{\lambda}$;dp110^{CAAX}*), or overexpression of catalytically inactive Drak (*repo>dEGFR$^{\lambda}$;dp110^{CAAX};Drak^{KD}*) decreased brain overgrowth relative to *repo>dEGFR$^{\lambda}$; dp110^{CAAX}*.

(B, C) (B) Total volumes (in μm^3) of 3rd instar larval brains, measured using Imaris. *repo>dEGFR$^{\lambda}$;dp110^{CAAX}*(n=3), *repo>dEGFR$^{\lambda}$;dp110^{CAAX};Drak$^{dsRNA\#1}$*(n=5), *repo>dEGFR$^{\lambda}$;dp110^{CAAX};Drak$^{dsRNA\#2}$*(n=5), *Drak^{null};repo>dEGFR$^{\lambda}$;dp110^{CAAX}*(n=3), *repo>dEGFR$^{\lambda}$;dp110^{CAAX};Drak^{KD}*(n=3), *repo>dEGFR$^{\lambda}$;dp110^{CAAX};Rho1$^{dsRNA\#1}$*(n=4), *repo>dEGFR$^{\lambda}$;dp110^{CAAX};Rho1$^{dsRNA\#2}$*(n=5), *wild-type*(n=3). (C) Glial cell numbers in representative 3 μm optical projections of 3rd instar brain hemispheres (n=3 per genotype). Statistics generated using One-Way ANOVA, ****p<0.0001.

(D-I) 3 μm optical projections of brain hemispheres, age-matched 3rd instar larvae. Frontal sections, midway through brains. Anterior up; midline to left. Repo (magenta) labels glial cell nuclei; CD8-GFP (green) labels glial cell bodies; anti-HRP (blue) counter-stains for neurons and neuropil. (D) *repo>dEGFR$^{\lambda}$;dp110^{CAAX}* showed increased glial cell numbers (magenta nuclei, green cell bodies) relative to (I) wild-type. (E-G) Drak knockdown (Drak^{dsRNA}), genetic reduction of Drak using a null allele (*Drak^{null}*), or overexpression of catalytically inactive Drak (*Drak^{KD}*) significantly reduced glial cells compared to *repo>dEGFR$^{\lambda}$;dp110^{CAAX}*.

Data generated in (A-I) by Alexander S. Chen, with assistance from Deidre Wright, Nilang Shah, and Renee D. Read.

Drak cooperates with EGFR to promote glial transformation

Because Drak reduction suppressed glial neoplasia in the context of constitutive EGFR-PI3K and EGFR signaling, we tested whether Drak overexpression cooperates with constitutive EGFR signaling. We found that glial-specific Drak overexpression had no obvious effect on normal larval glia morphology or number compared to wild-type (Figure 2.2A-C). Glial-specific $dEGFR^{\lambda}$ overexpression induced a significant increase in glial cell numbers compared to wild-type controls (Figure 2.2A-D). (49). Co-overexpression of Drak and $dEGFR^{\lambda}$ increased glial cell numbers, and these glia lost their normal stellate shape and formed abnormal cellular aggregates that disrupted normal larval brain architecture, indicative of neoplastic transformation (Figure 2.2A-E). We previously showed that overexpression of human $EGFR^{vIII}$ ($hEGFR^{vIII}$), an oncogenic constitutively active mutant variant of EGFR found in GBM, cooperates with $dp110^{CAAX}$ to drive neoplastic glial transformation, which was suppressed by Drak RNAi (50). Similar to $dEGFR^{\lambda}$, $hEGFR^{vIII}$ overexpression caused glial hyperplasia (50), and Drak and $hEGFR^{vIII}$ co-overexpression cooperated to drive increased proliferation and alterations in larval glial morphology consistent with neoplastic transformation (Supplemental Figure S2.2A-D). Thus, while Drak overexpression alone has little effect in glia, Drak co-overexpression augments the ability of constitutively active EGFR to promote tumorigenesis. Thus, Drak acts as a bona fide genetic modifier in that Drak loss or gain exerts the observed effects only in the context of other oncogenic mutations.

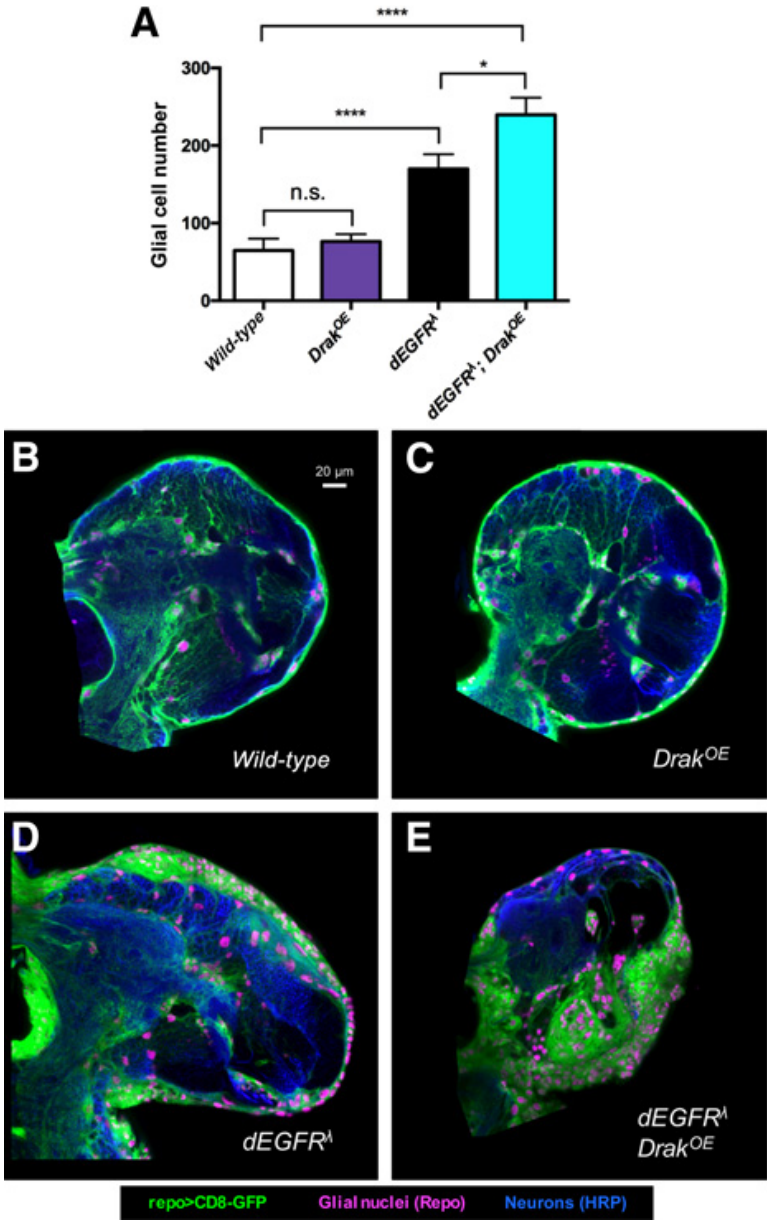

Figure 2.2. Drak cooperates with EGFR to promote glial transformation.

(A) Glial cell numbers in representative 3 µm optical projections of 3rd instar brain hemispheres. Statistics generated using One-Way ANOVA, ****p<0.0001. Comparisons of *wild-type* to $Drak^{OE}$ and $dEGFR^{\lambda}$ to $dEGFR^{\lambda};Drak^{OE}$ were performed using paired parametric T-Tests, n.s: p>0.05, *p<0.05. *wild-type*(n=5), $repo>Drak^{OE}$(n=7), $repo>dEGFR^{\lambda}$(n=4), $repo>Drak^{OE};dEGFR^{\lambda}$ (n=3).

(B-E) 3 μm optical projections of brain hemispheres from 3rd instar larvae, approximately 130 hrs old. Frontal sections, midway through brains. Repo (magenta) labels glial cell nuclei; CD8-GFP (green) labels glial cell bodies; anti-HRP (blue) counter-stains for neurons and neuropil. (A-B) Drak overexpression (*Drak^{OE})* using *repo-Gal4* had no obvious effect on glial cell development compared to wild-type. (A, C) *dEGFR$^{\lambda}$* overexpression alone increased glial cells compared to wild-type. (D) *repo>dEGFR$^{\lambda}$;Drak^{OE}* showed increased numbers of abnormal glia (magenta nuclei, green cell bodies), compared to *Drak^{OE}* or *dEGFR$^{\lambda}$* alone, which lost their normal stellate shape and formed aggregates that disrupt normal brain architecture and stunt brain development, evidenced by decreased neural tissue (HRP-stain).

Data generated in (A) by Alexander S. Chen and in (B-E) by Joanna Wardwell-Ozgo and Nilang Shah.

Drak acts downstream of oncogenic EGFR to phosphorylate Sqh

We next sought to understand the mechanism whereby Drak contributes to glial transformation. Given that Drak catalytic activity was essential for EGFR-PI3K glial neoplasia, we predicted that Spaghetti squash (Sqh), which is the *Drosophila* ortholog of human NMII regulatory light chain (MRLC) and only known Drak substrate (129), would be essential for EGFR-PI3K glial neoplasia. Prior studies have shown that DAP family kinases, including STK17A, the human ortholog of Drak, phosphorylate MRLC at serine and threonine residues (Thr-18 and Ser-19) (118, 129, 132). Similarly, Drak phosphorylates Sqh at the conserved serine residue (Ser-21 in Sqh is equivalent to Ser-19 in MRLC) (118, 129, 132). Phosphorylated Sqh binds to and stimulates the ATPase-dependent motor activity of Zipper, the sole NMII ortholog, which functions in cellular processes that require cytoskeletal contractility, such as cell migration, cytokinesis, and morphogenesis; all processes that play pivotal roles in tumorigenesis (132, 205, 206).

We found that, similar to *Drak* knockdown, glial-specific *sqh* knockdown significantly reduced glial cell numbers and rescued brain size in dEGFR$^{\lambda}$-dp110^{CAAX} mutants (Figure 2.3A-F), which suggests that Drak activates Sqh by phosphorylation in transformed glia. To test this hypothesis, we used a validated phospho-specific antibody to examine levels of Ser-21-phosphorylated Sqh (Sqh-S21-P) protein in dEGFR$^{\lambda}$-dp110^{CAAX} mutant glia in the presence or absence of Drak (201). dEGFR$^{\lambda}$-dp110^{CAAX} mutant glia showed increased Sqh-S21-P compared to wild-type glia, with mitotic cells showing cortical enrichment of Sqh-S21-P (Figure 2.3G), consistent with published observations regarding Sqh phosphorylation during cytokinesis (27). Drak RNAi reduced Sqh-S21-P levels (Figure 2.3G), indicative of loss of Sqh activation.

We next asked whether concurrent activation of EGFR and Drak signaling influences levels of activated Sqh. Consistent with Drak activity to phosphorylate Sqh, we observed increased levels of Sqh-S21-P in *dEGFR$^{\lambda}$;Drak^{OE}* glia compared to Drak-over expressing glia (Figure 2.3G). By western blot, we observed increased levels of Sqh-S21-P with *Drak^{OE};hEGFR^{vIII}* glia compared to hEGFR^{vIII}-overexpressing glia (Supplemental Figure S2.2E). These data are consistent with a model in which Drak increases the amount of activated, phosphorylated Sqh, which in turn supports EGFR-dependent tumorigenesis.

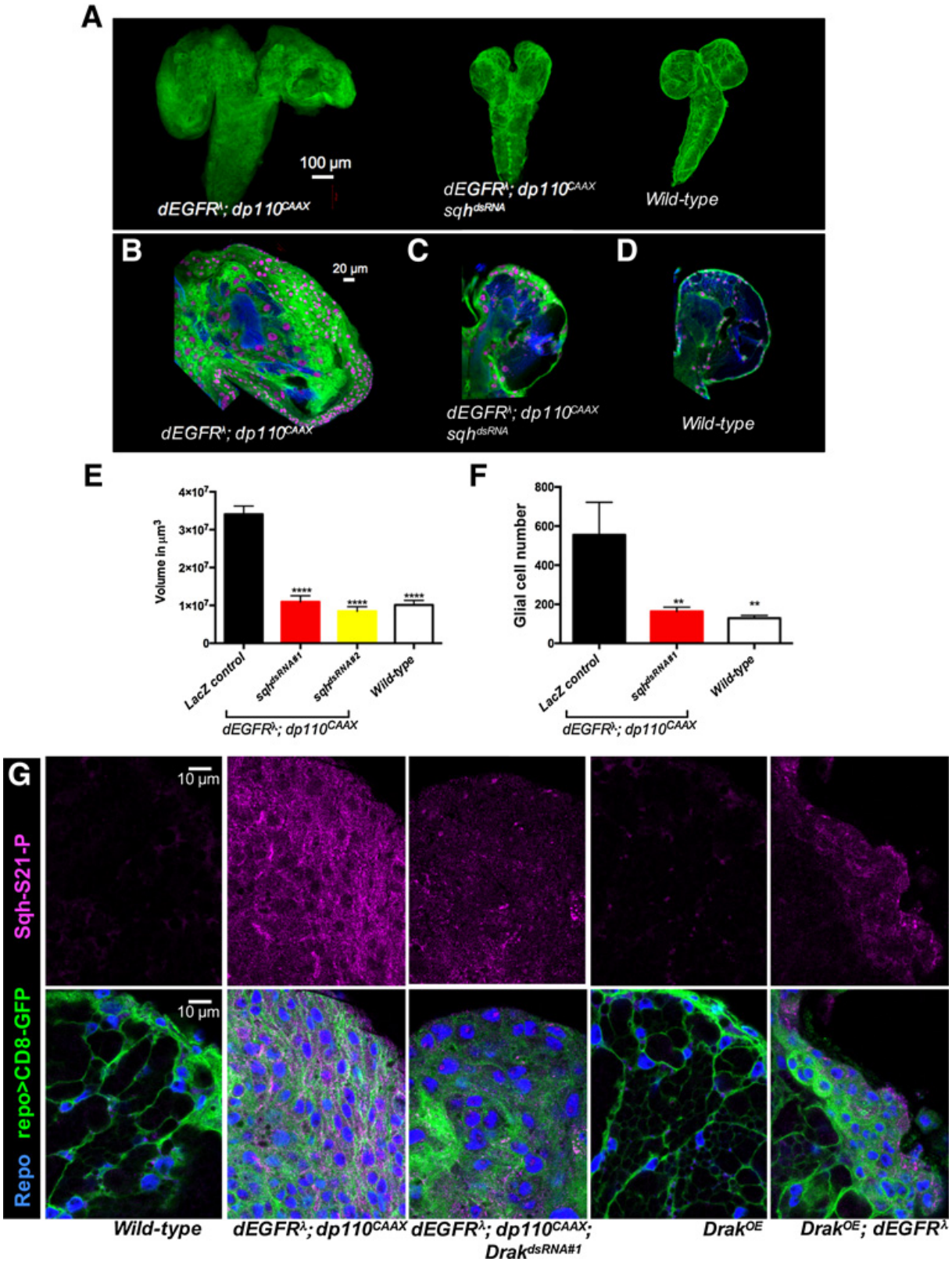
A
100 µm
dEGFRλ; dp110CAAX
dEGFRλ; dp110CAAX
sqhdsRNA
Wild-type
B
20 µm
dEGFRλ; dp110CAAX
C
dEGFRλ; dp110CAAX
sqhdsRNA
D
Wild-type
E
Volume in µm3
4×10⁷
3×10⁷
2×10⁷
1×10⁷
0
****
****
****
LacZ control
sqhdsRNA#1
sqhdsRNA#2
Wild-type
dEGFRλ; dp110CAAX
F
Glial cell number
800
600
400
200
0
**
**
LacZ control
sqhdsRNA#1
Wild-type
dEGFRλ; dp110CAAX
G
10 µm
Sqh-S21-P
10 µm
repo>CD8-GFP
Repo
Wild-type
dEGFRλ; dp110CAAX
dEGFRλ; dp110CAAX;
Drakdsrna#1
DrakOE
DrakOE; dEGFRλ

Figure 2.3. Drak acts downstream of oncogenic EGFR to phosphorylate Sqh.

(A) Optical projections of whole brain-nerve cord complexes from 3rd instar larvae approximately 130 hrs old. Dorsal view; anterior up. CD8-GFP (green) labels glia. Sqh knockdown (*repo>dEGFR$^{\lambda}$;dp110^{CAAX};sqh^{dsRNA}*) decreased neoplastic overgrowth relative to *repo>dEGFR$^{\lambda}$;dp110^{CAAX}*.

(B-D) 3 μm optical projections of brain hemispheres from age-matched 3rd instar larvae. Frontal sections, midway through brains. Repo (magenta) labels glial cell nuclei; CD8-GFP (green) labels glial cell bodies; anti-HRP (blue) counter-stains for neurons and neuropil. (B) *repo>dEGFR$^{\lambda}$;dp110^{CAAX}* showed increased glial cell numbers (magenta nuclei, green cell bodies) relative to (D) wild-type. (C) *Drak* knockdown dramatically reduced neoplastic glial proliferation compared to controls.

(E) Total volumes (in μm^3) of 3rd instar larval brains, measured using Imaris. *sqh* RNAi in the context of *dEGFR$^{\lambda}$;dp110^{CAAX}* reduced brain volume compared to *dEGFR$^{\lambda}$;dp110^{CAAX}* controls. Statistics generated using One-Way ANOVA, **** p<0.0001. *repo>dEGFR$^{\lambda}$;dp110^{CAAX}*(n=3), *repo>dEGFR$^{\lambda}$;dp110^{CAAX};sqh$^{dsRNA\#1}$*(n=5), *repo>dEGFR$^{\lambda}$;dp110^{CAAX};sqh$^{dsRNA\#2}$* (n=4), *wild-type* (n=3).

(F) Glial cell numbers in representative 3 μm optical projections of 3rd instar brain hemispheres. Statistics generated using One-Way ANOVA, **p<0.01 (n=3 per genotype).

(G) 3 μm optical projections of brain hemispheres from 3rd instar larvae. Repo (blue) labels glial cell nuclei; CD8-GFP (green) labels glial cell bodies; and Sqh-S21-P (magenta, Sqh-S21-P alone top panels, merge bottom panels). *repo>dEGFR$^{\lambda}$;dp110^{CAAX}* brains (second panel from left) showed increased Sqh-P21-P compared to wild-type (leftmost panel). *Drak* knockdown in *dEGFR$^{\lambda}$;dp110^{CAAX}* glia (middle panel) reduced Sqh-P21-P compared to *repo>dEGFR$^{\lambda}$;dp110^{CAAX}*

glia (second panel from left). Co-overexpression of *Drak* and *dEGFR*$^{\lambda}$ increased Sqh-P21-P levels (rightmost panel) compared to *Drak* overexpression alone (second panel from right).

Data generated in (A-F) by Alexander S. Chen with assistance from Deidre Wright and in (G) by Renee D. Read and Joanna Wardwell-Ozgo.

If Sqh phosphorylation promotes EGFR-dependent neoplasia, then overexpression of a phospho-mimetic version of Sqh should enhance oncogenic EGFR. A prior study engineered a Sqh transgene with serine-21 and threonine-20 converted to aspartic acid (Sqh^{D20D21}) to mimic the phosphorylated state (207). As predicted, Sqh^{D20D21} and $dEGFR^{\lambda}$ co-overexpression increased numbers of small proliferative glia that disturbed normal larval brain architecture; these changes are indicative of enhanced hyperplasia and/or neoplastic transformation (Figure 2.4A-4E). Thus, Sqh is a functionally relevant Drak substrate in EGFR-PI3K-mediated glial neoplasia. Taken together, our data provide strong support for a model in which Drak cooperates with oncogenic EGFR signaling to create and sustain a pool of activated, phosphorylated Sqh necessary for glial cell transformation.

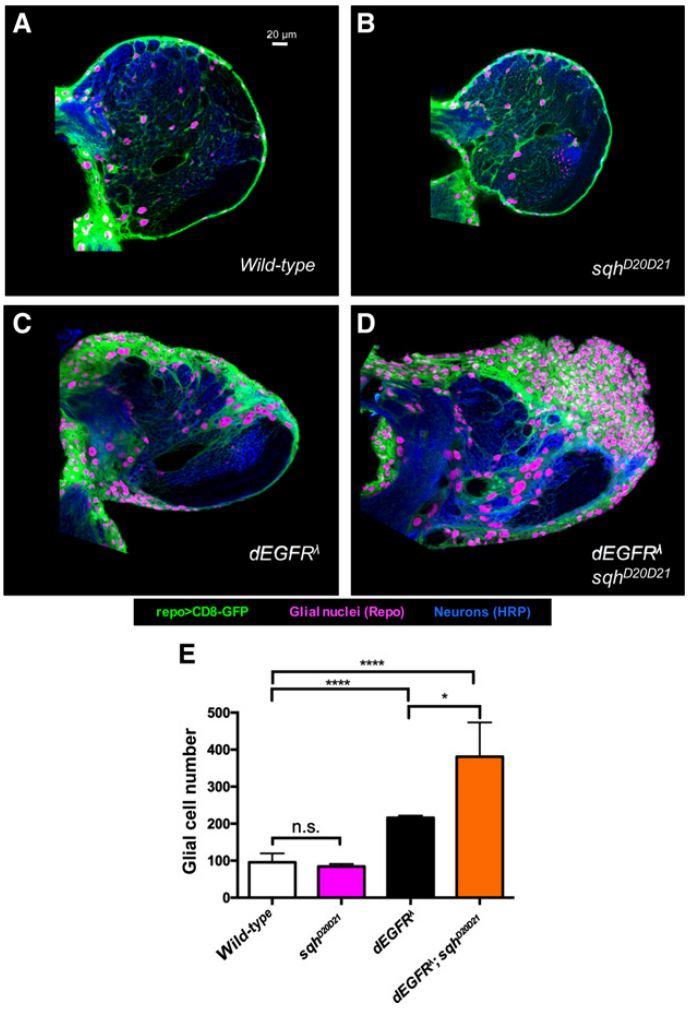

Figure 2.4. Sqh is a functionally relevant Drak substrate in glial neoplasia.

(A-D) 3 μm optical projections of brain hemispheres from 3rd instar larvae approximately 130 hrs old. Frontal sections, midway through brains. Repo (magenta) labels glial cell nuclei; CD8-GFP (green) labels glial cell bodies; anti-HRP (blue) counter-stains for neurons and neuropil. (B) sqh^{D20D21} overexpression in glia caused no observable phenotype compared to (A) wild-type. (D) sqh^{D20D21} and $dEGFR^{\lambda}$ co-overexpression yielded small proliferative glia that disturbed normal brain architecture, as compared to (A) wild-type and (C) $dEGFR^{\lambda}$ alone brains.

(E) Glial cell numbers in representative 3 μm optical projections of 3rd instar brain hemispheres. Statistics generated using One-Way ANOVA, ****$p<0.0001$; cell numbers of *wild-type* flies to sqh^{D20D21} flies compared using unpaired parametric T-Tests, n.s: $p>0.05$; $dEGFR^{\lambda}$ flies to $dEGFR^{\lambda};sqh^{D20D21}$ compared using paired parametric T-Tests, *$p<0.05$ (n=4 per genotype).

Data generated in (A-E) by Renee D. Read and Alexander S. Chen.

A Sqh binding partner, Anillin, is required for neoplastic growth.

Following determination that glial neoplasia in our GBM model requires Sqh, we next sought to determine which processes downstream of Sqh are essential in neoplastic glia. We used our *Drosophila* GBM model to test RNAi constructs against eight published Sqh binding partners (Supplemental Table 2.2). We found that glial-specific RNAi of *anillin*, which encodes a well-established Sqh binding partner and actin-binding scaffolding protein important for cytoskeletal reorganization during cytokinesis (199), significantly reduced dEGFR$^{\lambda}$-dp110^{CAAX} mutant glia proliferation (Figure 2.5A-F). Thus, *anillin* RNAi in glial cells may interfere with cytokinesis, thereby inhibiting tumor cell proliferation.

To determine if Anillin is an effector of dEGFR-Drak-Sqh signaling, we tested glial-specific *anillin* knockdown in either *dEGFR$^{\lambda}$;Drak^{OE}* or *dEGFR$^{\lambda}$;sqh^{D20D21}* mutant glia, and observed a significant reduction in glial proliferation (Supplemental Figure S2.3A-G), indicating that Anillin operates downstream of dEGFR-Drak-Sqh signaling. In contrast, *anillin* knockdown in wild-type glia had no impact on glial cell proliferation compared to wild-type controls (Supplemental Figure S2.3A-G), showing a differential requirement for the Drak-Sqh-Anillin pathway in neoplastic glia, but not wild-type glia.

MRLC phosphorylation mediates cellular processes that require NMII-dependent cytoskeletal contractility, including mitosis and cytokinesis (132, 205, 206). Previous studies demonstrate that phosphorylated Sqh recruits Anillin to the cortex during mitosis, where it coordinates cytokinesis by linking actin and NMII/Zipper proteins in the contractile ring (199). During embryonic cellularization, Drak phosphorylation of Sqh is responsible for proper organization of contractile rings (208), most likely because Sqh phosphorylation was necessary for binding of Anillin to Zipper. To determine if Drak-dependent phosphorylation of Sqh is

necessary for Anillin binding and/or localization in mitosis, we examined Anillin localization in relation to Sqh-S21-P in neoplastic dEGFR$^{\lambda}$-dp110^{CAAX} glia. Consistent with their binding in mitotic glia, Sqh-S21-P and Anillin were co-localized and enriched at the cortex and cleavage furrow (observed in mitotic cells in all *dEGFR$^{\lambda}$;dp110^{CAAX}* brains imaged, n=8), and this enrichment was lost upon Drak depletion (in all *dEGFR$^{\lambda}$;dp110^{CAAX};Drak$^{dsRNA\#1}$* brains imaged, n=6) (Figure 2.5G). Moreover, overall Anillin levels were reduced by Drak depletion (Figure 2.5G). Thus, our data support a model wherein Drak-dependent phosphorylation of Sqh promotes Anillin binding to coordinately drive cytokinesis and proliferation in neoplastic glia.

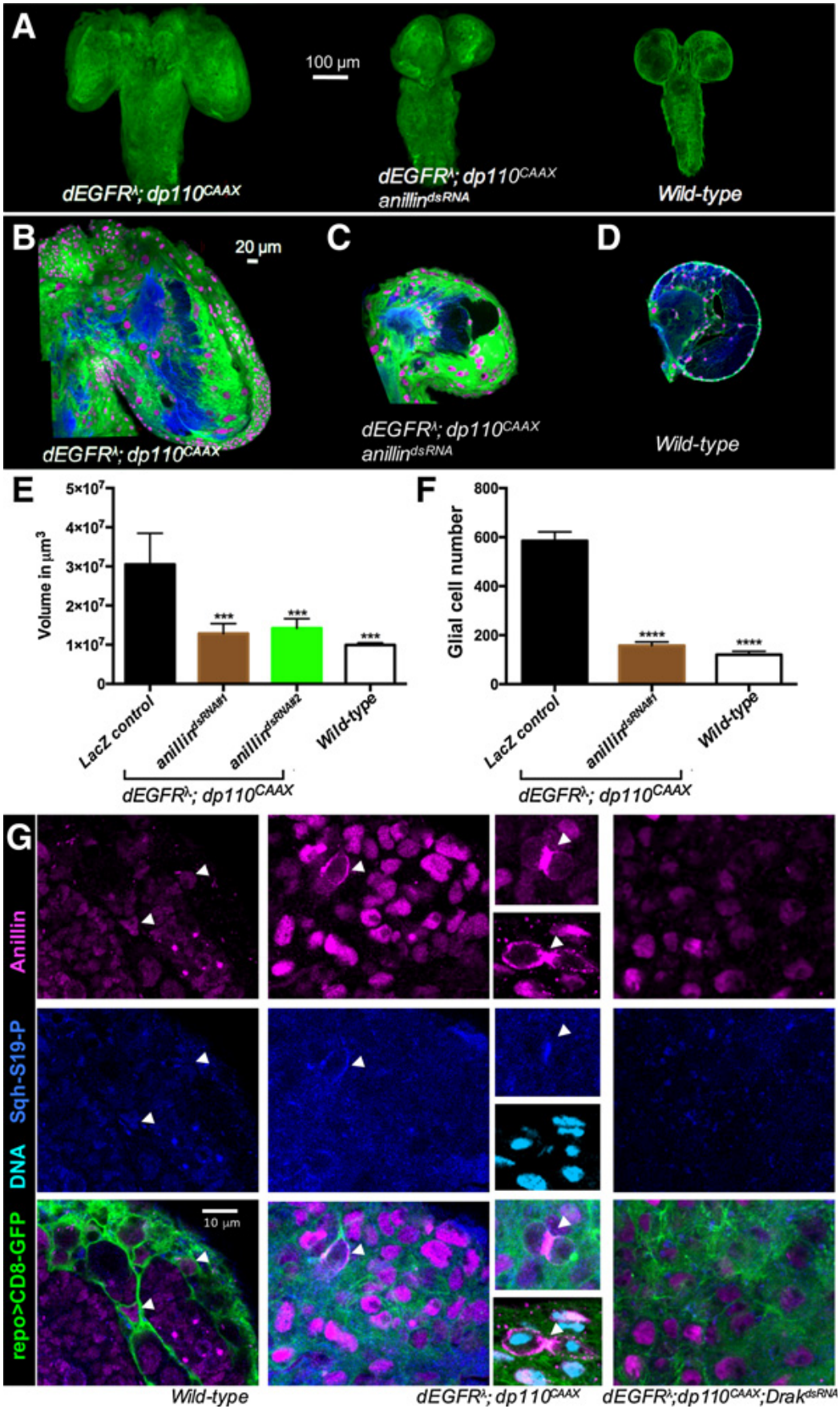
A
100 µm
dEGFRλ; dp110CAAX
dEGFRλ; dp110CAAX
anillindsRNA
Wild-type
B
20 µm
dEGFRλ; dp110CAAX
C
dEGFRλ; dp110CAAX
anillindsRNA
D
Wild-type
E
Volume in µm3
5×10^7
4×10^7
3×10^7
2×10^7
1×10^7
0
***
***
***
LacZ control
anillindsRNA#1
anillindsRNA#2
Wild-type
dEGFRλ; dp110CAAX
F
Glial cell number
800
600
400
200
0
****
****
LacZ control
anillindsRNA#1
Wild-type
dEGFRλ; dp110CAAX
G
Anillin
Sqh-S19-P
DNA
repo>CD8-GFP
10 µm
Wild-type
dEGFRλ; dp110CAAX
dEGFRλ;dp110CAAX;DrakdsRNA

Figure 2.5. A Sqh binding partner, Anillin, is required for neoplastic growth.

(A) Optical projections of whole brain-nerve cord complexes from 3rd instar larvae approximately 130 hrs old. Dorsal view; anterior up. CD8-GFP labels glia (green). Knockdown of *anillin* (*repo>dEGFR$^{\lambda}$;dp110^{CAAX};anillin^{dsRNA}*) show decreased neoplastic brain overgrowth relative to *repo>dEGFR$^{\lambda}$;dp110^{CAAX}*.

(B-D) 3 μm optical projections of brain hemispheres from age-matched 3rd instar larvae. Frontal sections, midway through brains. Repo (magenta) labels glial cell nuclei; CD8-GFP (green) labels glial cell bodies; anti-HRP (blue) counter-stains for neurons and neuropil. (C) *anillin* knockdown dramatically reduced neoplastic glial proliferation in the context of *dEGFR$^{\lambda}$;dp110^{CAAX}* compared to *repo>dEGFR$^{\lambda}$;dp110^{CAAX}* controls (B).

(E) The total volume (in μm^3) of 3rd instar larval brains, measured using Imaris. *anillin* knockdown drastically reduced brain volume in the context of *dEGFR$^{\lambda}$;dp110^{CAAX}*. Statistics generated using One-Way ANOVA, ***p<0.001. *repo>dEGFR$^{\lambda}$;dp110^{CAAX}* (n=3), *repo>dEGFR$^{\lambda}$;dp110^{CAAX};anillin$^{dsRNA\#1}$*(n=4), *repo>dEGFR$^{\lambda}$;dp110^{CAAX};anillin$^{dsRNA\#2}$*(n=4), *wild-type*(n=3).

(F) Glial cell numbers in representative 3 μm optical projections of brain hemispheres from 3rd instar larvae. Statistics generated using One-Way ANOVA with multiple comparisons, ****p<0.0001 (n=3 per genotype).

(G) 3 μm optical projections, 3rd instar larval brains. CD8-GFP (green) labels glial cell membranes. (F) immunostaining showed low levels of Anillin protein (magenta, upper panel) and Sqh-S21-P (blue, middle panel) in glia (white arrows, green, lower panel) and neighboring neurons (GFP-negative) in wild-type. (G) high levels of Anillin protein (magenta, upper panels) and Sqh-S21-P (blue, middle panel) were detected in *dEGFR$^{\lambda}$;dp110^{CAAX}* neoplastic glia (lower panel), with

Anillin showing nuclear localization and Sqh-S21-P showing cytoplasmic localization in non-mitotic cells. In mitotic cells (white arrow, in large panel), Anillin and Sqh-S21-P showed membrane and cytoplasmic co-localization. In cytokinesis, Anillin localized to the cleavage furrow (white arrows in insets), with upper inset showing cells in cytokinesis co-stained with Anillin and Sqh-S21-P with the lower inset showing cells in cytokinesis co-stained Anillin and DRAQ7 DNA dye (cyan) to show cell nuclei. (H) immunostaining revealed reduced levels of Anillin protein (magenta, upper panel) and Sqh-S21-P (blue, middle panel) upon *Drak* RNAi in $dEGFR^{\lambda};dp110^{CAAX}$ glia.

Data generated in (A-F) by Alexander S. Chen with assistance from Deidre Wright and Joanna Wardwell-Ozgo and in (G) by Renee D. Read.

STK17A expression correlates with EGFR status, phosphorylated MRLC levels, and ANLN expression in human tumors

To determine whether the Drak-Sqh-Anillin pathway operates in human GBM and/or LGGs, we examined expression and function of the human orthologs of Drak, STK17A and STK17B, and found that STK17A is overexpressed in GBMs (50). We next examined STK17A levels in a panel of patient-derived human GBM stem-cell containing gliomasphere (GSC) cultures. Compared to cultured normal human neural progenitor cells (HNPCs), $EGFR^{vIII}$-positive and EGFR-mutant GSC cultures express higher levels of STK17A and ANLN (Figure 2.6A). Moreover, in GSC cultures with high STK17A levels, we also saw a modest increase in Ser-19-phosphorylated MRLC (MRLC-S19-P) relative to HNPCs (Figure 2.6A). Thus, at the protein level, we observed that the relationships between EGFR, STK17A, ANLN (Anillin), and MRLC phosphorylation in GBM cells recapitulate our observations from *Drosophila.*

To further explore pathway conservation, we examined STK17A function and localization in serum-cultured GBM cell lines and GSC lines using RNAi and immunofluorescence. Consistent with prior reports (128), we found that, in serum cultured lines, STK17A is required for proliferation, with STK17A knockdown inducing slower proliferation, apoptosis, reduced MRLC-S19-P levels, and altered cell shape and adhesion (Figure 2.6B, Supplemental Figure S2.4A-B), which is consistent with alterations in MRLC regulation (209-211). We examined the effects of STK17A loss in GSCs treated with or without ZVAD to control for the effects of apoptosis, and we found that STK17A knockdown caused GSC adhesion defects, slower proliferation, apoptosis, and reduced levels of MRLC-S19-P and ANLN levels relative to control GSCs (Figure 2.6C-D, Supplemental Figure S2.4C-D). We also observed that total MRLC levels were reduced upon STK17A knockdown, suggesting that phosphorylation may regulate total MRLC protein in GBM

cells. This is consistent with published studies showing MRLC levels are regulated by proteosomal turn-over (212). Furthermore, we examined STK17A localization in $EGFR^{vIII}$-positive GBM cells and observed that STK17A protein, in conjunction with MRLC-S19-P and ANLN, was upregulated in mitotic cells and localized to the cleavage furrow in tumor cells undergoing cytokinesis (Figure 2.6E-F). Thus, STK17A expression is required to promote MRLC phosphorylation and ANLN upregulation in GBM cells to coordinately regulate cytokinesis and proliferation.

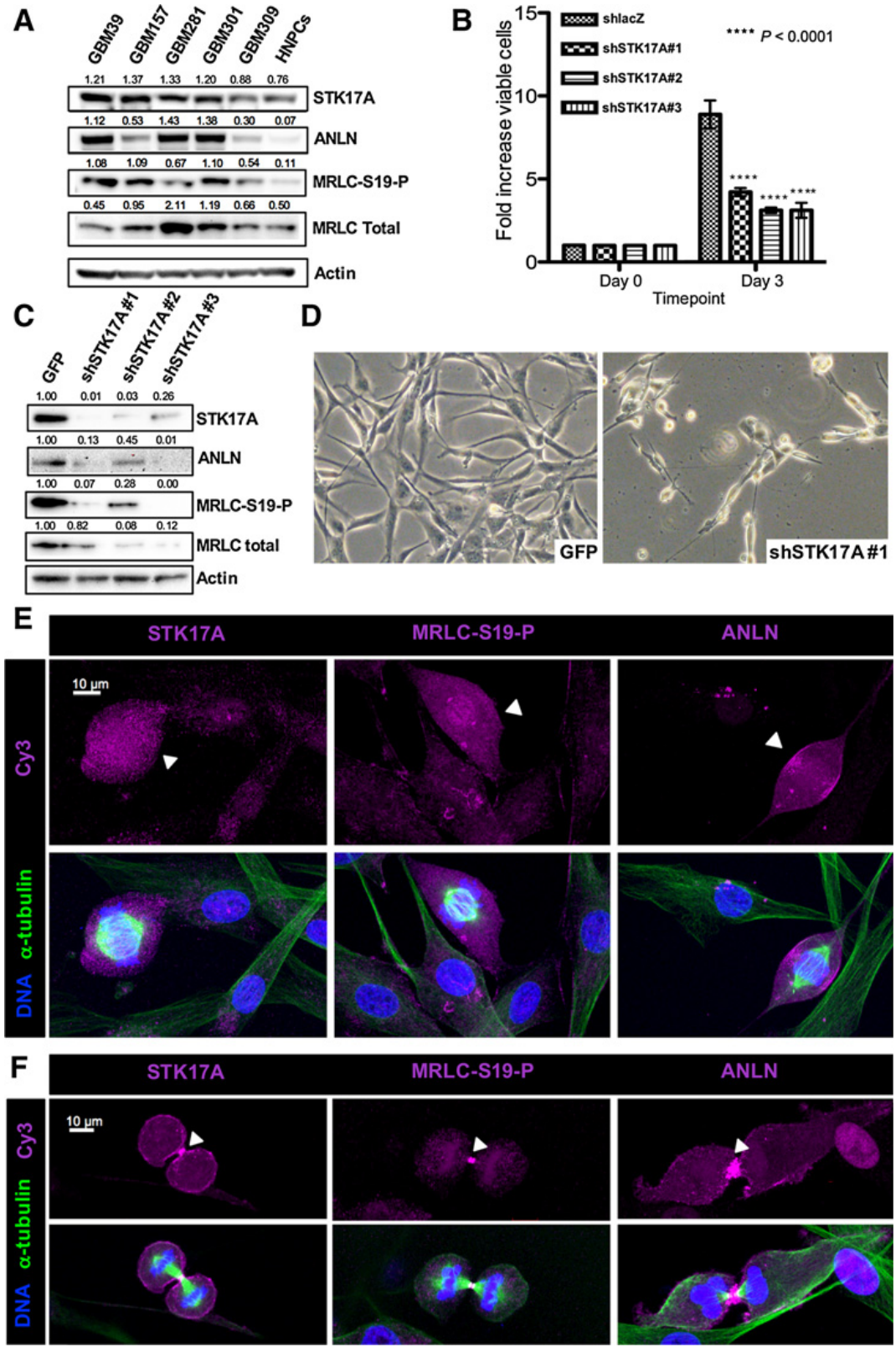
A
GBM39
GBM157
GBM281
GBM301
GBM309
HNPCs
1.21 1.37 1.33 1.20 0.88 0.76
STK17A
1.12 0.53 1.43 1.38 0.30 0.07
ANLN
1.08 1.09 0.67 1.10 0.54 0.11
MRLC-S19-P
0.45 0.95 2.11 1.19 0.66 0.50
MRLC Total
Actin
B
shlacZ
shSTK17A#1
shSTK17A#2
shSTK17A#3
**** P < 0.0001
Fold increase viable cells
15
10
5
0
****
****
****
Day 0
Day 3
Timepoint
C
GFP
shSTK17A #1
shSTK17A #2
shSTK17A #3
1.00 0.01 0.03 0.26
STK17A
1.00 0.13 0.45 0.01
ANLN
1.00 0.07 0.28 0.00
MRLC-S19-P
1.00 0.82 0.08 0.12
MRLC total
Actin
D
GFP
shSTK17A #1
E
STK17A
MRLC-S19-P
ANLN
Cy3
DNA α-tubulin
10 μm
F
STK17A
MRLC-S19-P
ANLN
Cy3
DNA α-tubulin
10 μm

Figure 2.6. STK17A function is required for GBM cell proliferation, and regulates MRLC phosphorylation and ANLN expression.

(A) Panel of GBM gliomasphere cultures. GBM39 and GBM301 harbor amplified $EGFR^{VIII}$; GBM281 harbors an activated variant mutant EGFR; GBM157 is PDGFR-overexpressing; GBM309 has neither (50, 88). Band intensities were normalized to Actin (numbers above bands).

(B) WST-1 Assay on U87 cells. Following selection for shRNA expression, U87 cell proliferation was measured by WST-1 reagent and quantified as fold-increase in absorbance between day 0 and day 3 after plating, normalized to controls treated with nontargeting shRNA. 3 shRNAs tested for STK17A. p-values from One-Way ANOVA with Dunnett post-test.

(C) STK17A knockdown using 3 separate shRNAs in GBM301 decreased expression of ANLN and MRLC-S19-P compared to control cells treated with GFP shRNAs; all samples treated with ZVAD (Supplemental Figure S2.4C-D shows non-ZVAD treated cells). Cells were infected with lentiviral vectors 3 days prior to harvest. Band intensities were normalized to Actin (numbers above bands), reported as fold changes relative to control cells.

(D) Adherently cultured GBM301 cells 3 days after infection with control lentivirus or shSTK17A#1, which reduced proliferation and altered cell shape and reduced adhesion; cells treated with ZVAD for 24 hrs prior to imaging.

(E, F) U87-$EGFR^{VIII}$ cells were fixed and probed for either STK17A, phosphorylated MRLC (MRLC-S19-P), or ANLN (magenta) and α-tubulin (green) and DRAQ7 to label DNA (blue). (E) STK17A, MRLC-S19-P, and ANLN were upregulated in tumor cells undergoing mitosis (cells marked with white arrows). (F) STK17A, MRLC-S19-P, and ANLN were localized in the cleavage furrow of tumor cells undergoing cytokinesis (cells marked with white arrows).

Data generated in (A) by Renee D. Read (blots) with technical assistance from Alexander S. Chen (densitometry) and materials and protocols from Harley I. Kornblum, in (B, E, and F) by Renee D. Read, and in (C) by Joanna Wardwell-Ozgo and Alexander S. Chen (densitometry).

We used immunohistochemistry to examine protein expression of STK17A, EGFR, MRLC-S19-P, and ANLN in a collection of graded human tumor specimens. In LGG tissue microarrays (TMA), specimens with high STK17A expression showed a statistically significant correlation with high EGFR, MRLC-S19-P, and ANLN expression (Figure 2.7A). In GBM TMAs, we observed high expression of EGFR, STK17A, MRLC-S19-P, and ANLN in the majority of specimens (Figure 2.7B). However, we observed some GBM specimens with high STK17A but low MRLC-S19-P expression (Figure 2.7B): in these surgical GBM specimens, it is possible that the MRLC-S19-P phospho-epitope was not properly fixed and preserved. Thus, in human tumors, elevated STK17A levels co-occur with elevated EGFR, MRLC-S19-P, and ANLN levels, which recapitulates the relationship we observed between EGFR, Drak, Sqh, and Anillin in *Drosophila*.

We used cBioportal to process genomic data catalogued by The Cancer Genome Atlas (TCGA) to assess prevalence of *STK17A* mRNA expression and copy gain alterations and to examine relationships between STK17A alterations and well-characterized genetic lesions in gliomas (7, 189, 190, 203, 204). Well-characterized lesions include full or partial amplification of chromosome 7, which includes regions encoding both *EGFR* and *STK17A* (213), and focal *EGFR* amplification and mutation. In TCGA cohorts of LGGs and GBMs, *STK17A* mRNA expression was significantly correlated with copy number gain in 13p on chromosome 7 (7p13) (Figure 2.7C-D). To understand whether *STK17A* mRNA overexpression is specific or is passively driven by copy gain, we examined mRNA expression of neighboring genes on chromosome 7. We found that genes in close proximity to *STK17A* (i.e. *NACAD)* showed no statistically significant difference in mRNA expression between LGG specimens with chromosome 7 copy gain compared to LGG specimens with no observable copy number alterations in the same region of chromosome

7 (Figure 2.7E), indicating that *STK17A* mRNA expression may be selectively upregulated. Thus, increased *STK17A* expression may have a specific role in glioma pathology.

To further assess whether STK17A is a driver of gliomagenesis, we used cBioportal to examine *STK17A* mRNA expression relative to IDH1 status in LGG patients. *IDH1* mutation is a common genetic alteration in LGG, and patients who harbor *IDH1* mutations have a better prognosis than those with wild-type *IDH1* (214-216). LGG patients with wild-type *IDH1* have more aggressive tumors that behave much like primary GBMs (189, 214). Furthermore, wild-type *IDH1*, not mutant *IDH1*, is typically found in gliomas with chromosome 7 alterations (189, 214). In LGG, we found elevated *STK17A* mRNA expression in tumors with wild-type *IDH1* compared to tumors with mutant *IDH1* (Figure 2.7F). In *IDH1* mutant LGGs, there was not a statistically significant difference between *STK17A* mRNA expression between tumors with or without chromosome 7 gain (Figure 2.7G), suggesting that STK17A levels are not as relevant to progression in *IDH1* mutant tumors. Our observations are consistent with a previous study showing *STK17A* mRNA overexpression in LGGs is correlated with disease severity and worse prognosis (128).

To investigate associations between *STK17A* expression and patient survival, we analyzed cBioportal TCGA data to find that LGG and GBM patients with at least two-fold *STK17A* copy gain showed worse overall survival compared to patients with no *STK17A* copy gain (Supplemental Figure S5A-B). Thus, LGG and GBM patients with STK17A copy gain have a worse overall prognosis.

Together, our results suggest that elevated STK17A expression drives MRLC and ANLN dependent cytoskeletal changes during mitosis and cytokinesis to facilitate disease progression

(Figure 2.7H), validating our identification of the STK17A ortholog Drak as a driver of tumorigenesis in our *Drosophila* GBM model.

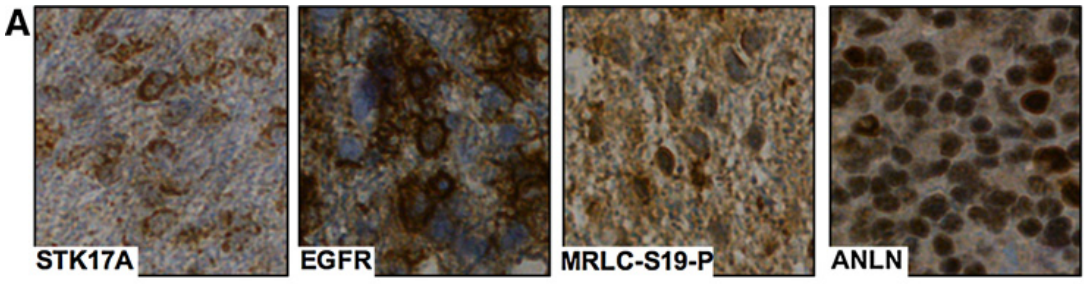

	EGFR Low	EGFR High
STK17A Low	10	4
STK17A High	2	10

$P < 0.01$, **

	MRLC Low	MRLC High
STK17A Low	11	9
STK17A High	4	16

$P < 0.05$, *

	Anillin Low	Anillin High
STK17A Low	8	5
STK17A High	1	10

$P < 0.05$, *

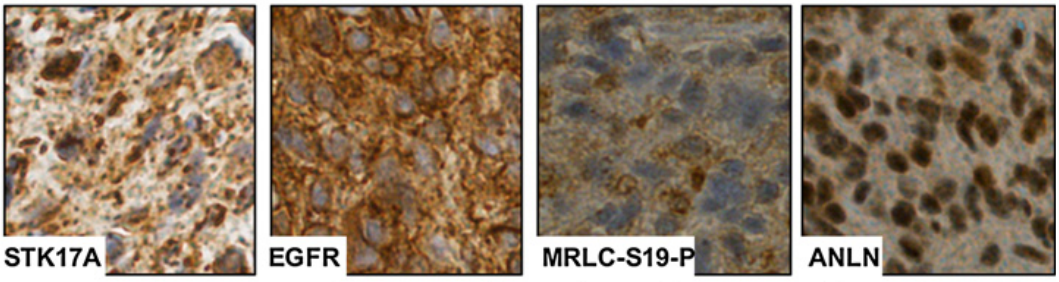

	EGFR Low	EGFR High
STK17A Low	0	0
STK17A High	3	15

	MRLC Low	MRLC High
STK17A Low	0	0
STK17A High	8	11

	Anillin Low	Anillin High
STK17A Low	0	0
STK17A High	2	16

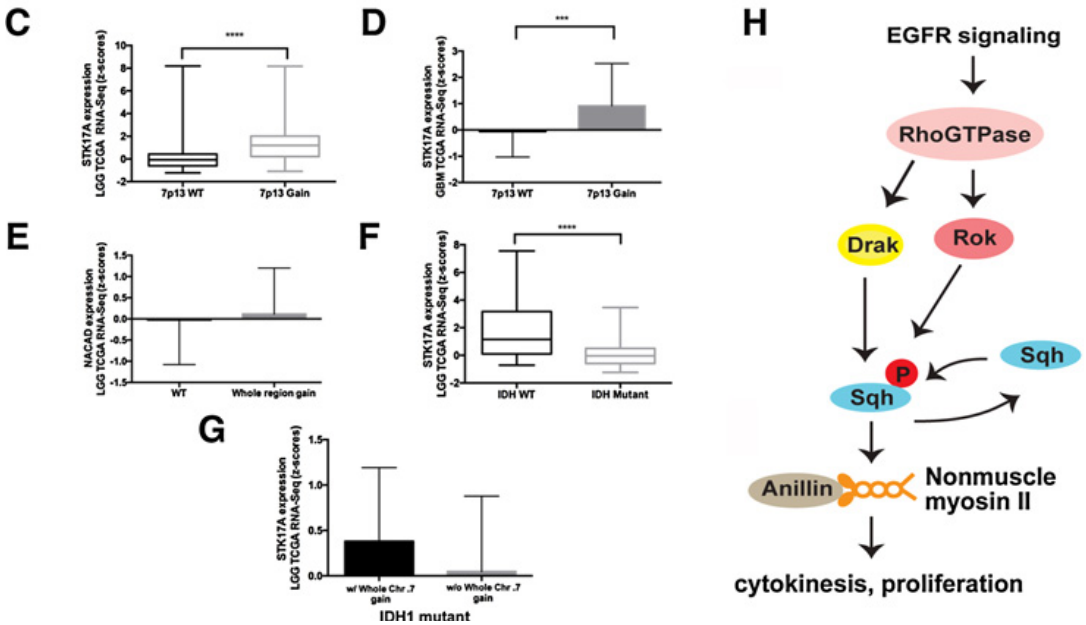

Figure 2.7. STK17A expression correlates with EGFR status, MRLC-S19-P levels, and ANLN expression in human tumors.

(A, B) Immunohistochemistry on TMAs of human (A) LGG tissue or (B) GBM tissue for STK17A, EGFR, MRLC-S19-P, or ANLN (reddish brown) showing cytoplasmic enrichment in tumor cells. Hematoxilin counterstain. Statistical analysis of low grade glioma of (A) LGG tumor specimens expressing STK17A show a statistically significant (Fisher's Exact Test) correlation between high STK17A expression and high EGFR expression, high MRLC-S19-P expression, and high ANLN expression. (B, lower) Table of the number of GBM tumor specimens with either high or low expression of STK17A and high or low expression of either EGFR, MRLC-S19-P, or ANLN.

(C-G) Analysis of *STK17A* mRNA expression in relation to chromosome 7 gain, NACAD expression, and IDH1 status in LGGs and GBMs using TCGA datasets. Statistics generated using Mann-Whitney *U* test, ****$p<0.0001$, ***$p<0.001$ (number of TCGA cases used: C:282, D:160, E:281, F:250, G:219).

(H) Diagram depicting the role of Drak/STK17A in promoting gliomas.

Data generated in (A, B) by Alexander S. Chen (images and statistics) with assistance from Krishanthan Vigneswaran, Daniel J. Brat, Christina Appin (sample selection, TMA generation, IHC scoring), and Renee D. Read (IHC scoring), (C-G) by Alexander S. Chen, and diagram in (H) created by Joanna Wardwell-Ozgo.

2.5 Discussion

Though EGFR and PI3K pathways play important roles in glioma progression and maintenance, effective therapies targeting these pathways remain elusive (194). We developed a *Drosophila melanogaster* GBM model based on co-activation of EGFR and PI3K in glia in order to gain insight into genetic and cellular mechanisms underlying gliomas (49, 50). Using our system, we identified a pathway through which the cytoplasmic serine/threonine kinase Drak specifically drives neoplastic proliferation. Consistent with published results (128), we show that the orthologous kinase STK17A drives proliferation human GBM cells, through a conserved pathway that regulates cytokinesis.

During *Drosophila* development, Drak acts downstream of EGFR and Rho-GTPase signaling to regulate epithelial tissue morphogenesis through Sqh phosphorylation (129, 130). Activated Sqh, like human MRLC, modulates cytoskeletal reorganization in cellular processes such as cytokinesis (206, 207, 217), which is fundamental to cancer progression (218). Drak harbors latent oncogenic activity, as it can cooperate with constitutively active EGFR to stimulate glial transformation. Similarly, in human LGG and GBM, STK17A is frequently subject to copy gain and overexpression in association with EGFR and chromosome 7 alterations. We show that, in *Drosophila* and human tumor cells, Sqh/MRLC is a key mediator of Drak/STK17A: Sqh/MRLC is phosphorylated at equivalent conserved sites in EGFR-PI3K mutant tumor cells in a Drak/STK17A-dependent manner, and is necessary for neoplastic growth. Thus, Sqh/MRLC is a functionally relevant and evolutionarily conserved substrate of Drak/STK17A in the context of EGFR-PI3K-driven glial tumorigenesis. This corroborates studies that have shown MRLC hyper-phosphorylation occurs in GBM tumors and that targeted inhibition of MRLC activity inhibits

GBM growth and invasion (209-211, 219, 220). Together, our results establish STK17A as a disease-relevant MRLC kinase in gliomas.

MRLC phosphorylation regulates many cellular processes that require NMII-dependent contractility (132, 205, 206). To distinguish which of these processes are most relevant to Drak/STK17A function, we used a genetic approach and found that, among known Sqh binding partners, Anillin is essential in neoplastic glia. Anillin is a scaffolding protein that acts downstream of RhoGTPase to organize the cytoskeleton and contractile ring in cytokinesis (199, 221-224). As part of this functionality, Anillin binds to Zipper (NMII) when Sqh is phosphorylated and activated (199). Drak-dependent activation of Sqh promotes Anillin binding to Zipper and organization into contractile rings during cytokinesis (206, 208). We observed that phosphorylated Sqh and Anillin co-localize in a Drak-dependent manner at the cleavage furrow in EGFR-PI3K mutant glia undergoing cytokinesis. Similarly, we observed that elevated levels of phosphorylated MRLC, ANLN, and STK17A co-occur in human gliomas, and that these proteins co-localize at the cleavage furrow in EGFR-mutant GBM cells undergoing cytokinesis. Our results suggest that the primary role of Drak/STK17A in neoplastic glia is to promote cytokinesis to drive proliferation.

Two other MRLC kinases, MLCK and ROCK, and two different NMII isoforms, including NMIIA and NMIIB, regulate GBM cell migration (209-211, 219, 220). Previous studies also show that STK17A promotes GBM cell migration *in vitro* (128). Therefore, we did not study STK17A function in tumor cell invasion; instead, given the effects of Drak loss, we focused on Drak/STK17A function in GBM proliferation and cytokinesis. While regulation of cytokinesis in glioma cells is not well understood, our results imply that cytokinesis in glioma cells is differentially regulated relative to normal developing glia or neural stem cells. In other tumor cell types, cytokinesis is preferentially controlled by NMIIC, which is also expressed in GBM cells

(219), and may therefore mediate STK17A function. Further work is needed to determine mechanisms of Drak/STK17A dependent regulation of cytokinesis, and whether defective cytokinesis actively provokes growth arrest and apoptosis in GBM cells.

While Drak overexpression alone causes no phenotype, Drak overexpression intensified the proliferative output of EGFR and PI3K signaling pathways through Sqh. Given that Drak modifies glial EGFR-PI3K-driven neoplasia but does not affect normal glial development, Drak and STK17A may require other signaling outputs downstream of EGFR or PI3K to drive proliferation. This is consistent with known requirements for RTK and PI3K activity in cytokinesis and other NMII-dependent processes (206). For example, previous reports indicate that increased phosphorylation of NMII occurs in GBM cells in response to EGFR signaling (211). Thus, perhaps EGFR-dependent differential phosphorylation and activation of NMII underlies the mechanism by which Drak-Sqh and EGFR cooperate to drive tumorigenesis, and the lack of NMII phosphorylation underlies the inability of Drak to promote glial proliferation when overexpressed alone. Further studies are required to explore mechanisms by which Drak/STK17A cooperates with EGFR activation to promote tumorigenesis.

In summary, our data validate use of invertebrate model organisms as a means to elucidate new aspects of glioma biology. Our research reveals that Drak/STK17A dependency may provide a molecular vulnerability and therapeutically relevant target for GBM and LGG.

2.6 Supplementary Material

Supplemental Table 1: Testing dsRNAs targeting Drak pathway

Table legend: VDRC stock ID numbers prefaced by "v," Bloomington stock ID numbers prefaced by "b." Bold highlights stocks that yielded reproducible genetic interactions and clear phenotypic alterations. Key to genetic interactions: S: moderate suppressor, SS: strong suppressor, WS: weak suppressor; no effect indicates that there were no obvious phenotypic differences between the dsRNA and control animals; nd indicates not determined.

stock ID number	CG number	gene name	*dEGFRλ;dp110^{CAAX}* phenotype	*wild-type* phenotype
v32960	CG32666	Drak	SS	no obvious effect
v107263	CG32666	Drak	SS	no obvious effect
b9909	CG8416	Rho1	SS	no obvious effect
b9910	CG8416	Rho1	SS	no obvious effect
b27727	CG8416	Rho1	SS	no obvious effect
b29002	CG8416	Rho1	SS	no obvious effect
b29003	CG8416	Rho1	SS	semi-lethal
b31542	CG3595	Sqh	SS	no obvious effect
b32439	CG3595	Sqh	SS	no obvious effect
b38222	CG3595	Sqh	S	nd
b32841	CG9366	RhoL	no effect	nd
b33723	CG9366	RhoL	no effect	nd
b28985	CG2248	Rac1	partial suppression	nd
b34910	CG2248	Rac1	no effect	nd
b28021	CG12530	Cdc42	partial suppression	nd
b29004	CG12530	Cdc42	no effect	nd
b35756	CG12530	Cdc42	no effect	nd
b42861	CG12530	Cdc42	no effect	nd
b28797	CG9774	rok	no effect	nd
b34324	CG9774	rok	no effect	nd

Data generated by Renee D. Read

Supplemental Table 2: Screening dsRNAs to target Sqh binding partners

Table legend: VDRC stock ID numbers prefaced by "v," Bloomington stock ID numbers prefaced by "b." Bold highlights stocks that yielded reproducible genetic interactions and clear phenotypic alterations. Key to genetic interactions: WS: weak suppressor, S: moderate suppressor, SS: strong suppressor, WE: weak enhancer, E: moderate enhancer, SE: strong enhancer; no effect indicates that there were no obvious phenotypic differences between the dsRNA and control animals.

stock ID number	CG number	gene name	*dEGFRλ;dp110^{CAAX}* interaction
v6455	CG8098	Picot	no effect
v19696	CG15811	Rop	no effect
v30915	CG11811		no effect
v30917	CG11811		no effect
v31620	CG12021	Patj	no effect
v33465	**CG2092**	**anillin**	**SS**
v40079	CG17492	mib2	no effect
v40101	CG17746		no effect
v40102	CG17746		no effect
v47469	CG17153	ssp	no effect
v100178	CG17746		no effect
v101082	CG8098	Picot	no effect
v101877	CG12021	Patj	no effect
v104674	**CG2092**	**anillin**	**SS**
v106242	CG15811	Rop	no effect
v106301	CG17153	ssp	no effect
v108947	CG17492	mib2	no effect
v110740	CG11811		no effect
b25920	CG8098	Picot	no effect
b26282	CG12021	Patj	no effect
b28929	CG15811	Rop	SS
b29358	CG17153	ssp	no effect
b33347	CG17746		no effect
b35747	CG12021	Patj	no effect
b51925	CG15811	Rop	no effect
b57833	CG17492	mib2	no effect
b53358	**CG2092**	**anillin**	**SS**
b65108	CG11811		no effect

UAS-dsRNA constructs that target published Sqh binding partners were tested in the *repo>dEGFR$^{\lambda}$;dp110^{CAAX}* background. All published binding partners were identified using Flybase database searches (www.Flybase.org). CG11811, CG17746, Picot, Rop, and ssp from Guruharsha et al 2011. Patj from Sen et al 2012. Mib2 from Carrasco-Rando and Ruiz-Gomez 2008. Anillin from D'Avino et al. 2008.

Data generated by Renee D. Read

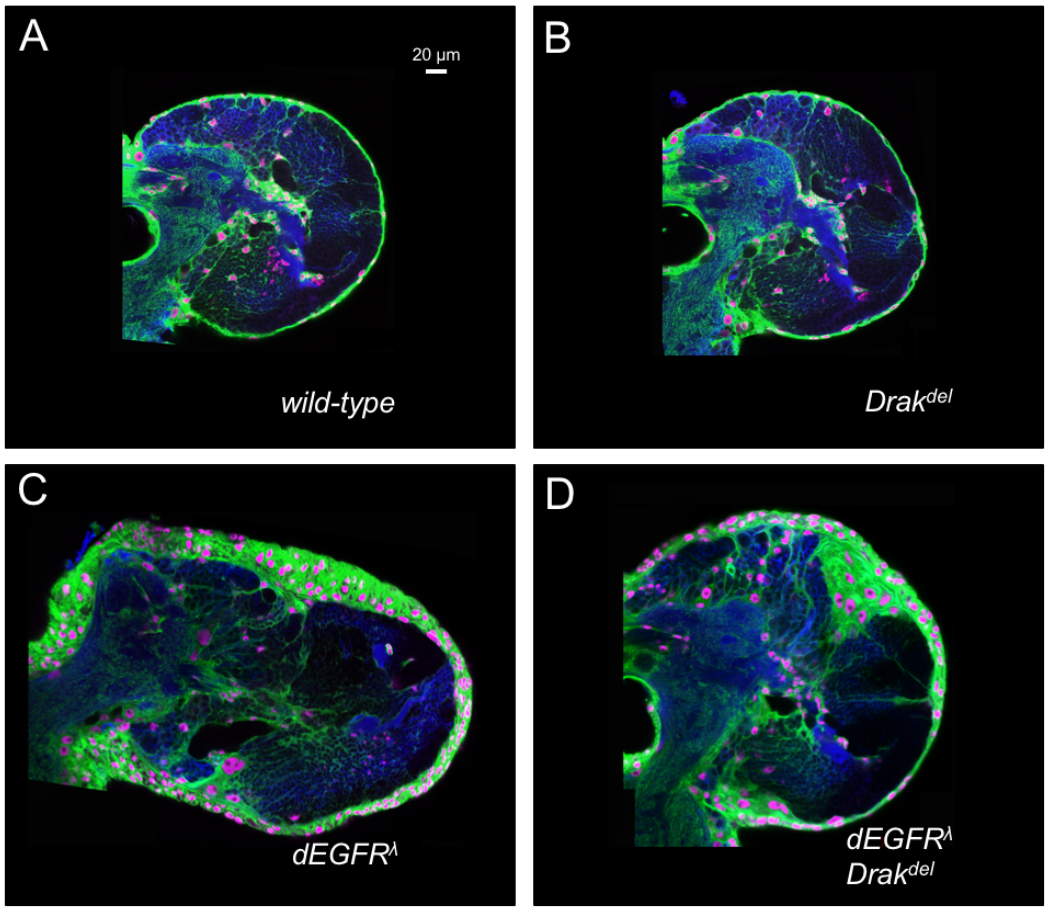

Supplemental Figure S2.1. Loss of *Drak* function suppresses EGFR-dependent glial hyperplasia

(A-D) 3 µm optical projections of brain hemispheres from late 3rd instar larvae approximately 130 hrs old, displayed at the same scale. Frontal sections, midway through brains. Anterior up; midline to left. Glial cell nuclei labeled with Repo (magenta); glial cell bodies labeled with GFP (green, CD8-GFP expressed using the *repo-Gal4* driver). Brains counter-stained with anti-HRP (blue), which reveals neuropil at high intensity and neuronal cell bodies at low intensity. *Drak* loss of function ($Drak^{del}$ null allele, B) had no obvious effect on glial cell morphology or number of glial cells compared to wild-type (A). Overexpression of $dEGFR^{\lambda}$ alone (C) yielded increased glial cells compared to wild-type controls (A). $Drak^{del}$; *repo*>$dEGFR^{\lambda}$ (D) showed reduction of glial hyperplasia compared to *repo*>$dEGFR^{\lambda}$ alone.

Data generated by Renee D. Read.

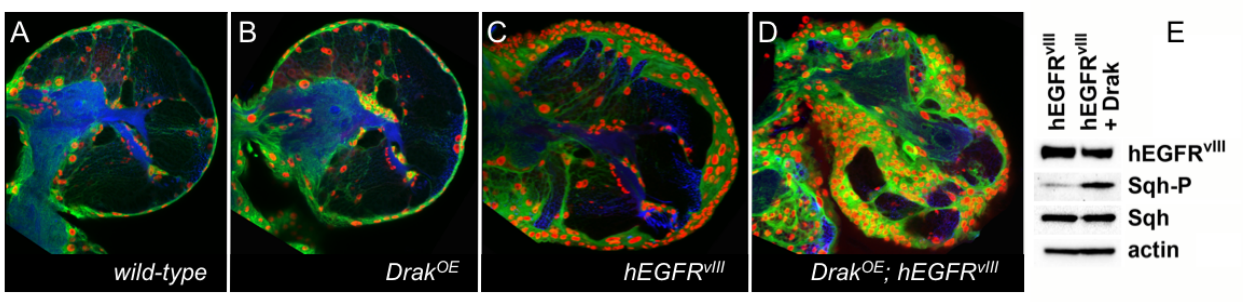

Supplemental Figure S2.2. Drak cooperates with hEGFR^{vIII} to promote glial transformation.

(A-D) 3 µm optical projections of brain hemispheres from late 3rd instar larvae approximately 130 hrs old, displayed at the same scale. Frontal sections, midway through brains. Anterior up; midline to left. Glial cell nuclei labeled with Repo (red); glial cell bodies labeled with CD8-GFP (green). Brains counter-stained with anti-HRP (blue), which reveals neuropil at high intensity and neuronal cell bodies at low intensity. *Drak* overexpression (*Drak^{OE}*) using the *repo-Gal4* driver (B) had no obvious effect on glial cell morphology or number of glial cells compared to wild-type (A). Overexpression of *hEGFR^{vIII}* alone (C) yielded increased glial cells compared to wild-type controls (A). *repo>Drak^{OE};hEGFR^{vIII}* (D) showed increased numbers of abnormal glia (red nuclei, green) as compared to *Drak^{OE}* or *hEGFR^{vIII}* alone, and these excess glia lost the normal stellate shape and created large aggregates of small clustered cells that disrupted normal larval brain architecture and stunted larval brain development as evidenced by the decreased neurons cells present (HRP-stain). (E) Levels of phosphorylated Sqh (Sqh-S19-P) are elevated in *repo>Drak^{OE}; hEGFR^{vIII}* brains compared to *repo>hEGFR^{vIII}* brains.

Data generated by Renee D. Read.

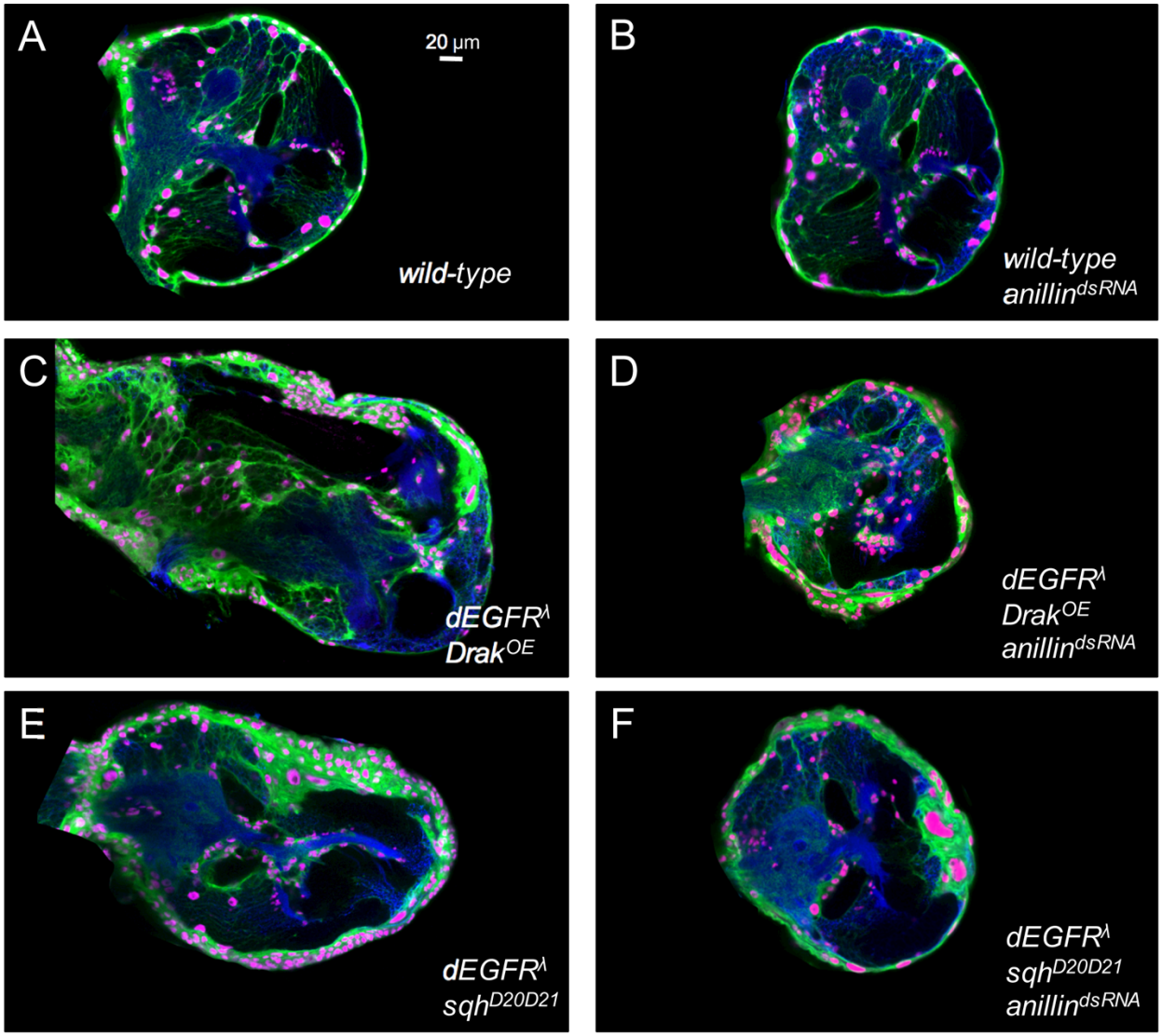
A
20 µm
wild-type
B
wild-type
anillin^dsRNA
C
dEGFR^λ
Drak^OE
D
dEGFR^λ
Drak^OE
anillin^dsRNA
E
dEGFR^λ
sqh^D20D21
F
dEGFR^λ
sqh^D20D21
anillin^dsRNA

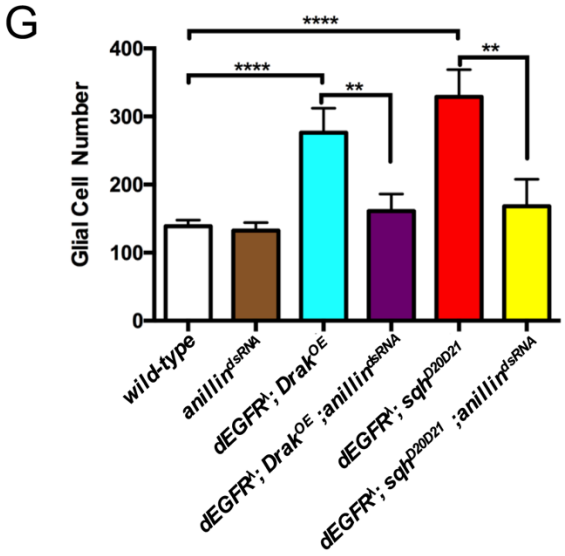
G
Glial Cell Number
400
300
200
100
0
****
****
**
**
wild-type
anillin^dsRNA
dEGFR^λ; Drak^OE
dEGFR^λ; Drak^OE ;anillin^dsRNA
dEGFR^λ; sqh^D20D21
dEGFR^λ; sqh^D20D21 ;anillin^dsRNA

Supplemental Figure S2.3. Anillin operates downstream of the Drak/Sqh pathway to promote glial transformation.

(A-F) 3 μm optical projections of brain hemispheres from late 3rd instar larvae approximately 130 hrs old, displayed at the same scale. Frontal sections, midway through brains. Anterior up; midline to left. Glial cell nuclei labeled with Repo (red); glial cell bodies labeled with CD8-GFP (green). Brains counter-stained with anti-HRP (blue), which reveals neuropil at high intensity and neuronal cell bodies at low intensity. Knockdown of *anillin* using the *repo-Gal4* driver (B) had no obvious effect on glial cell morphology or number of glial cells compared to wild-type (A). *repo>dEGFR$^{\lambda}$;Drak^{OE}* (C) yielded increased glial cells compared to wild-type controls (A). *repo>dEGFR$^{\lambda}$;Drak^{OE};anillin^{dsRNA}* (D) showed a reduction in numbers of abnormal glia (magenta nuclei, green cell bodies) as compared to *repo>dEGFR$^{\lambda}$;Drak^{OE}* (C), and these excess glia lost the normal stellate shape and created aggregates of small cells that disrupted normal larval brain architecture and stunt brain development, as evidenced by the decreased neural tissue present (HRP-stain). *repo>dEGFR$^{\lambda}$;sqh^{D20D21}* (E) yielded increased glial cells compared to wild-type controls (A). *repo>dEGFR$^{\lambda}$;sqh^{D20D21};anillin^{dsRNA}* (F) showed a reduction in numbers of abnormal glia (magenta nuclei, green cell bodies) as compared to *repo>dEGFR$^{\lambda}$;sqh^{D20D21}* (E), and these excess glia lost the normal stellate shape and created large aggregates of small cells that disrupted normal larval brain architecture and stunt brain development as evidenced by the decreased neural tissue present (HRP-stain).

(G) Glial cell numbers in representative 3 μm optical projections of brain hemispheres from late 3rd instar larvae approximately 130 hrs old, matched for section plane; Repo-positive nuclei were counted manually. Statistics generated using One-Way ANOVA with multiple comparisons, ****$p<0.0001$. Statistics comparing glial cell numbers of *wild-type* flies to *anillin^{dsRNA}* flies were

generated using paired parametric T-Tests, n.s: p>0.05. Statistics comparing glial cell numbers of *repo>dEGFR$^{\lambda}$;Drak^{OE}* flies to *repo>dEGFR$^{\lambda}$;Drak^{OE};anillin^{dsRNA},* and *repo>dEGFR$^{\lambda}$;sqh^{D20D21}* flies to *repo>dEGFR$^{\lambda}$;sqh^{D20D21};anillin^{dsRNA}* were generated using paired parametric T-Tests, **p<0.01 (four larval brains were counted for each condition).

Data generated by Alexander S. Chen.

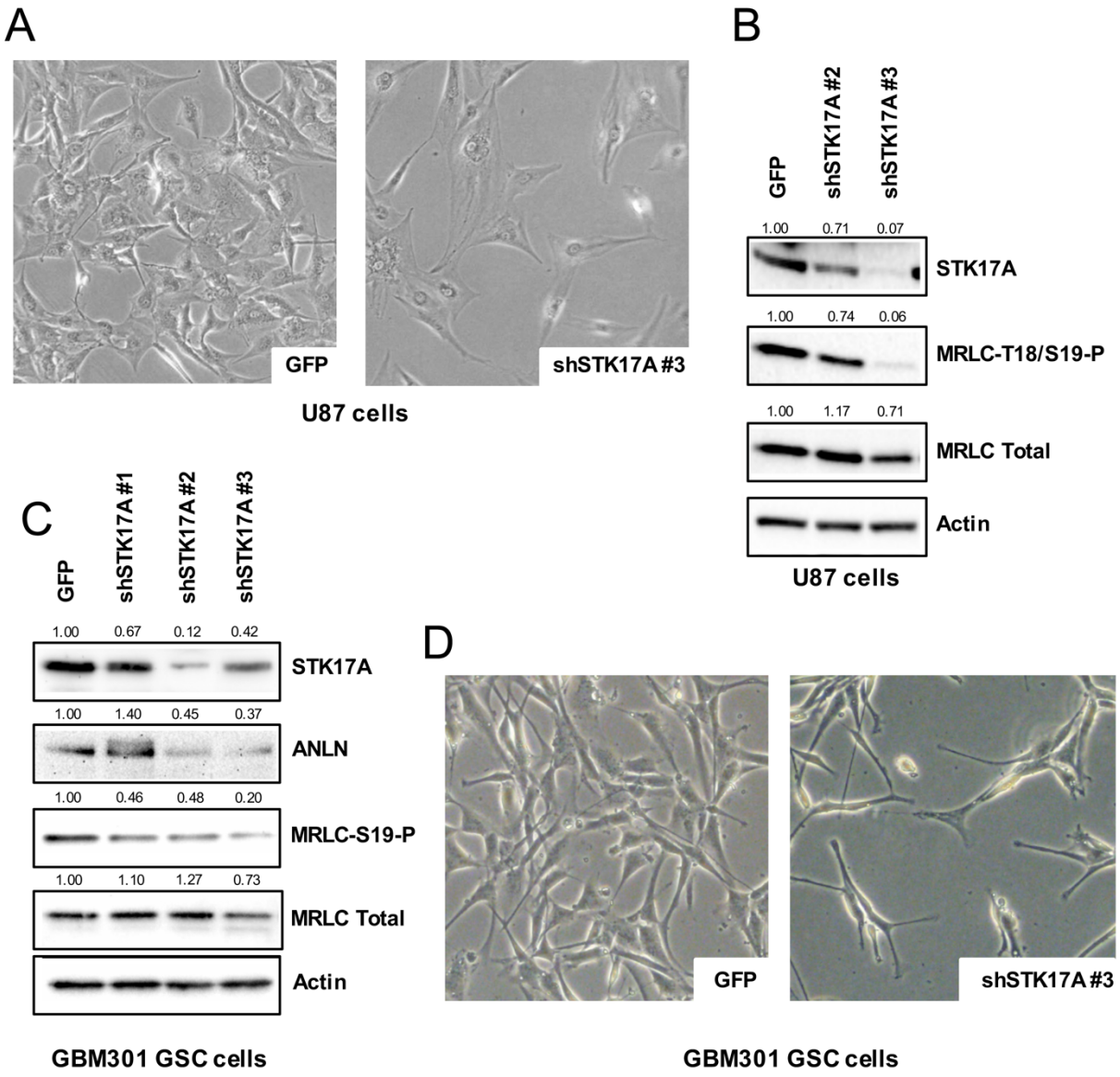

Supplemental Figure S2.4. Knockdown of STK17A in GBM cells showed a decrease in proliferation and MRLC-S19-P levels.

(A) Following selection for shRNA expression, U87 cells show reduced proliferation upon Stk17A knockdown. Cells were infected with lentiviral vectors, wither either control lentivirus or STK17A shRNAs, 3 days prior to selection for 2 days with puromycin.

(B) Knockdown of STK17A using 2 separate shRNAs in U87 cells decreased expression levels of MRLC-S19-P compared to control cells treated with GFP shRNAs, cells not treated with ZVAD.

Band intensities were normalized to Actin (numbers above each band), and band intensities were reported as fold changes relative to control cells treated with GFP shRNA.

(C) Knockdown of STK17A using 3 separate shRNAs in GBM301 cells decreased expression levels of ANLN and MRLC-S19-P compared to control cells treated with GFP shRNAs, cells not treated with ZVAD. Cells were infected with lentiviral vectors 3 days prior to harvest. Band intensities were normalized to Actin (numbers above each band), and band intensities were reported as fold changes relative to control cells treated with GFP shRNA.

(D) Adherently cultured GBM301 cells harvested 3 days after infection with either control lentivirus or shSTK17A#1. GBM301 cells showed reduced proliferation, altered cell shape, and reduced adhesion. GBM301 cells were not treated with ZVAD.

Data generated by Renee D. Read.

A **B**

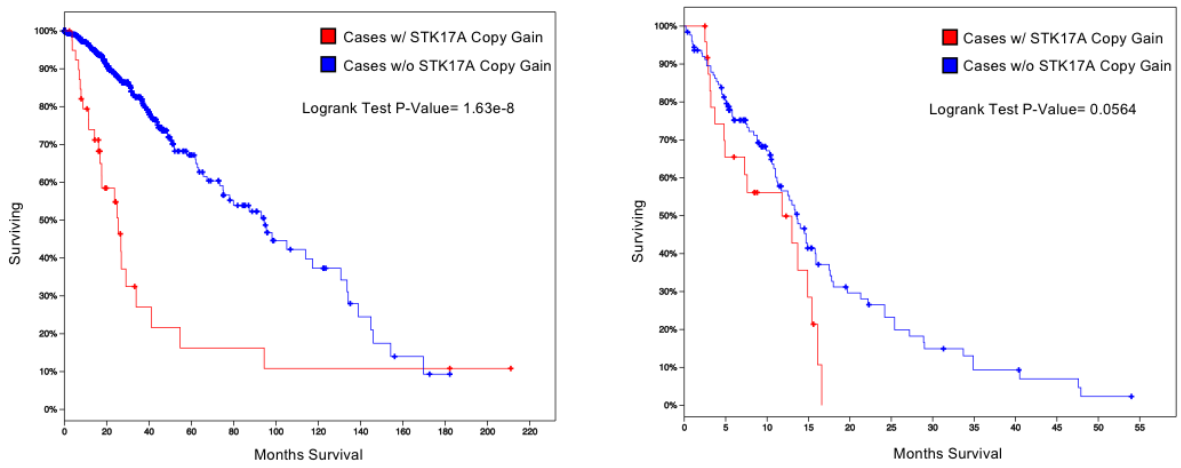

Supplemental Figure S2.5. *STK17A* is overexpressed in gliomas

(A) Overall survival of LGG TCGA cases with *STK17A* copy gain (z-score threshold of +/- 2) compared to cases without *STK17A* copy gain. 513 cases were analyzed and the overall survival was depicted as Kaplan-Meier curves. Cases with *STK17A* copy gain showed a worse prognosis compared to cases with no *STK17A* copy gain (Logrank Test P-Value= 1.63e-8).

(B) Overall survival of GBM TCGA cases (*Cell,* 2013 cohort) with *STK17A* copy gain (z-score threshold of +/- 2) compared to cases without *STK17A* copy gain. 151 cases were analyzed and the overall survival was depicted as Kaplan-Meier curves. Cases with *STK17A* copy gain showed a worse prognosis compared to cases with no *STK17A* copy gain, but was not statistically significant (Logrank Test P-Value= 0.0564).

Data generated by Alexander S. Chen.

Chapter 3. RIOK2-IMP3-TORC2 complex drives neoplastic glial proliferation through modulation of MYC

Alexander S. Chen, Jhomar Marquez, Nathaniel H. Boyd, Se-Yeong Oh, Riley Gulbronson, Jamie A.G. Hamilton, Emily R. Legan, and Renee D. Read.

3.1 Abstract

Glioblastoma multiforme (GBM) is the most common primary malignant brain tumor and is resistant to current therapies. Here, using a combination of proteomic and genetic approaches in both *Drosophila* and human GBM models, we identify novel signaling effectors that act downstream of EGFR and PI3K signaling pathways, which drive GBM. Our results indicate that RIOK2, an atypical serine/threonine kinase, forms a complex with the RNA-binding protein, IMP3 (Imp in *Drosophila*), and that the dRIOK2/RIOK-Imp/IMP3 pathway is necessary for tumorigenesis. Furthermore, our results indicate that RIOK2 catalytic activity is important for neoplasia and recruits TORC2 to phosphorylate IMP3. Finally, the dRIOK2-Imp pathway regulates protein levels of dMyc, a known Imp target mRNA, and these key findings were recapitulated in human GBM models. Collectively, our data indicates that RIOK2 catalytic activity promotes the activation of TORC2 and recruitment of IMP3, which in turn, modulates MYC mRNA and protein levels to promote tumorigenesis.

3.2 Introduction

Glioblastoma multiforme (GBM), which is classified by the World Health Organization Classification System as grade IV neoplasms (2), is the most common adult primary malignant brain tumor. GBM originates from glia and glial progenitor cells and characteristically shows rapid cell proliferation and extensive brain infiltration. With current treatment, surgery followed by radiation and temozolomide therapy, the median survival for GBM patients remains poor at 12-15 months (225). To better understand the basic biology of GBM in order to develop improved treatments for this disease, a concerted effort has been made to genomically characterize mutations in GBM and to understand the biological mechanisms by which these mutations drive tumorigenesis.

Genomic analyses reveal that common genetic lesions in GBM alter receptor tyrosine kinase/RAS/phosphatidylinositol-3 kinase (RTK/RAS/PI3K) signaling pathways, occurring in 88% of GBMs (7). The RTK Epidermal Growth Factor Receptor (EGFR) is amplified in 40-50% of GBM cases and is typically subject to gain-of-function mutations (7, 215), the most common of which is $EGFR^{vIII}$ (191), leading to constitutive activation of the kinase which conveys proliferative and survival advantages (188, 192). Both wild-type EGFR and $EGFR^{vIII}$ signal through the PI3K pathway, which is commonly dysregulated in GBM (226). Genetic lesions that activate components of the PI3K pathway typically occur in 90% of GBMs (7), often as a consequence of inactivating mutations in PTEN phosphatase or activating mutations in PIK3CA and PIK3R1 (7), resulting in constitutive activation of PI3K signaling. To understand how these mutations specifically drive initiation and progression of GBM, there is a need to identify novel biological processes activated downstream of EGFR-PI3K signaling in glia. Through

understanding novel mechanisms and new factors involved in GBM, we hope to uncover new potential therapeutic targets that may be used to develop new treatments for GBM patients.

To identify and investigate new downstream effectors of the EGFR-PI3K signaling pathways, we utilized a *Drosophila* GBM model (49). *Drosophila melanogaster* have several advantages as a model for neurologic cancers. *Drosophila* have a fully sequenced and annotated genome, versatile tools to allow for *in vivo* cell-type specific gene manipulation, and *Drosophila* neural and glial cell types are homologous to human neurons and glial cells (32-36, 196). Furthermore, *Drosophila* have functional orthologs for approximately 75% of human genes including many involved in gliomagenesis (37, 195). In *Drosophila*, co-overexpression of constitutively active forms of EGFR and PI3K in glial progenitor cells produces invasive malignant neoplastic tumors that recapitulate key aspects of human GBM, including a reliance on gliomagenic core kinases like mTor and transcription factors like dMyc to drive tumorigenesis (49).

Using genetic screens in our *Drosophila* GBM models, our lab previously found that right open reading frame kinase 2 (RIOK2) is required for EGFR-PI3K-dependent glial tumorigenesis (50). RIOK2 belongs to the RIO family of proteins, which are conserved evolutionarily in organisms from *Archaea* to humans (133), comprised of at least four members (RIOK1, RIOK2, RIOK3, and RIOKB), and defined by the presence of a RIO kinase domain (133). RIO family members are considered atypical protein kinases in that the RIO kinase domain has sequence similarity to eukaryotic protein kinases (133, 227) but lacks the activation loop and substrate binding domains found in traditional eukaryotic protein kinases (133). Studies have shown that RIOK2 has functionally distinct roles in processing 18s rRNA and assembly and maturation of the 40S ribosomal subunit (144, 146, 228, 229). In GBM tumor cells, RIOK2,

which is overexpressed in EGFR amplified/mutant GBM cells, is upregulated in response to AKT activation downstream of EGFR signaling, and RIOK2 binds to and activates the mTOR complex 2 (TORC2), which in turn, phosphorylates AKT and maintains AKT activation to drive tumorigenesis (50). However, other downstream effectors of RIOK2 in tumorigenesis are unknown.

In this manuscript, we show that RIOK2 promotes GBM tumorigenesis in a novel mechanism apart from RIOK2's known function in ribosome assembly by interacting with the RNA-binding protein, IGF2BP3 (IMP3). IMP3 belongs to the IGF2BP family of RNA-binding proteins, consisting of IMP1, IMP2, and IMP3, which are characterized by two N-terminal RNA-recognition motifs (RRMs) and four C-terminal hnRNP-K homology (KH) domains (160). IMP3, like other members of the IGF2BP family, regulates the localization, stability, and translation of cytoplasmic target mRNAs (160, 172). IMP3 is considered an oncofetal protein, in that IMP3 is normally highly expressed during embryogenesis and sparingly expressed in adult tissue, but is highly expressed in cancers (160). IMP3 expression acts as a biomarker for high-grade disease and poor prognosis in cancer patients, including GBM patients (172, 174, 230). Furthermore, studies show that IMP3 binds to and regulates mRNA of several well-established drivers of gliomagenesis including IGF2 and MYC (172, 174, 177). Our data here reveal that RIOK2 promotes GBM tumorigenesis by forming a complex with IMP3 to mediate phosphorylation of IMP3 by TORC2 to modulate MYC protein levels.

3.3 Materials and Methods

Drosophila Strains and culture conditions

Drosophila stocks were obtained from the Bloomington stock center and VDRC : *UAS-Imp^{dsRNA}* (Bloomington #34977, VDRC #20321, VDRC #20322); *UAS-RIOK2^{dsRNA}* (VDRC #404701) ; *UAS-dMyc^{dsRNA}* (VDRC #2948). *UAS-dRIOK2^{WT}* and *UAS-dRIOK2^{KD}* transgenic *Drosophila* were created by BestGene Inc., and isogeneous stocks were bred for experimental use. Drosophila GBM models were previously established and crosses to create tumorous larval brains were performed as described (50). All stocks were cultured on standard corn meal molasses food at 25°C. All genotypes were established by standard genetic crossing.

Cloning

The *Drosophila* dRIOK2 MIP10156 cDNA was purchased from the *Drosophila* Genomics Resource Center and cloned into pUAS-T using standard techniques. Human RIOK2-flag cDNAs encoding isoform I (Origene) were cloned into pRev-Tre tetracycline inducible vectors (Clontech). Kinase dead (KD) versions of *Drosophila* and human RIOK2 (dRIOK2^{KD}, RIOK2^{KD}) were created using site directed mutagenesis (Lightning Quick Change Kit, Agilent) to make alanine substitutions at catalytic residues Lys-123 and Asp-246 in both human RIOK2 and dRIOK2 as described by other groups (146, 228).

Immunohistochemistry and Imaging

Larval brains were dissected with forceps, fixed in 4% paraformaldehyde, processed, stained, and imaged as previously described (49). The following antibodies were used: 8D12 mouse anti-Repo (1:10, Developmental Studies Hybridoma Bank), anti-dMyc (1:25,

Developmental Studies Hybridoma Bank), or anti-Imp (1:500, a gift from Paul MacDonald, (231)). Secondary antibodies were conjugated to Cy3, Alexa-488, or Alexa-647 (1:100-250, Jackson Laboratories). Brains were mounted on glass slides ventral side down in vectashield and whole mount imaged on a Zeiss LSM 700 confocal system. For experiments where protein levels were compared between genotypes, all samples were prepared, subjected to immunohistochemistry, imaged, and image processed in a parallel manner side by side. 6 or more brains were stained with each Ab combination, and representative images are shown for each result. All brain phenotypes shown were highly penetrant, with approximately 75-100% of animals showing the growth phenotypes described. Images were analyzed in Zeiss Zen Software and processed in Photoshop. For larval brains probed with anti-dMyc, to reduce particulate background from the antibody, a median filter setting as used for the Cy3 channel with a kernel size set at 5 across all genotypes. Larval *Drosophila* brain hemisphere volumes were analyzed using Imaris software. Larval glial cells were counted manually in representative optical sections of age-matched brain hemispheres, matched for section plane. Statistical analyses were done using Prism.

Mammalian tissue culture

GBM39, generously shared by C. David James, was created from human GBMs serially xenografted. GBM725, GBM730, GBM914, GBM131, GBM56, and GBM1219 neurosphere cultures were created from GBM surgical specimens collected at Emory University and maintained in culture as described (88). Human tumor specimens were collected from surgical specimens donated for research with written informed consent of patients and were collected and used according to recognized ethical guidelines (Declaration of Helsinki, CIOMS, Belmont

Report, GCP, Nuremberg Code) in a protocol (IRB00045732) approved by the Institutional Review Board at Emory University. HNPCs were obtained from Lonza. U87 and U87-EGFR^{vIII} cells were gifts of Frank Furnari. Cell culture was performed as previously described (50).

Lentiviral shRNAs for RIOK2 and IMP3 (Sigma, MISSION shRNA, TRCN0000197250, TRCN0000074675, TRCN0000074675) were transfected with packaging vectors in 293 cells using Lipofectamine 3000 reagent (Thermofisher), and viral supernatant was isolated and used to infect GBM cells. For lentiviral infection, adherently plated cells were incubated with lentiviral supernatant for 6-8 hours with polybrene to enhance viral entry. Adherent neurospheres were plated in serum-free media with Geltrex (Thermofisher) or Laminin (Sigma); and adherent U87 cells plated in 10% FBS. After infection, viral media was replaced with fresh media with zVAD caspase inhibitor if indicated, and cells were incubated for 72-96 hours prior to harvest.

U87 cells with doxycycline-inducible wild-type RIOK2 (Rev-Tre-RIOK2^{WT}) or kinase-dead RIOK2 (Rev-Tre RIOK2^{KD}) or empty vector (Rev-Tre alone) were created from cells engineered with the Tet3G tetracycline responsive transcriptional inducer (Clontech). Prior to collection for experiments, RIOK2 expression vectors were induced with 8 μg/ml of doxycycline and incubated for 48 or 72 hours. WST-1 assays were performed as per manufacturer's instructions (Takara) (50).

For immunofluorescence, U87-EGFR^{vIII} cells were grown on glass coverslips, fixed with 4% paraformaldehyde, and stained on the coverslips with anti-IMP3 (1:100, DAKO, clone 69.1), anti-RIOK2 (1:100, Sigma HPA005681), and DRAQ7 (1:200, Cell Signaling Technology) to stain nuclear DNA and chromosomes.

Sucrose gradient analytical fractionation for ribosome biogenesis

Ribosome profiling analysis was performed using a previously published protocol adapted for GBM cultures (232). GBM cells were cultured as described above, and to prevent apoptosis 20 μM zVAD was added for 48 hrs prior to harvest. For sucrose density gradient fractionation, hypotonic lysis (5 mM Tris pH 7.5, 2.5 mM $MgCl_2$, 1.5 mM KCl, 0.1% Triton-X100 with protease and phosphatase inhibitors) was performed on 8-10 million GBM cells per experimental sample. Briefly, cells were treated with cyclohexamide and RNAseOUT (Sigma) to block translation elongation to fix ribosomes and ribosomal subunits on RNAs. Following preparation of hypotonic supernatants, the OD260 of each sample was measured (NanoDrop, ThermoFisher), and, based on OD readings, equivalent amounts of ribosomes for each lysate was loaded onto each 10%-45% sucrose density gradient (BioComp Gradient Master machine) for ultracentrifugation at 33,000 rpm for 5 hours (Beckman Optima L80K Ultracentrifuge, SW41Ti rotor). For optimal detection of ribosomes, 4-10 ODs were used per experiment, with the same ODs loaded for each control and experiments per experiment. 10% of total cell lysate was saved as an input control. Fractions were isolated and measured using a Brandel density gradient fractionator system with a UV detector, fraction collector, and chart recorder (Teledyne ISCO), and UV absorbance was recorded and analyzed with the TracerDAQ software system (MicroDAQ). Fractions were concentrated using centrifugal filters, and analyzed by western blot for protein composition.

Immunoprecipitations

For immunoprecipitations used for proteomics analysis, either 2 million GBM301 cells or 5 x 10^5 U87 cells were lysed with hypotonic lysis buffer. 10% of the cell lysate was saved as input controls. For GBM301 and U87 cells, 10 μg of anti-RIOK2 (1:1000, Sigma, HPA005681),

or a non-specific IgG were conjugated to magnetic beads according to supplier recommendations (BIORAD, SureBeads, Protein A magnetic beads, 161-4013). In order to ensure equal amounts of protein was used for both conditions, cells were pooled and equal amounts of the pooled cells were added to each IP condition. For U87 overexpressing RIOK2 constructs, 50 μl of anti-FLAG M2 magnetic beads (Sigma, M8823) was used. In order to ensure equal amount of protein was used per IP, cell lysates were quantified and equal amount of protein was added to each IP condition. Samples were incubated for 8 hours with end-over-end rotation at 4°C and washed five times with washing buffer (5 mM Tris pH 7.5, 2.5 mM $MgCl_2$, 1.5 mM KCl). Samples were submitted to the Emory Integrated Proteomics Core for total proteomic processing according to published procedures (233). Samples for phospho-peptide mapping were submitted to the Taplin Mass Spectrometry Facility (Harvard University)

For protein-protein interactions, 2 million GBM39 cells were used per conditions and were lysed in hypotonic lysis buffer (5 mM Tris pH 7.5, 2.5 mM $MgCl_2$, 1.5 mM KCl) with protease and phosphatase inhibitors as above. 10% of the cell lysis was saved as input controls. 10 μg of either anti-IMP3 (Cell Signaling 57145), anti-RIOK2 (1:1000, Sigma, HPA005681), or a non-specific IgG were conjugated to magnetic beads according to supplier recommendations (BIORAD, SureBeads, Protein A magnetic beads, 161-4013). In order to ensure equal amounts of protein was used for both conditions, cells were pooled and equal amounts of the pooled cells were added to each IP condition. Samples were incubated for 4 hours with end-over-end rotation at 4°C and washed five times with washing buffer (150 mM NaCl, 10 mM HEPES, 1 mM EGTA, 0.1 mM $MgCl_2$, pH 7.4, and 0.1% Triton-X100). Beads were then incubated in 1X LDS sample buffer at 70°C for 10 min and analyzed using Western blot.

In vitro immunoprecipitations were prepared using 0.012 μg of recombinant RIOK2 protein and 0.012 μg of recombinant IMP3 protein in hypotonic lysis buffer (5 mM Tris, 2.5 mM $MgCl_2$, 1.5 mM KCl) with 0.1 mg/ml of Bovine Serum Albumin (BSA) as a competitor. 10 μg of anti-RIOK2 (1:1000, Sigma, HPA005681) or a non-specific IgG were conjugated to magnetic beads according to supplier recommendations (BIORAD, SureBeads, Protein A magnetic beads, 161-4013). Samples were incubated for 4 hours with end-over-end rotation at 4°C and washed five times with washing buffer (150 mM NaCl, 10 mM HEPES, 1 mM EGTA, 0.1 mM $MgCl_2$, pH 7.4, and 0.1% Triton-X100). Beads were then incubated in 1X LDS sample buffer at 70°C for 10 min and analyzed using Western blot.

For U87 immunoprecipitations for tetracycline inducible systems, 5 x 10^5 cells were plated for each condition and treated with 8 μg/ml of doxycycline for 72 hours. Cells were lysed in hypotonic lysis buffer, and 10% of total cell lysate was saved as an input control. The remaining cell lysate was quantified, and equal amounts were added to 50 μl of anti-FLAG M2 magnetic beads (Sigma, M8823) and incubated for 4 hours with end-over-end rotation at 4°C and washed five times with washing buffer (150 mM NaCl, 10 mM HEPES, 1 mM EGTA, 0.1 mM $MgCl_2$, pH 7.4, and 0.1% Triton-X100). Beads were then incubated in 1X LDS sample buffer at 70°C for 10 min and analyzed using Western blot.

Crosslinking Immunoprecipitations

Approximately 3 million GBM39 cells were used per condition. The crosslinking immunoprecipitation was ran according to Zlatic *et al* (234). 10 μg of anti-RIOK2 (1:1000, Sigma, HPA005681), anti-IMP3 (Cell Signaling 57145), or a non-specific IgG were conjugated to magnetic beads according to supplier recommendations (BIORAD, SureBeads, Protein A

magnetic beads, 161-4013). Following washes, beads were then incubated in 1X LDS sample buffer at 70°C for 10 min and analyzed using Western blot.

***In vitro* Kinase Assay**

10 µl reactions containing 1 µg of purified recombinant protein 1 µCi γ-[^{32}P] ATP in 50 mM Tris/HCl, pH 7.6, 200 mM NaCl, and 5 mM $MgCl_2$ (Kinase Buffer) were incubated at 37°C for 1 hour. Samples were then immunoprecipitated for 4 hours with end-over-end rotation at 4°C using magnetic beads conjugated with anti-IMP3 (Cell Signaling 57145) according to supplier recommendations (BIORAD, SureBeads, Protein A magnetic beads, 161-4013). Samples were washed five times with kinase buffer. Beads were then incubated in 1X LDS sample buffer at 70°C for 10 min and analyzed using phosphoimager.

Western Blot Analysis

The following antibodies were used for immunoblotting following the manufacturer's recommendations: anti-RIOK2 (1:1000, Sigma HPA005681; 1:1000, Origene Clone OTI3E11), anti-IMP3 (1:1000, Cell Signaling 57145; 1:1000, DAKO clone 69.1), anti-mTOR (1:1000, Cell Signaling 4517), anti-MYC (1:1000, Cell Signaling clones D3N8F and E5Q6W), anti-NOB1 (1:1000, Origene TA808793 clone OTI1C12), anti-phospho-Ser/Thr-Pro MPM-2 (1:500, Millipore-Sigma 05-368), and anti-actin (1:200, Developmental Studies Hybridoma Bank JLA20).

***in silico* Analysis**

Patient RNAseq data from The Cancer Genome Atlas (TCGA) was downloaded using Gliovis (235) (gliovis.bioinfo.cnio.es) and XY correlations were performed between *RIOK2*, *IMP3*, *MYC*, and *mTOR* mRNA expression (data from 528 GBM patients), as well as mRNA expression of *RIOK2* and *IMP3* by tumor grade (data from 620 glioma patients). Copy number analysis for *EGFR* and comparison with *IMP3* mRNA expression was performed using cBioportal (data from 201 patients).

RNA-binding Protein Immunoprecipitation

RNA-binding protein immunoprecipitation was run according to supplier recommendations (Millipore, Magna RIP Kit, 17-700). Beads were conjugated with 10 μg either anti-IMP3 (#1: MBL, RN009P, #2: Cell Signaling, 57145) or non-specific IgG. cDNA was generated from IPed RNA, PCRed with primers against MYC, and the PCR results were analyzed using DNA gel electrophoresis.

Statistical analyses

Larval brain volumes were analyzed using one-way ANOVA with multiple comparisons. Larval glial cell numbers were analyzed using two-tailed parametric T-Tests. WST-1 data was analyzed using two-tailed parametric T-Tests. TCGA microarray data analysis was downloaded and graphed using Graphpad Prism. Correlative data was analyzed using linear regression, and the slope and P value are reported as calculated from an F test that answers the question "is the slope significantly non-zero?" Tumor grade data and copy number analysis was analyzed using one-way ANOVA with multiple comparisons and are reported using p values. Comparisons between two groups were done using two-tailed parametric T-Tests.

3.4 Results

RIOK2 knockdown does not dramatically affect ribosome assembly in GBM cells

In human and yeast cells, RIOK2 kinases, which are not functionally redundant with other RIO kinases, promote assembly of the 40S ribosome subunit, and loss of RIOK2 function can decrease ribosome biogenesis (144, 146, 147, 228, 229, 236). We and others have observed that, in both *Drosophila* and human cells, RIOK2 RNAi can trigger dp53/P53 activation (50, 237). P53 transcriptional activation can occur as a result of the P53-dependent ribosome stress response, which is triggered by defects in ribosome biogenesis (238, 239). Thus, we hypothesized that, in GBM cells, RIOK2 loss or inhibition impairs ribosome biogenesis. In our cell-based GBM models, we performed sucrose gradient density analytical fractionation to characterize ribosome assembly defects caused by RIOK2 RNAi. Cells were treated with *RIOK2* shRNAi constructs combined with zVAD caspase inhibitor to block apoptosis, and lysed in hypotonic conditions so as to preserve cytoplasmic RNA macromolecules. Surprisingly, over 10 repeat experiments in three different cell types (2 EGFR mutant GBM stem cell cultures, U87 cell models), cells with efficient RIOK2 knockdown showed minor reductions in levels of the 40S and 60S ribosome subunit relative to monosomes as compared to control cells, and these changes were not consistent with significantly reduced ribosome assembly observed in other cell types upon RIOK2 loss (Figure S3.1A) (146). Of note, we observed that with RIOK2 knockdown sufficient for GBM cell growth arrest and apoptosis, residual RIOK2 protein was present in 40S subunit fractions (Figure S3.1B): this residual RIOK2 protein was likely sufficient for sustained ribosome biogenesis. Previous studies and our results (see below) suggest that catalytically inactive RIOK2 ($RIOK2^{KD}$) acts as a dominant negative when overexpressed,

although overexpression of RIOK2^{KD} also did not induce ribosome biogenesis defects (Figure S3.2A). Thus, our results indicate that reduced RIOK2 function does not primarily block tumor cell survival or growth through reduced ribosome biogenesis.

In these experiments, we examined ribosome fractions from GBM cells for other changes induced by RIOK2 knockdown. Prior studies show that TORC2 phosphorylates substrates in association with ribosomes, albeit independently of TORC2 assembly (240, 241). Because phosphorylation of TORC2 substrates is reduced by RIOK2 RNAi, we wondered if RIOK2 loss altered TORC2 association with ribosomes. We found that, upon RIOK2 knockdown, defining TORC2 components RICTOR and mTOR no longer co-fractionate with immature or mature ribosomes (Figure S3.1B). Thus, without substantially impacting ribosome assembly, RIOK2 knockdown impairs mTORC2 complex assembly, and thereby reduce mTORC2 activation (50). However, these data do not provide mechanistic insight into how RIOK2 modulates mTOR. While RIOK2 protein is predominantly associated with the 40S subunit peak in (Figure S3.1B), overexpressed cytoplasmic RIOK2 protein in GBM cells may acquire previously undescribed functions that impact TORC2.

Together with our published data showing a requirement for RIOK2 in EGFR mutant GBM cells (50), these results suggest that RIOK2 loss or inhibition affects other, as yet undiscovered, cellular processes in GBM.

IMP3 is an effector of RIOK2

To understand the mechanisms by which RIOK2 promotes GBM cell growth and survival, we performed immunoprecipitation (IP) experiments on endogenous and flag-epitope-tagged RIOK2 protein to identify novel binding partners. IP experiments were carried out in

RIOK2-dependent EGFR-PTEN-mutant GBM cells (U87-EGFR^{vIII} cells, GBM301 EGFR^{vIII} cells) under hypotonic lysis conditions to enrich for cytoplasmic RIOK2 and its binding partners. Controls were nonspecific rabbit IgG IPs and empty anti-flag IPs. Immunoprecipitation experiments were performed three times, and proteins associated with RIOK2 were proteomically profiled using mass spectrometry (Emory Integrated Proteomics Core) (242, 243). Datasets were compared and RIOK2 binding partners were identified that eluted with both endogenous RIOK2 and epitope-tagged RIOK2 to control for antibody-specific artifacts. Potentially significant RIOK2 binding partners reproducibly met three important criteria: 1) 2-fold or greater enrichment in RIOK2-specific IPs compared to either non-specific controls, 2) more than three spectral counts, and 3) contained 2 identified peptides.

We identified several well established RIOK2 binding proteins, including several ribosome assembly factors, including TSR1, LTV1, NOB1, and PNO1 (Figure 3.1A, Table S3.1), which validates our technique (244). Furthermore, we identified several novel RIOK2 binding proteins, almost all of which were RNA-binding proteins (RBPs). The identified RBPs include IMP3, G3BP1, ATXN2L, ILF3, and others (Figure 3.1A, Table S3.1), which have described primary functions in mRNA stability, transport, and translation (160). Several of these RBPs co-fractionate with RIOK2, each other, and with RBP-mRNA complexes in published studies (245, 246), increasing our confidence that they were legitimate RIOK2 partners. In our dataset, the RBP, IMP3 (also known as IGF2BP3), is a particularly interesting novel RIOK2 binding partner due to its previously described role in cancers, including GBM, where it is a biomarker for high-grade disease and poor patient prognosis (174).

To follow-up on our proteomics analysis, we identified RIOK2 partners with *Drosophila* orthologs (Table S3.1). We then assessed the physiological relevance of these proteomic hits

using an unbiased RNAi screen in our *Drosophila* GBM model in which glial-specific co-overexpression of constitutively active EGFR (*dEGFR*$^{\lambda}$) and PI3K (*dp110*^{CAAX}) orthologs causes glial neoplasia (Table S3.2). The rationale being that tumor-specific functionality of RIOK2 and its partners should be conserved between *Drosophila* and human GBM models, and that genetic analysis of the RIOK2 pathway could be done rapidly and economically in *Drosophila* (50). Corresponding RNAi constructs for *Drosophila* orthologs of these proteins were obtained from public sources and were tested *in vivo* in normal *Drosophila* glia and in neoplastic glia in our *repo>dEGFR*$^{\lambda}$*; dp110*^{CAAX} *Drosophila* GBM model as described (50) (Table S3.2). We found that glial-specific RNAi of ribosome assembly factors and essential RBPs significantly impaired growth and proliferation of both neoplastic and normal glia (Table S3.2, Figure S3.3). In contrast, glial-specific RNAi of Imp, the sole IMP3 ortholog (247), significantly blocked growth and survival of neoplastic glia but had no detectable effect on the growth and survival of normal glia. Thus, Imp knockdown phenocopies the effects of dRIOK2 knockdown and catalytic inhibition in our *Drosophila* models (50) (see below), which suggests that Imp functions with dRIOK2 in a conserved pathway.

To understand the mode of interaction between RIOK2 and IMP3 in GBM, we confirmed RIOK2-IMP3 binding with reciprocal IPs of endogenous IMP3 in EGFR^{vIII} mutant RIOK2-dependent patient-derived GBM stem cells (GBM39) and confirmed by western blot that RIOK2 was pulled down (Figure 3.1B). In contrast, while control normal human neural progenitor/stem cells (HNPCs) express both IMP3 and RIOK2, but IMP3 was not associated with RIOK2 by co-IP (Figure 3.1C). This suggests that the interaction between RIOK2 and IMP3 is enriched in tumor cells. Of note, ribosome assembly factors such as NOB1 were not detected in the RIOK2-IMP3 IPs from GBM cells, suggesting that the RIOK2-IMP3 complex is distinct from the

RIOK2-ribosome assembly factor complexes (Figure 3.1B). Thus, RIOK2 may have novel functions independent of ribosome assembly.

Next, in order to determine whether RIOK2 and IMP3 directly bind each other, we performed *in vitro* co-IPs with purified recombinant RIOK2 and IMP3. We observed co-IP of both IMP3 and RIOK2 with each other, indicating that RIOK2 and IMP3 form a direct interaction (Figure 3.1D). Thus, collectively, our data show that IMP3 is a bona fide direct binding partner of RIOK2 that may drive GBM tumorigenesis through a novel mechanism outside of well-established RIOK2 function in ribosome assembly.

A

human protein	IP: IgG Control (Spectral Counts)	IP: RIOK2 (Spectral Counts)	IP: IgG Control (Number of Unique Peptides)	IP: RIOK2 (Number of Unique Peptides)
RIOK2	0	22	0	11
IMP3	0	8	0	6
G3BP2	0	8	0	6
ATXN2L	2	8	1	6
ILF3	0	13	0	11
TSR1	0	30	0	22
LTV1	0	21	0	13
NOB1	0	12	0	9
PNO1	0	18	0	7

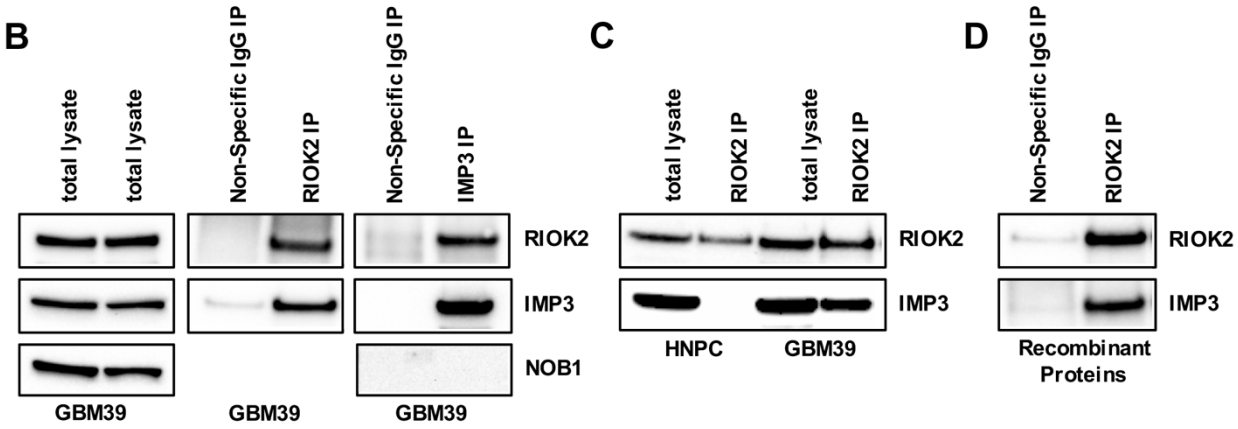

Figure 3.1. IMP3 is a binding partner and downstream effector of RIOK2.

(A) Proteomic Analysis of RIOK2 immunoprecipitations (IPs) from U87-EGFR^{vIII} GBM cells performed with antibodies against either endogenous RIOK2 or with a non-specific IgG control. Values are reported in spectral counts and number of unique peptides. Spectral counts are the total number of spectra identified for a protein and is a relative measurement of the quantity of a given protein, while the number of unique peptides refers to the number of peptides that matches the protein in question. Names of RNA-binding proteins are colored red, and names of ribosome

assembly factors are colored blue.

(B) IPs from GBM39 cells using antibodies against either RIOK2 or IMP3 demonstrated reciprocal co-IP of endogenous IMP3 and RIOK2, respectively. IMP3 IPs showed no detectable co-IP of endogenous NOB1, a ribosome assembly factor and established RIOK2 binding partner. Both endogenous RIOK2 and IMP3 were detected in total cell lysates.

(C) co-IPs of endogenous RIOK2 showed enrichment of endogenous IMP3 from GBM39 cells compared to human neural progenitor cells (HNPCs). Both endogenous RIOK2 and IMP3 were detected in total cell lysates of HNPCs and GBM39s.

(D) co-IP of purified recombinant RIOK2 and IMP3 protein with RIOK2 antibody demonstrate direct binding of IMP3 to RIOK2. RIOK2 protein was pretreated with 0.1 mg/ml of Bovine Serum Albumin (BSA 0.1mg/ml) binding competitor to reduce non-specific binding of recombinant IMP3.

Data generated by Alexander S. Chen with technical assistance from Duc Duong.

Imp is overexpressed in EGFR-PI3K mutant neoplastic glia, and is specifically required for glial neoplasia

Imp, the *Drosophila* ortholog of IMP3, is the sole member of the IGF2BP (IMP) family of RNA-binding proteins, which is composed of three members in humans (IMP1, IMP2, and IMP3). Because of the lack of putative redundancies in *Drosophila* compared to human GBM models and the conserved requirement for dRIOK2 signaling in GBM (50), we further utilized our *in vivo Drosophila* GBM model to investigate the impact of knockdown of IMP family proteins in glial neoplasia. Using immunohistochemistry, we found that Imp is upregulated in neoplastic $dEGFR^{\lambda}$; $dp110^{CAAX}$ mutant glia compared to wild-type glia, which is consistent with previously published reports showing that IMP3 is upregulated in GBM (Figure 3.2A) (174, 248). We next used confocal imaging to characterize the effect of Imp functional reduction on normal and neoplastic glia. We observed that glial-specific Imp knockdown by RNAi significantly reduced both brain volume and neoplastic glial proliferation in the GBM model (Figure 3.2B-H). The reduction of neoplastic glia proliferation and brain volume was similar between Imp knockdown and dRIOK2 knockdown in *repo>*$dEGFR^{\lambda}$; $dp110^{CAAX}$ animals, indicating that Imp may be a potential downstream effector of dRIOK2 (Figure 3.2B-H). Furthermore, Imp knockdown in wild-type glia yielded grossly normal brain morphology and glial cell development (Figure S3.4A-D), and animals with glial-specific Imp knockdown were viable. This result indicates that the reduction in neoplastic glial cell growth was not due to non-specific cellular lethality as a consequence of Imp knockdown, and that Imp is not essential for normal glial proliferation and development. Thus, collectively, our data suggests that similar to dRIOK2 (50), Imp is essential for proliferation of neoplastic tumorous EGFR-PI3K mutant glia, which is consistent with reports that IMP3 is required for proliferation of GBM cell lines (174,

248, 249).

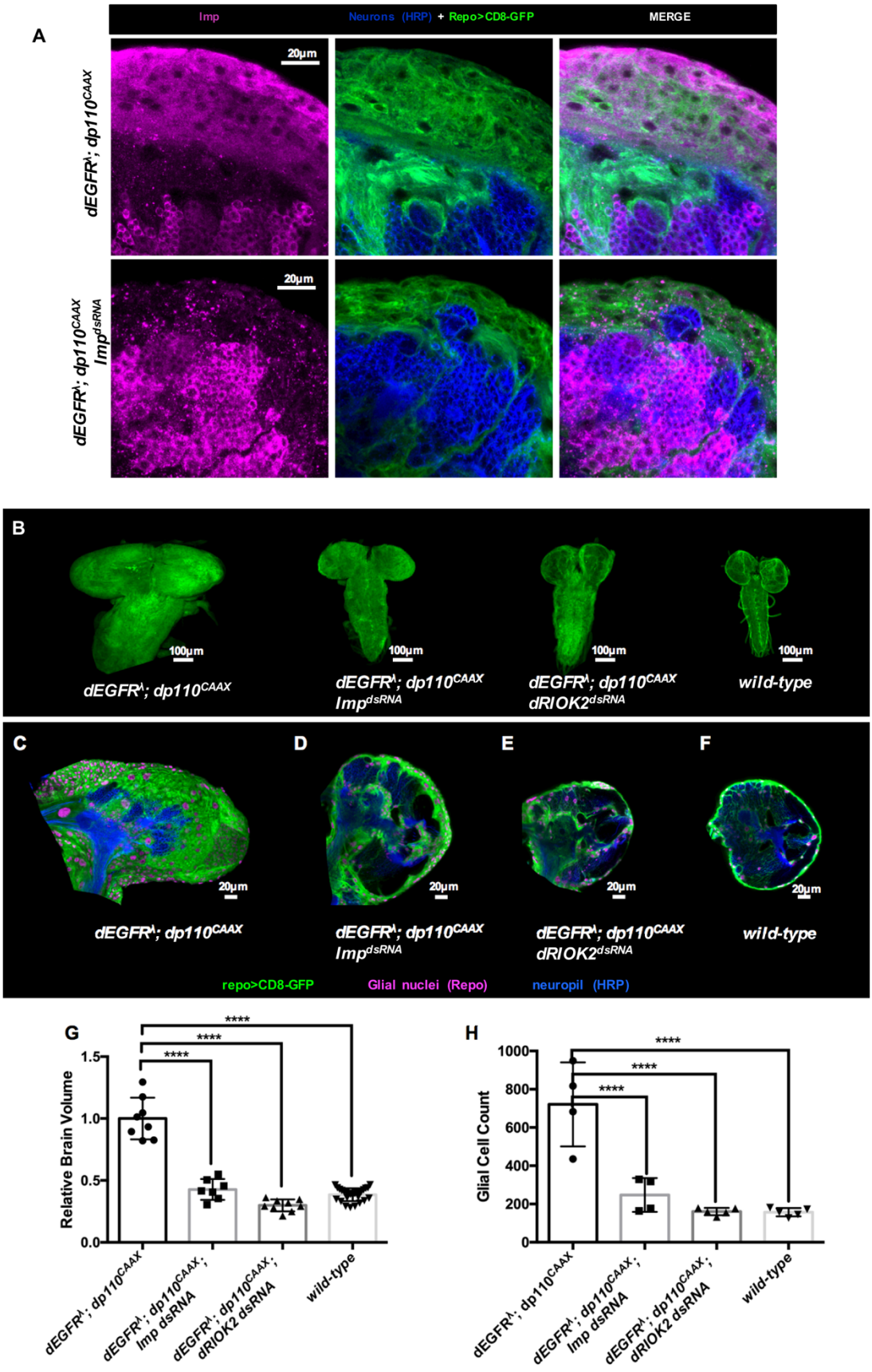
A
Imp
Neurons (HRP) + Repo>CD8-GFP
MERGE
20µm
dEGFRλ; dp110CAAX
dEGFRλ; dp110CAAX ImpdsRNA
B
100µm
dEGFRλ; dp110CAAX
dEGFRλ; dp110CAAX ImpdsRNA
dEGFRλ; dp110CAAX dRIOK2dsRNA
wild-type
C
D
E
F
20µm
repo>CD8-GFP
Glial nuclei (Repo)
neuropil (HRP)
G
Relative Brain Volume
1.5
1.0
0.5
0.0
****
dEGFRλ; dp110CAAX
dEGFRλ; dp110CAAX; Imp dsRNA
dEGFRλ; dp110CAAX; dRIOK2 dsRNA
wild-type
H
Glial Cell Count
1000
800
600
400
200
0

Figure 3.2. Imp knockdown mimics dRIOK2 knockdown in a *Drosophila* GBM model.

(A) 3 μm optical projections of brain hemispheres, aged-matched 3rd instar larvae. CD8-GFP (green) labels glial cell bodies; anti-HRP (blue) counterstains for neurons and neuropil; and magenta labels Imp protein (alone leftmost panels, GFP-HRP merge center panels, and Imp-GFP-HRP merge rightmost panels). Imp knockdown (*repo>dEGFR$^{\lambda}$;dp110^{CAAX};Imp^{dsRNA}*) (bottom panels) reduced Imp protein levels in glia (green cells in bottom panel) compared to control *repo>dEGFR$^{\lambda}$;dp110^{CAAX}* brains (top panels).

(B) Optical projections of whole brain-nerve cord complexes from 3rd instar larvae approximately 6 days old. Dorsal view; anterior up. CD8-GFP (green) labels glial cell bodies. Imp knockdown (*repo>dEGFR$^{\lambda}$;dp110^{CAAX};Imp^{dsRNA}*) decreased neoplastic brain overgrowth relative to *repo>dEGFR$^{\lambda}$;dp110^{CAAX}* controls and mimics dRIOK2 knockdown (*repo>dEGFR$^{\lambda}$;dp110^{CAAX};dRIOK2^{dsRNA}*), restoring brain sizes similar to wild-type animals.

(C-F) 3 μm optical projections of brain hemispheres, aged-matched 3rd instar larvae. Frontal sections, midway through brains. Anterior up; midline to the left. Repo (magenta) labels glial cell nuclei; CD8-GFP (green) labels glial cell bodies; anti-HRP (blue) counterstains for neurons and neuropil. (C) *repo>dEGFR$^{\lambda}$;dp110^{CAAX}* showed drastically increased brain sizes and glial cell number (magenta) compared to (F) wild-type brains. (C-E) Imp knockdown (*repo>dEGFR$^{\lambda}$;dp110^{CAAX};Imp^{dsRNA}*) and dRIOK2 (*repo>dEGFR$^{\lambda}$;dp110^{CAAX};dRIOK2^{dsRNA}*) significantly decreased numbers of neoplastic glia compared to *repo>dEGFR$^{\lambda}$;dp110^{CAAX}*.

(G) Total volumes of (in μm^3) of 3rd instar larval brains were measured using confocal microcopy couples with Imaris and normalized to *repo>dEGFR$^{\lambda}$;dp110^{CAAX}* larval brains. (*repo>dEGFR$^{\lambda}$;dp110^{CAAX}*: n=8, *repo>dEGFR$^{\lambda}$;dp110^{CAAX};Imp^{dsRNA}*: n=7, *repo>dEGFR$^{\lambda}$;dp110^{CAAX};dRIOK2^{dsRNA}*: n=9, wild-type: n=27). Statistics generated using One-

Way ANOVA, ****p<0.0001.

(H) Glial cell numbers counted in representative 3 μm optical projections of 3rd instar larval brain hemispheres. (*repo>dEGFR$^{\lambda}$;dp110^{CAAX}*: n=4, *repo>dEGFR$^{\lambda}$;dp110^{CAAX};Imp^{dsRNA}*: n=4, *repo>dEGFR$^{\lambda}$;dp110^{CAAX};dRIOK2^{dsRNA}*: n=5, wild-type: n=5). Statistics generated using two-tailed TTESTs, ****p<0.0001.

Data generated in (A-F, H) by Alexander S. Chen and in (G) by Alexander S. Chen and Riley Gulbronson.

RIOK2 and IMP3 are co-overexpressed and co-localized in GBM cells

While our results showed that dRIOK2 and Imp are physiologically relevant in our *Drosophila* GBM model, we wanted to determine if IMP3 and RIOK2 are of equal importance in human GBM cells. We first performed western blot analysis of a panel of patient-derived GBM neurosphere cultures from EGFR amplified tumors, which are enriched for GBM stem cells, and observed that RIOK2 and IMP3 are co-overexpressed in GBM relative to cultured HNPCs (Figure 3.3A). This finding is consistent with previous studies that showed that IMP3 is overexpressed in GBM tumor tissue (174). To assess whether RIOK2 and IMP3 are co-overexpressed in GBM tumor tissues, we used cBioportal and Gliovis to download and analyze tumor genomic data cataloged by The Cancer Genome Atlas (TCGA). Our data show that both *RIOK2* and *IMP3* mRNA are overexpressed to the greatest degree in grade IV gliomas (GBMs) relative to grade II and grade III gliomas (Figure 3.3B). Furthermore, analysis of TCGA reveal that *RIOK2* and *IMP3* mRNA expression levels are positively correlated in that high expression levels of *RIOK2* mRNA co-occur with high expression levels of *IMP3* mRNA, indicating that they may operate together to promote tumorigenesis (Figure 3.3B). Moreover, tumors with EGFR amplification have significantly higher expression levels of *IMP3* mRNA, indicating that IMP3 overexpression is maybe upregulated by EGFR signaling (Figure 3.3B). Collectively, analysis of publicly available TCGA datasets reveal that RIOK2 and IMP3 are co-overexpressed in GBM.

To further investigate whether RIOK2 and IMP3 regulate each other in GBM cells, we conducted immunofluorescence experiments to assess their localization pattern in GBM cells overexpressing $EGFR^{vIII}$. Our data show that RIOK2 and IMP3 are both predominantly localized in the cytoplasm of these cells, with both RIOK2 and IMP3 exhibiting a perinuclear staining

pattern consistent with previously published IMP3 localization patterns (Figure 3.3C) (163, 250). These results suggest that RIOK2 and IMP3 may promote GBM tumorigenesis primarily in the cytoplasm.

Collectively, our data support that IMP3 and RIOK2 are co-overexpressed and co-localized in GBM tumors, consistent with the possibility that they form a functional pathway; however, the mechanism by which RIOK2 and IMP3 promote GBM tumorigenesis is unclear.

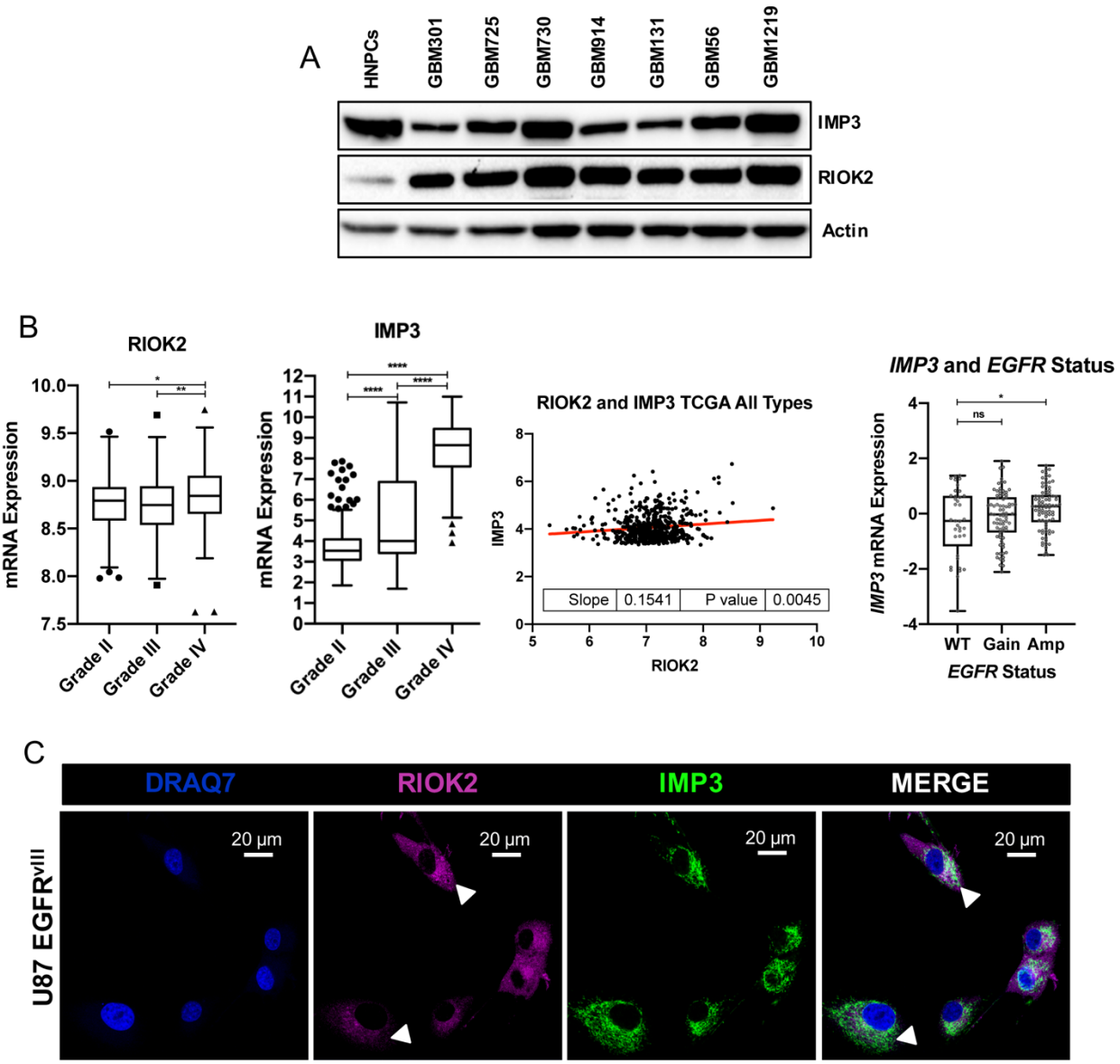
A
HNPCs
GBM301
GBM725
GBM730
GBM914
GBM131
GBM56
GBM1219
IMP3
RIOK2
Actin
B
RIOK2
mRNA Expression
Grade II
Grade III
Grade IV
IMP3
RIOK2 and IMP3 TCGA All Types
Slope
0.1541
P value
0.0045
IMP3 and EGFR Status
IMP3 mRNA Expression
WT
Gain
Amp
EGFR Status
ns
C
DRAQ7
RIOK2
IMP3
MERGE
U87 EGFRvIII
20 µm

Figure 3.3. RIOK2 and IMP3 are co-overexpressed in human GBMs.

(A) A panel of lysates from human neural progenitor cells (HNPCs) or short-term patient-derived GBM neurosphere cultures derived from tumors with loss of PTEN and amplification of EGFR (GBM301, GBM725, GBM914, GBM1219) or other RTKs (NTRK2: GBM131, MET: GBM730, GBM56) show elevated RIOK2 expression compared to HNPCs; all cultures express endogenous IMP3.

(B) Analysis of TCGA GBM tumor profiling data show significantly increased expression of both *RIOK2* and *IMP3* mRNA in grade IV gliomas compared to lower grade gliomas. Increased expression of *RIOK2* and *IMP3* mRNA are significantly correlated with each other across all TCGA glioma grades. *IMP3* mRNA expression is significantly increased in high grade gliomas with EGFR amplification compared to tumors without EGFR amplification.

(C) U87-EGFR^{vIII} cells were fixed and stained to label nuclear DNA (DRAQ7, blue), RIOK2 (magenta), and IMP3 (green). RIOK2 and IMP3 were co-localized predominantly in the cytosol, with both RIOK2 and IMP3 also exhibiting a perinuclear localization pattern (denoted by white arrows).

Data generated in (A) by Renee D. Read with technical assistance from Colleen Mosley, in (B) by Nathaniel H. Boyd, and in (C) by Jamie A.G. Hamilton and Renee D. Read.

RIOK2 catalytic activity promotes tumorigenesis

Because RIOK2 is thought to be a kinase and an ATPase, we sought to assess the importance of RIOK2 catalytic activity in promoting GBM tumorigenesis to determine if RIOK2 catalytic activity is required for tumorigenesis and if RIOK2 phosphorylates IMP3. For this purpose, we tested catalytically inactive (KD) versions of RIOK2 in *Drosophila* and human GBM cells.

In our *Drosophila* GBM model, we overexpressed catalytically inactive dRIOK2 ($dRIOK2^{KD}$) or, as a control, dRIOK2 wild-type ($dRIOK2^{WT}$) in neoplastic glia in *repo>dEGFR$^{\lambda}$; dp110^{CAAX}* animals and compared their phenotypes to control *repo>dEGFR$^{\lambda}$; dp110^{CAAX}* animals that overexpressed a lacZ construct. $dRIOK2^{KD}$ overexpression, but not $RIOK2^{WT}$ overexpression, significantly reduced both glial proliferation and brain volume in the GBM model (Figure 3.4A-F). In contrast, in normal wild-type glial cells, $dRIOK2^{KD}$ overexpression did not cause obvious or detectable defects in glial progenitor cells (*repo-Gal4*) or in neural stem cells (*wor-Gal4, dpn-Gal4*), and even whole animals (*actin-Gal4*) were grossly normal and viable with $dRIOK2^{KD}$ overexpression (Figure S3.5A-D, data not shown). Thus, $dRIOK2^{KD}$ can specifically act as a dominant negative, and block tumorigenesis, while sparing normal cells. This suggests that dRIOK2 adopts a differential or neomorphic function in tumor cells, and that $dRIOK^{KD}$ overexpression specifically counteracts this function.

To determine if kinase-dead RIOK2 ($RIOK2^{KD}$) similarly provokes growth arrest in human GBM cells, we overexpressed $RIOK2^{KD}$ in cultured cells. We had difficulty recovering GBM cells that constitutively overexpress $RIOK2^{KD}$ from viral vectors (not shown), suggesting that $RIOK2^{KD}$ blocks GBM cell growth and survival. Thus, we tested $RIOK2^{KD}$ using tetracycline inducible vectors to find that $RIOK2^{KD}$ overexpression significantly reduced growth

of PTEN-null U87 GBM cells, which are sensitive to RIOK2 levels, as measured by WST-1 assays (Figure 3.4G), whereas wild-type RIOK2 (RIOK2^{WT}) overexpression enhanced cell growth, consistent with our published data showing that RIOK2 confers a proliferation advantage to PTEN mutant cells (50). Thus, RIOK2 catalytic function promotes tumorigenesis.

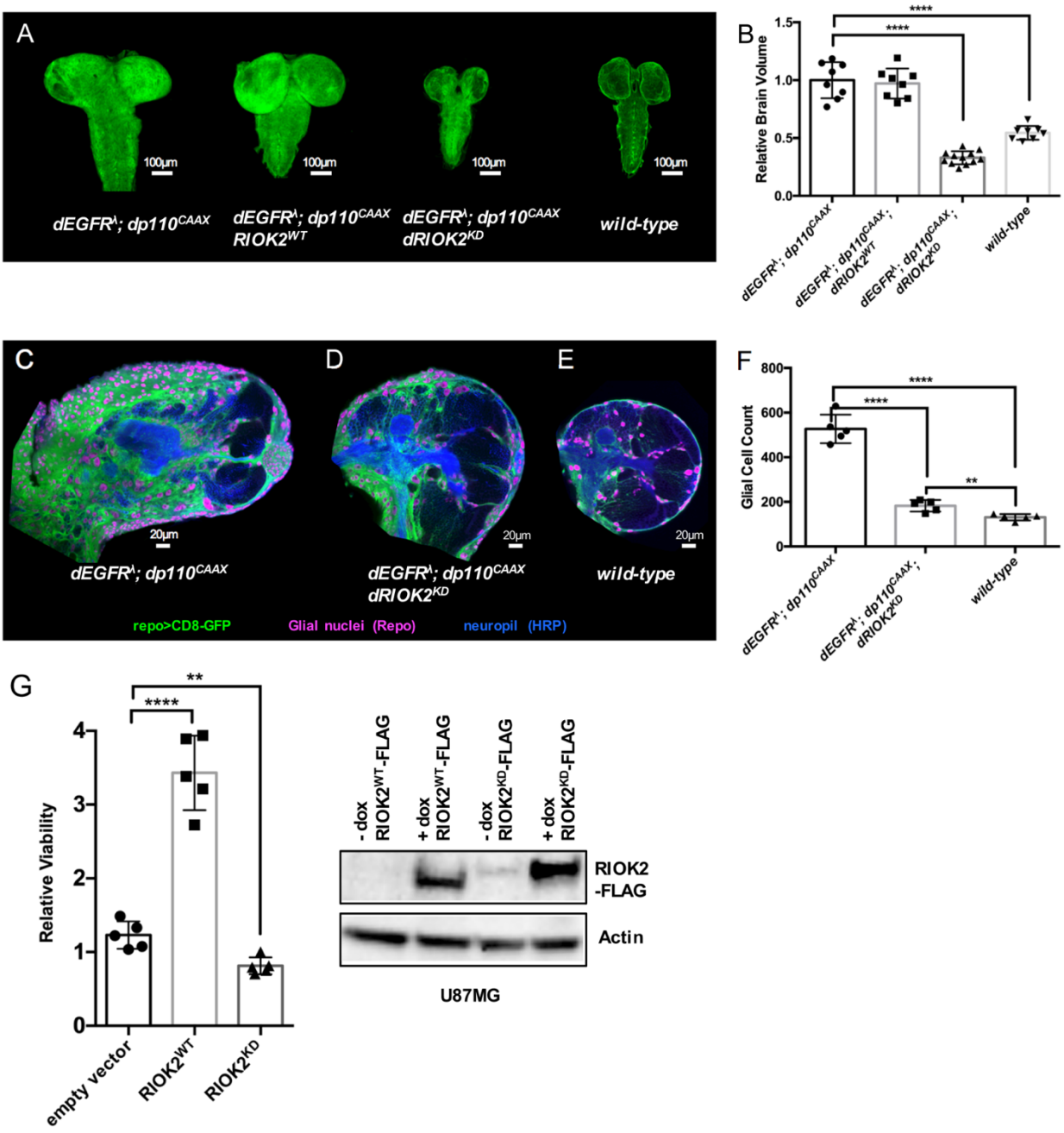

Figure 3.4. dRIOK2/RIOK2 catalytic activity drives tumorigenesis and mediates IMP3 binding.

(A) Optical projections of whole brain-nerve cord complexes from 3rd instar larvae approximately 6 days old. Dorsal view; anterior up. CD8-GFP (green) labels glial cell bodies. *repo>dEGFR$^{\lambda}$;dp110^{CAAX}* and overexpression of wild-type dRIOK2 (*repo>dEGFR$^{\lambda}$;dp110^{CAAX};dRIOK2^{WT}*) increased larval brain size relative to wild-type. Overexpression of catalytically inactive dRIOK2 (*repo>dEGFR$^{\lambda}$;dp110^{CAAX};dRIOK2^{KD}*) decreased larval brain size relative to *repo>dEGFR$^{\lambda}$;dp110^{CAAX}* and *repo>dEGFR$^{\lambda}$;dp110^{CAAX};dRIOK2^{WT}* animals.

(B) Total volumes of (in μm^3) of 3rd instar larval brains were measured using confocal microscopy coupled with Imaris and normalized to wild-type larval brains. (*repo>dEGFR$^{\lambda}$;dp110^{CAAX}*: n=8, *repo>dEGFR$^{\lambda}$;dp110^{CAAX};dRIOK2^{WT}*: n=8, *repo>dEGFR$^{\lambda}$;dp110^{CAAX};dRIOK2^{KD}*: n=12, wild-type: n=8). Statistics generated using One-Way ANOVA with multiple comparisons, ****p<0.0001.

(C-E) 3 μm optical projections of brain hemispheres, aged-matched 3rd instar larvae. Frontal sections, midway through brains. Anterior up; midline to the left. Repo (magenta) labels glial cell nuclei; CD8-GFP (green) labels glial cell bodies; anti-HRP (blue) counterstains for neurons and neuropil. (B) *repo>dEGFR$^{\lambda}$;dp110^{CAAX}* and overexpression of wild-type RIOK2 (*repo>dEGFR$^{\lambda}$;dp110^{CAAX};dRIOK2^{WT}*) showed drastically increased glial cell number (magenta) and brain size compared to (E) wild-type brains. Overexpression of catalytically inactive RIOK2 (*repo>dEGFR$^{\lambda}$;dp110^{CAAX}*; *dRIOK2^{KD}*) showed drastically reduced glial cell number and decreased brain sizes compared to *repo>dEGFR$^{\lambda}$;dp110^{CAAX}* and *repo>dEGFR$^{\lambda}$;dp110^{CAAX};dRIOK2^{WT}* animals.

(F) Glial cell numbers in representative 3 μm optical projections of 3rd instar larval brain hemispheres. (*repo>dEGFR$^{\lambda}$;dp110^{CAAX}*: n=5, *repo>dEGFR$^{\lambda}$;dp110^{CAAX};dRIOK2^{KD}*: n=5, wild-type: n=5). Statistics generated using two-tailed Student TTESTS, ****p<0.0001, **p<0.01.

(G) WST-1 assays on U87 GBM cells overexpressing either empty vector control, FLAG-tagged wild-type RIOK2 (RIOK2^{WT}-FLAG), or FLAG-tagged catalytically inactive RIOK2 (RIOK2^{KD}-FLAG). RIOK2 constructs were induced for 48 hr by doxycycline (dox). RIOK2^{KD}-FLAG overexpressing cells displayed reduced viability and/or proliferation compared to RIOK2^{WT}-FLAG overexpressing cells, which showed increased proliferation relative to vector control cells. Five samples were used for each condition. Statistics generated using two-tailed Student TTESTS, **p<0.01, ****p<0.0001. Western blots confirming overexpression of RIOK2^{WT}-FLAG and RIOK2^{KD}-FLAG upon doxycycline induction.

Data generated in (A-B) by Alexander S. Chen and Emily Legan and in (C-F) by Alexander S. Chen with assistance from Renee D. Read and in (G) by Renee D. Read.

The RIOK2-IMP3 complex depends on RIOK2 catalytic activity and recruits TORC2 to phosphorylate IMP3

To assess the contribution of RIOK2 catalytic function to RIOK2-IMP3 interactions, we performed co-IP experiments on U87 cells overexpressing RIOK2^{KD} or control cells expressing either RIOK2^{WT} or an empty vector. Proteomics analysis of these co-IPs indicated that IMP3 displayed reduced binding to RIOK2^{KD} compared to RIOK2^{WT}, and that both RIOK2^{KD} and RIOK2^{WT} specifically co-fractionated with established RIOK2 binding partners, including ribosome assembly factors and other RBPs found to co-IP with endogenous RIOK2 (Table S3.3). These results were confirmed by western blot (Figure 3.5A), which demonstrate that IMP3 binding is regulated by RIOK2 catalytic activity *in vivo*.

Given the requirement for RIOK2 catalytic activity for IMP3 binding, we hypothesized that IMP3 is a potential substrate of RIOK2. Our *in vitro* kinase assays revealed that RIOK2 autophosphorylates and phospho-proteomic analysis identified RIOK2 autophosphorylation sites consistent with published literature (139) (Figure S3.6A and S3.6B). *In vitro* kinase assays and phospho-proteomic analysis also revealed that RIOK2 does not directly phosphorylate IMP3 (Figure S3.6C). These results are consistent with reports that RIOK2 can exert its function in the context of 40S ribosome assembly without directly phosphorylating a substrate (146). Furthermore, recent studies have shown that instead of directly phosphorylating substrates, RIOK2 may act as an ATPase, where the phosphoryl transfer from ATP to Asp257 in the RIOK2 active site and the subsequent hydrolysis of aspartylphosphate induces a conformational change that releases RIOK2 from the pre-40S particle along with other *trans*-acting factors such DIM, LTV1, and NOB1 (146, 147). Therefore, we suspected that RIOK2 may undergo a conformational change that depends on its catalytic activity to recruit other proteins to act as

intermediaries in IMP3 regulation.

To identify additional proteins in the RIOK2-IMP3 complex, we performed crosslinking IPs on endogenous RIOK2 and IMP3 in patient-derived $EGFR^{vIII}$ mutant RIOK2-dependent GBM stem cells (GBM39) using DSP, an anime-reactive crosslinker with NHS ester reactive ends that specifically recognize proteins, combined with stringent washes, to identify transient protein-protein interactions (Figure 3.5B). We observed IMP3 and RIOK2 co-IP from DSP treated cells, and, by blotting for additional proteins, we found that mTOR and RICTOR, a component of mTOR Complex 2 (TORC2), were enriched in our RIOK2 IPs compared to non-specific IgG controls (Figure 3.5C). Our results are consistent with our previous studies which show that RIOK2 forms a complex with TORC2, that binding of RIOK2 to mTOR depends on RIOK2 catalytic activity, and that RIOK2 catalytic activity is necessary to drive TORC2 activation (50). Therefore, RIOK2 may recruit IMP3 to the TORC2 complex.

Previous studies show that mTOR directly phosphorylates IMP3 at Ser184 (173). To determine if mTOR phosphorylates IMP3 in the RIOK2-IMP3 complex, we performed crosslinking co-IP on endogenous IMP3 in patient-derived GBM stem cells (GBM39) followed by western blots with an antibody that should recognize the phosphorylated Ser184 site (MPM2, recognizes phospho-Ser/Thr adjacent to Pro), and we detected presumptive phosphorylated IMP3 in the RIOK2-IMP3-mTOR complex (Figure 3.5D). Furthermore, in GBM39, RIOK2 knockdown reduced phosphorylation of IMP3 at Ser184 and Thr529, a second site also adjacent to a Pro residue, supporting the hypothesis that phosphorylation at these sites is regulated by RIOK2 (Figure S3.6D). Together, our data support a model in which RIOK2 catalytic activity allows for recruitment of IMP3 and TORC2, which in turn phosphorylates IMP3, and forms a stable RIOK-IMP3 complex.

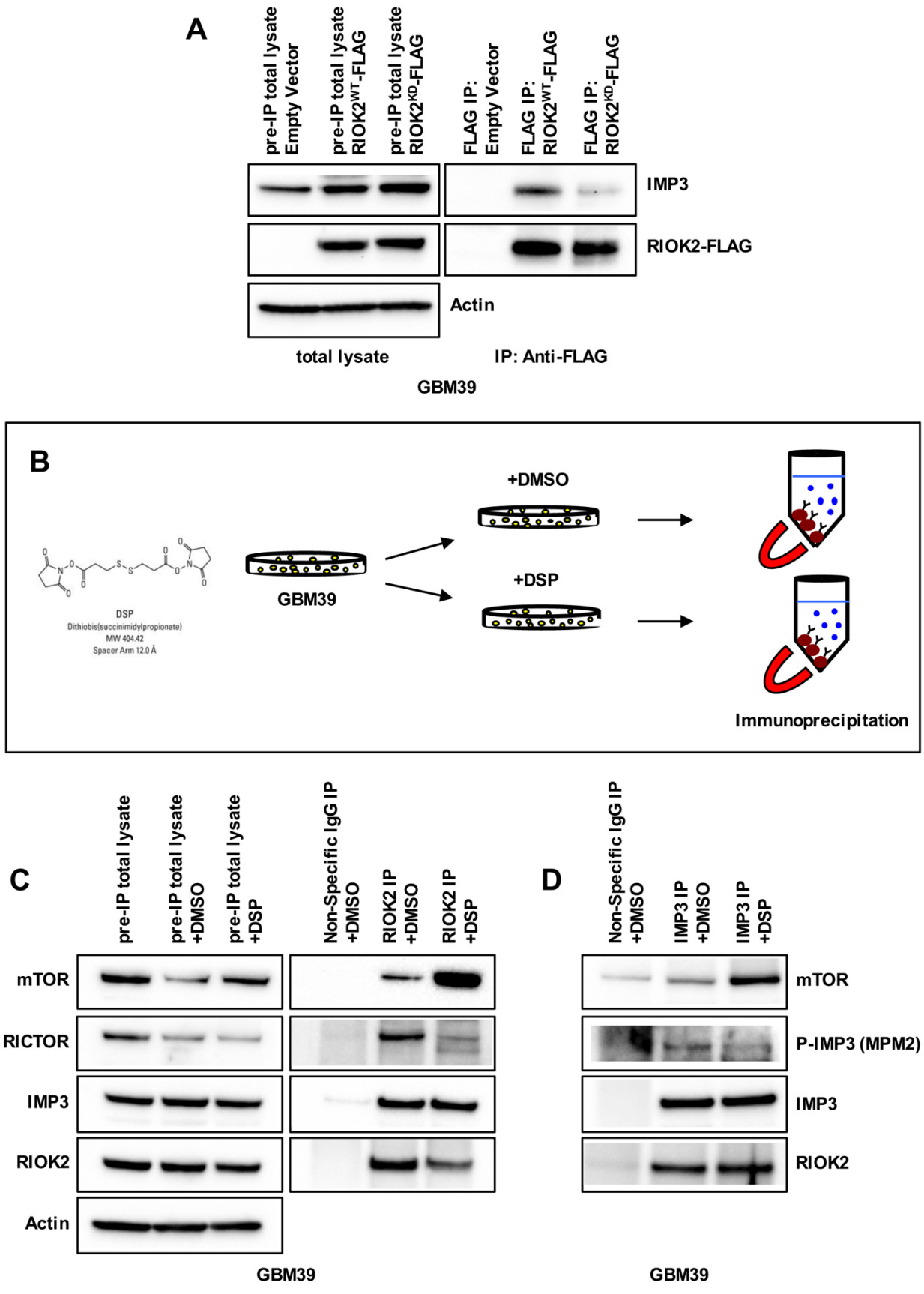
A
pre-IP total lysate Empty Vector
pre-IP total lysate RIOK2WT-FLAG
pre-IP total lysate RIOK2KD-FLAG
FLAG IP: Empty Vector
FLAG IP: RIOK2WT-FLAG
FLAG IP: RIOK2KD-FLAG
IMP3
RIOK2-FLAG
Actin
total lysate
IP: Anti-FLAG
GBM39
B
DSP
Dithiobis(succinimidylpropionate)
MW 404.42
Spacer Arm 12.0 Å
GBM39
+DMSO
+DSP
Immunoprecipitation
C
pre-IP total lysate
pre-IP total lysate +DMSO
pre-IP total lysate +DSP
Non-Specific IgG IP +DMSO
RIOK2 IP +DMSO
RIOK2 IP +DSP
mTOR
RICTOR
IMP3
RIOK2
Actin
GBM39
D
Non-Specific IgG IP +DMSO
IMP3 IP +DMSO
IMP3 IP +DSP
mTOR
P-IMP3 (MPM2)
IMP3
RIOK2
GBM39

Figure 3.5. The RIOK2-IMP3 complex recruits TORC2 to phosphorylate IMP3.

(A) RIOK2^{WT}-FLAG or RIOK2^{KD}-FLAG overexpression was induced in U87 cells with 8 μg/ml doxycycline for 72 hrs, and proteins were IPed with Mouse M2 Anti-FLAG magnetic beads. Westerns blots on total cell lysates set aside prior to IP show that endogenous IMP3 was expressed across all samples, and that FLAG-tagged RIOK2^{WT}-FLAG and RIOK2^{KD}-FLAG were sufficiently induced by doxycycline treatment. Western blots of show that a significantly reduced amount of IMP3 co-IPed with RIOK2^{KD}-FLAG compared to RIOK2^{WT}-FLAG.

(B) Diagram of experimental workflow for DSP crosslinking and IPs from GBM39 cells.

(C) GBM39 cells were treated with either DMSO or DSP crosslinker (1mM) for 2 hrs. Western blot analysis show that GBM39 total cell lysates set aside prior to IPs endogenously expressed mTOR, RICTOR, IMP3, and RIOK2. Western blots of RIOK2 IPs from GBM39 cells indicate enrichment of endogenous mTOR and RICTOR protein in the RIOK2-IMP3 complex as compared to control non-specific IgG IPs.

(D) GBM39 treated with either DMSO or DSP crosslinker (1 mM) for 2 hrs prior to IPs with either IMP3 antibody or a non-specific IgG control. Western blots show enrichment of endogenous mTOR protein in the IMP3-RIOK2 co-IPed complex, as well as phosphorylated IMP3 (detected with MPM2 antibody).

Data generated by Alexander S. Chen.

RIOK2 and IMP3 regulate MYC levels in an evolutionarily conserved pathway

IMP family RBPs regulate target mRNA transport, stability, and translation (160). Previous studies in human cells show that IMP3 regulates several target mRNAs that encode established gliomagenic oncogenes including IGF2 and MYC (159). Notably, MYC is the founding member of the MYC family of "super-transcription factors," so called because they regulate at least 15% of all known genes, many of which have established functions in a variety of pro-tumor pathways such as cell proliferation, cell growth, metabolism, ribosome biogenesis, and stem cell self-renewal (178, 180). Recent studies in *Drosophila* have identified that in neurogenesis, Imp upregulates dMyc protein levels by increasing *dMyc* mRNA stability, which in turn leads to increased proliferation and size of *Drosophila* neural stem cells, known as neuroblasts (251). Moreover, studies in human leukemia cells have shown that IMP3 binds to the 3' UTR of *MYC* mRNA, and deletions in the RNA-binding domain of IMP3 prevented binding of IMP3 to MYC and in turn, reduced *MYC* mRNA stability (177). Together, these studies make a compelling case that IMP3 regulates *MYC* mRNA levels. However, no previous studies have connected RIOK2 to regulation of IMP3 or MYC.

Using our *Drosophila* GBM model, we tested whether dRIOK2 and Imp knockdown affect dMyc protein levels. Using antibodies specific to dMyc protein, our data show that dMyc protein levels are reduced with glial-specific knockdown of dRIOK2 and Imp in the GBM model compared to control animals (Figure 3.6A). These results are consistent with a hypothesis that a dRIOK2-Imp complex may drive glial tumorigenesis by modulating protein levels of dMyc, which is required for EGFR-PI3K driven glial tumorigenesis (49).

We next wanted to determine if IMP3 and RIOK2 regulate *MYC* mRNA in human GBM cells. To determine whether IMP3 binds to *MYC* mRNA in GBM, we performed RNA-binding

protein immunoprecipitations (RIP) in GBM stem cells (GBM39), using two separate IMP3 antibodies. Our data show that *MYC* mRNA is enriched in samples IPed with IMP3 compared to non-specific antibody immunoprecipitation (Figure 3.6B), indicating that *MYC* is a bona fide target mRNA of IMP3 in GBM cells. To determine if RIOK2 and IMP3 regulate MYC levels in human GBM cells, we knocked down RIOK2 and IMP3 in GBM39 and GBM301 cells, and observed reduced levels of *MYC* mRNA and protein in these cells (Figure 3.6C and 3.6D, Figure S3.7A-B), indicating that MYC expression is upregulated by RIOK2 and IMP3. Consistent with this interpretation, analysis of TAGC data indicate that higher RIOK2 and IMP3 expression levels are significantly correlated with higher MYC mRNA expression levels, particularly in tumors that show EGFR gain and amplification (Figure S3.7C-D).

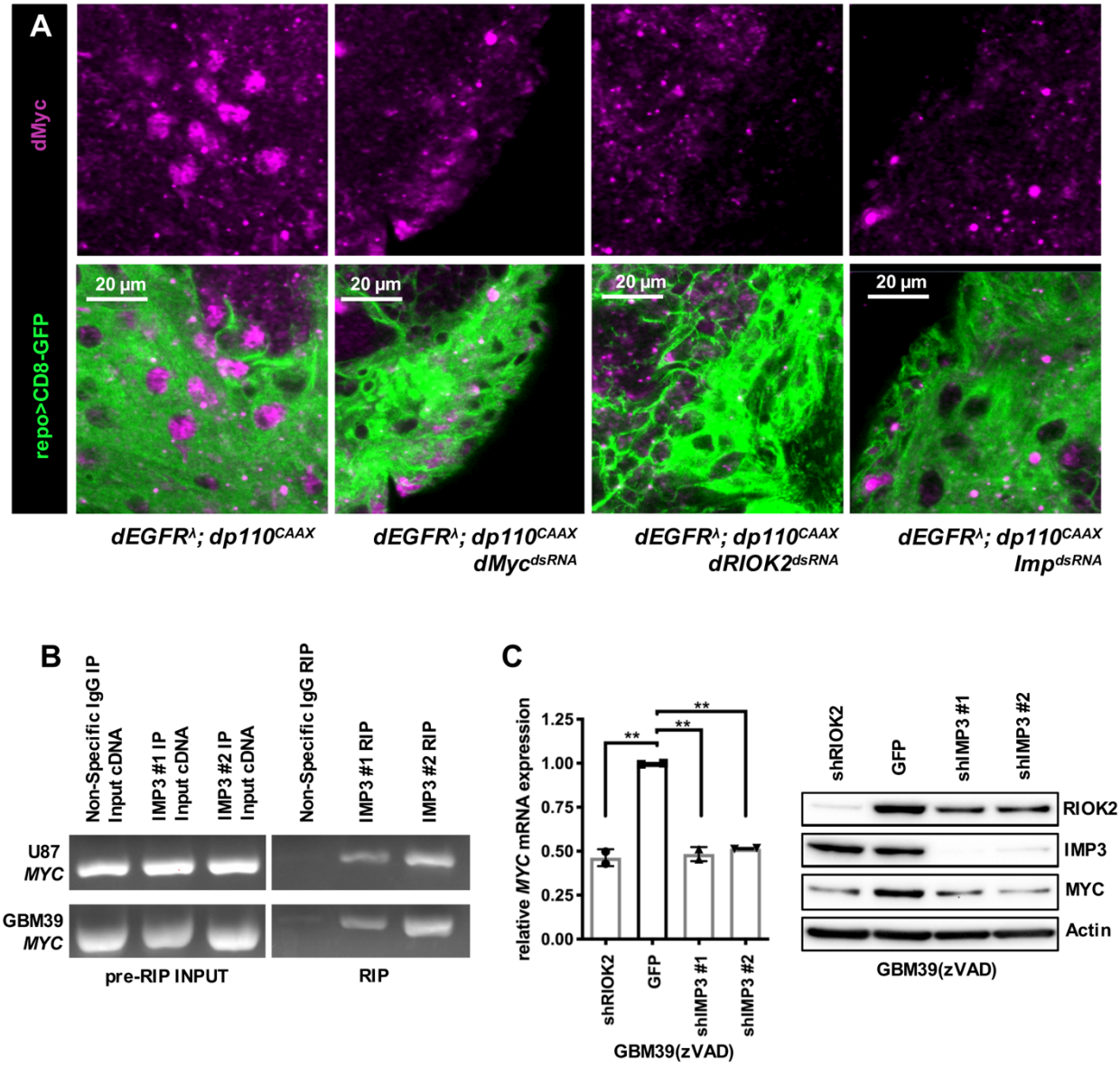

Figure 3.6. dRIOK2/RIOK2 and Imp/IMP3 modulate dMyc/MYC expression in a conserved pathway.

(A) 3 µm optical projections of brain hemispheres, aged-matched 3rd instar larvae. CD8-GFP (green) labels glial cell bodies and magenta labels dMyc protein (alone in top panels, merged in bottom panels). dMyc knockdown was used as a control to determine background in dMyc antibody stains. dRIOK2 knockdown (*repo>dEGFR$^{\lambda}$;dp110^{CAAX};dRIOK2^{dsRNA}*) (Third panel

from the left) reduced dMyc levels compared to *repo>dEGFR$^{\lambda}$;dp110^{CAAX}* brains (rightmost panel) and showed similar levels as dMyc knockdown(*repo>dEGFR$^{\lambda}$;dp110^{CAAX};dMyc^{dsRNA}*) (second panel of the left). Imp knockdown (*repo>dEGFR$^{\lambda}$;dp110^{CAAX};Imp^{dsRNA}*) (rightmost panel) reduced dMyc levels compared to *repo>dEGFR$^{\lambda}$;dp110^{CAAX}* brains (leftmost panel) and showed similar levels as dMyc knockdown (*repo>dEGFR$^{\lambda}$;dp110^{CAAX};dMyc^{dsRNA}*) (second panel of the left).

(B) IMP3 was IPed with two different antibodies (anti-IMP3 #1 and anti-IMP3 #2) from GBM39 cells. IP with non-specific IgG was used as a negative control. Co-IPed IMP3-bound mRNAs were extracted and cDNAs were generated. cDNA was PCRed with primers against *MYC*, and DNA gel electrophoresis showed specific MYC PCR products, indicating that *MYC* mRNA was bound to IMP3 in GBM cells expressing RIOK2.

(C) RIOK2 or IMP3 knockdown was performed in GBM39 cells using verified lentiviral shRNAs. GBM cells were treated with 20 μM zVAD to prevent apoptosis. Cells were harvested 96 hrs after infection. GBM39 cells with RIOK2 and IMP3 knockdown showed reduced expression of endogenous *MYC* mRNA, as measured by qPCR, and MYC protein, as measured by western blot, compared to control cells infected with GFP shRNA. Two replicates were used per conditions. Statistics generated using unpaired two-tailed Student TTESTS, **$p<0.01$.

Data generated in (A, B) by Alexander S. Chen and in (C) by Se-Yeong Oh.

Collectively, our data reveal a novel mechanism in which RIOK2 recruits TORC2 and IMP3 in a complex, where mTOR phosphorylates IMP3, and together, drive GBM tumorigenesis by modulating MYC levels (Figure 3.7).

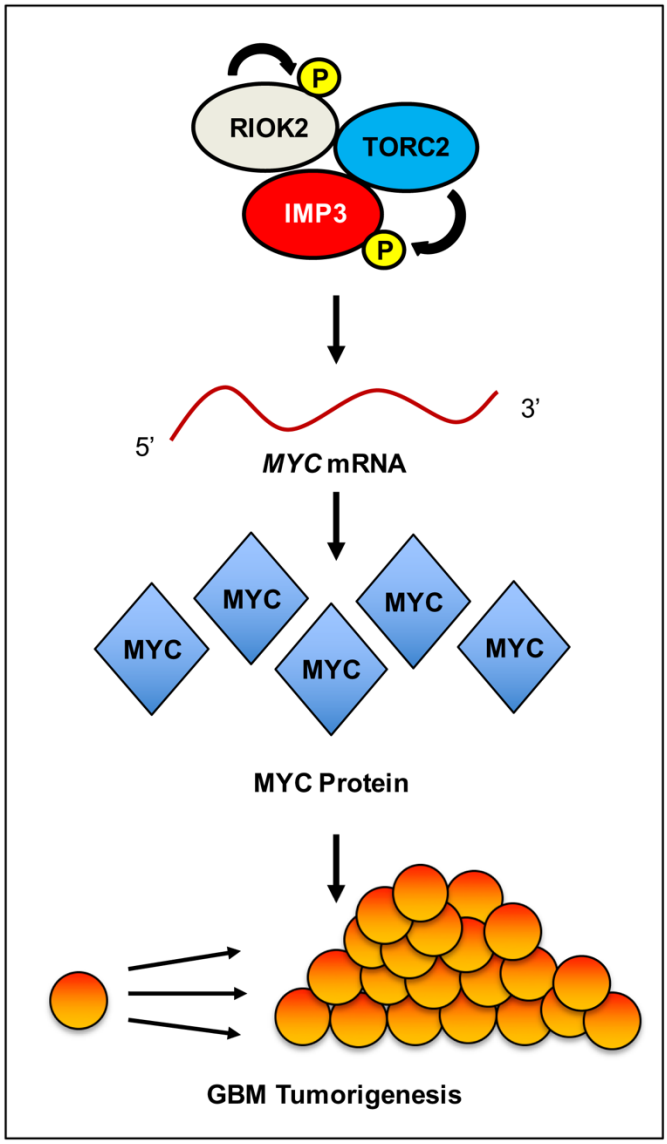

Figure 3.7. A model for the role of the RIOK2-IMP3-TORC2 complex in regulating MYC expression to promote GBM tumorigenesis.

RIOK2 catalytic activity promotes autophosphorylation to allow for binding to IMP3 and TORC2. IMP3 is phosphorylated by TORC2 and this complex modulates *MYC* mRNA to promote increased levels of MYC protein to promote GBM tumorigenesis.

Diagram generated by Alexander S. Chen.

3.5 Discussion

EGFR and PI3K are commonly altered in GBM and play key roles in regulating GBM initiation and progression (194). Utilizing complementary experimental approaches in a *Drosophila* GBM model developed by Read *et al.* and in cell-based models of human GBM (49), we identified a new pathway in which the atypical serine/threonine kinase, RIOK2, drives GBM tumorigenesis by forming a complex with the RNA-binding protein, IMP3. The connection between RIOK2 and IMP3 is novel, and, based on what is known about IMP3, may explain the tumor cell-type-specific aspects of RIOK2 function.

Previous literature hinted at alternative functions for RIOK2 proteins aside from their conserved role in ribosome biogenesis: more than half of all Rio2p is not associated with pre-40S subunits, and, under metabolic stress, cytoplasmic Rio2p localizes to RNA granules (236, 252). Therefore, we hypothesized that RIOK2 must instead operate through a mechanism outside of ribosome assembly to promote GBM tumorigenesis. Our data supports a new model whereby RIOK2 drives GBM tumorigenesis by forming a stable and direct interaction with IMP3, which, in GBM cells, is part of a larger protein complex that includes TORC2 and likely includes other RBPs identified in our proteomic analysis of RIOK2 IPs. This concept of RIOK2 and IMP3 operating as part of a larger RBP complex to drive GBM tumorigenesis is consistent with literature supporting that RBPs act as part of messenger ribonucleoprotein particles that are regulated by other proteins recruited to regulate the activity of these particles, including kinases (152, 155, 156). Several of the other RBPs that co-IPed with RIOK2 and IMP3 bind to different regions on mRNAs, suggesting that they may associate with each other and RIOK2 in larger-scale complexes coordinately bound to target RNAs: for example, ATXN2L/ATXN2 binds to 5' UTRs in mRNAs and PABPC4 binds to polyA tails (Supplemental Table S3.1).

RIOK2 has been postulated to be a kinase based on the core sequence similarities between the RIO domain and other protein kinases, and has been shown to autophosphorylate itself, although no other substrates have been identified. Our data shows that RIOK2 does not directly phosphorylate IMP3, but that RIOK2 does autophosphorylate itself, and that in our *Drosophila* GBM model and human cell-based models, RIOK2 catalytic function is necessary for proliferation of tumorous glia cells. Our previously published findings in patient-derived GBM stem cells using RIOK2 RNAi or overexpression of dominant negative catalytically inactive RIOK2 ($RIOK2^{KD}$) reveal that RIOK2 catalytic activity is required for TORC2 activation (50). Here, our IP experiments in GBM cell culture show that RIOK2 catalytic activity is required for binding formation of the RIOK2-IMP3-TORC2 complex. Therefore, we propose a model by which RIOK2 catalytic activation and autophosphorylation results in a conformational change to allow for the recruitment of IMP3 and TORC2, which in turn, allows mTOR to phosphorylate IMP3, which is consistent with previous studies that have shown, as part of the TORC2 complex, mTOR directly phosphorylates IMP3 to regulate translation of *IGF2* mRNA (173). It is possible that RIOK2 and IMP3 may also promote GBM tumorigenesis through modulating TORC2 activity towards other RBPs and RNAs, although additional experiments will need to be performed to determine the mechanisms whereby RIOK2, IMP3, and TOCR2 interact with each other and larger RNA particles as well as the functional impact of those interactions on target mRNAs.

Furthermore, our *Drosophila* GBM model has identified that both dRIOK2 and the *Drosophila* ortholog of IMP3, Imp, modulates dMyc protein levels. *MYC* is a known target mRNA of IMP3 (177), and MYC has an established role in modulating GBM tumorigenesis by regulating downstream effectors involved in ribosome biogenesis, cell proliferation,

differentiation, survival, and immune surveillance (178, 180). Importantly, our data in patient-derived GBM stem cells recapitulates key findings in our *Drosophila* GBM model, indicating that this pathway is implicated in the human disease. Our data in GBM stem cells show that similarly to our *Drosophila* GBM model, RIOK2 and IMP3 co-localize, and that RIOK2 catalytic activity is important in GBM tumorigenesis. Moreover, knockdown experiments in patient-derived GBM stem cells reveal that both RIOK2 and IMP3 knockdown reduces MYC protein levels, indicating that RIOK2 and IMP3 are important in modulating MYC protein levels. However, the precise mechanism in which the RIOK2-IMP3-TORC2 complex modulates *MYC* target mRNA is currently unknown. Compelling findings by Samuels *et al.* show that during development, Imp, the *Drosophila* ortholog of IMP3, stabilizes *dMyc* mRNA to increase dMyc protein levels and in turn, results in faster division rates by neuroblasts (251). It is possible that the RIOK2-IMP3, in this context, may operate in a similar fashion to increase MYC protein levels by increasing the stability of *MYC* mRNA, and that the activity of IMP3 in this context is stimulated by TORC2-dependent phosphorylation (173).

Collectively, our data shows a novel pathway in which RIOK2 promotes GBM tumorigenesis. RIOK2 autophosphorylates to allow for the recruitment of both TORC2 and IMP3 into the complex. TORC2 then phosphorylates IMP3 which turn increases MYC protein expression to drive GBM tumorigenesis. While additional experiments need to be conducted in order to further elucidate the mechanism in which RIOK2-IMP3 promotes GBM tumorigenesis, our findings have uncovered important aspects of GBM tumor biology. By identifying how RIOK2 may regulate RNA-binding proteins in GBM tumors, we may better develop more effective therapeutic strategies and in turn, improve GBM patient prognosis.

3.6 Supplementary Material

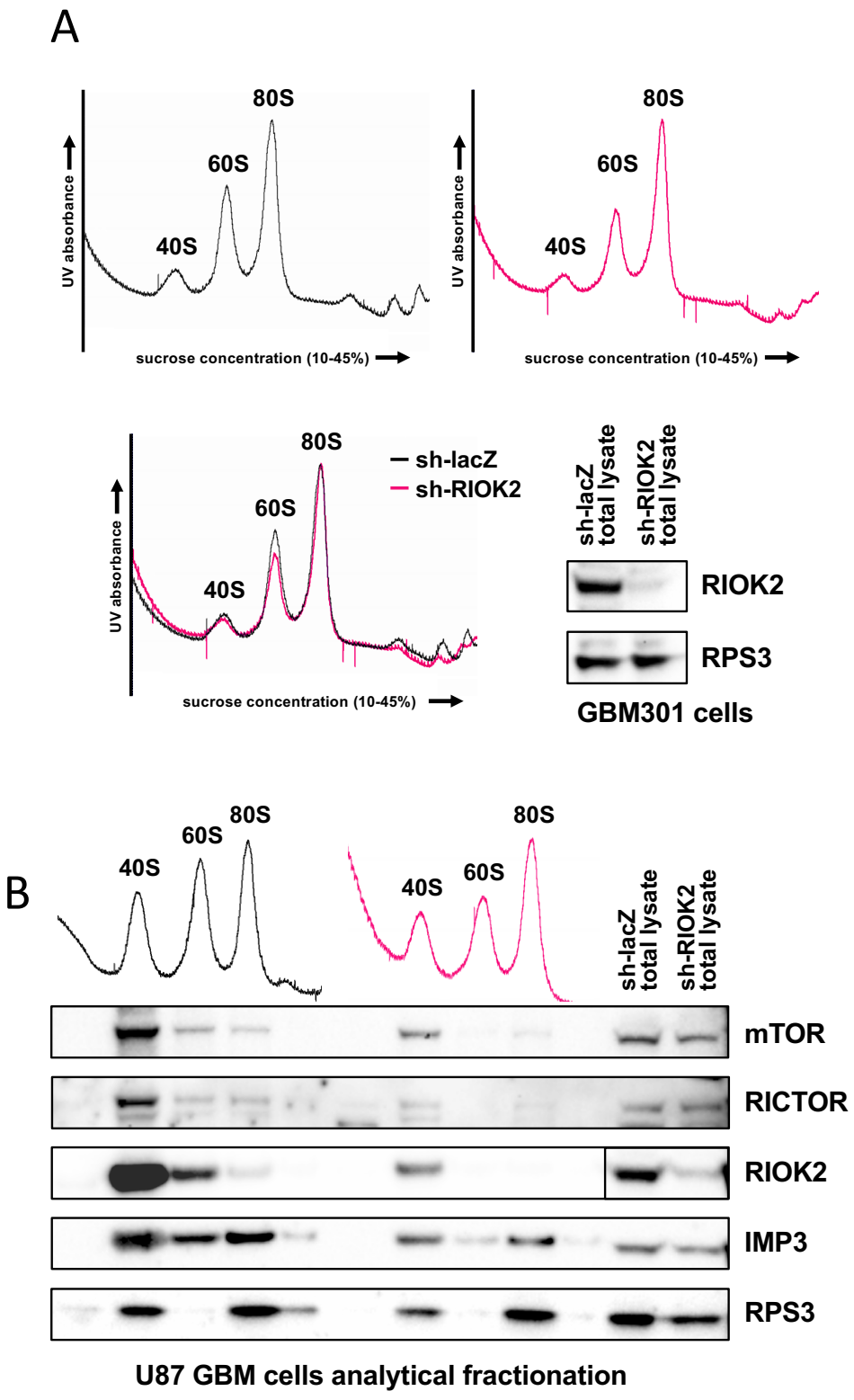

Figure S3.1. RIOK2 RNAi induces minor defects in ribosome biogenesis and disrupts TORC2 activation.

A) Analytical sucrose density gradient fractionation of GBM301 cells treated with either a lentiviral control lacZ shRNA or a validated RIOK2 shRNA. Cells were infected with shRNAs, treated with 20 μM zVAD, and harvested 72 hrs following infection. Western blots of total cell lysates (right) confirmed RIOK2 knockdown and equivalent expression levels of ribosomal proteins between control and RIOK2 knockdown samples. 4 ODs from each lysate were ultracentrifuged in a sucrose density gradient of 10%-45%, and eluted into several fractions while a UV lamp was used to detect ribosome subunits. Annotated UV traces show that RIOK2 knockdown slightly reduced levels of 40S and 60S subunits relative to levels of mature 80S monosomes.

B) RIOK2 co-fractionates with mTor and Rictor in association with the 40S ribosome subunit in GBM cells by analytical sucrose density gradient fractionation. RIOK2 knockdown efficiency confirmed by western blot on total cell lysate, right two lanes. Annotated UV traces for each sample (9 ODs used for each) is shown above western blot results for concentrated matched fractions, which show that RIOK2 knockdown induced a slight reduction in levels of 40S and 60S subunits relative to mature 80S monosomes. RIOK2, mTOR, and RICTOR proteins are enriched in the concentrated fractions collected for the 40S peak, as confirmed by the presence of the small subunit protein RPS3. RIOK2 knockdown inhibited mTOR-RICTOR co-fractionation with the 40S ribosome subunit. IMP3 also co-fractionated with mature and immature ribosomes. These results may indicate either direct association or independent co-fractionation of RIOK2-IMP3-mTOR-RICTOR complexes with ribosome subunits.

Data generated in (A, B) by Jhomar Marquez and Renee D. Read.

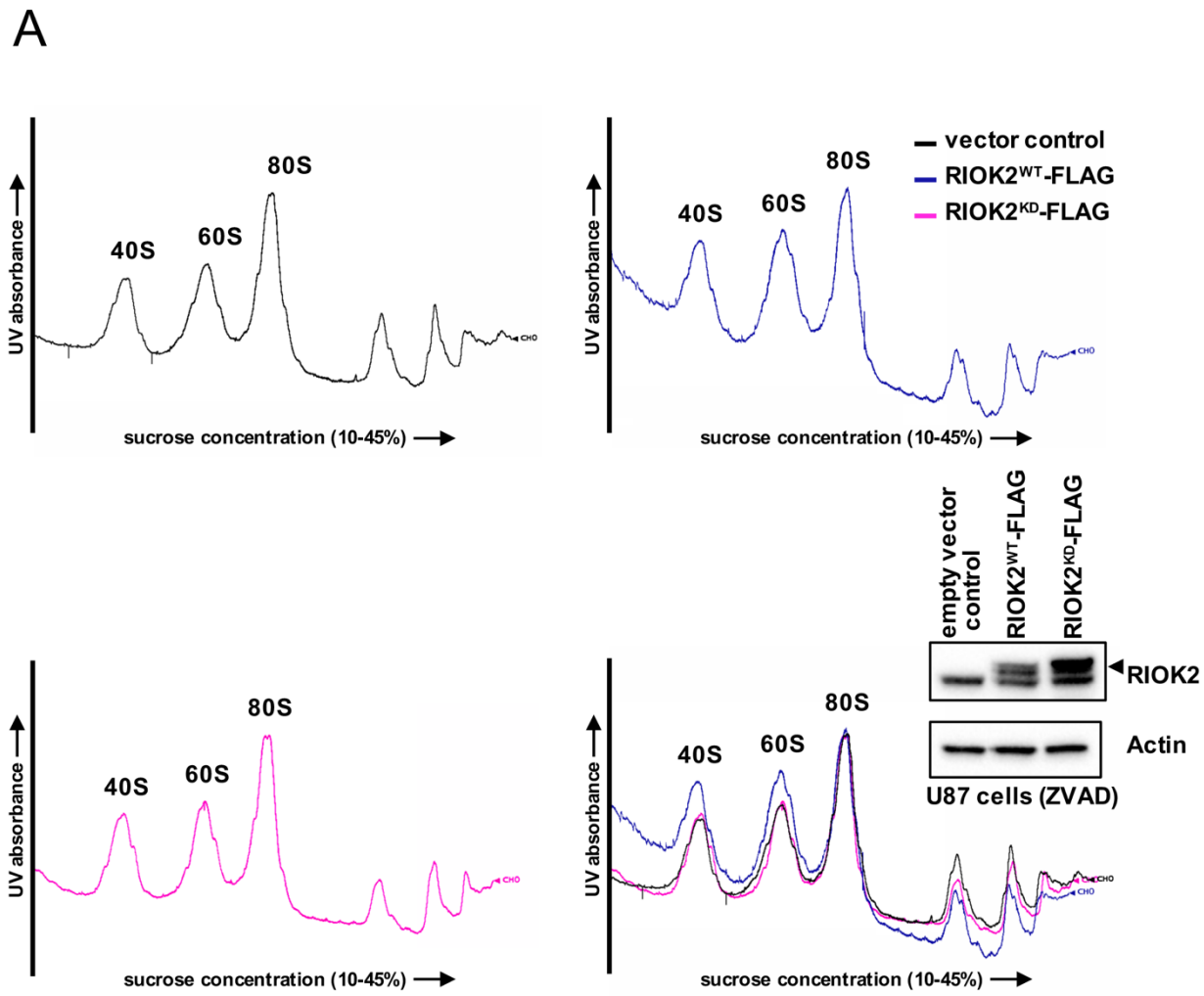

Figure S3.2. Overexpressed catalytically inactive RIOK2 does not induce defects in ribosome biogenesis.

A) Analytical sucrose density gradient fractionation of from U87 GBM cells overexpressing either empty vector control, FLAG-tagged wild-type RIOK2 (RIOK2^{WT}-FLAG), or FLAG-tagged catalytically inactive RIOK2 (RIOK2^{KD}-FLAG). RIOK2 constructs were induced for 48 hr by doxycycline prior to harvesting cells. RIOK2-FLAG induction efficiency confirmed by western blot on total cell lysate (arrow indicates higher molecular weight epitope-tagged

RIOK2).10 ODs from each lysate were ultracentrifuged in a sucrose density gradient of 10%-45%, and eluted into several fractions while a UV lamp was used to detect ribosome subunits. Annotated UV traces show that compared to empty vector control U87 cells (black trace), $RIOK2^{KD}$-FLAG overexpression did not affect levels of 40S and 60S subunits relative to levels of mature 80S monosomes in U87 cells (magenta trace), whereas $RIOK2^{WT}$-FLAG overexpression slightly increased levels of 40S and 60S subunits relative to levels of mature 80S monosomes in U87 cells (blue trace). Bottom right shows all UV traces overlaid normalized to 80S peak height.

Data generated in (A) by Alexander S. Chen and Renee D. Read with technical assistance from Coston Rowe.

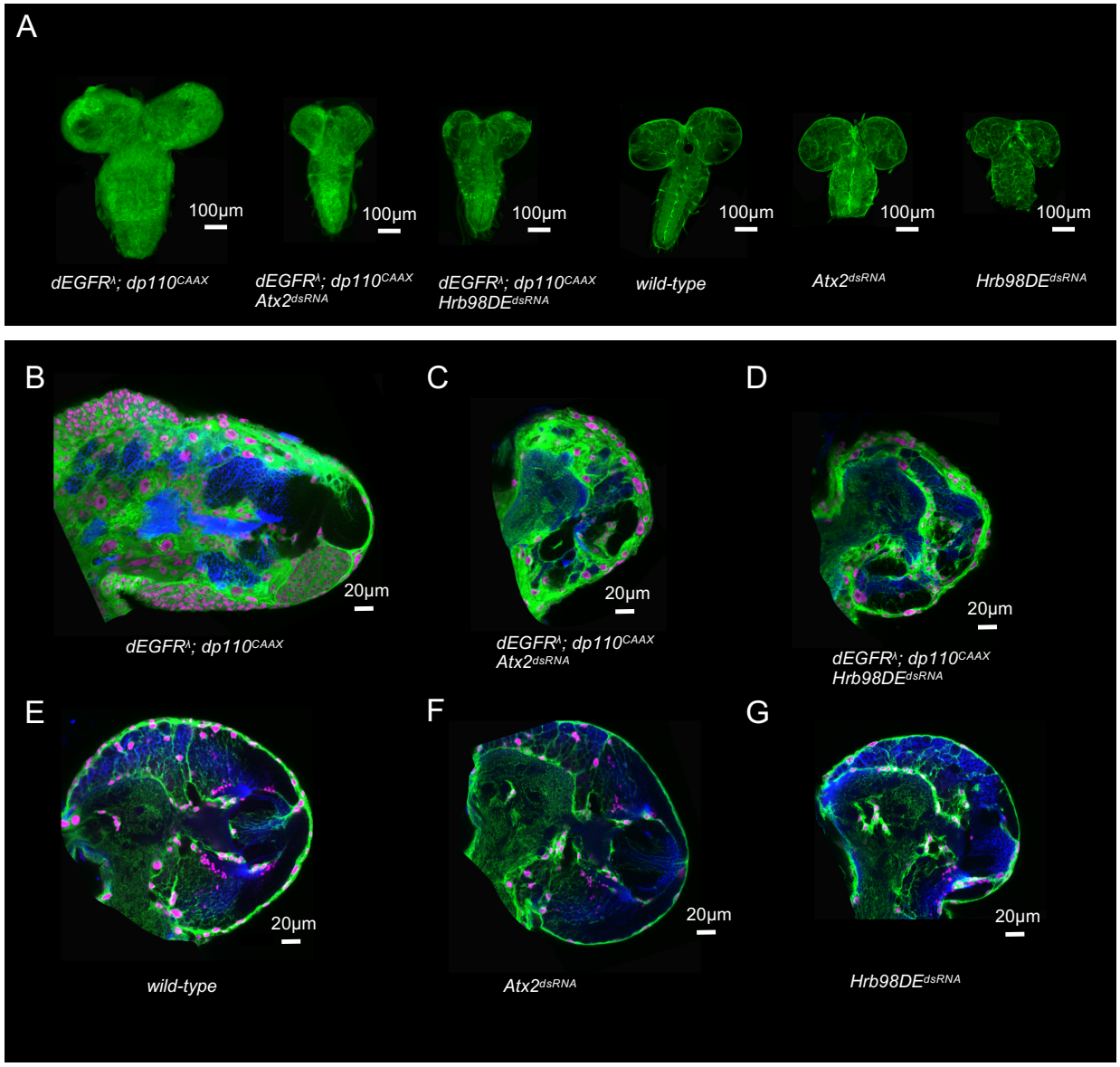

Figure S3.3. *Drosophila* orthologs of RIOK2 associated RNA-binding proteins are required for EGFR-PI3K glial neoplasia.

(A) Optical projections of whole brain-nerve cord complexes from 3rd instar larvae approximately 6 days old. Dorsal view; anterior up. CD8-GFP (green) labels glial cell bodies. Knockdown of RBPs Atx2 (*repo>dEGFR$^{\lambda}$;dp110^{CAAX};Atx2^{dsRNA}*) or Hrb98DE (*repo>dEGFR$^{\lambda}$;dp110^{CAAX};Hrb98DE^{dsRNA}*) decreased brain overgrowth relative to

repo>dEGFR$^{\lambda}$;dp110^{CAAX}. Glia-specific knockdown of Atx2 (*repo>Atx2^{dsRNA}*) or Hrb98DE (*repo>Hrb98DE^{dsRNA}*) induced no obvious defects as compared to wild-type control brains. (B-G) 3 μm optical projections of brain hemispheres, aged-matched 3rd instar larvae. Frontal sections, midway through brains. Anterior up; midline to the left. Repo (magenta) labels glial cell nuclei; CD8-GFP (green) labels glial cell bodies; anti-HRP (blue) counterstains for neurons and neuropil. Knockdown of RBPs (C) Atx2 (*repo>dEGFR$^{\lambda}$;dp110^{CAAX};Atx2^{dsRNA}*) or (D) Hrb98DE (*repo>dEGFR$^{\lambda}$;dp110^{CAAX};Hrb98DE^{dsRNA}*) decreased the numbers of neoplastic glia compared to (B) *repo>dEGFR$^{\lambda}$;dp110^{CAAX}*. Glia-specific knockdown of (F) Atx2 (*repo>Atx2^{dsRNA}*) or (G) Hrb98DE (*repo>Hrb98DE^{dsRNA}*) induced no drastic differences in glial cell numbers or morphology as compared to (E) wild-type animals.

Data generated by Alexander S. Chen and Riley Gulbronson.

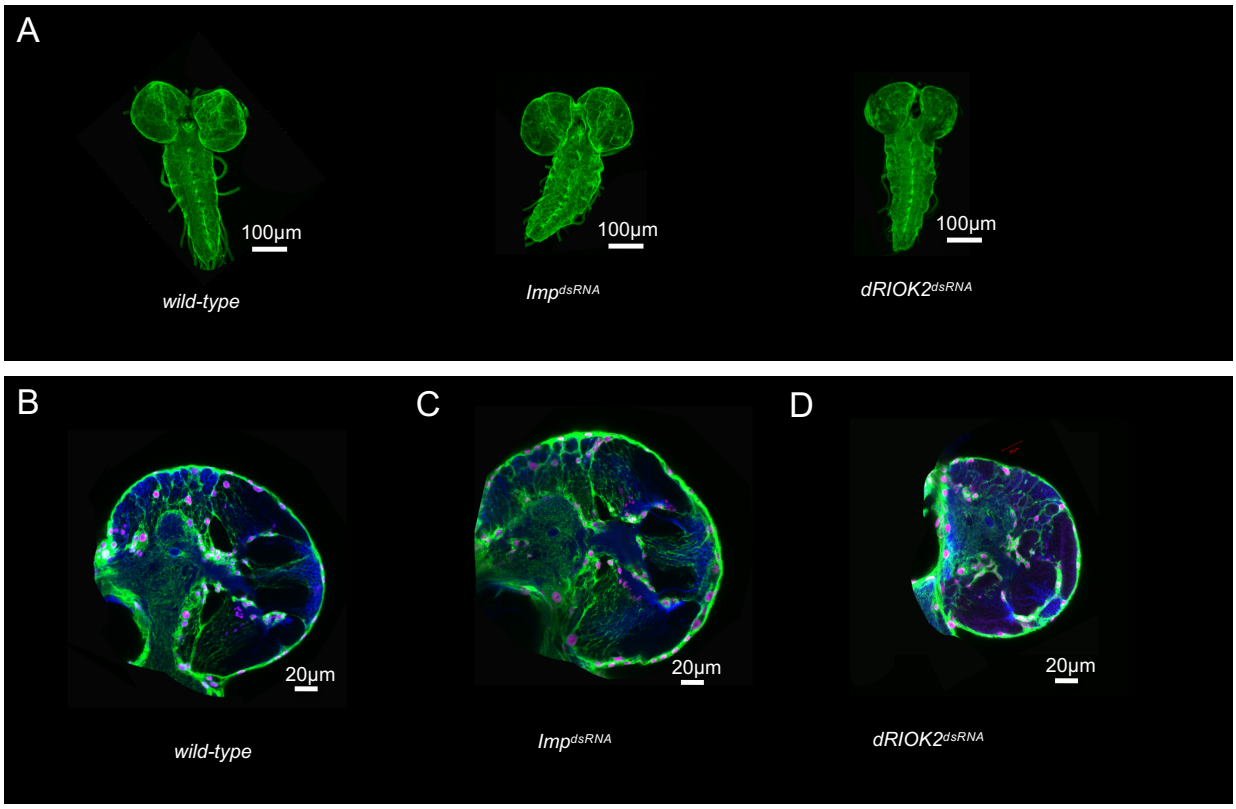

Figure S3.4. Imp and dRIOK2 knockdown in wild-type background produced no gross morphological defects in *Drosophila* glia.

(A) Optical projections of whole brain-nerve cord complexes from 3rd instar larvae approximately 6 days old. Dorsal view; anterior up. CD8-GFP (green) labels glial cell bodies. Imp (*repo>Imp^{dsRNA}*) or dRIOK2 (*repo>dRIOK2^{dsRNA}*) knockdown induced no drastic morphological differences in glia compared to wild-type control animals.

(B-D) 3 μm optical projections of brain hemispheres, aged-matched 3rd instar larvae. Frontal sections, midway through brains. Anterior up; midline to the left. Repo (magenta) labels glial cell nuclei; CD8-GFP (green) labels glial cell bodies; anti-HRP (blue) counterstains for neurons and neuropil. Compared to (A) wild-type animals, neither (B) *Imp* knockdown *(repo>Imp^{dsRNA}*)

nor (D) dRIOK2 knockdown (*repo>dRIOK2*^{dsRNA}) showed drastic defects in glial cell numbers or morphology.

Data generated by Alexander S. Chen and Riley Gulbronson.

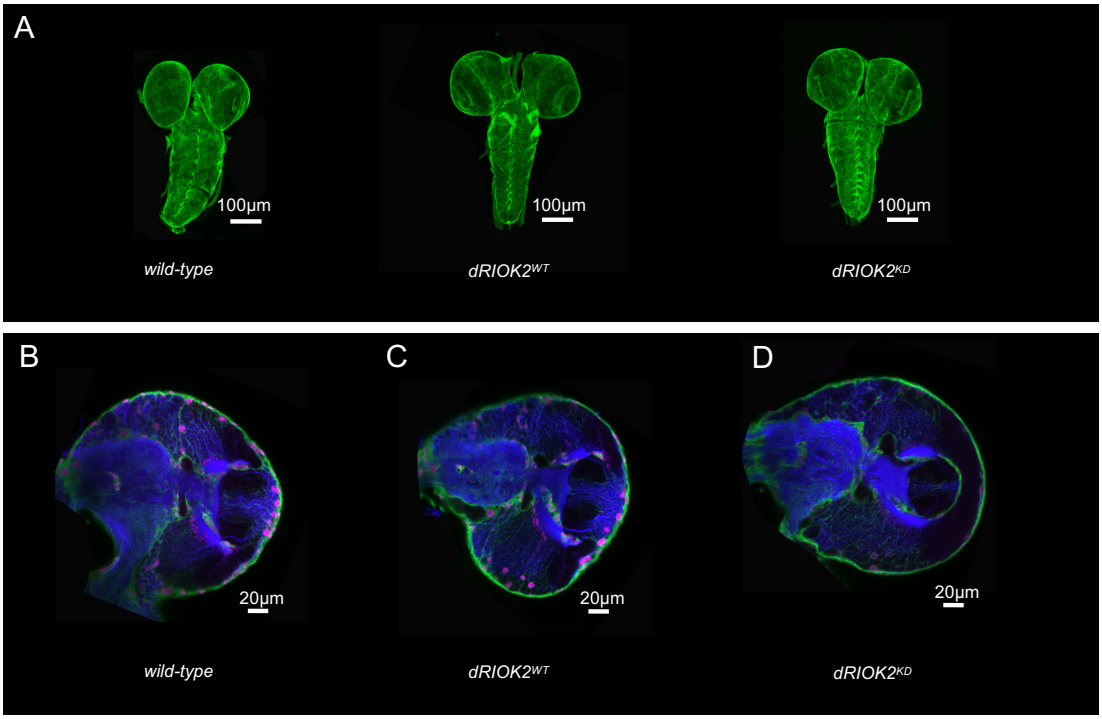

Figure S3.5. dRIOK2 or kinase-dead dRIOK2 overexpression induced no gross development or morphological defects in *Drosophila* glia.

(A) Optical projections of whole brain-nerve cord complexes from 3rd instar larvae approximately 6 days old. Dorsal view; anterior up. CD8-GFP (green) labels glial cell bodies. Overexpression of either wild-type dRIOK2 (*repo>dRIOK2^{WT}*) or kinase-dead dRIOK2 (*repo>dRIOK2^{KD}*) induced no drastic morphological differences in the brain compared to wild-type control animals.

(B-D) 3 µm optical projections of brain hemispheres, aged-matched 3rd instar larvae. Frontal sections, midway through brains. Anterior up; midline to the left. Repo (magenta) labels glial cell nuclei; CD8-GFP (green) labels glial cell bodies; anti-HRP (blue) counterstains for neurons and neuropil. Compared to wild-type animals (A), (B) overexpression of wild-type dRIOK2 (*repo>dRIOK2^{WT}*) or overexpression of kinase-dead dRIOK2 (*repo>dRIOK2^{KD}*) produced no drastic morphological differences compared to wild-type animals showed drastically different

brain morphology.

Data generated by Alexander S. Chen and Emily Legan.

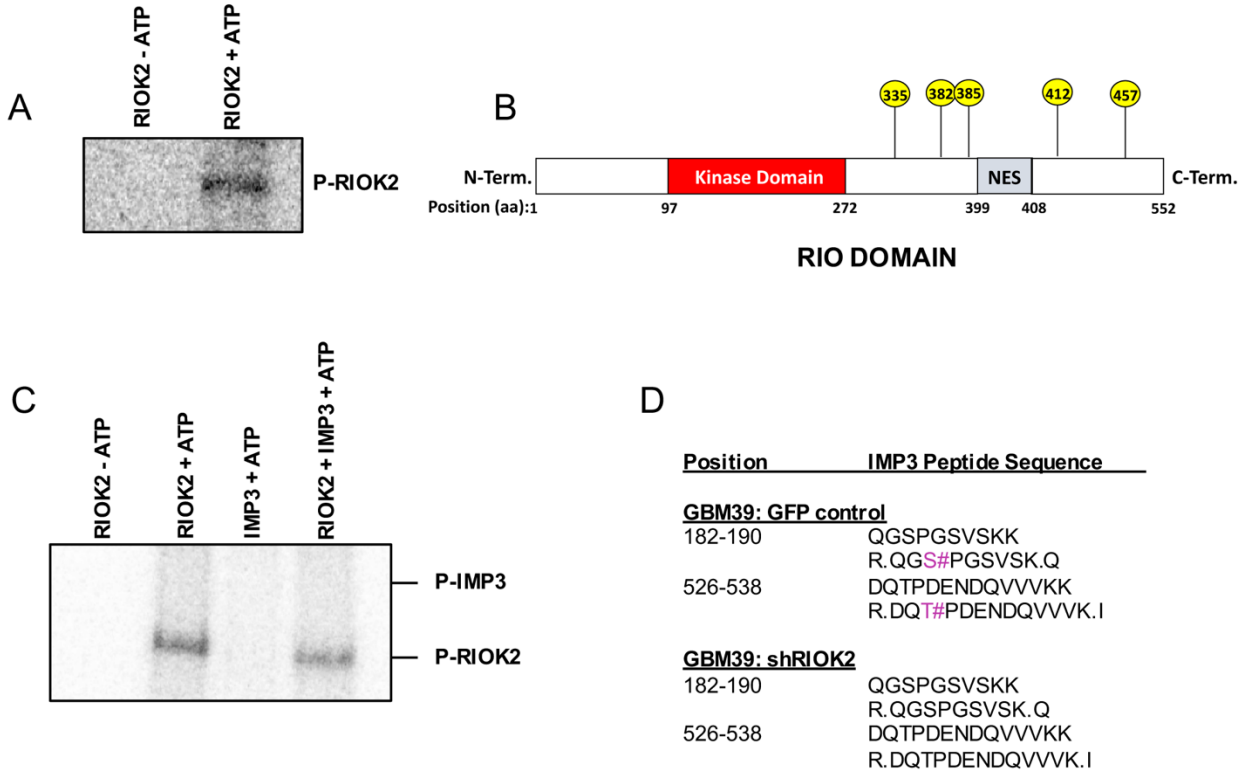

Figure S3.6: RIOK2 autophosphorylates itself but does not directly phosphorylate IMP3.

(A) Phospho-image of *in vitro* kinase assay using purified recombinant RIOK2 protein and radiolabeled ATP show that RIOK2 is autophosphorylated.

(B) Representative image of RIOK2 phospho-sites identified using phospho-proteomics.

(C) Phospho-image of *in vitro* kinase assay using purified recombinant RIOK2 and/or IMP3 protein and radiolabeled ATP show that RIOK2 is autophosphorylated, but does not directly phosphorylated IMP3.

(D) Phospho-peptide profiling of endogenous IMP3. RIOK2 knockdown was performed in GBM39 cells using verified lentiviral shRNAs. GBM cells were treated with 20 μM zVAD to

prevent apoptosis. Cells were harvested 72 hrs after infection, and IMP3 was IPed. RIOK2 knockdown was verified by western blot. GBM39 cells with RIOK2 knockdown showed reduced IMP3 phosphorylation on Ser184 and Ser528 (magenta) compared to IMP3 from control cells. Data generated by Alexander S. Chen with technical assistance from the Taplin Biological Mass Spectrometry Facility.

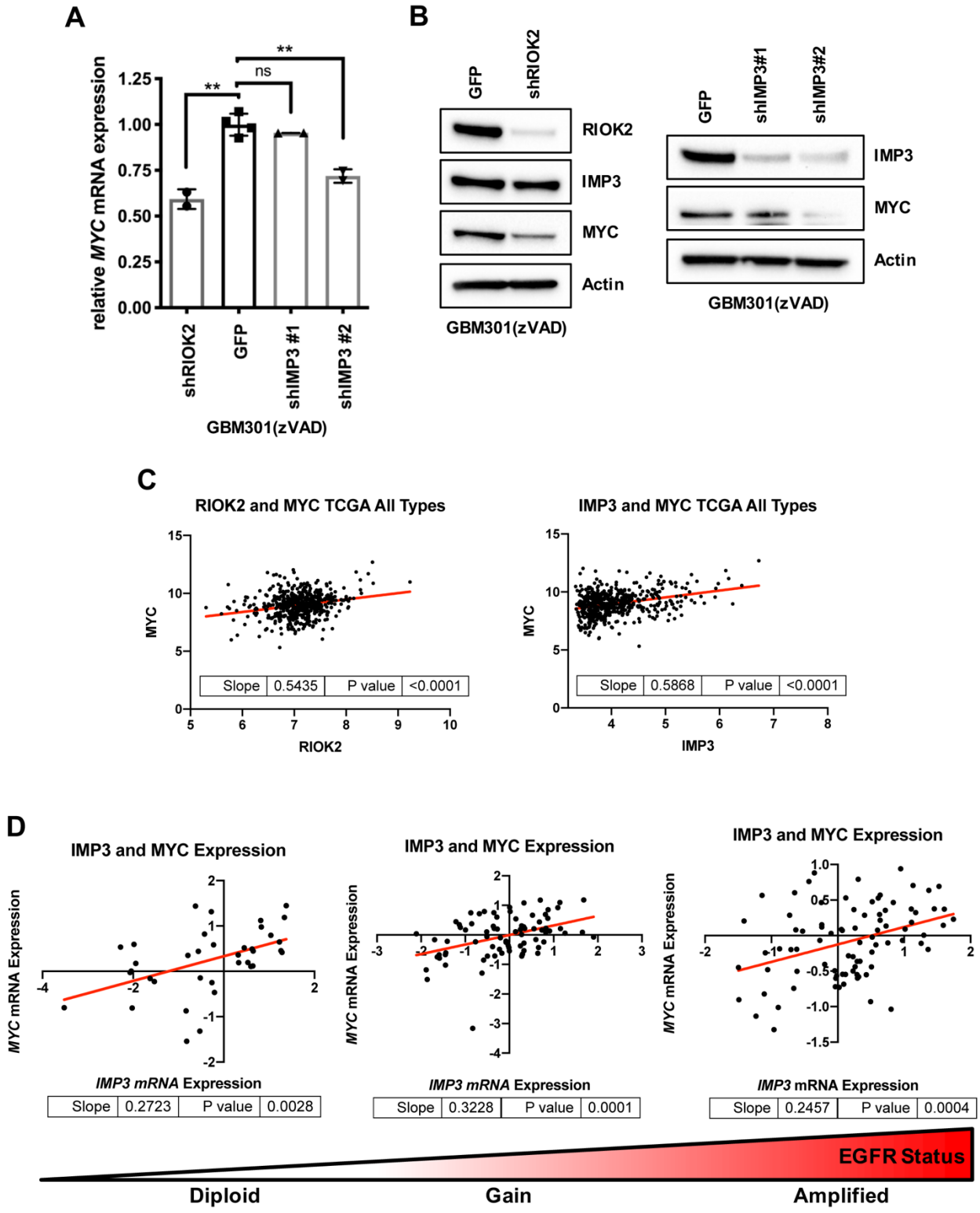
A
relative MYC mRNA expression
1.25
1.00
0.75
0.50
0.25
0.00
**
**
ns
shRIOK2
GFP
shIMP3 #1
shIMP3 #2
GBM301(zVAD)
B
GFP
shRIOK2
RIOK2
IMP3
MYC
Actin
GBM301(zVAD)
GFP
shIMP3#1
shIMP3#2
IMP3
MYC
Actin
GBM301(zVAD)
C
RIOK2 and MYC TCGA All Types
MYC
RIOK2
Slope 0.5435 P value <0.0001
IMP3 and MYC TCGA All Types
MYC
IMP3
Slope 0.5868 P value <0.0001
D
IMP3 and MYC Expression
MYC mRNA Expression
IMP3 mRNA Expression
Slope 0.2723 P value 0.0028
IMP3 and MYC Expression
MYC mRNA Expression
IMP3 mRNA Expression
Slope 0.3228 P value 0.0001
IMP3 and MYC Expression
MYC mRNA Expression
IMP3 mRNA Expression
Slope 0.2457 P value 0.0004
EGFR Status
Diploid
Gain
Amplified

Figure S3.7: RIOK2 and IMP3 modulate MYC expression in GBM cells in a conserved pathway.

RIOK2 or IMP3 knockdown was performed in GBM 301cells using verified lentiviral shRNAs. GBM301 cells were treated with 20 μM zVAD to prevent apoptosis. GBM301 cells with RIOK2 and IMP3 knockdown showed reduced expression of endogenous *MYC* mRNA, as measured by qPCR, and MYC protein, as measured by western blot, compared to control cells infected with GFP shRNA. The samples shown in this figure were harvested 72 hrs after infection, although by 96 hrs after infection we observed a stronger effect on MYC protein levels as shown in Figure 6C, suggesting that MYC levels drop following a prolonged reduction of IMP3 protein. Two replicates were used per condition. Statistics generated using unpaired two-tailed Student TTESTS, **$p<0.01$.

(C, D) Analysis of TCGA glioma tumor profiling data show significant correlation between increased expression of both *RIOK2* and *IMP3* mRNA and *MYC* mRNA expression across all TCGA glioma grades (C). Increased expression of *IMP3* and *MYC* mRNA are significantly correlated with each other and significantly increased in grade IV gliomas with EGFR gain and amplification compared to tumors diploid for EGFR (D).

Data generated by in (A, B) by Alexander S. Chen, Se-Yeong Oh, and Nathaniel H. Boyd, and in (C-D) by Nathaniel H. Boyd.

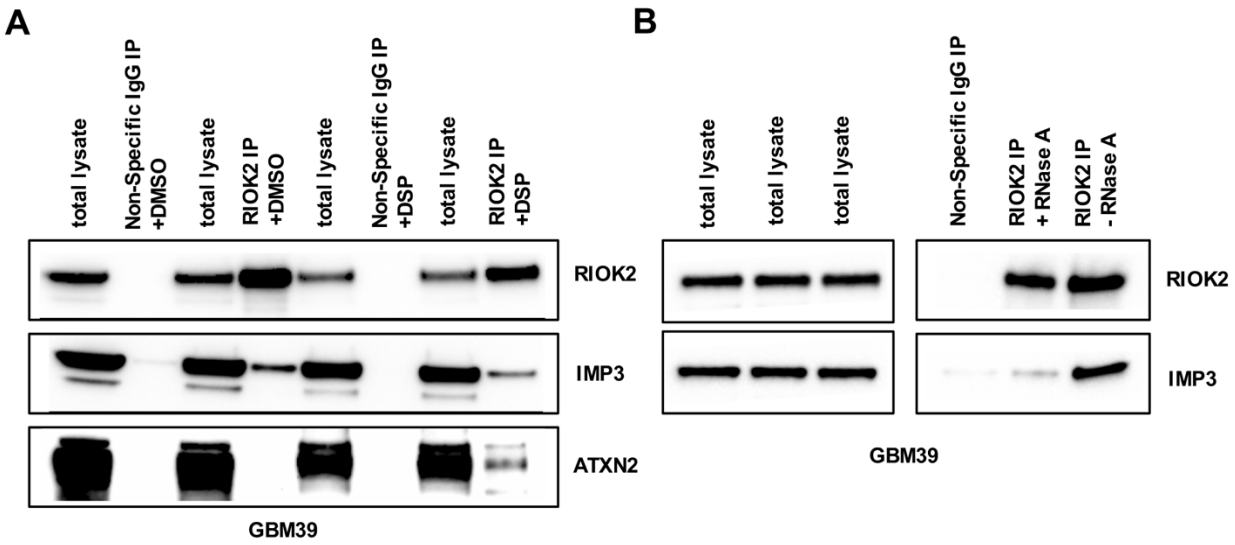

Figure S3.8: RIOK2-IMP3 complexes include other RNA-binding proteins and rely on the presence of RNA.

A). GBM39 treated with either DMSO or DSP crosslinker (1 mM) for 2 hrs prior to IPs with either a RIOK2 antibody or a non-specific IgG control. Western blots show enrichment of endogenous ATXN2 protein in the RIOK2 IP samples treated with DSP.

B). GBM39 treated with RNAse A (100µg/ml) prior to IPs with either a RIOK2 antibody or a non-specific IgG control. Western blots show decrease levels of IMP3 protein when in the sample treated with RNase A.

Data generated by Alexander S. Chen.

Table S1:Proteomic approach to identify endogenous RIOK2 binding proteins									
		U87				GBM301			
		Non-Specific IgG IP		RIOK2 IP		Non-Specific IgG IP		RIOK2 IP	
GENE	FLY Homolog	Spectral Counts	Unique Peptide	Spectral Counts	Unique Peptide	Spectral Counts	Unique Peptide	Spectral Counts	Unique Peptide
LTV1	CG7686	0	0	21	13	0	0	23	14
NOB1	CG2972	0	0	12	9	2	2	10	8
PNO1	lethal (1) G0004	0	0	18	7	2	2	18	10
G3BP2	rasputin	0	0	8	6	4	2	13	8
ILF3	Zn72D	0	0	13	11	17	12	29	22
RIOK2	**RIOK2**	0	0	22	11	0	0	14	12
IMP3	**Imp**	0	0	8	6	0	0	5	3
BYSL	bys	0	0	17	12	2	2	18	11
TSR1	CG7338	0	0	30	22	0	0	28	19
SEC23IP	PAPLA1	1	1	17	12	1	1	5	5
GIGYF2	CG11148	1	1	9	5	1	1	14	12
G3BP1	rasputin	4	4	27	13	7	7	3	1
PABPC4	pAbp	6	1	28	8	10	8	17	6
ATXN2L	Atx2	2	1	8	6	4	3	10	8
RRBP1	alt	5	4	19	1	28	28	57	47
DDX1	Ddx1	8	6	26	12	7	6	21	15
HNRNPUL1	CG30122	1	1	3	1	13	11	6	4
DDX5	CG10077	10	4	29	13	7	3	19	9
HNRNPA3	Hrb98DE, Hrb87F	5	4	13	1	11	8	13	11
DDX17	CG10077	13	7	19	8	7	3	21	12
HNRNPL	smooth	4	3	5	5	2	2	6	6

Table S3.1: Proteomic approach to identify endogenous RIOK2 binding proteins.

Proteomic analysis of IPs from U87-EGFR^{vIII} cells and GBM301 cells performed with antibodies against endogenous RIOK2 or a non-specific IgG control. Values are reported in spectral counts (PSM) or number of unique peptides. Spectral counts are the total number of spectra identified for a protein and is a relative measurement of the quantity of a given protein, while the number of unique peptides refers to the number of peptides that matches the protein in question. Names of the human genes are given along with the name of the associated fly homolog.

Data generated by Alexander S. Chen with technical assistance from Duc Duong.

Table S2: RNAi screen of *Drosophila* orthologs for RIOK2 binding proteins

Stock ID Number	CG Number	Gene Name	dEGFR$^{\lambda}$;dp110^{CAAX} Phenotype	wild-type Phenotype
v49919	CG18212	alt	NE	NE
v108279	CG18212	alt	NE	NE
v108843	CG5166	Atx2	NE	NE
v34955	CG5166	Atx2	NE	NE
v34956	CG5166	Atx2	S	NE
b36114	CG5166	Atx2	S	NE
b44012	CG5166	Atx2	SS	S
b34876	CG1430	bys	SS	S
b29017	CG9054	Ddx1	NE	NE
v103365	CG9054	Ddx1	S	NE
v29019	CG9054	Ddx1	NE	nd
b61289	CG9054	Ddx1	NE	NE
b27531	CG9054	Ddx1	NE	NE
b55744	CG9054	Ddx1	NE	NE
b27484	CG6203	Fmr1	NE	nd
b6929	CG6203	Fmr1	NE	NE
b6930	CG6203	Fmr1	NE	NE
b28896	CG11148	Gyf	NE	NE
v105985	CG11148	Gyf	NE	NE
v18158	CG11148	Gyf	NE	nd
v18159	CG11148	Gyf	NE	NE
v51759	CG12749	Hrb87F	SS	SS
b31472	CG12749	Hrb87F	NE	nd
b31244	CG12749	Hrb87F	NE	NE
b52937	CG12749	Hrb87F	NE	NE
v29523	CG9983	Hrb98DE	NE	SS
b32351	CG9983	Hrb98DE	SS	SS
b31303	CG9983	Hrb98DE	NE	NE
v27963	CG7338	Tsr1	SS	SS
v27965	CG7338	Tsr1	SS	SS

Table S2: RNAi screen of *Drosophila* orthologs for RIOK2 binding proteins

Stock ID Number	CG Number	Gene Name	dEGFR$^{\lambda}$;dp110^{CAAX} Phenotype	Wild-Type Phenotype
v20321	CG1691	Imp	NE	nd
v20322	CG1691	Imp	SS	NE
b34977	CG1691	Imp	SS	NE
b55645	CG1691	Imp	NE	NE
v16289	CG11738	l(1)G0004	SS	NE
v33649	CG7686	LTV1	NE	NE
v33650	CG7686	LTV1	SS	SS
v62514	CG7686	LTV1	SS	nd
v22007	CG5119	pAbp	NE	SS
b36127	CG5119	pAbp	NE	nd
b28821	CG5119	pAbp	NE	nd
b53247	CG5119	pAbp	NE	nd
v35956	CG8552	PAPLA1	NE	NE
v35957	CG8552	PAPLA1	NE	NE
v108121	CG8552	PAPLA1	NE	NE
b63605	CG8552	PAPLA1	NE	NE
b44638	CG8552	PAPLA1	NE	NE
v29113	CG9412	rin	NE	SS
v109911	CG9412	rin	S	NE
b33392	CG9412	rin	NE	nd
b57694	CG9412	rin	NE	NE
b9303	CG9412	rin	NE	NE
v108351	CG9218	Sm	NE	NE
b32669	CG5215	Zn72D	NE	nd
v104991	CG2972		SS	NE
v48771	CG2972		SS	nd
v106984	CG30122		NE	NE
b55209	CG30122		NE	NE
b32388	CG10077		NE	nd

Table S3.2. RNAi screen of *Drosophila* orthologs for RIOK2 binding proteins.

UAS-dsRNA stocks were obtained for *Drosophila* orthologs of RIOK2 binding proteins and tested to determine the effects of RNAi knockdown of their target genes on neoplastic glia using the *repo>dEGFR$^{\lambda}$;dp110^{CAAX}* GBM model and, for comparison, on wild-type glia using *repo-Gal4*. Not all UAS-dsRNA stocks tested have been validated for their RNAi efficacy. VDRC stock ID numbers prefaced with a "v," Bloomington stock ID numbers are prefaced by a "b". Key to genetics interactions: WS: weak suppressor, S: moderate suppressor, SS: strong suppressor; NE: no effect indicates that there were no obvious phenotypic differences between dsRNA and control animals; nd indicates no determined.

Data generated by Alexander S. Chen.

Table S3: Proteomics approach to identify RIOK2-FLAG binding proteins						
	Vector Control		RIOK2^{WT} FLAG IP		RIOK2^{KD} FLAG IP	
Human Gene	Spectral Counts	Unique Peptide	Spectral Counts	Unique Peptide	Spectral Counts	Unique Peptide
LTV1	0	0	8	6	11	7
NOB1	0	0	7	4	8	7
PNO1	1	1	11	5	12	7
G3BP2	4	3	6	4	6	5
ILF3	4	4	5	3	11	5
RIOK2	0	0	78	23	78	23
IMP3	2	2	5	2	2	1
BYSL	0	0	4	3	2	2
TSR1	1	1	18	11	6	6
SEC23IP	3	3	5	5	8	5
GIGYF2	2	2	3	3	2	2
G3BP1	11	7	14	8	17	9
PABPC4	9	2	11	1	15	4
ATXN2L	5	4	7	5	10	9
RRBP1	8	7	13	1	14	1
DDX1	8	6	11	5	15	9
HNRNPUL1	1	1	5	3	4	4
DDX5	23	14	38	17	29	16
HNRNPA3	13	9	17	1	7	6
DDX17	9	6	21	9	17	7
HNRNPL	9	8	11	8	17	11

Table S3.3. IMP3 does not strongly co-immunoprecipitate with catalytically inactive RIOK2.

Proteomic analysis of RIOK2^{WT}-FLAG or catalytically inactive RIOK2^{KD}-FLAG, both with an N-terminal FLAG epitope tag, and empty vector control cells. RIOK2-FLAG constructs were overexpressed using doxycycline inducible vectors. Cells were treated with 8 μg/ml of doxycycline and incubated for 72 hrs and then lysed under hypotonic conditions. Using M2 antibodies to the FLAG epitope tag, IPs were performed on total cell lysates from all three samples, and subjected to proteomic analysis. Values are reported in spectral counts (PSM) and number of unique peptides. Spectral counts are the total number of spectra identified for a protein and is a relative measurement of the quantity of a given protein, while the number of unique peptides refers to the number of peptides that matches the protein in question.

Data generated by Alexander S. Chen with technical assistance from Duc Duong.

Chapter 4. Discussion

Glioblastoma multiforme (GBM) continues to pose a considerable challenge, as the most common primary malignant adult brain tumor with a relatively poor patient overall survival of approximately 14.6 months (1). Due to the highly invasive, heterogeneous, and infiltrative nature of these tumors, there has been marginal progress in the development of treatment strategies that extend survival (2, 3). Efforts to genomically characterize this disease have identified a number of genes that are frequently altered in GBM, such as genes in the EGFR and PI3K signaling axes. However, efforts to therapeutically target these pathways have been largely unsuccessful in improving patient outcomes (7, 8, 27-30). Therefore, there has been a concerted effort to better understand the underlying tumor biology of GBM, focusing on frequently altered signaling transduction pathways implicated in disease progression, and how downstream effectors of these pathways contribute to the overall morbidity of this disease.

Given the high prevalence of genomic mutations and overexpression of RTKs, such as EGFR, and of activating mutations in PI3K signaling pathway components (7), investigation of how these signaling pathways rely on aberrant activation of novel downstream effectors has been the primary focus of my dissertation. The development of a *Drosophila* GBM model with glial-specific activation of EGFR and PI3K by Dr. Renee D. Read (49) and recent advancements in cell culture-based approaches that more closely model essential GBM tumor biology (109), have positioned our laboratory to be uniquely suited for mechanistic studies of how the EGFR and PI3K downstream pathways coordinately drive GBM tumorigenesis. My research focuses on two novel kinases, which were first identified in a kinome-wide screen performed using the *Drosophila* GBM model (50), that function downstream of EGFR-PI3K signaling to drive GBM tumorigenesis through two novel and disparate mechanisms. My second chapter focuses on

investigating the mechanisms by which STK17A/Drak operates downstream of EGFR-PI3K signaling pathways in order to phosphorylate Sqh/MRLC, which in turn activates the Anillin adaptor protein to coordinately regulate cytokinesis to promote GBM tumorigenesis. My third chapter focuses on exploring how RIOK2 forms a complex with RNA-binding protein, IMP3, and TORC2 to modulate MYC protein levels to drive GBM tumorigenesis. Collectively, my dissertation adds to our overall understanding of how EGFR-PI3K pathways activates two novel kinases, STK17A and RIOK2, to promote GBM tumorigenesis through disparate mechanisms. By understanding how STK17A/Drak and the RIOK2-IMP3-TORC2 complex specifically contribute to GBM tumor biology, we may be able to design more effective targeted therapies against these kinases and improve patient treatment strategies.

4.1 Drak/STK17A in EGFR driven gliomagenesis

In the second chapter, I outline a novel function where STK17A/Drak drives GBM tumorigenesis by regulating cytokinesis. Cytokinesis has long been an interest in the context of GBM tumorigenesis. Disruption of this mechanism can have a number of functional consequences ranging from unequal distribution of genetic material to uncontrolled cellular proliferation and growth. Both of which are conducive to glial neoplasia. To assess the mechanisms in which Drak promotes tumorigenesis, I utilized our *Drosophila* GBM model system to discover that Drak, the *Drosophila* ortholog of STK17A, specifically drives glial tumorigenesis downstream of EGFR-PI3K signaling in a kinase-dependent manner. Furthermore, the use of our *Drosophila* GBM model has identified known downstream effectors of Drak, such as Sqh and Anillin, and both of these effectors have a prominent influence on GBM tumorigenesis. Interestingly, I observed that Drak, activated Sqh, and Anillin all co-localized to

the cleavage furrow of mitotic glial cells, suggesting that Drak, Sqh, and Anillin may play a key role in cytokinesis to promote GBM tumorigenesis. Importantly, these results were recapitulated in human GBM cells, suggesting that this pathway is evolutionarily conserved. Collectively, these results identify a novel mechanism in which GBM tumor cells hi-jack cytokinesis in order to promote uncontrolled cellular proliferation and growth. In the developing fly, studies show that Drak/Sqh/Anillin regulates the actin cytoskeleton (129-132). Our data in human GBM models reveal that GBM can adopt this essential evolutionarily conserved developmental pathway, resulting in uncontrolled tumor cell proliferation.

While our studies on STK17A/Drak have made major contributions to our understanding of GBM tumor biology, there still remains a number of questions regarding how STK17A regulates cytokinesis. While our data shows that STK17A/Drak, MRLC/Sqh, and Anillin co-localize to the cleavage furrow of mitotic glial cells, the precise manner in which these members contribute to the formation of the cleavage furrow is currently unknown. In the future, we can use live-imaging approaches of fluorescently labeled actin subunits to address how STK17A/Drak defects may influence cytoskeletal remodeling at the cleavage furrow and whether these defects directly influence the proliferation of neoplastic glia.

Furthermore, while our studies show that STK17A promotes GBM tumorigenesis by phosphorylating MRLC, the precise nonmuscle myosin type II isoform that contributes to glial cell proliferation is currently unknown. Studies show that NMII isoform C may regulate cytokinesis and is expressed in GBM (219). In order to determine whether the STK17A pathway regulates NMIIC, we can perform immunoprecipitations to validate whether NMIIC found in the complex. While questions remain regarding how precisely the Drak/STK17A, Sqh/MRLC, Anillin complex regulates the cytoskeletal remodeling necessary for cytokinesis, our findings

have made major contributions to the understanding of basic tumor GBM biology. By better understanding how protein kinases contribute to the formation of the cleavage furrow, a crucial step in mitosis, we can better understand how cancer cells proliferate and in turn, potentially develop more effective targeted therapies to treat GBM tumor patients.

4.2 RIOK2 and IMP3 in gliomagenesis

The mechanism in which oncogenic mRNAs are regulated is a growing area of research in the field of GBM tumor biology. In the third chapter, I identified how the RIOK2-IMP3-TORC2 complex contributes to GBM tumorigenesis by modulating MYC protein expression. What is fascinating about this project is that it demonstrates how proteins operating in the context of a larger protein complex may convey functions outside of their typically understood role. RIOK2 is typically understood to have a role in the maturation of the 40S ribosomal subunit (141, 144), although our results indicated that ribosome biogenesis is largely unaffected when RIOK2 overexpression is blocked by RNAi. Instead, our data demonstrates that, in GBM cells, RIOK2 is part of a complex with IMP3 and the TORC2 complex, and that these proteins forms a complex distinct from the 40S ribosome subunit and the RIOK2-associated ribosome assembly factors, such as NOB1. Our laboratory identified Imp, the *Drosophila* ortholog of IMP3, through an unbiased screening approach using our *Drosophila* GBM model, as an important effector downstream of dRIOK2 in promoting GBM tumorigenesis. The identification of Imp is interesting given its previously described role as a biomarker in predicting poor patient prognosis (174). Our data in human GBM cells show that RIOK2 form a complex with IMP3 and TORC2, and that RIOK2 catalytic activity is important for the formation of this complex. Additionally, data in both our *Drosophila* GBM model and human GBM stem cells show that dRIOK2/RIOK2

and Imp/IMP3 knockdown reduce levels of MYC protein, indicating that the dRIOK2/RIOK2-Imp/IMP3-TORC2 complex drives GBM tumorigenesis by modulating levels of dMyc/MYC protein.

Our data elucidate how RNA-binding proteins are involved in promoting GBM tumorigenesis. IMP3 is typically understood to be an oncofetal protein and is highly expressed early in development and is only expressed in certain tissues late in development. As such, IMP3 promotes the translation, transport, and stability of target mRNAs involved in essential biological processes vital during early development like migration and cellular growth and proliferation. Our data demonstrates that aberrant activation of EGFR-PI3K signaling in GBM can hi-jack this essential developmental pathway. By operating as a part of a larger complex with IMP3 and TORC2, it is possible that RIOK2 can then quickly modulate the activity of oncogenic target mRNAs through a variety of mechanisms including promoting their stability and/or translation. By regulating a known IMP3 target mRNAs that encode oncogenes, such as MYC and CYCLIN D1, the RIOK2-IMP3-TORC2 complex can promote uncontrolled glial cell growth and proliferation, resulting in GBM tumorigenesis. By understanding how the RIOK2-IMP3 complex contributes to glial cell proliferation in a tumor-specific manner, we can identify new pathways that may serve as more effective therapeutic targets to combat GBM disease progression.

In terms of our understanding of the RIOK2-IMP3 pathway there are a number of aspects relating to the mechanism that are currently unknown. While our data conveys compelling evidence that RIOK2-IMP3-TORC2 complex modulates MYC protein levels, the precise manner in which this complex regulates *MYC* mRNA remains to be determined. Recent data in *Drosophila* show that Imp regulates *dMyc* mRNA stability during development (251). It is possible that in GBM, IMP3, the human ortholog of Imp, may also regulate *MYC* mRNA

stability in this context. In order to address this issue, we can perform actinomycin D mRNA stability assays. Actinomycin D inhibits transcription by intercalating into DNA, and prevents the unwinding of the DNA double-helix, thus, inhibiting DNA-dependent RNA-polymerase activity. By knocking down either RIOK2 or IMP3 in GBM stem cells, we can observe whether reduction of RIOK2 or IMP3 protein levels has any effect on *MYC* mRNA half-life. If *MYC* mRNA half-life is reduced, then RIOK2 and IMP3 have a role in promoting *MYC* mRNA stability.

While I identified mTOR as a component in the RIOK2-IMP3 complex, it is unclear how mTOR regulates IMP3 activity. Does inhibiting mTOR from binding to the complex impact IMP3 activity, and does mTOR directly phosphorylate IMP3 in this context? Ideally, we can use a number of previously described experimental approaches to address these questions. In order to address whether mTOR inhibition may influence IMP3 activity, we can treat GBM stem cells with a mTOR inhibitor such as rapamycin and observe whether mTOR inhibition prevents IMP3 binding to the complex via immunoprecipitation experiments. In order to address whether mTOR directly phosphorylates IMP3, we can utilize our previously described *in vitro* kinase assay.

Finally, while we identified *MYC* as a potential target mRNA of the RIOK2-IMP3 complex, given recent developments in RNA-sequencing technology, we are uniquely suited to identify novel mRNA targets of the RIOK2-IMP3 complex. IMP3 can regulate hundreds of different target mRNAs (159). It will be interesting to observe using RNA-sequencing technologies how knocking down RIOK2 may influence which target mRNAs are bound to IMP3.

4.3 Conclusions

Collectively, these studies on both STK17A/Drak and RIOK2 further emphasizes the importance of *Drosophila melanogaster* as a model organism to study essential GBM tumor biology. Using the *Drosophila* GBM model, I identified two novel protein kinases, and how they regulate two disparate mechanisms to promote GBM tumorigenesis. Moreover, key findings uncovered in our *Drosophila* GBM model were recapitulated in human GBM using cell-based approaches, human tissue microarrays, and TCGA data sets. These results indicate that *Drosophila melanogaster* can successfully model the human GBM disease. By identifying novel pathways quickly and efficiently in *Drosophila* and then translating these findings into human models, we can more quickly develop targeted therapies against novel pathways that promote GBM tumorigenesis and in turn, improve patient prognosis.

Going forward, the well-documented advantages of *Drosophila* models will be crucial for investigating many emerging areas in glioma biology. Due to the ease of genetic manipulation and the availability of powerful imaging modalities, *Drosophila* models are well suited to study tumor microenvironments, where a complex network of different cell types operate within distinct microenvironments that, through local and systemic cues, regulate normal and tumor stem/progenitor cell proliferation and differentiation (253). Studies show that *IDH1/2* mutations are a powerful predictor of GBM patient outcomes (2), and by manipulating *Drosophila* Idh, the ortholog of human IDH1/2, researchers may better understand how *IDH1/2* mutations contribute to glial tumorigenicity (254). Moreover, many human epigenetic regulators were first discovered in *Drosophila* and have functional orthologs in *Drosophila*, such that *Drosophila* models could be effective for determining how mutations in epigenetic regulators, such as *TET2*, promote GBM tumorigenesis (255-257). *Drosophila* models may also be effective tools to test complex,

multi-targeted combinations of pharmacological agents in order to discover effective combinations that can be translated to treat human GBM patients (258). Of note, while *Drosophila* lack an adaptive immune system, they possess a functional innate immune system where *Drosophila* glial cell types perform microglia-like functions during development and injury (38). Therefore, *Drosophila* may be an effective tool to better understand how the innate immune system responds to GBM tumors.

In the future, *Drosophila* will likely continue to reveal novel biological pathways and mechanisms involved in gliomagenesis, and eventually this knowledge may contribute to the development of effective treatment strategies to improve patient outcomes.

References

1. Weller M, van den Bent M, Tonn JC, Stupp R, Preusser M, Cohen-Jonathan-Moyal E, Henriksson R, Le Rhun E, Balana C, Chinot O, Bendszus M, Reijneveld JC, Dhermain F, French P, Marosi C, Watts C, Oberg I, Pilkington G, Baumert BG, Taphoorn MJB, Hegi M, Westphal M, Reifenberger G, Soffietti R, Wick W. European Association for Neuro-Oncology (EANO) guideline on the diagnosis and treatment of adult astrocytic and oligodendroglial gliomas. The Lancet Oncology. 2017;18(6):e315-e29. Epub 2017/05/10. doi: 10.1016/s1470-2045(17)30194-8. PubMed PMID: 28483413.
2. Louis DN, Ohgaki H, Wiestler OD, Cavenee WK, Burger PC, Jouvet A, Scheithauer BW, Kleihues P. The 2007 WHO classification of tumours of the central nervous system. Acta neuropathologica. 2007;114(2):97-109. Epub 2007/07/10. doi: 10.1007/s00401-007-0243-4. PubMed PMID: 17618441; PMCID: PMC1929165.
3. Furnari FB, Fenton T, Bachoo RM, Mukasa A, Stommel JM, Stegh A, Hahn WC, Ligon KL, Louis DN, Brennan C, Chin L, DePinho RA, Cavenee WK. Malignant astrocytic glioma: genetics, biology, and paths to treatment. Genes & development. 2007;21(21):2683-710. Epub 2007/11/03. doi: 10.1101/gad.1596707. PubMed PMID: 17974913.
4. Maher EA, Brennan C, Wen PY, Durso L, Ligon KL, Richardson A, Khatry D, Feng B, Sinha R, Louis DN, Quackenbush J, Black PM, Chin L, DePinho RA. Marked genomic differences characterize primary and secondary glioblastoma subtypes and identify two distinct molecular and clinical secondary glioblastoma entities. Cancer Res. 2006;66(23):11502-13. Epub 2006/11/23. doi: 10.1158/0008-5472.Can-06-2072. PubMed PMID: 17114236.
5. Phillips HS, Kharbanda S, Chen R, Forrest WF, Soriano RH, Wu TD, Misra A, Nigro JM, Colman H, Soroceanu L, Williams PM, Modrusan Z, Feuerstein BG, Aldape K. Molecular subclasses of high-grade glioma predict prognosis, delineate a pattern of disease progression, and resemble stages in neurogenesis. Cancer Cell. 2006;9(3):157-73. Epub 2006/03/15. doi: 10.1016/j.ccr.2006.02.019. PubMed PMID: 16530701.
6. Zong H, Parada LF, Baker SJ. Cell of origin for malignant gliomas and its implication in therapeutic development. Cold Spring Harbor perspectives in biology. 2015;7(5). Epub 2015/01/31. doi: 10.1101/cshperspect.a020610. PubMed PMID: 25635044; PMCID: PMC4448618.
7. Comprehensive genomic characterization defines human glioblastoma genes and core pathways. Nature. 2008;455(7216):1061-8. Epub 2008/09/06. doi: 10.1038/nature07385. PubMed PMID: 18772890; PMCID: PMC2671642.
8. Brennan CW, Verhaak RG, McKenna A, Campos B, Noushmehr H, Salama SR, Zheng S, Chakravarty D, Sanborn JZ, Berman SH, Beroukhim R, Bernard B, Wu CJ, Genovese G, Shmulevich I, Barnholtz-Sloan J, Zou L, Vegesna R, Shukla SA, Ciriello G, Yung WK, Zhang W, Sougnez C, Mikkelsen T, Aldape K, Bigner DD, Van Meir EG, Prados M, Sloan A, Black KL, Eschbacher J, Finocchiaro G, Friedman W, Andrews DW, Guha A, Iacocca M, O'Neill BP, Foltz G, Myers J, Weisenberger DJ, Penny R, Kucherlapati R, Perou CM, Hayes DN, Gibbs R, Marra M, Mills GB, Lander E, Spellman P, Wilson R, Sander C, Weinstein J, Meyerson M, Gabriel S, Laird PW, Haussler D, Getz G, Chin L. The somatic genomic landscape of glioblastoma. Cell. 2013;155(2):462-77. Epub 2013/10/15. doi: 10.1016/j.cell.2013.09.034. PubMed PMID: 24120142; PMCID: PMC3910500.
9. Humphrey PA, Wong AJ, Vogelstein B, Zalutsky MR, Fuller GN, Archer GE, Friedman HS, Kwatra MM, Bigner SH, Bigner DD. Anti-synthetic peptide antibody reacting at the fusion junction of deletion-mutant epidermal growth factor receptors in human glioblastoma. Proceedings of the National Academy of Sciences of the United States of America. 1990;87(11):4207-11. Epub 1990/06/01. PubMed PMID: 1693434; PMCID: PMC54077.
10. Wong AJ, Ruppert JM, Bigner SH, Grzeschik CH, Humphrey PA, Bigner DS, Vogelstein B. Structural alterations of the epidermal growth factor receptor gene in human gliomas. Proceedings of the National Academy of Sciences of the United States of America. 1992;89(7):2965-9. Epub 1992/04/01. PubMed PMID: 1557402; PMCID: PMC48784.

11. Boockvar JA, Kapitonov D, Kapoor G, Schouten J, Counelis GJ, Bogler O, Snyder EY, McIntosh TK, O'Rourke DM. Constitutive EGFR signaling confers a motile phenotype to neural stem cells. Molecular and cellular neurosciences. 2003;24(4):1116-30. Epub 2003/12/31. PubMed PMID: 14697673.
12. Bachoo RM, Maher EA, Ligon KL, Sharpless NE, Chan SS, You MJ, Tang Y, DeFrances J, Stover E, Weissleder R, Rowitch DH, Louis DN, DePinho RA. Epidermal growth factor receptor and Ink4a/Arf: convergent mechanisms governing terminal differentiation and transformation along the neural stem cell to astrocyte axis. Cancer Cell. 2002;1(3):269-77. Epub 2002/06/28. PubMed PMID: 12086863.
13. Ozawa T, Brennan CW, Wang L, Squatrito M, Sasayama T, Nakada M, Huse JT, Pedraza A, Utsuki S, Yasui Y, Tandon A, Fomchenko EI, Oka H, Levine RL, Fujii K, Ladanyi M, Holland EC. PDGFRA gene rearrangements are frequent genetic events in PDGFRA-amplified glioblastomas. Genes & development. 2010;24(19):2205-18. Epub 2010/10/05. doi: 10.1101/gad.1972310. PubMed PMID: 20889717; PMCID: PMC2947772.
14. Nagane M, Levitzki A, Gazit A, Cavenee WK, Huang HJ. Drug resistance of human glioblastoma cells conferred by a tumor-specific mutant epidermal growth factor receptor through modulation of Bcl-XL and caspase-3-like proteases. Proceedings of the National Academy of Sciences of the United States of America. 1998;95(10):5724-9. Epub 1998/05/20. PubMed PMID: 9576951; PMCID: PMC20446.
15. Samuels Y, Wang Z, Bardelli A, Silliman N, Ptak J, Szabo S, Yan H, Gazdar A, Powell SM, Riggins GJ, Willson JK, Markowitz S, Kinzler KW, Vogelstein B, Velculescu VE. High frequency of mutations of the PIK3CA gene in human cancers. Science (New York, NY). 2004;304(5670):554. Epub 2004/03/16. doi: 10.1126/science.1096502. PubMed PMID: 15016963.
16. Gallia GL, Rand V, Siu IM, Eberhart CG, James CD, Marie SK, Oba-Shinjo SM, Carlotti CG, Caballero OL, Simpson AJ, Brock MV, Massion PP, Carson BS, Sr., Riggins GJ. PIK3CA gene mutations in pediatric and adult glioblastoma multiforme. Molecular cancer research : MCR. 2006;4(10):709-14. Epub 2006/10/20. doi: 10.1158/1541-7786.mcr-06-0172. PubMed PMID: 17050665.
17. Mizoguchi M, Nutt CL, Mohapatra G, Louis DN. Genetic alterations of phosphoinositide 3-kinase subunit genes in human glioblastomas. Brain pathology (Zurich, Switzerland). 2004;14(4):372-7. Epub 2004/12/21. PubMed PMID: 15605984.
18. Haas-Kogan D, Shalev N, Wong M, Mills G, Yount G, Stokoe D. Protein kinase B (PKB/Akt) activity is elevated in glioblastoma cells due to mutation of the tumor suppressor PTEN/MMAC. Current biology : CB. 1998;8(21):1195-8. Epub 1998/11/04. PubMed PMID: 9799739.
19. Baeza N, Weller M, Yonekawa Y, Kleihues P, Ohgaki H. PTEN methylation and expression in glioblastomas. Acta neuropathologica. 2003;106(5):479-85. Epub 2003/08/09. doi: 10.1007/s00401-003-0748-4. PubMed PMID: 12904991.
20. Li J, Yen C, Liaw D, Podsypanina K, Bose S, Wang SI, Puc J, Miliaresis C, Rodgers L, McCombie R, Bigner SH, Giovanella BC, Ittmann M, Tycko B, Hibshoosh H, Wigler MH, Parsons R. PTEN, a putative protein tyrosine phosphatase gene mutated in human brain, breast, and prostate cancer. Science (New York, NY). 1997;275(5308):1943-7. Epub 1997/03/28. PubMed PMID: 9072974.
21. Lee Y, Koh J, Kim SI, Won JK, Park CK, Choi SH, Park SH. The frequency and prognostic effect of TERT promoter mutation in diffuse gliomas. Acta neuropathologica communications. 2017;5(1):62. Epub 2017/08/31. doi: 10.1186/s40478-017-0465-1. PubMed PMID: 28851427; PMCID: PMC5574236.
22. Holland EC, Celestino J, Dai C, Schaefer L, Sawaya RE, Fuller GN. Combined activation of Ras and Akt in neural progenitors induces glioblastoma formation in mice. Nature genetics. 2000;25(1):55-7. Epub 2000/05/10. doi: 10.1038/75596. PubMed PMID: 10802656.
23. Li L, Dutra A, Pak E, Labrie JE, 3rd, Gerstein RM, Pandolfi PP, Recht LD, Ross AH. EGFRvIII expression and PTEN loss synergistically induce chromosomal instability and glial tumors. Neuro-oncology. 2009;11(1):9-21. Epub 2008/09/25. doi: 10.1215/15228517-2008-081. PubMed PMID: 18812521; PMCID: PMC2718963.
24. Zheng H, Ying H, Yan H, Kimmelman AC, Hiller DJ, Chen AJ, Perry SR, Tonon G, Chu GC, Ding Z, Stommel JM, Dunn KL, Wiedemeyer R, You MJ, Brennan C, Wang YA, Ligon KL, Wong WH, Chin L, dePinho RA. Pten and p53 converge on c-Myc to control differentiation, self-renewal, and

transformation of normal and neoplastic stem cells in glioblastoma. Cold Spring Harbor symposia on quantitative biology. 2008;73:427-37. Epub 2009/01/20. doi: 10.1101/sqb.2008.73.047. PubMed PMID: 19150964.
25. Fomchenko EI, Dougherty JD, Helmy KY, Katz AM, Pietras A, Brennan C, Huse JT, Milosevic A, Holland EC. Recruited cells can become transformed and overtake PDGF-induced murine gliomas in vivo during tumor progression. PloS one. 2011;6(7):e20605. Epub 2011/07/15. doi: 10.1371/journal.pone.0020605. PubMed PMID: 21754979; PMCID: PMC3130733.
26. Holland EC, Hively WP, DePinho RA, Varmus HE. A constitutively active epidermal growth factor receptor cooperates with disruption of G1 cell-cycle arrest pathways to induce glioma-like lesions in mice. Genes & development. 1998;12(23):3675-85. Epub 1998/12/16. PubMed PMID: 9851974; PMCID: PMC317252.
27. Cloughesy TF, Yoshimoto K, Nghiemphu P, Brown K, Dang J, Zhu S, Hsueh T, Chen Y, Wang W, Youngkin D, Liau L, Martin N, Becker D, Bergsneider M, Lai A, Green R, Oglesby T, Koleto M, Trent J, Horvath S, Mischel PS, Mellinghoff IK, Sawyers CL. Antitumor activity of rapamycin in a Phase I trial for patients with recurrent PTEN-deficient glioblastoma. PLoS medicine. 2008;5(1):e8. Epub 2008/01/25. doi: 10.1371/journal.pmed.0050008. PubMed PMID: 18215105; PMCID: PMC2211560.
28. Mellinghoff IK, Wang MY, Vivanco I, Haas-Kogan DA, Zhu S, Dia EQ, Lu KV, Yoshimoto K, Huang JH, Chute DJ, Riggs BL, Horvath S, Liau LM, Cavenee WK, Rao PN, Beroukhim R, Peck TC, Lee JC, Sellers WR, Stokoe D, Prados M, Cloughesy TF, Sawyers CL, Mischel PS. Molecular determinants of the response of glioblastomas to EGFR kinase inhibitors. N Engl J Med. 2005;353(19):2012-24. Epub 2005/11/12. doi: 10.1056/NEJMoa051918. PubMed PMID: 16282176.
29. Raizer JJ, Abrey LE, Lassman AB, Chang SM, Lamborn KR, Kuhn JG, Yung WK, Gilbert MR, Aldape KA, Wen PY, Fine HA, Mehta M, Deangelis LM, Lieberman F, Cloughesy TF, Robins HI, Dancey J, Prados MD. A phase II trial of erlotinib in patients with recurrent malignant gliomas and nonprogressive glioblastoma multiforme postradiation therapy. Neuro-oncology. 2010;12(1):95-103. Epub 2010/02/13. doi: 10.1093/neuonc/nop015. PubMed PMID: 20150372; PMCID: PMC2940554.
30. Szerlip NJ, Pedraza A, Chakravarty D, Azim M, McGuire J, Fang Y, Ozawa T, Holland EC, Huse JT, Jhanwar S, Leversha MA, Mikkelsen T, Brennan CW. Intratumoral heterogeneity of receptor tyrosine kinases EGFR and PDGFRA amplification in glioblastoma defines subpopulations with distinct growth factor response. Proceedings of the National Academy of Sciences of the United States of America. 2012;109(8):3041-6. Epub 2012/02/11. doi: 10.1073/pnas.1114033109. PubMed PMID: 22323597; PMCID: PMC3286976.
31. Gonzalez C. Drosophila melanogaster: a model and a tool to investigate malignancy and identify new therapeutics. Nature reviews Cancer. 2013;13(3):172-83. Epub 2013/02/08. doi: 10.1038/nrc3461. PubMed PMID: 23388617.
32. Lee T, Luo L. Mosaic analysis with a repressible cell marker for studies of gene function in neuronal morphogenesis. Neuron. 1999;22(3):451-61. Epub 1999/04/10. PubMed PMID: 10197526.
33. Bellen HJ, Levis RW, Liao G, He Y, Carlson JW, Tsang G, Evans-Holm M, Hiesinger PR, Schulze KL, Rubin GM, Hoskins RA, Spradling AC. The BDGP gene disruption project: single transposon insertions associated with 40% of Drosophila genes. Genetics. 2004;167(2):761-81. Epub 2004/07/09. doi: 10.1534/genetics.104.026427. PubMed PMID: 15238527; PMCID: PMC1470905.
34. Brand AH, Perrimon N. Targeted gene expression as a means of altering cell fates and generating dominant phenotypes. Development. 1993;118(2):401-15. PubMed PMID: 8223268.
35. Dietzl G, Chen D, Schnorrer F, Su KC, Barinova Y, Fellner M, Gasser B, Kinsey K, Oppel S, Scheiblauer S, Couto A, Marra V, Keleman K, Dickson BJ. A genome-wide transgenic RNAi library for conditional gene inactivation in Drosophila. Nature. 2007;448(7150):151-6. Epub 2007/07/13. doi: 10.1038/nature05954. PubMed PMID: 17625558.
36. St Johnston D. The art and design of genetic screens: Drosophila melanogaster. Nature reviews Genetics. 2002;3(3):176-88. Epub 2002/04/25. doi: 10.1038/nrg751. PubMed PMID: 11972155.

37. Reiter LT, Potocki L, Chien S, Gribskov M, Bier E. A systematic analysis of human disease-associated gene sequences in Drosophila melanogaster. Genome research. 2001;11(6):1114-25. Epub 2001/05/31. doi: 10.1101/gr.169101. PubMed PMID: 11381037; PMCID: PMC311089.
38. Freeman MR. Drosophila Central Nervous System Glia. Cold Spring Harbor perspectives in biology. 2015;7(11). Epub 2015/02/28. doi: 10.1101/cshperspect.a020552. PubMed PMID: 25722465; PMCID: PMC4632667.
39. Speder P, Brand AH. Systemic and local cues drive neural stem cell niche remodelling during neurogenesis in Drosophila. eLife. 2018;7. Epub 2018/01/05. doi: 10.7554/eLife.30413. PubMed PMID: 29299997; PMCID: PMC5754201.
40. Read RD. Pvr receptor tyrosine kinase signaling promotes post-embryonic morphogenesis, and survival of glia and neural progenitor cells in Drosophila. Development (Cambridge, England). 2018;145(23). Epub 2018/10/18. doi: 10.1242/dev.164285. PubMed PMID: 30327326.
41. Coutinho-Budd JC, Sheehan AE, Freeman MR. The secreted neurotrophin Spatzle 3 promotes glial morphogenesis and supports neuronal survival and function. Genes & development. 2017;31(20):2023-38. Epub 2017/11/16. doi: 10.1101/gad.305888.117. PubMed PMID: 29138279; PMCID: PMC5733495.
42. Leiserson WM, Harkins EW, Keshishian H. Fray, a Drosophila serine/threonine kinase homologous to mammalian PASK, is required for axonal ensheathment. Neuron. 2000;28(3):793-806. Epub 2001/02/13. PubMed PMID: 11163267.
43. Auld VJ, Fetter RD, Broadie K, Goodman CS. Gliotactin, a novel transmembrane protein on peripheral glia, is required to form the blood-nerve barrier in Drosophila. Cell. 1995;81(5):757-67. Epub 1995/06/02. PubMed PMID: 7539719.
44. Gateff E. Malignant neoplasms of genetic origin in Drosophila melanogaster. Science (New York, NY). 1978;200(4349):1448-59. Epub 1978/06/30. PubMed PMID: 96525.
45. Gateff E. Tumor suppressor and overgrowth suppressor genes of Drosophila melanogaster: developmental aspects. The International journal of developmental biology. 1994;38(4):565-90. Epub 1994/12/01. PubMed PMID: 7779680.
46. St John MA, Xu T. Understanding human cancer in a fly? American journal of human genetics. 1997;61(5):1006-10. Epub 1997/11/05. doi: 10.1086/301619. PubMed PMID: 9345112; PMCID: PMC1716045.
47. Artavanis-Tsakonas S, Muskavitch MA, Yedvobnick B. Molecular cloning of Notch, a locus affecting neurogenesis in Drosophila melanogaster. Proceedings of the National Academy of Sciences of the United States of America. 1983;80(7):1977-81. Epub 1983/04/01. PubMed PMID: 6403942; PMCID: PMC393735.
48. Fan X, Khaki L, Zhu TS, Soules ME, Talsma CE, Gul N, Koh C, Zhang J, Li YM, Maciaczyk J, Nikkhah G, Dimeco F, Piccirillo S, Vescovi AL, Eberhart CG. NOTCH pathway blockade depletes CD133-positive glioblastoma cells and inhibits growth of tumor neurospheres and xenografts. Stem cells (Dayton, Ohio). 2010;28(1):5-16. Epub 2009/11/12. doi: 10.1002/stem.254. PubMed PMID: 19904829; PMCID: PMC2878196.
49. Read RD, Cavenee WK, Furnari FB, Thomas JB. A drosophila model for EGFR-Ras and PI3K-dependent human glioma. PLoS Genet. 2009;5(2):e1000374. Epub 2009/02/14. doi: 10.1371/journal.pgen.1000374. PubMed PMID: 19214224.
50. Read RD, Fenton TR, Gomez GG, Wykosky J, Vandenberg SR, Babic I, Iwanami A, Yang H, Cavenee WK, Mischel PS, Furnari FB, Thomas JB. A kinome-wide RNAi screen in Drosophila Glia reveals that the RIO kinases mediate cell proliferation and survival through TORC2-Akt signaling in glioblastoma. PLoS Genet. 2013;9(2):e1003253. Epub 2013/03/06. doi: 10.1371/journal.pgen.1003253 PGENETICS-D-12-01408 [pii]. PubMed PMID: 23459592.
51. Park NI, Guilhamon P, Desai K, McAdam RF, Langille E, O'Connor M, Lan X, Whetstone H, Coutinho FJ, Vanner RJ, Ling E, Prinos P, Lee L, Selvadurai H, Atwal G, Kushida M, Clarke ID, Voisin V, Cusimano MD, Bernstein M, Das S, Bader G, Arrowsmith CH, Angers S, Huang X, Lupien M, Dirks PB. ASCL1 Reorganizes Chromatin to Direct Neuronal Fate and Suppress Tumorigenicity of

Glioblastoma Stem Cells. Cell stem cell. 2017;21(3):411. Epub 2017/09/09. doi: 10.1016/j.stem.2017.08.008. PubMed PMID: 28886368.
52. Witte HT, Jeibmann A, Klambt C, Paulus W. Modeling glioma growth and invasion in Drosophila melanogaster. Neoplasia (New York, NY). 2009;11(9):882-8. Epub 2009/09/03. PubMed PMID: 19724682; PMCID: PMC2735809.
53. Chen AS, Wardwell-Ozgo J, Shah NN, Wright D, Appin CL, Vigneswaran K, Brat DJ, Kornblum HI, Read RD. Drak/STK17A drives neoplastic glial proliferation through modulation of MRLC signaling. Cancer research. 2018. Epub 2018/12/12. doi: 10.1158/0008-5472.can-18-0482. PubMed PMID: 30530503.
54. Chen X, Wanggou S, Bodalia A, Zhu M, Dong W, Fan JJ, Yin WC, Min HK, Hu M, Draghici D, Dou W, Li F, Coutinho FJ, Whetstone H, Kushida MM, Dirks PB, Song Y, Hui CC, Sun Y, Wang LY, Li X, Huang X. A Feedforward Mechanism Mediated by Mechanosensitive Ion Channel PIEZO1 and Tissue Mechanics Promotes Glioma Aggression. Neuron. 2018;100(4):799-815.e7. Epub 2018/10/23. doi: 10.1016/j.neuron.2018.09.046. PubMed PMID: 30344046.
55. Frattini V, Pagnotta SM, Tala, Fan JJ, Russo MV, Lee SB, Garofano L, Zhang J, Shi P, Lewis G, Sanson H, Frederick V, Castano AM, Cerulo L, Rolland DCM, Mall R, Mokhtari K, Elenitoba-Johnson KSJ, Sanson M, Huang X, Ceccarelli M, Lasorella A, Iavarone A. A metabolic function of FGFR3-TACC3 gene fusions in cancer. Nature. 2018;553(7687):222-7. Epub 2018/01/13. doi: 10.1038/nature25171. PubMed PMID: 29323298; PMCID: PMC5771419.
56. Kim SN, Jeibmann A, Halama K, Witte HT, Walte M, Matzat T, Schillers H, Faber C, Senner V, Paulus W, Klambt C. ECM stiffness regulates glial migration in Drosophila and mammalian glioma models. Development (Cambridge, England). 2014;141(16):3233-42. Epub 2014/07/27. doi: 10.1242/dev.106039. PubMed PMID: 25063458.
57. Chi KC, Tsai WC, Wu CL, Lin TY, Hueng DY. An Adult Drosophila Glioma Model for Studying Pathometabolic Pathways of Gliomagenesis. Molecular neurobiology. 2018. Epub 2018/10/26. doi: 10.1007/s12035-018-1392-2. PubMed PMID: 30357574.
58. Agnihotri S, Golbourn B, Huang X, Remke M, Younger S, Cairns RA, Chalil A, Smith CA, Krumholtz SL, Mackenzie D, Rakopoulos P, Ramaswamy V, Taccone MS, Mischel PS, Fuller GN, Hawkins C, Stanford WL, Taylor MD, Zadeh G, Rutka JT. PINK1 Is a Negative Regulator of Growth and the Warburg Effect in Glioblastoma. Cancer research. 2016;76(16):4708-19. Epub 2016/06/22. doi: 10.1158/0008-5472.can-15-3079. PubMed PMID: 27325644.
59. Cheng P, Wang J, Waghmare I, Sartini S, Coviello V, Zhang Z, Kim SH, Mohyeldin A, Pavlyukov MS, Minata M, Valentim CL, Chhipa RR, Bhat KP, Dasgupta B, La Motta C, Kango-Singh M, Nakano I. FOXD1-ALDH1A3 Signaling Is a Determinant for the Self-Renewal and Tumorigenicity of Mesenchymal Glioma Stem Cells. Cancer research. 2016;76(24):7219-30. Epub 2016/08/30. doi: 10.1158/0008-5472.can-15-2860. PubMed PMID: 27569208; PMCID: PMC5161538.
60. Silies M, Yuva Y, Engelen D, Aho A, Stork T, Klambt C. Glial cell migration in the eye disc. The Journal of neuroscience : the official journal of the Society for Neuroscience. 2007;27(48):13130-9. Epub 2007/11/30. doi: 10.1523/jneurosci.3583-07.2007. PubMed PMID: 18045907.
61. Green P, Hartenstein AY, Hartenstein V. The embryonic development of the Drosophila visual system. Cell and tissue research. 1993;273(3):583-98. Epub 1993/09/01. PubMed PMID: 8402833.
62. Rich JN, Reardon DA, Peery T, Dowell JM, Quinn JA, Penne KL, Wikstrand CJ, Van Duyn LB, Dancey JE, McLendon RE, Kao JC, Stenzel TT, Ahmed Rasheed BK, Tourt-Uhlig SE, Herndon JE, 2nd, Vredenburgh JJ, Sampson JH, Friedman AH, Bigner DD, Friedman HS. Phase II trial of gefitinib in recurrent glioblastoma. Journal of clinical oncology : official journal of the American Society of Clinical Oncology. 2004;22(1):133-42. Epub 2003/11/26. doi: 10.1200/jco.2004.08.110. PubMed PMID: 14638850.
63. Funa K, Sasahara M. The roles of PDGF in development and during neurogenesis in the normal and diseased nervous system. Journal of neuroimmune pharmacology : the official journal of the Society on NeuroImmune Pharmacology. 2014;9(2):168-81. Epub 2013/06/19. doi: 10.1007/s11481-013-9479-z. PubMed PMID: 23771592; PMCID: PMC3955130.

64. Singh D, Chan JM, Zoppoli P, Niola F, Sullivan R, Castano A, Liu EM, Reichel J, Porrati P, Pellegatta S, Qiu K, Gao Z, Ceccarelli M, Riccardi R, Brat DJ, Guha A, Aldape K, Golfinos JG, Zagzag D, Mikkelsen T, Finocchiaro G, Lasorella A, Rabadan R, Iavarone A. Transforming fusions of FGFR and TACC genes in human glioblastoma. Science (New York, NY). 2012;337(6099):1231-5. Epub 2012/07/28. doi: 10.1126/science.1220834. PubMed PMID: 22837387; PMCID: 3677224.
65. Di Stefano AL, Fucci A, Frattini V, Labussiere M, Mokhtari K, Zoppoli P, Marie Y, Bruno A, Boisselier B, Giry M, Savatovsky J, Touat M, Belaid H, Kamoun A, Idbaih A, Houillier C, Luo FR, Soria JC, Tabernero J, Eoli M, Paterra R, Yip S, Petrecca K, Chan JA, Finocchiaro G, Lasorella A, Sanson M, Iavarone A. Detection, Characterization, and Inhibition of FGFR-TACC Fusions in IDH Wild-type Glioma. Clinical cancer research : an official journal of the American Association for Cancer Research. 2015;21(14):3307-17. Epub 2015/01/23. doi: 10.1158/1078-0432.CCR-14-2199. PubMed PMID: 25609060; PMCID: 4506218.
66. Miroshnikova YA, Mouw JK, Barnes JM, Pickup MW, Lakins JN, Kim Y, Lobo K, Persson AI, Reis GF, McKnight TR, Holland EC, Phillips JJ, Weaver VM. Tissue mechanics promote IDH1-dependent HIF1alpha-tenascin C feedback to regulate glioblastoma aggression. Nature cell biology. 2016;18(12):1336-45. Epub 2016/11/08. doi: 10.1038/ncb3429. PubMed PMID: 27820599; PMCID: PMC5361403.
67. Kai F, Laklai H, Weaver VM. Force Matters: Biomechanical Regulation of Cell Invasion and Migration in Disease. Trends in cell biology. 2016;26(7):486-97. Epub 2016/04/09. doi: 10.1016/j.tcb.2016.03.007. PubMed PMID: 27056543; PMCID: PMC4970516.
68. Northey JJ, Przybyla L, Weaver VM. Tissue Force Programs Cell Fate and Tumor Aggression. Cancer Discov. 2017;7(11):1224-37. Epub 2017/10/19. doi: 10.1158/2159-8290.cd-16-0733. PubMed PMID: 29038232; PMCID: PMC5679454.
69. Oudin MJ, Weaver VM. Physical and Chemical Gradients in the Tumor Microenvironment Regulate Tumor Cell Invasion, Migration, and Metastasis. Cold Spring Harbor symposia on quantitative biology. 2016;81:189-205. Epub 2017/04/21. doi: 10.1101/sqb.2016.81.030817. PubMed PMID: 28424337.
70. Murthy SE, Dubin AE, Patapoutian A. Piezos thrive under pressure: mechanically activated ion channels in health and disease. Nature reviews Molecular cell biology. 2017;18(12):771-83. Epub 2017/10/05. doi: 10.1038/nrm.2017.92. PubMed PMID: 28974772.
71. Cox CD, Bae C, Ziegler L, Hartley S, Nikolova-Krstevski V, Rohde PR, Ng CA, Sachs F, Gottlieb PA, Martinac B. Removal of the mechanoprotective influence of the cytoskeleton reveals PIEZO1 is gated by bilayer tension. Nature communications. 2016;7:10366. Epub 2016/01/21. doi: 10.1038/ncomms10366. PubMed PMID: 26785635; PMCID: PMC4735864.
72. Lewis AH, Grandl J. Mechanical sensitivity of Piezo1 ion channels can be tuned by cellular membrane tension. eLife. 2015;4. Epub 2015/12/10. doi: 10.7554/eLife.12088. PubMed PMID: 26646186; PMCID: PMC4718726.
73. Kim SE, Coste B, Chadha A, Cook B, Patapoutian A. The role of Drosophila Piezo in mechanical nociception. Nature. 2012;483(7388):209-12. Epub 2012/02/22. doi: 10.1038/nature10801. PubMed PMID: 22343891; PMCID: PMC3297676.
74. He L, Si G, Huang J, Samuel ADT, Perrimon N. Mechanical regulation of stem-cell differentiation by the stretch-activated Piezo channel. Nature. 2018;555(7694):103-6. Epub 2018/02/08. doi: 10.1038/nature25744. PubMed PMID: 29414942; PMCID: PMC6101000.
75. Overington JP, Al-Lazikani B, Hopkins AL. How many drug targets are there? Nature reviews Drug discovery. 2006;5(12):993-6. Epub 2006/12/02. doi: 10.1038/nrd2199. PubMed PMID: 17139284.
76. Ulrich TA, de Juan Pardo EM, Kumar S. The mechanical rigidity of the extracellular matrix regulates the structure, motility, and proliferation of glioma cells. Cancer Res. 2009;69(10):4167-74. Epub 2009/05/14. doi: 10.1158/0008-5472.can-08-4859. PubMed PMID: 19435897; PMCID: PMC2727355.

77. Moore SW, Roca-Cusachs P, Sheetz MP. Stretchy proteins on stretchy substrates: the important elements of integrin-mediated rigidity sensing. Developmental cell. 2010;19(2):194-206. Epub 2010/08/17. doi: 10.1016/j.devcel.2010.07.018. PubMed PMID: 20708583; PMCID: PMC5319208.
78. Bokel C, Brown NH. Integrins in development: moving on, responding to, and sticking to the extracellular matrix. Developmental cell. 2002;3(3):311-21. Epub 2002/10/04. PubMed PMID: 12361595.
79. Ginsberg MH. Integrin activation. BMB reports. 2014;47(12):655-9. Epub 2014/11/13. PubMed PMID: 25388208; PMCID: PMC4345508.
80. Warburg O. On respiratory impairment in cancer cells. Science (New York, NY). 1956;124(3215):269-70. Epub 1956/08/10. PubMed PMID: 13351639.
81. Deberardinis RJ, Sayed N, Ditsworth D, Thompson CB. Brick by brick: metabolism and tumor cell growth. Current opinion in genetics & development. 2008;18(1):54-61. Epub 2008/04/05. doi: 10.1016/j.gde.2008.02.003. PubMed PMID: 18387799; PMCID: PMC2476215.
82. Vander Heiden MG, Cantley LC, Thompson CB. Understanding the Warburg effect: the metabolic requirements of cell proliferation. Science (New York, NY). 2009;324(5930):1029-33. Epub 2009/05/23. doi: 10.1126/science.1160809. PubMed PMID: 19460998; PMCID: PMC2849637.
83. Gandhi S, Wood-Kaczmar A, Yao Z, Plun-Favreau H, Deas E, Klupsch K, Downward J, Latchman DS, Tabrizi SJ, Wood NW, Duchen MR, Abramov AY. PINK1-associated Parkinson's disease is caused by neuronal vulnerability to calcium-induced cell death. Molecular cell. 2009;33(5):627-38. Epub 2009/03/17. doi: 10.1016/j.molcel.2009.02.013. PubMed PMID: 19285945; PMCID: PMC2724101.
84. Wang X, Winter D, Ashrafi G, Schlehe J, Wong YL, Selkoe D, Rice S, Steen J, LaVoie MJ, Schwarz TL. PINK1 and Parkin target Miro for phosphorylation and degradation to arrest mitochondrial motility. Cell. 2011;147(4):893-906. Epub 2011/11/15. doi: 10.1016/j.cell.2011.10.018. PubMed PMID: 22078885; PMCID: PMC3261796.
85. Singh SK, Hawkins C, Clarke ID, Squire JA, Bayani J, Hide T, Henkelman RM, Cusimano MD, Dirks PB. Identification of human brain tumour initiating cells. Nature. 2004;432(7015):396-401. Epub 2004/11/19. doi: 10.1038/nature03128. PubMed PMID: 15549107.
86. Ignatova TN, Kukekov VG, Laywell ED, Suslov ON, Vrionis FD, Steindler DA. Human cortical glial tumors contain neural stem-like cells expressing astroglial and neuronal markers in vitro. Glia. 2002;39(3):193-206. Epub 2002/08/31. doi: 10.1002/glia.10094. PubMed PMID: 12203386.
87. Galli R, Binda E, Orfanelli U, Cipelletti B, Gritti A, De Vitis S, Fiocco R, Foroni C, Dimeco F, Vescovi A. Isolation and characterization of tumorigenic, stem-like neural precursors from human glioblastoma. Cancer Res. 2004;64(19):7011-21. Epub 2004/10/07. doi: 10.1158/0008-5472.can-04-1364. PubMed PMID: 15466194.
88. Laks DR, Masterman-Smith M, Visnyei K, Angenieux B, Orozco NM, Foran I, Yong WH, Vinters HV, Liau LM, Lazareff JA, Mischel PS, Cloughesy TF, Horvath S, Kornblum HI. Neurosphere formation is an independent predictor of clinical outcome in malignant glioma. Stem cells (Dayton, Ohio). 2009;27(4):980-7. Epub 2009/04/09. doi: 10.1002/stem.15. PubMed PMID: 19353526; PMCID: PMC3177534.
89. Lathia JD, Mack SC, Mulkearns-Hubert EE, Valentim CL, Rich JN. Cancer stem cells in glioblastoma. Genes & development. 2015;29(12):1203-17. Epub 2015/06/26. doi: 10.1101/gad.261982.115. PubMed PMID: 26109046; PMCID: PMC4495393.
90. Hannenhalli S, Kaestner KH. The evolution of Fox genes and their role in development and disease. Nature reviews Genetics. 2009;10(4):233-40. Epub 2009/03/11. doi: 10.1038/nrg2523. PubMed PMID: 19274050; PMCID: PMC2733165.
91. Nakano I. Transcription factors as master regulator for cancer stemness: remove milk from fox? Expert review of anticancer therapy. 2014;14(8):873-5. Epub 2014/07/16. doi: 10.1586/14737140.2014.940324. PubMed PMID: 25017123.
92. Koga M, Matsuda M, Kawamura T, Sogo T, Shigeno A, Nishida E, Ebisuya M. Foxd1 is a mediator and indicator of the cell reprogramming process. Nature communications. 2014;5:3197. Epub 2014/02/06. doi: 10.1038/ncomms4197. PubMed PMID: 24496101.

93. Mao P, Joshi K, Li J, Kim SH, Li P, Santana-Santos L, Luthra S, Chandran UR, Benos PV, Smith L, Wang M, Hu B, Cheng SY, Sobol RW, Nakano I. Mesenchymal glioma stem cells are maintained by activated glycolytic metabolism involving aldehyde dehydrogenase 1A3. Proceedings of the National Academy of Sciences of the United States of America. 2013;110(21):8644-9. Epub 2013/05/08. doi: 10.1073/pnas.1221478110. PubMed PMID: 23650391; PMCID: PMC3666732.
94. Berninger B, Guillemot F, Gotz M. Directing neurotransmitter identity of neurones derived from expanded adult neural stem cells. The European journal of neuroscience. 2007;25(9):2581-90. Epub 2007/06/15. doi: 10.1111/j.1460-9568.2007.05509.x. PubMed PMID: 17561834.
95. Chanda S, Ang CE, Davila J, Pak C, Mall M, Lee QY, Ahlenius H, Jung SW, Sudhof TC, Wernig M. Generation of induced neuronal cells by the single reprogramming factor ASCL1. Stem cell reports. 2014;3(2):282-96. Epub 2014/09/26. doi: 10.1016/j.stemcr.2014.05.020. PubMed PMID: 25254342; PMCID: PMC4176533.
96. Mukherjee S, Kong J, Brat DJ. Cancer stem cell division: when the rules of asymmetry are broken. Stem cells and development. 2015;24(4):405-16. Epub 2014/11/11. doi: 10.1089/scd.2014.0442. PubMed PMID: 25382732; PMCID: PMC4313409.
97. Knoblich JA. Mechanisms of asymmetric stem cell division. Cell. 2008;132(4):583-97. Epub 2008/02/26. doi: 10.1016/j.cell.2008.02.007. PubMed PMID: 18295577.
98. Homem CC, Knoblich JA. Drosophila neuroblasts: a model for stem cell biology. Development (Cambridge, England). 2012;139(23):4297-310. Epub 2012/11/08. doi: 10.1242/dev.080515. PubMed PMID: 23132240.
99. Caussinus E, Gonzalez C. Induction of tumor growth by altered stem-cell asymmetric division in Drosophila melanogaster. Nature genetics. 2005;37(10):1125-9. Epub 2005/09/06. doi: 10.1038/ng1632. PubMed PMID: 16142234.
100. Betschinger J, Mechtler K, Knoblich JA. Asymmetric segregation of the tumor suppressor brat regulates self-renewal in Drosophila neural stem cells. Cell. 2006;124(6):1241-53. Epub 2006/03/28. doi: 10.1016/j.cell.2006.01.038. PubMed PMID: 16564014.
101. Chen G, Kong J, Tucker-Burden C, Anand M, Rong Y, Rahman F, Moreno CS, Van Meir EG, Hadjipanayis CG, Brat DJ. Human Brat ortholog TRIM3 is a tumor suppressor that regulates asymmetric cell division in glioblastoma. Cancer Res. 2014;74(16):4536-48. Epub 2014/06/21. doi: 10.1158/0008-5472.can-13-3703. PubMed PMID: 24947043; PMCID: PMC4134737.
102. Mukherjee S, Tucker-Burden C, Zhang C, Moberg K, Read R, Hadjipanayis C, Brat DJ. Drosophila Brat and Human Ortholog TRIM3 Maintain Stem Cell Equilibrium and Suppress Brain Tumorigenesis by Attenuating Notch Nuclear Transport. Cancer research. 2016;76(8):2443-52. Epub 2016/02/20. doi: 10.1158/0008-5472.can-15-2299. PubMed PMID: 26893479; PMCID: PMC4873416.
103. Mukherjee S, Tucker-Burden C, Kaissi E, Newsam A, Duggireddy H, Chau M, Zhang C, Diwedi B, Rupji M, Seby S, Kowalski J, Kong J, Read R, Brat DJ. CDK5 Inhibition Resolves PKA/cAMP-Independent Activation of CREB1 Signaling in Glioma Stem Cells. Cell reports. 2018;23(6):1651-64. Epub 2018/05/10. doi: 10.1016/j.celrep.2018.04.016. PubMed PMID: 29742423; PMCID: PMC5987254.
104. Hirschhaeuser F, Menne H, Dittfeld C, West J, Mueller-Klieser W, Kunz-Schughart LA. Multicellular tumor spheroids: an underestimated tool is catching up again. J Biotechnol. 2010;148(1):3-15. Epub 2010/01/26. doi: 10.1016/j.jbiotec.2010.01.012. PubMed PMID: 20097238.
105. Deschavanne PJ, Fertil B. A review of human cell radiosensitivity in vitro. Int J Radiat Oncol Biol Phys. 1996;34(1):251-66. Epub 1996/01/01. doi: 10.1016/0360-3016(95)02029-2. PubMed PMID: 12118559.
106. Hecht BK, Turc-Carel C, Chatel M, Grellier P, Gioanni J, Attias R, Gaudray P, Hecht F. Cytogenetics of malignant gliomas: I. The autosomes with reference to rearrangements. Cancer Genet Cytogenet. 1995;84(1):1-8. Epub 1995/10/01. doi: 10.1016/0165-4608(95)00091-7. PubMed PMID: 7497435.
107. Pardal R, Clarke MF, Morrison SJ. Applying the principles of stem-cell biology to cancer. Nature reviews Cancer. 2003;3(12):895-902. Epub 2004/01/23. doi: 10.1038/nrc1232. PubMed PMID: 14737120.

108. Romer J, Curran T. Targeting medulloblastoma: small-molecule inhibitors of the Sonic Hedgehog pathway as potential cancer therapeutics. Cancer Res. 2005;65(12):4975-8. Epub 2005/06/17. doi: 10.1158/0008-5472.Can-05-0481. PubMed PMID: 15958535.
109. Lee J, Kotliarova S, Kotliarov Y, Li A, Su Q, Donin NM, Pastorino S, Purow BW, Christopher N, Zhang W, Park JK, Fine HA. Tumor stem cells derived from glioblastomas cultured in bFGF and EGF more closely mirror the phenotype and genotype of primary tumors than do serum-cultured cell lines. Cancer Cell. 2006;9(5):391-403. Epub 2006/05/16. doi: S1535-6108(06)00117-6 [pii] 10.1016/j.ccr.2006.03.030. PubMed PMID: 16697959.
110. Yuan X, Curtin J, Xiong Y, Liu G, Waschsmann-Hogiu S, Farkas DL, Black KL, Yu JS. Isolation of cancer stem cells from adult glioblastoma multiforme. Oncogene. 2004;23(58):9392-400. Epub 2004/11/24. doi: 10.1038/sj.onc.1208311. PubMed PMID: 15558011.
111. Gunther HS, Schmidt NO, Phillips HS, Kemming D, Kharbanda S, Soriano R, Modrusan Z, Meissner H, Westphal M, Lamszus K. Glioblastoma-derived stem cell-enriched cultures form distinct subgroups according to molecular and phenotypic criteria. Oncogene. 2008;27(20):2897-909. Epub 2007/11/27. doi: 10.1038/sj.onc.1210949. PubMed PMID: 18037961.
112. Kawai T, Matsumoto M, Takeda K, Sanjo H, Akira S. ZIP kinase, a novel serine/threonine kinase which mediates apoptosis. Molecular and cellular biology. 1998;18(3):1642-51. Epub 1998/03/06. doi: 10.1128/mcb.18.3.1642. PubMed PMID: 9488481; PMCID: PMC108879.
113. Kawai T, Nomura F, Hoshino K, Copeland NG, Gilbert DJ, Jenkins NA, Akira S. Death-associated protein kinase 2 is a new calcium/calmodulin-dependent protein kinase that signals apoptosis through its catalytic activity. Oncogene. 1999;18(23):3471-80. Epub 1999/06/22. doi: 10.1038/sj.onc.1202701. PubMed PMID: 10376525.
114. Kogel D, Plottner O, Landsberg G, Christian S, Scheidtmann KH. Cloning and characterization of Dlk, a novel serine/threonine kinase that is tightly associated with chromatin and phosphorylates core histones. Oncogene. 1998;17(20):2645-54. Epub 1998/12/05. doi: 10.1038/sj.onc.1202204. PubMed PMID: 9840928.
115. Inbal B, Shani G, Cohen O, Kissil JL, Kimchi A. Death-associated protein kinase-related protein 1, a novel serine/threonine kinase involved in apoptosis. Molecular and cellular biology. 2000;20(3):1044-54. Epub 2000/01/11. doi: 10.1128/mcb.20.3.1044-1054.2000. PubMed PMID: 10629061; PMCID: PMC85221.
116. Farag AK, Roh EJ. Death-associated protein kinase (DAPK) family modulators: Current and future therapeutic outcomes. Med Res Rev. 2019;39(1):349-85. Epub 2018/06/28. doi: 10.1002/med.21518. PubMed PMID: 29949198.
117. Temmerman K, Simon B, Wilmanns M. Structural and functional diversity in the activity and regulation of DAPK-related protein kinases. Febs j. 2013;280(21):5533-50. Epub 2013/06/12. doi: 10.1111/febs.12384. PubMed PMID: 23745726.
118. Sanjo H, Kawai T, Akira S. DRAKs, novel serine/threonine kinases related to death-associated protein kinase that trigger apoptosis. J Biol Chem. 1998;273(44):29066-71. Epub 1998/10/24. PubMed PMID: 9786912.
119. Deiss LP, Feinstein E, Berissi H, Cohen O, Kimchi A. Identification of a novel serine/threonine kinase and a novel 15-kD protein as potential mediators of the gamma interferon-induced cell death. Genes & development. 1995;9(1):15-30. Epub 1995/01/01. doi: 10.1101/gad.9.1.15. PubMed PMID: 7828849.
120. Cohen O, Feinstein E, Kimchi A. DAP-kinase is a Ca2+/calmodulin-dependent, cytoskeletal-associated protein kinase, with cell death-inducing functions that depend on its catalytic activity. Embo j. 1997;16(5):998-1008. Epub 1997/03/03. doi: 10.1093/emboj/16.5.998. PubMed PMID: 9118961; PMCID: PMC1169700.
121. Dioletis E, Dingley AJ, Driscoll PC. Structural and functional characterization of the recombinant death domain from death-associated protein kinase. PloS one. 2013;8(7):e70095. Epub 2013/08/08. doi: 10.1371/journal.pone.0070095. PubMed PMID: 23922916; PMCID: PMC3726526.

122. Stevens C, Lin Y, Sanchez M, Amin E, Copson E, White H, Durston V, Eccles DM, Hupp T. A germ line mutation in the death domain of DAPK-1 inactivates ERK-induced apoptosis. J Biol Chem. 2007;282(18):13791-803. Epub 2007/01/25. doi: 10.1074/jbc.M605649200. PubMed PMID: 17244621.
123. Tian X, Shi Y, Liu N, Yan Y, Li T, Hua P, Liu B. Upregulation of DAPK contributes to homocysteine-induced endothelial apoptosis via the modulation of Bcl2/Bax and activation of caspase 3. Mol Med Rep. 2016;14(5):4173-9. Epub 2016/10/26. doi: 10.3892/mmr.2016.5733. PubMed PMID: 27633052; PMCID: PMC5101913.
124. Qin Y, Ye GX, Wu CJ, Wang S, Pan DB, Jiang JY, Fu J, Xu SQ. Effect of DAPK1 gene on proliferation, migration, and invasion of carcinoma of pancreas BxPC-3 cell line. Int J Clin Exp Pathol. 2014;7(11):7536-44. Epub 2015/01/01. PubMed PMID: 25550789; PMCID: PMC4270545.
125. Zhao J, Zhao D, Poage GM, Mazumdar A, Zhang Y, Hill JL, Hartman ZC, Savage MI, Mills GB, Brown PH. Death-associated protein kinase 1 promotes growth of p53-mutant cancers. The Journal of clinical investigation. 2015;125(7):2707-20. Epub 2015/06/16. doi: 10.1172/jci70805. PubMed PMID: 26075823; PMCID: PMC4563671.
126. Schlegel CR, Georgiou ML, Misterek MB, Stocker S, Chater ER, Munro CE, Pardo OE, Seckl MJ, Costa-Pereira AP. DAPK2 regulates oxidative stress in cancer cells by preserving mitochondrial function. Cell Death Dis. 2015;6:e1671. Epub 2015/03/06. doi: 10.1038/cddis.2015.31. PubMed PMID: 25741596; PMCID: PMC4385915.
127. Park Y, Kim W, Lee JM, Park J, Cho JK, Pang K, Lee J, Kim D, Park SW, Yang KM, Kim SJ. Cytoplasmic DRAK1 overexpressed in head and neck cancers inhibits TGF-beta1 tumor suppressor activity by binding to Smad3 to interrupt its complex formation with Smad4. Oncogene. 2015;34(39):5037-45. Epub 2014/12/23. doi: 10.1038/onc.2014.423. PubMed PMID: 25531329.
128. Mao P, Hever-Jardine MP, Rahme GJ, Yang E, Tam J, Kodali A, Biswal B, Fadul CE, Gaur A, Israel MA, Spinella MJ. Serine/threonine kinase 17A is a novel candidate for therapeutic targeting in glioblastoma. PLoS One. 2013;8(11):e81803. Epub 2013/12/07. doi: 10.1371/journal.pone.0081803 PONE-D-13-25674 [pii]. PubMed PMID: 24312360.
129. Neubueser D, Hipfner DR. Overlapping roles of Drosophila Drak and Rok kinases in epithelial tissue morphogenesis. Mol Biol Cell. 2010;21(16):2869-79. Epub 2010/06/25. doi: E10-04-0328 [pii] 10.1091/mbc.E10-04-0328. PubMed PMID: 20573980.
130. Robertson F, Pinal N, Fichelson P, Pichaud F. Atonal and EGFR signalling orchestrate rok- and Drak-dependent adherens junction remodelling during ommatidia morphogenesis. Development. 2012;139(18):3432-41. Epub 2012/08/10. doi: dev.080762 [pii] 10.1242/dev.080762. PubMed PMID: 22874916.
131. Vicente-Manzanares M, Ma X, Adelstein RS, Horwitz AR. Non-muscle myosin II takes centre stage in cell adhesion and migration. Nature reviews Molecular cell biology. 2009;10(11):778-90. doi: 10.1038/nrm2786. PubMed PMID: 19851336; PMCID: 2834236.
132. Heissler SM, Manstein DJ. Nonmuscle myosin-2: mix and match. Cell Mol Life Sci. 2013;70(1):1-21. Epub 2012/05/09. doi: 10.1007/s00018-012-1002-9. PubMed PMID: 22565821; PMCID: PMC3535348.
133. LaRonde-LeBlanc N, Wlodawer A. A family portrait of the RIO kinases. J Biol Chem. 2005;280(45):37297-300. Epub 2005/09/27. doi: 10.1074/jbc.R500013200. PubMed PMID: 16183636.
134. LaRonde NA. The ancient microbial RIO kinases. J Biol Chem. 2014;289(14):9488-92. Epub 2014/02/21. doi: 10.1074/jbc.R113.538090. PubMed PMID: 24554707; PMCID: PMC3974999.
135. Hanks SK, Hunter T. Protein kinases 6. The eukaryotic protein kinase superfamily: kinase (catalytic) domain structure and classification. Faseb j. 1995;9(8):576-96. Epub 1995/05/01. PubMed PMID: 7768349.
136. LaRonde-LeBlanc N, Wlodawer A. Crystal structure of A. fulgidus Rio2 defines a new family of serine protein kinases. Structure. 2004;12(9):1585-94. Epub 2004/09/03. doi: 10.1016/j.str.2004.06.016. PubMed PMID: 15341724.
137. Knighton DR, Zheng JH, Ten Eyck LF, Ashford VA, Xuong NH, Taylor SS, Sowadski JM. Crystal structure of the catalytic subunit of cyclic adenosine monophosphate-dependent protein kinase.

Science (New York, NY). 1991;253(5018):407-14. Epub 1991/07/26. doi: 10.1126/science.1862342. PubMed PMID: 1862342.
138. Laronde-Leblanc N, Guszczynski T, Copeland T, Wlodawer A. Structure and activity of the atypical serine kinase Rio1. Febs j. 2005;272(14):3698-713. Epub 2005/07/13. doi: 10.1111/j.1742-4658.2005.04796.x. PubMed PMID: 16008568.
139. LaRonde-LeBlanc N, Guszczynski T, Copeland T, Wlodawer A. Autophosphorylation of Archaeoglobus fulgidus Rio2 and crystal structures of its nucleotide-metal ion complexes. Febs j. 2005;272(11):2800-10. Epub 2005/06/10. doi: 10.1111/j.1742-4658.2005.04702.x. PubMed PMID: 15943813.
140. Angermayr M, Bandlow W. RIO1, an extraordinary novel protein kinase. FEBS Lett. 2002;524(1-3):31-6. Epub 2002/07/24. doi: 10.1016/s0014-5793(02)02993-9. PubMed PMID: 12135737.
141. Geerlings TH, Faber AW, Bister MD, Vos JC, Raue HA. Rio2p, an evolutionarily conserved, low abundant protein kinase essential for processing of 20 S Pre-rRNA in Saccharomyces cerevisiae. J Biol Chem. 2003;278(25):22537-45. Epub 2003/04/12. doi: 10.1074/jbc.M300759200. PubMed PMID: 12690111.
142. Gajiwala KS, Burley SK. Winged helix proteins. Curr Opin Struct Biol. 2000;10(1):110-6. Epub 2000/02/19. doi: 10.1016/s0959-440x(99)00057-3. PubMed PMID: 10679470.
143. Wolberger C, Campbell R. New perch for the winged helix. Nat Struct Biol. 2000;7(4):261-2. Epub 2000/03/31. doi: 10.1038/74004. PubMed PMID: 10742162.
144. Vanrobays E, Gelugne JP, Gleizes PE, Caizergues-Ferrer M. Late cytoplasmic maturation of the small ribosomal subunit requires RIO proteins in Saccharomyces cerevisiae. Molecular and cellular biology. 2003;23(6):2083-95. Epub 2003/03/04. PubMed PMID: 12612080; PMCID: PMC149469.
145. Giaever G, Chu AM, Ni L, Connelly C, Riles L, Veronneau S, Dow S, Lucau-Danila A, Anderson K, Andre B, Arkin AP, Astromoff A, El-Bakkoury M, Bangham R, Benito R, Brachat S, Campanaro S, Curtiss M, Davis K, Deutschbauer A, Entian KD, Flaherty P, Foury F, Garfinkel DJ, Gerstein M, Gotte D, Guldener U, Hegemann JH, Hempel S, Herman Z, Jaramillo DF, Kelly DE, Kelly SL, Kotter P, LaBonte D, Lamb DC, Lan N, Liang H, Liao H, Liu L, Luo C, Lussier M, Mao R, Menard P, Ooi SL, Revuelta JL, Roberts CJ, Rose M, Ross-Macdonald P, Scherens B, Schimmack G, Shafer B, Shoemaker DD, Sookhai-Mahadeo S, Storms RK, Strathern JN, Valle G, Voet M, Volckaert G, Wang CY, Ward TR, Wilhelmy J, Winzeler EA, Yang Y, Yen G, Youngman E, Yu K, Bussey H, Boeke JD, Snyder M, Philippsen P, Davis RW, Johnston M. Functional profiling of the Saccharomyces cerevisiae genome. Nature. 2002;418(6896):387-91. Epub 2002/07/26. doi: 10.1038/nature00935. PubMed PMID: 12140549.
146. Zemp I, Wild T, O'Donohue MF, Wandrey F, Widmann B, Gleizes PE, Kutay U. Distinct cytoplasmic maturation steps of 40S ribosomal subunit precursors require hRio2. J Cell Biol. 2009;185(7):1167-80. Epub 2009/07/01. doi: jcb.200904048 [pii] 10.1083/jcb.200904048. PubMed PMID: 19564402.
147. Ferreira-Cerca S, Sagar V, Schafer T, Diop M, Wesseling AM, Lu H, Chai E, Hurt E, LaRonde-LeBlanc N. ATPase-dependent role of the atypical kinase Rio2 on the evolving pre-40S ribosomal subunit. Nat Struct Mol Biol. 2012;19(12):1316-23. Epub 2012/10/30. doi: nsmb.2403 [pii] 10.1038/nsmb.2403. PubMed PMID: 23104056.
148. Weinberg F, Reischmann N, Fauth L, Taromi S, Mastroianni J, Köhler M, Halbach S, Becker AC, Deng N, Schmitz T, Uhl FM, Herbener N, Riedel B, Beier F, Swarbrick A, Lassmann S, Dengjel J, Zeiser R, Brummer T. The Atypical Kinase RIOK1 Promotes Tumor Growth and Invasive Behavior. EBioMedicine. 2017;20:79-97. Epub 2017/05/14. doi: 10.1016/j.ebiom.2017.04.015. PubMed PMID: 28499923; PMCID: PMC5478185.
149. Zhang T, Ji D, Wang P, Liang D, Jin L, Shi H, Liu X, Meng Q, Yu R, Gao S. The atypical protein kinase RIOK3 contributes to glioma cell proliferation/survival, migration/invasion and the AKT/mTOR signaling pathway. Cancer Lett. 2018;415:151-63. Epub 2017/12/14. doi: 10.1016/j.canlet.2017.12.010. PubMed PMID: 29233656.

150. Song Y, Li C, Jin L, Xing J, Sha Z, Zhang T, Ji D, Yu R, Gao S. RIOK2 is negatively regulated by miR-4744 and promotes glioma cell migration/invasion through epithelial-mesenchymal transition. J Cell Mol Med. 2020. Epub 2020/03/04. doi: 10.1111/jcmm.15107. PubMed PMID: 32125767.
151. Liu K, Chen H-L, Wang S, Gu M-M, Chen X-M, Zhang S-L, Yu K-J, You Q-S. High Expression of RIOK2 and NOB1 Predict Human Non-small Cell Lung Cancer Outcomes. Scientific Reports. 2016;6(1):28666. doi: 10.1038/srep28666.
152. Muller-McNicoll M, Neugebauer KM. How cells get the message: dynamic assembly and function of mRNA-protein complexes. Nature reviews Genetics. 2013;14(4):275-87. Epub 2013/03/13. doi: 10.1038/nrg3434. PubMed PMID: 23478349.
153. Baltz AG, Munschauer M, Schwanhausser B, Vasile A, Murakawa Y, Schueler M, Youngs N, Penfold-Brown D, Drew K, Milek M, Wyler E, Bonneau R, Selbach M, Dieterich C, Landthaler M. The mRNA-bound proteome and its global occupancy profile on protein-coding transcripts. Molecular cell. 2012;46(5):674-90. Epub 2012/06/12. doi: 10.1016/j.molcel.2012.05.021. PubMed PMID: 22681889.
154. Ascano M, Hafner M, Cekan P, Gerstberger S, Tuschl T. Identification of RNA-protein interaction networks using PAR-CLIP. Wiley Interdiscip Rev RNA. 2012;3(2):159-77. Epub 2012/01/04. doi: 10.1002/wrna.1103. PubMed PMID: 22213601; PMCID: PMC3711140.
155. Moore MJ, Proudfoot NJ. Pre-mRNA processing reaches back to transcription and ahead to translation. Cell. 2009;136(4):688-700. Epub 2009/02/26. doi: 10.1016/j.cell.2009.02.001. PubMed PMID: 19239889.
156. Schoenberg DR, Maquat LE. Regulation of cytoplasmic mRNA decay. Nature reviews Genetics. 2012;13(4):246-59. Epub 2012/03/07. doi: 10.1038/nrg3160. PubMed PMID: 22392217; PMCID: PMC3351101.
157. Nielsen FC, Nielsen J, Christiansen J. A family of IGF-II mRNA binding proteins (IMP) involved in RNA trafficking. Scand J Clin Lab Invest Suppl. 2001;234:93-9. Epub 2001/11/21. PubMed PMID: 11713986.
158. Yaniv K, Yisraeli JK. The involvement of a conserved family of RNA binding proteins in embryonic development and carcinogenesis. Gene. 2002;287(1-2):49-54. Epub 2002/05/07. doi: 10.1016/s0378-1119(01)00866-6. PubMed PMID: 11992722.
159. Degrauwe N, Suvà ML, Janiszewska M, Riggi N, Stamenkovic I. IMPs: an RNA-binding protein family that provides a link between stem cell maintenance in normal development and cancer. Genes & development. 2016;30(22):2459-74. Epub 2016/12/13. doi: 10.1101/gad.287540.116. PubMed PMID: 27940961; PMCID: PMC5159662.
160. Bell JL, Wachter K, Muhleck B, Pazaitis N, Kohn M, Lederer M, Huttelmaier S. Insulin-like growth factor 2 mRNA-binding proteins (IGF2BPs): post-transcriptional drivers of cancer progression? Cellular and molecular life sciences : CMLS. 2013;70(15):2657-75. Epub 2012/10/17. doi: 10.1007/s00018-012-1186-z. PubMed PMID: 23069990; PMCID: PMC3708292.
161. Nielsen J, Christiansen J, Lykke-Andersen J, Johnsen AH, Wewer UM, Nielsen FC. A family of insulin-like growth factor II mRNA-binding proteins represses translation in late development. Molecular and cellular biology. 1999;19(2):1262-70. Epub 1999/01/16. PubMed PMID: 9891060; PMCID: 116055.
162. Nielsen J, Kristensen MA, Willemoes M, Nielsen FC, Christiansen J. Sequential dimerization of human zipcode-binding protein IMP1 on RNA: a cooperative mechanism providing RNP stability. Nucleic Acids Res. 2004;32(14):4368-76. Epub 2004/08/18. doi: 10.1093/nar/gkh754. PubMed PMID: 15314207; PMCID: PMC514376.
163. Wachter K, Kohn M, Stohr N, Huttelmaier S. Subcellular localization and RNP formation of IGF2BPs (IGF2 mRNA-binding proteins) is modulated by distinct RNA-binding domains. Biol Chem. 2013;394(8):1077-90. Epub 2013/05/04. doi: 10.1515/hsz-2013-0111. PubMed PMID: 23640942.
164. Chao JA, Patskovsky Y, Patel V, Levy M, Almo SC, Singer RH. ZBP1 recognition of beta-actin zipcode induces RNA looping. Genes & development. 2010;24(2):148-58. Epub 2010/01/19. doi: 10.1101/gad.1862910. PubMed PMID: 20080952; PMCID: 2807350.
165. Hafner M, Landthaler M, Burger L, Khorshid M, Hausser J, Berninger P, Rothballer A, Ascano M, Jr., Jungkamp AC, Munschauer M, Ulrich A, Wardle GS, Dewell S, Zavolan M, Tuschl T.

Transcriptome-wide identification of RNA-binding protein and microRNA target sites by PAR-CLIP. Cell. 2010;141(1):129-41. Epub 2010/04/08. doi: 10.1016/j.cell.2010.03.009. PubMed PMID: 20371350; PMCID: PMC2861495.
166. Conway AE, Van Nostrand EL, Pratt GA, Aigner S, Wilbert ML, Sundararaman B, Freese P, Lambert NJ, Sathe S, Liang TY, Essex A, Landais S, Burge CB, Jones DL, Yeo GW. Enhanced CLIP Uncovers IMP Protein-RNA Targets in Human Pluripotent Stem Cells Important for Cell Adhesion and Survival. Cell reports. 2016;15(3):666-79. Epub 2016/04/14. doi: 10.1016/j.celrep.2016.03.052. PubMed PMID: 27068461; PMCID: PMC4839292.
167. Boylan KL, Mische S, Li M, Marques G, Morin X, Chia W, Hays TS. Motility screen identifies Drosophila IGF-II mRNA-binding protein--zipcode-binding protein acting in oogenesis and synaptogenesis. PLoS Genet. 2008;4(2):e36. Epub 2008/02/20. doi: 10.1371/journal.pgen.0040036. PubMed PMID: 18282112; PMCID: PMC2242817.
168. Zhang HL, Eom T, Oleynikov Y, Shenoy SM, Liebelt DA, Dictenberg JB, Singer RH, Bassell GJ. Neurotrophin-induced transport of a beta-actin mRNP complex increases beta-actin levels and stimulates growth cone motility. Neuron. 2001;31(2):261-75. Epub 2001/08/15. doi: 10.1016/s0896-6273(01)00357-9. PubMed PMID: 11502257.
169. Tiruchinapalli DM, Oleynikov Y, Kelic S, Shenoy SM, Hartley A, Stanton PK, Singer RH, Bassell GJ. Activity-dependent trafficking and dynamic localization of zipcode binding protein 1 and beta-actin mRNA in dendrites and spines of hippocampal neurons. The Journal of neuroscience : the official journal of the Society for Neuroscience. 2003;23(8):3251-61. Epub 2003/04/30. PubMed PMID: 12716932.
170. Hansen TV, Hammer NA, Nielsen J, Madsen M, Dalbaeck C, Wewer UM, Christiansen J, Nielsen FC. Dwarfism and impaired gut development in insulin-like growth factor II mRNA-binding protein 1-deficient mice. Molecular and cellular biology. 2004;24(10):4448-64. Epub 2004/05/04. doi: 10.1128/mcb.24.10.4448-4464.2004. PubMed PMID: 15121863; PMCID: PMC400488.
171. Nishino J, Kim S, Zhu Y, Zhu H, Morrison SJ. A network of heterochronic genes including Imp1 regulates temporal changes in stem cell properties. eLife. 2013;2:e00924. Epub 2013/11/07. doi: 10.7554/eLife.00924. PubMed PMID: 24192035; PMCID: PMC3817382.
172. Lederer M, Bley N, Schleifer C, Huttelmaier S. The role of the oncofetal IGF2 mRNA-binding protein 3 (IGF2BP3) in cancer. Semin Cancer Biol. 2014;29:3-12. Epub 2014/07/30. doi: 10.1016/j.semcancer.2014.07.006. PubMed PMID: 25068994.
173. Dai N, Christiansen J, Nielsen FC, Avruch J. mTOR complex 2 phosphorylates IMP1 cotranslationally to promote IGF2 production and the proliferation of mouse embryonic fibroblasts. Genes Dev. 2013;27(3):301-12. Epub 2013/02/08. doi: 27/3/301 [pii] 10.1101/gad.209130.112. PubMed PMID: 23388827.
174. Suvasini R, Shruti B, Thota B, Shinde SV, Friedmann-Morvinski D, Nawaz Z, Prasanna KV, Thennarasu K, Hegde AS, Arivazhagan A, Chandramouli BA, Santosh V, Somasundaram K. Insulin growth factor-2 binding protein 3 (IGF2BP3) is a glioblastoma-specific marker that activates phosphatidylinositol 3-kinase/mitogen-activated protein kinase (PI3K/MAPK) pathways by modulating IGF-2. J Biol Chem. 2011;286(29):25882-90. Epub 2011/05/27. doi: 10.1074/jbc.M110.178012. PubMed PMID: 21613208; PMCID: 3138258.
175. Rivera Vargas T, Boudoukha S, Simon A, Souidi M, Cuvellier S, Pinna G, Polesskaya A. Post-transcriptional regulation of cyclins D1, D3 and G1 and proliferation of human cancer cells depend on IMP-3 nuclear localization. Oncogene. 2014;33(22):2866-75. Epub 2013/07/03. doi: 10.1038/onc.2013.252. PubMed PMID: 23812426.
176. Samanta S, Pursell B, Mercurio AM. IMP3 protein promotes chemoresistance in breast cancer cells by regulating breast cancer resistance protein (ABCG2) expression. J Biol Chem. 2013;288(18):12569-73. Epub 2013/03/30. doi: 10.1074/jbc.C112.442319. PubMed PMID: 23539627; PMCID: PMC3642304.
177. Palanichamy JK, Tran TM, Howard JM, Contreras JR, Fernando TR, Sterne-Weiler T, Katzman S, Toloue M, Yan W, Basso G, Pigazzi M, Sanford JR, Rao DS. RNA-binding protein IGF2BP3 targeting

of oncogenic transcripts promotes hematopoietic progenitor proliferation. The Journal of clinical investigation. 2016;126(4):1495-511. Epub 2016/03/15. doi: 10.1172/JCI80046. PubMed PMID: 26974154; PMCID: 4811152.
178. Dang CV, O'Donnell KA, Zeller KI, Nguyen T, Osthus RC, Li F. The c-Myc target gene network. Semin Cancer Biol. 2006;16(4):253-64. Epub 2006/08/15. doi: 10.1016/j.semcancer.2006.07.014. PubMed PMID: 16904903.
179. Chen H, Liu H, Qing G. Targeting oncogenic Myc as a strategy for cancer treatment. Signal Transduction and Targeted Therapy. 2018;3(1):5. doi: 10.1038/s41392-018-0008-7.
180. Meyer N, Penn LZ. Reflecting on 25 years with MYC. Nature reviews Cancer. 2008;8(12):976-90. Epub 2008/11/26. doi: 10.1038/nrc2231. PubMed PMID: 19029958.
181. Bjornsti MA, Houghton PJ. The TOR pathway: a target for cancer therapy. Nature reviews Cancer. 2004;4(5):335-48. Epub 2004/05/04. doi: 10.1038/nrc1362. PubMed PMID: 15122205.
182. Frost P, Moatamed F, Hoang B, Shi Y, Gera J, Yan H, Frost P, Gibbons J, Lichtenstein A. In vivo antitumor effects of the mTOR inhibitor CCI-779 against human multiple myeloma cells in a xenograft model. Blood. 2004;104(13):4181-7. Epub 2004/08/12. doi: 10.1182/blood-2004-03-1153. PubMed PMID: 15304393.
183. Chapuis N, Tamburini J, Green AS, Vignon C, Bardet V, Neyret A, Pannetier M, Willems L, Park S, Macone A, Maira SM, Ifrah N, Dreyfus F, Herault O, Lacombe C, Mayeux P, Bouscary D. Dual inhibition of PI3K and mTORC1/2 signaling by NVP-BEZ235 as a new therapeutic strategy for acute myeloid leukemia. Clinical cancer research : an official journal of the American Association for Cancer Research. 2010;16(22):5424-35. Epub 2010/10/05. doi: 10.1158/1078-0432.Ccr-10-1102. PubMed PMID: 20884625.
184. Yu K, Toral-Barza L, Discafani C, Zhang WG, Skotnicki J, Frost P, Gibbons JJ. mTOR, a novel target in breast cancer: the effect of CCI-779, an mTOR inhibitor, in preclinical models of breast cancer. Endocr Relat Cancer. 2001;8(3):249-58. Epub 2001/09/22. doi: 10.1677/erc.0.0080249. PubMed PMID: 11566616.
185. Sabatini DM. mTOR and cancer: insights into a complex relationship. Nature reviews Cancer. 2006;6(9):729-34. Epub 2006/08/18. doi: 10.1038/nrc1974. PubMed PMID: 16915295.
186. Sarbassov DD, Guertin DA, Ali SM, Sabatini DM. Phosphorylation and regulation of Akt/PKB by the rictor-mTOR complex. Science (New York, NY). 2005;307(5712):1098-101. Epub 2005/02/19. doi: 10.1126/science.1106148. PubMed PMID: 15718470.
187. Hresko RC, Mueckler M. mTOR.RICTOR is the Ser473 kinase for Akt/protein kinase B in 3T3-L1 adipocytes. J Biol Chem. 2005;280(49):40406-16. Epub 2005/10/14. doi: 10.1074/jbc.M508361200. PubMed PMID: 16221682.
188. Dunn GP, Rinne ML, Wykosky J, Genovese G, Quayle SN, Dunn IF, Agarwalla PK, Chheda MG, Campos B, Wang A, Brennan C, Ligon KL, Furnari F, Cavenee WK, Depinho RA, Chin L, Hahn WC. Emerging insights into the molecular and cellular basis of glioblastoma. Genes Dev. 2012;26(8):756-84. Epub 2012/04/18. doi: 10.1101/gad.187922.112. PubMed PMID: 22508724; PMCID: PMC3337451.
189. Cancer Genome Atlas Research N, Brat DJ, Verhaak RG, Aldape KD, Yung WK, Salama SR, Cooper LA, Rheinbay E, Miller CR, Vitucci M, Morozova O, Robertson AG, Noushmehr H, Laird PW, Cherniack AD, Akbani R, Huse JT, Ciriello G, Poisson LM, Barnholtz-Sloan JS, Berger MS, Brennan C, Colen RR, Colman H, Flanders AE, Giannini C, Grifford M, Iavarone A, Jain R, Joseph I, Kim J, Kasaian K, Mikkelsen T, Murray BA, O'Neill BP, Pachter L, Parsons DW, Sougnez C, Sulman EP, Vandenberg SR, Van Meir EG, von Deimling A, Zhang H, Crain D, Lau K, Mallery D, Morris S, Paulauskis J, Penny R, Shelton T, Sherman M, Yena P, Black A, Bowen J, Dicostanzo K, Gastier-Foster J, Leraas KM, Lichtenberg TM, Pierson CR, Ramirez NC, Taylor C, Weaver S, Wise L, Zmuda E, Davidsen T, Demchok JA, Eley G, Ferguson ML, Hutter CM, Mills Shaw KR, Ozenberger BA, Sheth M, Sofia HJ, Tarnuzzer R, Wang Z, Yang L, Zenklusen JC, Ayala B, Baboud J, Chudamani S, Jensen MA, Liu J, Pihl T, Raman R, Wan Y, Wu Y, Ally A, Auman JT, Balasundaram M, Balu S, Baylin SB, Beroukhim R, Bootwalla MS, Bowlby R, Bristow CA, Brooks D, Butterfield Y, Carlsen R, Carter S, Chin L, Chu A,

Chuah E, Cibulskis K, Clarke A, Coetzee SG, Dhalla N, Fennell T, Fisher S, Gabriel S, Getz G, Gibbs R, Guin R, Hadjipanayis A, Hayes DN, Hinoue T, Hoadley K, Holt RA, Hoyle AP, Jefferys SR, Jones S, Jones CD, Kucherlapati R, Lai PH, Lander E, Lee S, Lichtenstein L, Ma Y, Maglinte DT, Mahadeshwar HS, Marra MA, Mayo M, Meng S, Meyerson ML, Mieczkowski PA, Moore RA, Mose LE, Mungall AJ, Pantazi A, Parfenov M, Park PJ, Parker JS, Perou CM, Protopopov A, Ren X, Roach J, Sabedot TS, Schein J, Schumacher SE, Seidman JG, Seth S, Shen H, Simons JV, Sipahimalani P, Soloway MG, Song X, Sun H, Tabak B, Tam A, Tan D, Tang J, Thiessen N, Triche T, Jr., Van Den Berg DJ, Veluvolu U, Waring S, Weisenberger DJ, Wilkerson MD, Wong T, Wu J, Xi L, Xu AW, Yang L, Zack TI, Zhang J, Aksoy BA, Arachchi H, Benz C, Bernard B, Carlin D, Cho J, DiCara D, Frazer S, Fuller GN, Gao J, Gehlenborg N, Haussler D, Heiman DI, Iype L, Jacobsen A, Ju Z, Katzman S, Kim H, Knijnenburg T, Kreisberg RB, Lawrence MS, Lee W, Leinonen K, Lin P, Ling S, Liu W, Liu Y, Liu Y, Lu Y, Mills G, Ng S, Noble MS, Paull E, Rao A, Reynolds S, Saksena G, Sanborn Z, Sander C, Schultz N, Senbabaoglu Y, Shen R, Shmulevich I, Sinha R, Stuart J, Sumer SO, Sun Y, Tasman N, Taylor BS, Voet D, Weinhold N, Weinstein JN, Yang D, Yoshihara K, Zheng S, Zhang W, Zou L, Abel T, Sadeghi S, Cohen ML, Eschbacher J, Hattab EM, Raghunathan A, Schniederjan MJ, Aziz D, Barnett G, Barrett W, Bigner DD, Boice L, Brewer C, Calatozzolo C, Campos B, Carlotti CG, Jr., Chan TA, Cuppini L, Curley E, Cuzzubbo S, Devine K, DiMeco F, Duell R, Elder JB, Fehrenbach A, Finocchiaro G, Friedman W, Fulop J, Gardner J, Hermes B, Herold-Mende C, Jungk C, Kendler A, Lehman NL, Lipp E, Liu O, Mandt R, McGraw M, McLendon R, McPherson C, Neder L, Nguyen P, Noss A, Nunziata R, Ostrom QT, Palmer C, Perin A, Pollo B, Potapov A, Potapova O, Rathmell WK, Rotin D, Scarpace L, Schilero C, Senecal K, Shimmel K, Shurkhay V, Sifri S, Singh R, Sloan AE, Smolenski K, Staugaitis SM, Steele R, Thorne L, Tirapelli DP, Unterberg A, Vallurupalli M, Wang Y, Warnick R, Williams F, Wolinsky Y, Bell S, Rosenberg M, Stewart C, Huang F, Grimsby JL, Radenbaugh AJ, Zhang J. Comprehensive, Integrative Genomic Analysis of Diffuse Lower-Grade Gliomas. N Engl J Med. 2015;372(26):2481-98. doi: 10.1056/NEJMoa1402121. PubMed PMID: 26061751; PMCID: PMC4530011.

190. Brennan CW, Verhaak RGW, McKenna A, Campos B, Noushmehr H, Salama SR, Siyuan Zheng S, Chakravarty D, Sanborn JZ, Berman SH, Beroukhim R, Bernard B, Wu C-J, Genovese G, Shmulevich I, Barnholtz-Sloan J, Zou L, Vegesna R, Shukla SA, Ciriello G, Yung WK, Zhang W, Sougnez C, Mikkelsen T, Aldape K, Bigner DD, Van Meir EG, Prados M, Sloan A, Black KL, Eschbacher J, Finocchiaro G, Friedman W, Andrews DW, Guha A, Iacocca M, ONeill BP, Foltz G, Myers J, Weisenberger DJ, Penny R, Kucherlapati R, Perou CM, Hayes DN, Gibbs R, Marra M, Mills GB, Lander E, Spellman P, Wilson R, Sander C, Weinstein J, Meyerson M, Gabriel S, Laird PW, Haussler D, Getz G, Chin L, Network TR. The Somatic Genomic Landscape of Glioblastoma. Cell. 2013;155(2): 462-77.

191. Verhaak RG, Hoadley KA, Purdom E, Wang V, Qi Y, Wilkerson MD, Miller CR, Ding L, Golub T, Mesirov JP, Alexe G, Lawrence M, O'Kelly M, Tamayo P, Weir BA, Gabriel S, Winckler W, Gupta S, Jakkula L, Feiler HS, Hodgson JG, James CD, Sarkaria JN, Brennan C, Kahn A, Spellman PT, Wilson RK, Speed TP, Gray JW, Meyerson M, Getz G, Perou CM, Hayes DN. Integrated genomic analysis identifies clinically relevant subtypes of glioblastoma characterized by abnormalities in PDGFRA, IDH1, EGFR, and NF1. Cancer Cell. 2010;17(1):98-110. Epub 2010/02/05. doi: S1535-6108(09)00432-2 [pii] 10.1016/j.ccr.2009.12.020. PubMed PMID: 20129251.

192. Nishikawa R, Ji XD, Harmon RC, Lazar CS, Gill GN, Cavenee WK, Huang HJ. A mutant epidermal growth factor receptor common in human glioma confers enhanced tumorigenicity. Proc Natl Acad Sci U S A. 1994;91(16):7727-31. Epub 1994/08/02. PubMed PMID: 8052651.

193. Zhu H, Acquaviva J, Ramachandran P, Boskovitz A, Woolfenden S, Pfannl R, Bronson RT, Chen JW, Weissleder R, Housman DE, Charest A. Oncogenic EGFR signaling cooperates with loss of tumor suppressor gene functions in gliomagenesis. Proc Natl Acad Sci U S A. 2009;106(8):2712-6. doi: 10.1073/pnas.0813314106. PubMed PMID: 19196966; PMCID: 2650331.

194. Cloughesy TF, Cavenee WK, Mischel PS. Glioblastoma: from molecular pathology to targeted treatment. Annual review of pathology. 2014;9:1-25. doi: 10.1146/annurev-pathol-011110-130324. PubMed PMID: 23937436.

195. Reiter LT, Bier E. Using Drosophila melanogaster to uncover human disease gene function and potential drug target proteins. Expert Opin Ther Targets. 2002;6(3):387-99. PubMed PMID: 12223075.
196. Freeman MR, Doherty J. Glial cell biology in Drosophila and vertebrates. Trends Neurosci. 2006;29(2):82-90. Epub 2005/12/27. doi: S0166-2236(05)00307-3 [pii] 10.1016/j.tins.2005.12.002. PubMed PMID: 16377000.
197. Lin Y, Hupp TR, Stevens C. Death-associated protein kinase (DAPK) and signal transduction: additional roles beyond cell death. The FEBS journal. 2010;277(1):48-57. Epub 2009/11/03. doi: 10.1111/j.1742-4658.2009.07411.x. PubMed PMID: 19878313.
198. Bialik S, Kimchi A. The death-associated protein kinases: structure, function, and beyond. Annu Rev Biochem. 2006;75:189-210. Epub 2006/06/08. doi: 10.1146/annurev.biochem.75.103004.142615. PubMed PMID: 16756490.
199. Straight AF, Field CM, Mitchison TJ. Anillin binds nonmuscle myosin II and regulates the contractile ring. Mol Biol Cell. 2005;16(1):193-201. Epub 2004/10/22. doi: 10.1091/mbc.E04-08-0758. PubMed PMID: 15496454; PMCID: PMC539163.
200. Tang HW, Wang YB, Wang SL, Wu MH, Lin SY, Chen GC. Atg1-mediated myosin II activation regulates autophagosome formation during starvation-induced autophagy. EMBO J. 2011;30(4):636-51. Epub 2010/12/21. doi: 10.1038/emboj.2010.338. PubMed PMID: 21169990; PMCID: PMC3041946.
201. Zhang L, Ward REt. Distinct tissue distributions and subcellular localizations of differently phosphorylated forms of the myosin regulatory light chain in Drosophila. Gene Expr Patterns. 2011;11(1-2):93-104. Epub 2010/10/06. doi: 10.1016/j.gep.2010.09.008. PubMed PMID: 20920606; PMCID: PMC3025304.
202. Giansanti MG, Vanderleest TE, Jewett CE, Sechi S, Frappaolo A, Fabian L, Robinett CC, Brill JA, Loerke D, Fuller MT, Blankenship JT. Exocyst-Dependent Membrane Addition Is Required for Anaphase Cell Elongation and Cytokinesis in Drosophila. PLoS Genet. 2015;11(11):e1005632. Epub 2015/11/04. doi: 10.1371/journal.pgen.1005632. PubMed PMID: 26528720; PMCID: PMC4631508.
203. Gao J, Aksoy BA, Dogrusoz U, Dresdner G, Gross B, Sumer SO, Sun Y, Jacobsen A, Sinha R, Larsson E, Cerami E, Sander C, Schultz N. Integrative analysis of complex cancer genomics and clinical profiles using the cBioPortal. Sci Signal. 2013;6(269):pl1. doi: 10.1126/scisignal.2004088. PubMed PMID: 23550210.
204. Cerami E, Gao J, Dogrusoz U, Gross BE, Sumer SO, Aksoy BA, Jacobsen A, Byrne CJ, Heuer ML, Larsson E, Antipin Y, Reva B, Goldberg AP, Sander C, Schultz N. The cBio cancer genomics portal: an open platform for exploring multidimensional cancer genomics data. Cancer Discov. 2012;2(5):401-4. Epub 2012/05/17. doi: 10.1158/2159-8290.CD-12-0095. PubMed PMID: 22588877; PMCID: PMC3956037.
205. Kasza KE, Zallen JA. Dynamics and regulation of contractile actin-myosin networks in morphogenesis. Curr Opin Cell Biol. 2011;23(1):30-8. Epub 2010/12/07. doi: 10.1016/j.ceb.2010.10.014. PubMed PMID: 21130639; PMCID: PMC3320050.
206. Cabernard C. Cytokinesis in Drosophila melanogaster. Cytoskeleton (Hoboken). 2012;69(10):791-809. Epub 2012/08/14. doi: 10.1002/cm.21060. PubMed PMID: 22888045.
207. Mitonaka T, Muramatsu Y, Sugiyama S, Mizuno T, Nishida Y. Essential roles of myosin phosphatase in the maintenance of epithelial cell integrity of Drosophila imaginal disc cells. Dev Biol. 2007;309(1):78-86. Epub 2007/07/31. doi: 10.1016/j.ydbio.2007.06.021. PubMed PMID: 17662709.
208. Chougule AB, Hastert MC, Thomas JH. Drak Is Required for Actomyosin Organization During Drosophila Cellularization. G3 (Bethesda). 2016;6(4):819-28. Epub 2016/01/29. doi: 10.1534/g3.115.026401. PubMed PMID: 26818071; PMCID: PMC4825652.
209. Gillespie GY, Soroceanu L, Manning TJ, Jr., Gladson CL, Rosenfeld SS. Glioma migration can be blocked by nontoxic inhibitors of myosin II. Cancer Res. 1999;59(9):2076-82. Epub 1999/05/08. PubMed PMID: 10232591.
210. Salhia B, Hwang JH, Smith CA, Nakada M, Rutka F, Symons M, Rutka JT. Role of myosin II activity and the regulation of myosin light chain phosphorylation in astrocytomas. Cell Motil Cytoskeleton. 2008;65(1):12-24. Epub 2007/09/27. doi: 10.1002/cm.20240. PubMed PMID: 17896341.

211. Ivkovic S, Beadle C, Noticewala S, Massey SC, Swanson KR, Toro LN, Bresnick AR, Canoll P, Rosenfeld SS. Direct inhibition of myosin II effectively blocks glioma invasion in the presence of multiple motogens. Mol Biol Cell. 2012;23(4):533-42. Epub 2012/01/06. doi: mbc.E11-01-0039 [pii] 10.1091/mbc.E11-01-0039. PubMed PMID: 22219380.
212. Bornhauser BC, Olsson PA, Lindholm D. MSAP is a novel MIR-interacting protein that enhances neurite outgrowth and increases myosin regulatory light chain. J Biol Chem. 2003;278(37):35412-20. Epub 2003/06/27. doi: 10.1074/jbc.M306271200. PubMed PMID: 12826659.
213. Beroukhim R, Getz G, Nghiemphu L, Barretina J, Hsueh T, Linhart D, Vivanco I, Lee JC, Huang JH, Alexander S, Du J, Kau T, Thomas RK, Shah K, Soto H, Perner S, Prensner J, Debiasi RM, Demichelis F, Hatton C, Rubin MA, Garraway LA, Nelson SF, Liau L, Mischel PS, Cloughesy TF, Meyerson M, Golub TA, Lander ES, Mellinghoff IK, Sellers WR. Assessing the significance of chromosomal aberrations in cancer: methodology and application to glioma. Proc Natl Acad Sci U S A. 2007;104(50):20007-12. Epub 2007/12/14. doi: 10.1073/pnas.0710052104. PubMed PMID: 18077431; PMCID: PMC2148413.
214. Yan H, Parsons DW, Jin G, McLendon R, Rasheed BA, Yuan W, Kos I, Batinic-Haberle I, Jones S, Riggins GJ, Friedman H, Friedman A, Reardon D, Herndon J, Kinzler KW, Velculescu VE, Vogelstein B, Bigner DD. IDH1 and IDH2 mutations in gliomas. N Engl J Med. 2009;360(8):765-73. Epub 2009/02/21. doi: 10.1056/NEJMoa0808710. PubMed PMID: 19228619; PMCID: PMC2820383.
215. Parsons DW, Jones S, Zhang X, Lin JC, Leary RJ, Angenendt P, Mankoo P, Carter H, Siu IM, Gallia GL, Olivi A, McLendon R, Rasheed BA, Keir S, Nikolskaya T, Nikolsky Y, Busam DA, Tekleab H, Diaz LA, Jr., Hartigan J, Smith DR, Strausberg RL, Marie SK, Shinjo SM, Yan H, Riggins GJ, Bigner DD, Karchin R, Papadopoulos N, Parmigiani G, Vogelstein B, Velculescu VE, Kinzler KW. An integrated genomic analysis of human glioblastoma multiforme. Science. 2008;321(5897):1807-12. Epub 2008/09/06. doi: 1164382 [pii]
10.1126/science.1164382. PubMed PMID: 18772396.
216. Guo C, Pirozzi CJ, Lopez GY, Yan H. Isocitrate dehydrogenase mutations in gliomas: mechanisms, biomarkers and therapeutic target. Curr Opin Neurol. 2011;24(6):648-52. Epub 2011/10/18. doi: 10.1097/WCO.0b013e32834cd415. PubMed PMID: 22002076; PMCID: PMC3640434.
217. Jordan P, Karess R. Myosin light chain-activating phosphorylation sites are required for oogenesis in Drosophila. J Cell Biol. 1997;139(7):1805-19. Epub 1998/02/07. PubMed PMID: 9412474.
218. Newell-Litwa KA, Horwitz R, Lamers ML. Non-muscle myosin II in disease: mechanisms and therapeutic opportunities. Disease models & mechanisms. 2015;8(12):1495-515. Epub 2015/11/07. doi: 10.1242/dmm.022103. PubMed PMID: 26542704; PMCID: PMC4728321.
219. Beadle C, Assanah MC, Monzo P, Vallee R, Rosenfeld SS, Canoll P. The role of myosin II in glioma invasion of the brain. Mol Biol Cell. 2008;19(8):3357-68. Epub 2008/05/23. doi: E08-03-0319 [pii]
10.1091/mbc.E08-03-0319. PubMed PMID: 18495866.
220. Wong SY, Ulrich TA, Deleyrolle LP, MacKay JL, Lin JM, Martuscello RT, Jundi MA, Reynolds BA, Kumar S. Constitutive activation of myosin-dependent contractility sensitizes glioma tumor-initiating cells to mechanical inputs and reduces tissue invasion. Cancer Res. 2015;75(6):1113-22. Epub 2015/01/31. doi: 10.1158/0008-5472.CAN-13-3426. PubMed PMID: 25634210; PMCID: PMC4359960.
221. Field CM, Coughlin M, Doberstein S, Marty T, Sullivan W. Characterization of anillin mutants reveals essential roles in septin localization and plasma membrane integrity. Development. 2005;132(12):2849-60. Epub 2005/06/03. doi: 10.1242/dev.01843. PubMed PMID: 15930114.
222. Field CM, Alberts BM. Anillin, a contractile ring protein that cycles from the nucleus to the cell cortex. J Cell Biol. 1995;131(1):165-78. Epub 1995/10/01. PubMed PMID: 7559773; PMCID: PMC2120607.
223. Thomas JH, Wieschaus E. src64 and tec29 are required for microfilament contraction during Drosophila cellularization. Development. 2004;131(4):863-71. Epub 2004/01/23. doi: 10.1242/dev.00989. PubMed PMID: 14736750.

224. Hickson GR, O'Farrell PH. Rho-dependent control of anillin behavior during cytokinesis. J Cell Biol. 2008;180(2):285-94. Epub 2008/01/23. doi: 10.1083/jcb.200709005. PubMed PMID: 18209105; PMCID: PMC2213597.
225. Stupp R, Mason WP, van den Bent MJ, Weller M, Fisher B, Taphoorn MJ, Belanger K, Brandes AA, Marosi C, Bogdahn U, Curschmann J, Janzer RC, Ludwin SK, Gorlia T, Allgeier A, Lacombe D, Cairncross JG, Eisenhauer E, Mirimanoff RO. Radiotherapy plus concomitant and adjuvant temozolomide for glioblastoma. N Engl J Med. 2005;352(10):987-96. Epub 2005/03/11. doi: 352/10/987 [pii]
10.1056/NEJMoa043330. PubMed PMID: 15758009.
226. Huang PH, Xu AM, White FM. Oncogenic EGFR signaling networks in glioma. Science signaling. 2009;2(87):re6. Epub 2009/09/10. doi: 10.1126/scisignal.287re6. PubMed PMID: 19738203.
227. LaRonde-LeBlanc N, Wlodawer A. The RIO kinases: an atypical protein kinase family required for ribosome biogenesis and cell cycle progression. Biochim Biophys Acta. 2005;1754(1-2):14-24. Epub 2005/09/27. doi: 10.1016/j.bbapap.2005.07.037. PubMed PMID: 16182620.
228. Widmann B, Wandrey F, Badertscher L, Wyler E, Pfannstiel J, Zemp I, Kutay U. The kinase activity of human Rio1 is required for final steps of cytoplasmic maturation of 40S subunits. Mol Biol Cell. 2011. Epub 2011/11/11. doi: mbc.E11-07-0639 [pii]
10.1091/mbc.E11-07-0639. PubMed PMID: 22072790.
229. Baumas K, Soudet J, Caizergues-Ferrer M, Faubladier M, Henry Y, Mougin A. Human RioK3 is a novel component of cytoplasmic pre-40S pre-ribosomal particles. RNA Biol. 2012;9(2):162-74. Epub 2012/03/16. doi: 18810 [pii]
10.4161/rna.18810. PubMed PMID: 22418843.
230. Del Gobbo A, Vaira V, Ferrari L, Patriarca C, Di Cristofori A, Ricca D, Caroli M, Rampini P, Bosari S, Ferrero S. The oncofetal protein IMP3: a novel grading tool and predictor of poor clinical outcome in human gliomas. BioMed research international. 2015;2015:413897. Epub 2015/02/20. doi: 10.1155/2015/413897. PubMed PMID: 25695077; PMCID: 4324486.
231. Geng C, Macdonald PM. Imp associates with squid and Hrp48 and contributes to localized expression of gurken in the oocyte. Molecular and cellular biology. 2006;26(24):9508-16. Epub 2006/10/13. doi: 10.1128/mcb.01136-06. PubMed PMID: 17030623; PMCID: PMC1698525.
232. Morita M, Alain T, Topisirovic I, Sonenberg N. Polysome Profiling Analysis. Bio-protocol. 2013;3(14):e833. doi: 10.21769/BioProtoc.833.
233. Soucek S, Zeng Y, Bellur DL, Bergkessel M, Morris KJ, Deng Q, Duong D, Seyfried NT, Guthrie C, Staley JP, Fasken MB, Corbett AH. The Evolutionarily-conserved Polyadenosine RNA Binding Protein, Nab2, Cooperates with Splicing Machinery to Regulate the Fate of pre-mRNA. Mol Cell Biol. 2016;36(21):2697-714. Epub 2016/08/17. doi: 10.1128/MCB.00402-16. PubMed PMID: 27528618; PMCID: PMC5064217.
234. Zlatic SA, Ryder PV, Salazar G, Faundez V. Isolation of labile multi-protein complexes by in vivo controlled cellular cross-linking and immuno-magnetic affinity chromatography. Journal of visualized experiments : JoVE. 2010(37). Epub 2010/03/11. doi: 10.3791/1855. PubMed PMID: 20216526; PMCID: 2925877.
235. Bowman RL, Wang Q, Carro A, Verhaak RG, Squatrito M. GlioVis data portal for visualization and analysis of brain tumor expression datasets. Neuro Oncol. 2017;19(1):139-41. Epub 2016/12/30. doi: 10.1093/neuonc/now247. PubMed PMID: 28031383; PMCID: PMC5193031.
236. Strunk BS, Novak MN, Young CL, Karbstein K. A translation-like cycle is a quality control checkpoint for maturing 40S ribosome subunits. Cell. 2012;150(1):111-21. Epub 2012/07/10. doi: S0092-8674(12)00645-9 [pii]
10.1016/j.cell.2012.04.044. PubMed PMID: 22770215.
237. Hasygar K, Hietakangas V. p53- and ERK7-dependent ribosome surveillance response regulates Drosophila insulin-like peptide secretion. PLoS Genet. 2014;10(11):e1004764. Epub 2014/11/14. doi: 10.1371/journal.pgen.1004764. PubMed PMID: 25393288; PMCID: 4230838.

238. Fumagalli S, Thomas G. The role of p53 in ribosomopathies. Semin Hematol. 2011;48(2):97-105. Epub 2011/03/26. doi: S0037-1963(11)00009-6 [pii] 10.1053/j.seminhematol.2011.02.004. PubMed PMID: 21435506.
239. Narla A, Ebert BL. Ribosomopathies: human disorders of ribosome dysfunction. Blood. 2010;115(16):3196-205. Epub 2010/03/03. doi: blood-2009-10-178129 [pii] 10.1182/blood-2009-10-178129. PubMed PMID: 20194897.
240. Oh WJ, Wu CC, Kim SJ, Facchinetti V, Julien LA, Finlan M, Roux PP, Su B, Jacinto E. mTORC2 can associate with ribosomes to promote cotranslational phosphorylation and stability of nascent Akt polypeptide. EMBO J. 2010;29(23):3939-51. Epub 2010/11/04. doi: emboj2010271 [pii] 10.1038/emboj.2010.271. PubMed PMID: 21045808.
241. Zinzalla V, Stracka D, Oppliger W, Hall MN. Activation of mTORC2 by association with the ribosome. Cell. 2011;144(5):757-68. Epub 2011/03/08. doi: S0092-8674(11)00128-0 [pii] 10.1016/j.cell.2011.02.014. PubMed PMID: 21376236.
242. Seyfried NT, Dammer EB, Swarup V, Nandakumar D, Duong DM, Yin L, Deng Q, Nguyen T, Hales CM, Wingo T, Glass J, Gearing M, Thambisetty M, Troncoso JC, Geschwind DH, Lah JJ, Levey AI. A Multi-network Approach Identifies Protein-Specific Co-expression in Asymptomatic and Symptomatic Alzheimer's Disease. Cell Syst. 2017;4(1):60-72 e4. Epub 2016/12/19. doi: 10.1016/j.cels.2016.11.006. PubMed PMID: 27989508; PMCID: PMC5269514.
243. Wingo TS, Duong DM, Zhou M, Dammer EB, Wu H, Cutler DJ, Lah JJ, Levey AI, Seyfried NT. Integrating Next-Generation Genomic Sequencing and Mass Spectrometry To Estimate Allele-Specific Protein Abundance in Human Brain. J Proteome Res. 2017;16(9):3336-47. Epub 2017/07/12. doi: 10.1021/acs.jproteome.7b00324. PubMed PMID: 28691493; PMCID: PMC5698003.
244. Campbell MG, Karbstein K. Protein-protein interactions within late pre-40S ribosomes. PLoS One. 2011;6(1):e16194. Epub 2011/02/02. doi: 10.1371/journal.pone.0016194. PubMed PMID: 21283762; PMCID: PMC3024409.
245. Hein MY, Hubner NC, Poser I, Cox J, Nagaraj N, Toyoda Y, Gak IA, Weisswange I, Mansfeld J, Buchholz F, Hyman AA, Mann M. A human interactome in three quantitative dimensions organized by stoichiometries and abundances. Cell. 2015;163(3):712-23. Epub 2015/10/27. doi: 10.1016/j.cell.2015.09.053. PubMed PMID: 26496610.
246. Varjosalo M, Sacco R, Stukalov A, van Drogen A, Planyavsky M, Hauri S, Aebersold R, Bennett KL, Colinge J, Gstaiger M, Superti-Furga G. Interlaboratory reproducibility of large-scale human protein-complex analysis by standardized AP-MS. Nat Methods. 2013;10(4):307-14. Epub 2013/03/05. doi: 10.1038/nmeth.2400. PubMed PMID: 23455922.
247. Hansen HT, Rasmussen SH, Adolph SK, Plass M, Krogh A, Sanford J, Nielsen FC, Christiansen J. Drosophila Imp iCLIP identifies an RNA assemblage coordinating F-actin formation. Genome Biol. 2015;16:123. Epub 2015/06/10. doi: 10.1186/s13059-015-0687-0. PubMed PMID: 26054396; PMCID: 4477473.
248. Bhargava S, Visvanathan A, Patil V, Kumar A, Kesari S, Das S, Hegde AS, Arivazhagan A, Santosh V, Somasundaram K. IGF2 mRNA binding protein 3 (IMP3) promotes glioma cell migration by enhancing the translation of RELA/p65. Oncotarget. 2017;8(25):40469-85. Epub 2017/05/04. doi: 10.18632/oncotarget.17118. PubMed PMID: 28465487; PMCID: PMC5522290.
249. Wu C, Ma H, Qi G, Chen F, Chu J. Insulin-like growth factor II mRNA-binding protein 3 promotes cell proliferation, migration and invasion in human glioblastoma. Onco Targets Ther. 2019;12:3661-70. Epub 2019/06/14. doi: 10.2147/ott.S200901. PubMed PMID: 31190868; PMCID: PMC6527097.
250. Liu T, Deng M, Li J, Tong X, Wei Q, Ye X. Phosphorylation of right open reading frame 2 (Rio2) protein kinase by polo-like kinase 1 regulates mitotic progression. J Biol Chem. 2011;286(42):36352-60. Epub 2011/09/02. doi: M111.250175 [pii] 10.1074/jbc.M111.250175. PubMed PMID: 21880710.

251. Samuels TJ, Jarvelin AI, Ish-Horowicz D, Davis I. Imp/IGF2BP levels modulate individual neural stem cell growth and division through myc mRNA stability. eLife. 2020;9. Epub 2020/01/15. doi: 10.7554/eLife.51529. PubMed PMID: 31934860; PMCID: PMC7025822.
252. Shah KH, Nostramo R, Zhang B, Varia SN, Klett BM, Herman PK. Protein kinases are associated with multiple, distinct cytoplasmic granules in quiescent yeast cells. Genetics. 2014;198(4):1495-512. Epub 2014/10/25. doi: 10.1534/genetics.114.172031. PubMed PMID: 25342717; PMCID: 4256768.
253. Bjornsson CS, Apostolopoulou M, Tian Y, Temple S. It takes a village: constructing the neurogenic niche. Developmental cell. 2015;32(4):435-46. Epub 2015/02/25. doi: 10.1016/j.devcel.2015.01.010. PubMed PMID: 25710530; PMCID: PMC4886554.
254. Reitman ZJ, Sinenko SA, Spana EP, Yan H. Genetic dissection of leukemia-associated IDH1 and IDH2 mutants and D-2-hydroxyglutarate in Drosophila. Blood. 2015;125(2):336-45. Epub 2014/11/16. doi: 10.1182/blood-2014-05-577940. PubMed PMID: 25398939; PMCID: PMC4287640.
255. Felsenfeld G. A brief history of epigenetics. Cold Spring Harbor perspectives in biology. 2014;6(1). Epub 2014/01/05. doi: 10.1101/cshperspect.a018200. PubMed PMID: 24384572; PMCID: PMC3941222.
256. García MG, Carella A, Urdinguio RG, Bayón GF, Lopez V, Tejedor JR, Sierra MI, García-Toraño E, Santamarina P, Perez RF, Mangas C, Astudillo A, Corte-Torres MD, Sáenz-de-Santa-María I, Chiara MD, Fernández AF, Fraga MF. Epigenetic dysregulation of TET2 in human glioblastoma. Oncotarget. 2018;9(40):25922-34. Epub 2018/06/15. doi: 10.18632/oncotarget.25406. PubMed PMID: 29899831; PMCID: PMC5995234.
257. Wang F, Minakhina S, Tran H, Changela N, Kramer J, Steward R. Tet protein function during Drosophila development. PloS one. 2018;13(1):e0190367. Epub 2018/01/13. doi: 10.1371/journal.pone.0190367. PubMed PMID: 29324752; PMCID: PMC5764297.
258. Das TK, Esernio J, Cagan RL. Restraining Network Response to Targeted Cancer Therapies Improves Efficacy and Reduces Cellular Resistance. Cancer Res. 2018;78(15):4344-59. Epub 2018/05/31. doi: 10.1158/0008-5472.can-17-2001. PubMed PMID: 29844121.